

KEMIAN LAITOS  
JYVÄSKYLÄN YLIOPISTO

## **Rigid medium-sized rings: applications and synthesis**

M.Sc. thesis

University of Jyväskylä

Department of Chemistry

09.12.2024

Sanna Stenfors



JYVÄSKYLÄN YLIOPISTO



## Tiivistelmä

Tämän *pro gradu*- tutkielman kirjallinen osa keskittyy keskikokoisten rengasrakenteisten yhdisteiden ominaisuuksiin, stereoselektiivisiin synteestrategioihin, esiintyvyyteen luonnonaineissa, sekä hyödyntämiseen lääkeainekemiassa. Kokeellisessa osassa tutkittiin fotokemiallista Cope toisiintumista mahdollisena uutena menetelmänä trisubstituoitujen alkeiden stereoselektiiviseen synteesein.

Kirjallisen osan alkupäässä käsitellään esim. keskikokoisten renkaiden jäykistäviä elementtejä, stereokemiaa sekä konformaatioanalyysiä. Keskikokoisten renkaiden synteesi orgaanisessa kemiassa on hyvin vaikeaa mm. jännittyneen rakenteen, destabiloivien transannulaaristen vuorovaikutusten sekä syklisaatioreaktioissa tapahtuvan entropian pieneneminen vuoksi. Kolmannessa luvussa käsitellään esimerkkejä renkaanlaajennus- ja syklisaatioreaktioista, joiden avulla on syntetisoitu keskikokoisia renkaita stereoselektiivisesti. Luvussa 4 esitellään keskikokoisen renkaan sisältäviä karbo- ja heterosyklisiä yhdisteitä lääkeainesuunnittelussa/lääkeainekemian näkökulmasta.

Synteesiin liittyvistä vaikeuksista huolimatta keskikokoiset renkaat ovat hyvin mielenkiintoisia rakenneyksiköitä lääkeaineissa, mikä on lisännyt kiinnostusta synteessimenetelmien kehittämiseen. Lisäksi esim. 8- ja 9-jäsenisiä renkaita esiintyy useissa luonnonaineissa kuten seskviterpeeneihin kuuluvassa karyofylleenissa, joka syntetisoitiin ensimmäisen kerran vuonna 1963. Keskikokoisten renkaiden synteessimenetelmien kehitys jatkuu edelleen, esimerkiksi Petri Pihkon tutkimusryhmän synteeseikohtena oleva humiliisini *E* on 9-renkaan sisältävä makrosykli.

Tämän tutkielman kokeellisessa osassa toteutettiin funktionalisoidun keskikokoisen renkaan lähtöaineen synteesi käyttämällä fotokemiallista isomerisaatiota avainvaiheena. Lähtöaineen hiilirunko syntetisoitiin alkylaation ja Weinreb-ketoni-synteesin avulla. Fotokemiallinen isomerisaatio onnistui, mutta reaktio ei ollut täysin stereoselektiivinen. Isomerisaatioreaktion päätuotteena saatiin funktionalisoitua trisubstituoitua *Z*-alkeenia, jota voitaisi edelleen hyödyntää 10-renkaisen laktonin synteesein.

## Abstract

The literature review section of this master's thesis focuses on the properties of compounds with medium-sized rings, stereoselective synthesis strategies, occurrence in natural products, and utilization in medicinal chemistry. In the experimental part, the photochemical Cope rearrangement was explored as a potential new method for the stereoselective synthesis of trisubstituted alkenes.

The beginning of the literature review discusses, for example, the rigidifying elements of medium-sized rings, stereochemistry, and conformational analysis. The synthesis of medium-sized rings in organic chemistry is very difficult, for example, due to the strained structure, destabilizing transannular interactions, and lowering of entropy in the cyclization reaction. The third chapter discusses examples of ring expansion and cyclization strategies that have been used to synthesize medium-sized rings stereoselectively. Lastly, carbo- and heterocyclic compounds containing medium-sized rings are presented from the perspective of medicinal chemistry and their applications.

Despite the difficulties associated with synthesis, medium-sized rings are very interesting structural units in the design of pharmaceuticals. This feature has increased interest in the development of synthesis methods. In addition, medium-sized rings, such as 8- and 9-membered rings, are found in several natural products. An example is the sesquiterpene caryophyllene, which was synthesized for the first time in 1963. The development of synthetic methods for medium-sized rings continues today. In current research, humilisin E, a macrocycle containing a 9-membered ring is a target of total synthesis in the research group of Petri Pihko.

In the experimental part of this thesis, a functionalized starting material for medium-sized ring synthesis was prepared using a photochemical isomerization reaction as the key step. The carbon backbone of the starting material was synthesized by alkylation and Weinreb ketone synthesis. The photochemical isomerization was successful, but the reaction was not completely stereoselective, and a functionalized trisubstituted *Z*-alkene was obtained as the major product.

## Preface

This master's thesis was completed in the Department of Organic Chemistry at the University of Jyväskylä during December 2024. The topic was mainly chosen based on my interests, especially related to synthesis methods and medicinal substances. The literature review of my thesis focuses on the structural properties of medium-sized rings, synthesis methods, and applications in medicine. JYKDOK and Google Scholar databases were used for the literature search. The experimental part focuses on developing the synthesis route for a model substrate for cyclizations into medium-sized rings, such as the 9-membered ring of humilisin E. In addition, the aim was to explore a photochemical Cope rearrangement as a potential new method for obtaining trisubstituted alkenes in a stereoselective manner.

This master's thesis was supervised by Prof. Petri Pihko, and the other supervisors were M.Sc. Aino Rolig and Dr. Pradip Mondal during the experimental part. I would like to thank all of them for their excellent guidance, help, and support during the process. Thank you also for trusting me and my abilities! I would also like to thank the entire Pihko Group for the good team spirit and help during my project, Associate Professor Fabien Cougnon for being the second examiner of my thesis, and Dr. Anniina Kiesilä for measuring the mass spectra. In addition, I would also like to thank Dr. Elina Sievänen for the NMR training and M.Sc. Esa Haapaniemi for the guidance with the TopSpin software.

Doing this thesis has been a stressful but rewarding learning experience. I was able to challenge myself a lot, especially during the experimental part. Nevertheless, I sometimes felt that: "Kuljen silmät kiinni tietämättä suuntaa" as one of my favorite artists, BEHM, sings in her song Unia. Despite the challenges, working on a master's thesis reminded me of how diverse and fascinating the world of chemistry is. This experience confirmed my hope that I would like to work on research and synthesis in one way or another in the future as well!

Last but not least, I would like to thank my family, partner, and friends. I can never put into words how much I appreciate each of you! Thank you for your patience, understanding, and above all support during the intense and challenging life situation that I have had this year. Your encouragement and faith in me have been invaluable to me!

In Jyväskylä

09.12.2024

Sanna Stenfors

## Table of contents

<b>Tiivistelmä</b> .....	<b>iii</b>
<b>Abstract</b> .....	<b>iv</b>
<b>Preface</b> .....	<b>v</b>
<b>Table of contents</b> .....	<b>vi</b>
<b>Abbreviations</b> .....	<b>ix</b>
<b>LITERATURE REVIEW</b> .....	<b>1</b>
<b>1 Introduction</b> .....	<b>2</b>
<b>2 Medium-sized rings</b> .....	<b>3</b>
2.1 Beneficial properties of medium-sized rings.....	4
2.1.1 Natural products.....	5
2.1.2 Medicinal chemistry: macrocycles and medium-sized rings.....	10
2.2 Challenges in synthesis.....	15
2.3 Rigidifying elements, stereochemistry, and atropisomerism.....	19
2.4 Conformational analysis.....	23
2.4.1 Methods of conformational analysis.....	26
2.4.2 Example of modern conformational analysis by DFT: nefopam.....	28
2.4.3 Cyclooctane.....	30
2.4.4 <i>N</i> -Acetylbenzazocine.....	33
<b>3 Synthetic methods for medium-sized rings</b> .....	<b>35</b>
3.1 Ring expansion reactions.....	36
3.1.1 Fragmentation reactions.....	38
3.1.2 Pericyclic ring-expansion reactions.....	43
3.1.3 Acyloin condensation followed by ring expansion.....	45
3.2 Cyclization reactions of acyclic precursors.....	47
3.2.1 Ring-closing metathesis (RCM).....	49
3.2.2 Samarium(II)-promoted cyclizations.....	50
3.2.3 Case study: Taxol®.....	52
<b>4 Medium-sized rings in pharmaceuticals and natural products</b> .....	<b>56</b>

4.1 Carbocycles .....	58
4.1.1 Paclitaxel .....	58
4.1.2 HIV protease inhibitors .....	61
4.2 Heterocycles .....	64
4.2.1 Nefopam .....	65
4.2.2 X-linked inhibitor of apoptosis protein (XIAP) and xevinapant .....	66
4.2.3 SMAC mimetics .....	69
<b>5 Conclusions of the literature review .....</b>	<b>73</b>
<b>EXPERIMENTAL PART .....</b>	<b>75</b>
<b>6 Introduction .....</b>	<b>76</b>
<b>7 Work plan .....</b>	<b>79</b>
<b>8 Execution of work plan .....</b>	<b>81</b>
8.1 TBS protection of 3-bromo-1-propanol.....	82
8.2 Alkylation reaction.....	82
8.3 Finkelstein reaction .....	85
8.4 Deprotection and lactonization attempts .....	85
8.5 Weinreb amide synthesis.....	88
8.6 Weinreb ketone synthesis.....	89
8.7 Shapiro reaction.....	91
8.8 Photo-Cope Rearrangement .....	94
<b>9 Conclusions .....</b>	<b>99</b>
<b>10 Experimental methods .....</b>	<b>101</b>
10.1 (3-bromopropoxy)( <i>tert</i> -butyl)dimethylsilane .....	102
10.2 1-iodo-3-( <i>tert</i> -butyldimethylsilyloxy)propane .....	103
10.3 ethyl-5-(( <i>tert</i> -butyldimethylsilyl)oxy)-2-(prop-1-en-2-yl)pentanoate.....	104
10.4 <i>N</i> -methoxy- <i>N</i> -methylbenzamide .....	105
10.5 5-(( <i>tert</i> -butyldimethylsilyl)oxy)- <i>N</i> -methoxy- <i>N</i> -methyl-2-(prop-1-en-2-yl)pentanamide .....	106
10.6 2,4,6-Triisopropylbenzenesulfonyl hydrazide.....	107
10.7 Cyclopentanone (2,4,6-Triisopropylbenzenesulfonyl)hydrazone .....	108
10.8 2-methyl-1-phenylprop-2-en-1-one.....	109

10.9 7-(( <i>tert</i> -butyldimethylsilyl)oxy)-2-methyl-4-(prop-1-en-2-yl)hept-1-en-3-one .....	110
10.10 5-(( <i>tert</i> -butyldimethylsilyl)oxy)-1-(cyclopent-1-en-1-yl)-2-(prop-1-en-2-yl)pentan-1-one .	111
10.11 methyl (2 <i>R</i> )-2-(( <i>Z</i> )-6-(( <i>tert</i> -butyldimethylsilyl)oxy)-2-methylhex-2-en-1-yl)cyclopentane-1-carboxylate .....	113
10.12 Attempted reactions.....	114
10.12.1 ethyl-5-(( <i>tert</i> -butyldimethylsilyl)oxy)-2-(prop-1-en-2-yl)pentanoate .....	114
10.12.2 3-(prop-1-en-2-yl)tetrahydro-2 <i>H</i> -pyran-2-one .....	115
10.12.3 1-Cyclopenten-1-ylphenylmethanone .....	117
10.12.4 1-(hydroxy(phenyl)methyl)-1-cyclopentene .....	117
10.12.5 methyl (2 <i>R</i> )-2-(( <i>Z</i> )-6-(( <i>tert</i> -butyldimethylsilyl)oxy)-2-methylhex-2-en-1-yl)cyclopentane-1-carboxylate .....	118
<b>References .....</b>	<b>119</b>
<b>Appendices .....</b>	<b>130</b>



**Abbreviations**

<b><math>^{13}\text{C}</math> NMR</b>	carbon-13 nuclear magnetic resonance
<b><math>^1\text{H}</math> NMR</b>	proton nuclear magnetic resonance
<b>ALK</b>	anaplastic lymphoma kinase
<b>API</b>	active pharmaceutical ingredient
<b>approx.</b>	approximately
<b>aq</b>	aqueous
<b>ATR</b>	attenuated total reflectance
<b>AVPI</b>	Ala1-Val2-Pro3-Ile4-motif
<b>BAX</b>	Bcl-2-associated X protein
<b>BB</b>	boat-boat
<b>BC</b>	boat-chair
<b>Bcl-2</b>	B-cell leukemia 2
<b>BHT</b>	butylated hydroxytoluene
<b>BIR</b>	baculoviral IAP repeat
<b>br</b>	broad
<b>brine</b>	salt water (sat. NaCl)
<b>bRo5</b>	beyond-rule-of-5
<b>Bu</b>	butyl group
<b>ca.</b>	circa
<b>CC</b>	chair-chair
<b>CCDC</b>	Cambridge Crystallographic Data Centre
<b><math>\text{CDCl}_3</math></b>	chloroform- $d_3$

<b>cIAP1/2</b>	cellular IAP 1 and 2
<b>COSY</b>	correlation spectroscopy
<b>CP</b>	complementary pairing
<b>CR</b>	crown
<b>CRE</b>	cyclization/ring expansion cascade
<b>CrEL</b>	Cremophor EL
<b>CRT</b>	chemoradiotherapy
<b>d</b>	doublet
<b>DABCO</b>	triethylenediamine
<b>DCM</b>	dichloromethane
<b>dd</b>	doublet of doublets
<b>DFT</b>	density functional theory
<b>DIBAL</b>	diisobutylaluminium hydride
<b>DIPEA</b>	<i>N,N</i> -Diisopropylethylamine
<b>DMAP</b>	4-dimethylaminopyridine
<b>DME</b>	dimethyl ether
<b>DMSO</b>	dimethyl sulfoxide
<b>DOS</b>	diversity-oriented synthesis
<b><i>E2</i></b>	second order elimination reaction
<b>ED<sub>50</sub></b>	median effective dose
<b><i>E<sub>h</sub></i></b>	Hartree energy
<b>EHO</b>	2-ethylheptane-5-olide
<b>EM</b>	effective molarity
<b>equiv</b>	equivalent

<b>ER</b>	endoplasmic reticulum
<b>ESI</b>	electrospray ionization
<b>Et</b>	ethyl group
<i>et al.</i>	and others
<b>Et<sub>2</sub>O</b>	diethyl ether
<b>EtOAc</b>	ethyl acetate
<b>EtOH</b>	ethanol
<b>EVL</b>	2-ethylidene-6-hepten-5-olide
<b>FADD</b>	fas-associated protein with death domain
<b>FDA</b>	Food and Drug Administration
<b>FTIR</b>	Fourier-Transform Infrared Spectroscopy
<b>G<sub>0</sub></b>	Gibbs free energy
<b>G-II</b>	Grubbs second-generation catalyst
<b>GluCl</b>	glutamate-gated chloride channel
<b>HBA</b>	hydrogen bond acceptor
<b>HBD</b>	hydrogen bond donor
<b>hex</b>	hexane
<b>HG-II</b>	Hoveyda–Grubbs second-generation catalyst
<b>HH COSY</b>	HH correlated spectroscopy
<b>HIV</b>	human immunodeficiency virus
<b>HL</b>	$\delta$ -hexalactone
<b>HPLC</b>	High Performance Liquid Chromatography
<b>HRMS</b>	High-Resolution Mass Spectrometry
<b>HSQC</b>	Heteronuclear Single Quantum Correlation

<b>IAP</b>	inhibitor of apoptosis protein
<b><i>i</i>-PrMgCl</b>	isopropylmagnesium chloride
<b>IMDA</b>	intramolecular Diels-Alder reaction
<b>IMHB</b>	intramolecular hydrogen bonds
<b><i>in vitro</i></b>	experiment performed outside of a living system
<b><i>in vivo</i></b>	experiment performed in a living organism
<b>IR</b>	Infrared Spectroscopy
<b><i>J</i></b>	coupling constant
<b><i>K<sub>i</sub></i></b>	inhibitory constant
<b>LA</b>	locally advanced
<b>LC/MS</b>	Liquid Chromatography-Mass Spectrometry
<b>LDA</b>	lithium diisopropylamide
<b>lit.</b>	literature
<b>m</b>	multiplet
<b><i>m/z</i></b>	mass-to-charge ratio
<b>MD</b>	molecular dynamics
<b>Me</b>	methyl
<b>MM</b>	molecular mechanics
<b>mp</b>	melting point
<b>MTA</b>	microtubule targeting agent
<b>MW</b>	molecular weight
<b>NaHMDS</b>	sodium bis(trimethylsilyl)amide
<b><i>n</i>-BuLi</b>	<i>n</i> -Butyllithium

<b>NFκB</b>	nuclear factor kappa-light-chain enhancer of activated B cells
<b>NIK</b>	NFκB-inducing kinase
<b>NMO</b>	<i>N</i> -methylnmorpholine <i>N</i> -oxide
<b>NMR</b>	Nucleic Magnetic Resonance
<b>NOE</b>	Nuclear Overhauser Effect
<b>NOESY</b>	Nuclear Overhauser Effect Spectroscopy
<b>NSAID</b>	non-steroidal anti-inflammatory drug
<b>Nu</b>	nucleophile
<b>ODRE</b>	Oxidative Dearomatization–Ring-Expanding rearomatization
<b>p</b>	para
<b>PES</b>	potential energy surface
<b>Pg</b>	protecting group
<b>PhOK</b>	potassium phenoxide
<b>ppm</b>	parts per million
<b>PSA</b>	polar surface area
<b><i>p</i>-TsOH</b>	<i>p</i> -Toluenesulfonic acid
<b>PTX</b>	paclitaxel
<b>q</b>	quartet
<b>QM</b>	quantum mechanical
<b>quint</b>	quintet
<b>R</b>	organic side chain
<b>RB</b>	rotatable bond

<b>RCM</b>	ring-closing metathesis
<b><i>R<sub>f</sub></i></b>	retention factor
<b>RIP1</b>	receptor-interacting serine/threonine-protein kinase 1
<b>Ro5</b>	rule of 5
<b>ROP</b>	ring-opening polymerization
<b>ROS</b>	reactive oxygen species
<b>ROS1</b>	c-ros onco gene 1
<b>rt.</b>	room temperature
<b>s</b>	singlet
<b>SAR</b>	structure-activity relationship
<b>sat.</b>	saturated
<b>SCCHN</b>	squamous cell carcinoma of the head and neck
<b>sept</b>	septet
<b>SMAC</b>	second mitochondria-derived activator of caspase
<b><i>S<sub>N</sub>2</i></b>	second-order nucleophilic substitution
<b><i>S<sub>N</sub>Ar</i></b>	intramolecular nucleophilic aromatic substitution
<b>SPS</b>	solvent purification system
<b>SuRE</b>	successive ring expansion
<b>t</b>	triplet
<b>T3P</b>	propanephosphonic acid anhydride
<b>TBAF</b>	<i>tetra-n</i> -butylammonium fluoride
<b>TBC</b>	twisted boat-chair
<b>TBDMSOTf</b>	<i>tert</i> -Butyldimethylsilyl trifluoromethanesulfonate
<b>TBSCl</b>	<i>tert</i> -Butyldimethylsilylchloride

<b>TC</b>	twist-chair
<b>TCC</b>	twist-chair-chair
<b>td</b>	triplet of doublets
<b>TES</b>	triethylsilane
<b>THF</b>	tetrahydrofuran
<b>TIPSOTf</b>	triisopropylsilyl trifluoromethanesulfonate
<b>TLC</b>	thin-layer chromatography
<b>TLR4</b>	toll-like receptor 4
<b>TMEDA</b>	tetramethylethylenediamine
<b>TMSOEt</b>	ethoxytrimethylsilane
<b>TNF</b>	tumor necrosis factor
<b>TOF</b>	time-of-flight
<b>TPAP</b>	tetrapropylammonium perruthenate
<b>TPSH</b>	2,4,6-triisopropylbenzenesulfonyl hydrazide
<b>UV</b>	ultraviolet
<i>via</i>	through
<b>VL</b>	$\delta$ -valerolactone
<b>XIAP</b>	X-linked inhibitors of apoptosis protein

**LITERATURE REVIEW**



## 1 Introduction

Medium-sized rings are ring structures composed of 8-11 carbon atoms, and they may also contain heteroatoms. Medium-sized rings are usually strained structures with transannular interactions between substituents. Steric clashes of substituents with each other cause destabilizing interactions, which are challenging to alleviate due to the minimal free space inside the medium-sized ring. Several low-energy conformations can typically be determined for medium-sized rings, e.g. using computational methods.<sup>1-3</sup> Rigidifying elements, such as benzene rings and double bonds, reduce the number of possible conformers and conformational freedom compared to the unsubstituted rings. On the other hand, rigidifying elements remove hydrogen atoms or CH bonds from the ring, reducing the transannular interactions.<sup>4,5</sup>

Medium-sized rings are found both in natural products as well as in the structures of pharmaceuticals.<sup>6,7</sup> Nevertheless, their synthesis is very challenging due to, for example, thermodynamic instability and competing side reactions/intermolecular coupling that traditional cyclization methods face.<sup>8,9</sup> Several studies have shown that ring size plays a key role in the outcome of the reaction: for example, ring expansion reactions may only be possible in synthesizing compounds that exceed a certain ring size.<sup>10</sup> The development of new experimental methods favoring macrocyclization, or the formation of medium-sized rings, is an important goal in the near future.

Currently, medium-sized rings are largely underrepresented in different screening libraries in medicinal chemistry, and aliphatic 5- and 6-membered rings are more common in approved drugs. This can be explained, among other things, by the entropic and enthalpic challenges associated with synthesis, which lead to variable yields. Cyclic frameworks improve binding affinity and bioavailability compared to linear structures, which is very important for drugs. The more compact the conformational space of the molecule, the smaller the entropy loss when the macrocycle binds to the target protein.<sup>11,12</sup> Research on macrocyclic compounds and their synthesis is very important for the discovery of molecules with medical significance and the development of synthesis strategies in medicine.

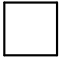
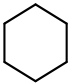
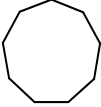
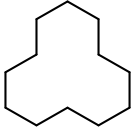
The purpose of this thesis is to study the properties, synthesis methods, and the occurrence of rigid medium-sized rings in various natural products and pharmaceuticals. The following Chapter covers the structure of medium-sized rings, the effect of rigidifying elements, and examples of conformational analysis. In addition, towards the end of the literature review part,

examples of drugs with a medium-sized ring are presented. Separate numbering has been used in the theoretical and experimental parts for clarity.

## 2 Medium-sized rings

Cyclic compounds are categorized by ring size and properties: small-sized rings (3-4 atoms), common-sized rings (5-7 atoms), medium-sized rings (8-11 atoms), and large-sized rings containing 12 or more atoms (see Table 2.1).<sup>1</sup> Rings of comparable sizes often possess many similarities but, for example, substituents have been shown to affect energies of conformations.<sup>1,13,14</sup> The ring size affects the properties of the ring: for example, strain is a significant part in terms of reactions. The ring strain affects compounds if the bonds are forced to angles that deviate from normal - in medium and large rings the conformational changes can lower the tension.<sup>1</sup>

**Table 2.1.** Comparison of different ring sizes and their calculated enthalpies ( $\Delta H$ ) and strain energies<sup>15</sup>

Number of atoms	Name	Structure	$\Delta H_f^\circ$ (gas, 25 °), kcal/mol	Strain energy (gas, 25 °) <sup>b</sup> , kcal/mol
4	Cyclobutane		+6.8	26.3
6	Cyclohexane		-29.5	1.4
9	Cyclononane		-31.7	15.5
12	Cyclododecane		-55.0, -50.5 (average: -52.8)	11.8

<sup>a</sup>experimental data <sup>b</sup>calculated energy values

The bond angles of tetrahedral  $sp^3$ -hybridized carbon are  $109.5^\circ$ . However, due to their cyclic structure, cycloalkanes are unable to form a perfect tetrahedral bond angle concerning each substituent. This causes strain in the bond angles of cycloalkanes. Puckering of the ring reduces the bond angles when examining the structure in three-dimensional space.<sup>16</sup> Small-sized rings are highly strained and rigid due to large deviations from ideal bond angles (angle strain) and eclipsing interactions (torsional strain). Common-sized rings have bond angles near the ideal value ( $109.5^\circ$ ) and substituents directed outward from the ring.<sup>1</sup> Medium-sized rings exhibit a unique type of steric strain called transannular interactions, which arise when ring substituents interact with each other causing a strong repulsion between non-bonded atoms.<sup>1,14</sup> Large-sized rings have relatively little strain and resemble open-chain compounds.<sup>1</sup>

Medium-sized rings can also contain different heteroatoms, contributing to the rigidity and reactivity of the ring structures. The addition of substituents changes the reactivity, and the desired reactions can be enabled, while unwanted ones are limited with good conformational control.<sup>17</sup> The rigidity of the ring structure contributes to stereocontrol because it defines the distances between atoms in the molecule. The distances between the functional groups play a significant role in the reaction. The synthesis and conformations of rigid medium-sized rings, as well as the effect of ring sizes, are discussed in later chapters.

## 2.1 Beneficial properties of medium-sized rings

As structures, medium-sized rings offer a combination of suitable flexibility and multiple different conformers, which makes them interesting and useful synthesis targets in organic chemistry. In substituted 8-membered rings, the presence of bulky groups can lead to a pseudoequatorial preference, influencing the energy landscape and conformational interchange.<sup>10,16,18</sup> The number of possible conformations sharply increases as the ring size increases. However, there is no specific algorithm or formula to determine the number of conformations.<sup>1</sup> The number of possible conformers decreases when the structure has rigidifying elements. Temperature also affects the number of conformations - the number is more limited at normal room temperature.<sup>18</sup>

Medium-sized rings are common in numerous bioactive natural products and many therapeutically significant molecules.<sup>10</sup> Synthesis of medium-sized rings is challenging (see subchapter 2.2) but the interest has grown in medicinal chemistry despite the difficulties.<sup>19,20</sup> Unique structural features of medium-sized rings, such as the combination of structural rigidity and wide conformational flexibility, may lead to new bioactive compounds that potentially

target previously undruggable biological targets.<sup>17</sup> The structure of medium-sized rings allows for greater flexibility compared to smaller ring sizes, facilitating the conformational changes required for receptor binding. Furthermore, medium-sized rings have shown increased metabolic stability and cell permeability, making them attractive candidates for drug discovery.<sup>21</sup>

The following subchapters discuss examples of natural products and pharmaceuticals that have medium-sized rings containing rigidifying elements. The examples are presented as introductory cases that give a general understanding of the structure and conformation of compounds containing a rigid medium-sized ring. The synthesis strategies of medium-sized rings and their applications in medicinal chemistry are discussed in more detail in Chapters 3 and 4.

### 2.1.1 Natural products

Macrocycles found in natural products often contain a variety of functional groups and substituents. This subchapter briefly introduces two groups of natural products: alkaloids and terpenes, both of which are extensive classes of natural products containing a wide range of biologically and pharmaceutically interesting compounds.<sup>22,23</sup> In addition, the natural product that inspired the work of the experimental part, humilisin E, belongs to the diterpenoids which are modified terpenes containing particularly oxygen as an additional functional group.<sup>24</sup>

Alkaloids are one of the major categories of natural compounds manufactured by a wide range of terrestrial and marine organisms, including bacteria, plants, and fungi. The production of alkaloids also conveys many environmental benefits to the host, including protection against predators and competitors and facilitating reproduction. As a result, alkaloids frequently possess remarkable pharmacological properties, thereby serving as ideal lead compounds in the design of therapies against human diseases.<sup>6</sup>

Nitrogen (*N*) heterocycles are present in thousands of known alkaloids. However, 8-membered *N*-heterocycles are rare compared to 5-7-membered heterocycles (for example imidazoles and pyridines).<sup>25</sup> As an example of 8-membered *N*-heterocycles in natural products, the okaramines possess an 8-membered azocine ring system. The okaramines are part of an azocinoindole family with a compound skeleton resembling deoxyisoaustamides **1** (see Figure 2.1.1.1).<sup>6</sup>

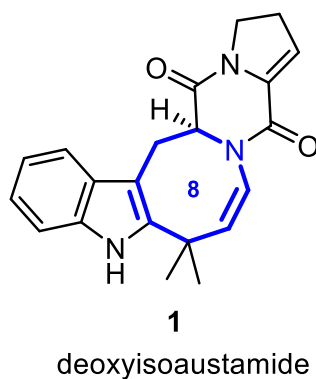


**Figure 2.1.1.1.** The structure of deoxyisoaustamide **1**.<sup>6</sup>

Okaramines A (**2**) and B (**3**) were isolated from the fungus *Penicillium simplicissimum*, a microorganism that had been isolated from a soil sample.<sup>26</sup> Okaramine A showed potent insecticidal activity causing the death of 90 % of *Bombyx mori* instar larvae at 30 ppm in 24 h. Okaramine B exhibited higher insecticidal activity compared to okaramine A ( $LD_{100} = 0.3$  ppm), activating insect glutamate-gated chloride channels (GluCl<sub>s</sub>).<sup>6</sup>

Although okaramines have an 8-membered ring in their structure, the 4-membered ring structure, azetidine, is more interesting from the point of view of biological activity. Structure-activity relationship (SAR) studies revealed the importance of the azetidine ring of okaramines B, C, and D for insecticidal properties: okaramine A, which does not possess the azetidine unit, was less active than okaramine B. However, despite having azetidine in the structure, okaramines **4** and **5** were inactive, suggesting that hydroxylation at C-12 negatively impacts insecticidal activity (Figure 2.1.1.2).<sup>6</sup>

The structures of okaramines **6-8** lack the C1'-C2' double bond and only weak insecticidal activity was observed ( $LD_{50} > 100$   $\mu\text{g/g}$ ). This result indicated that the decrease in insecticidal activity is due to the induced conformational change caused by the loss of the C1'-C2' double bond (see Figure 2.1.1.2).<sup>6</sup>

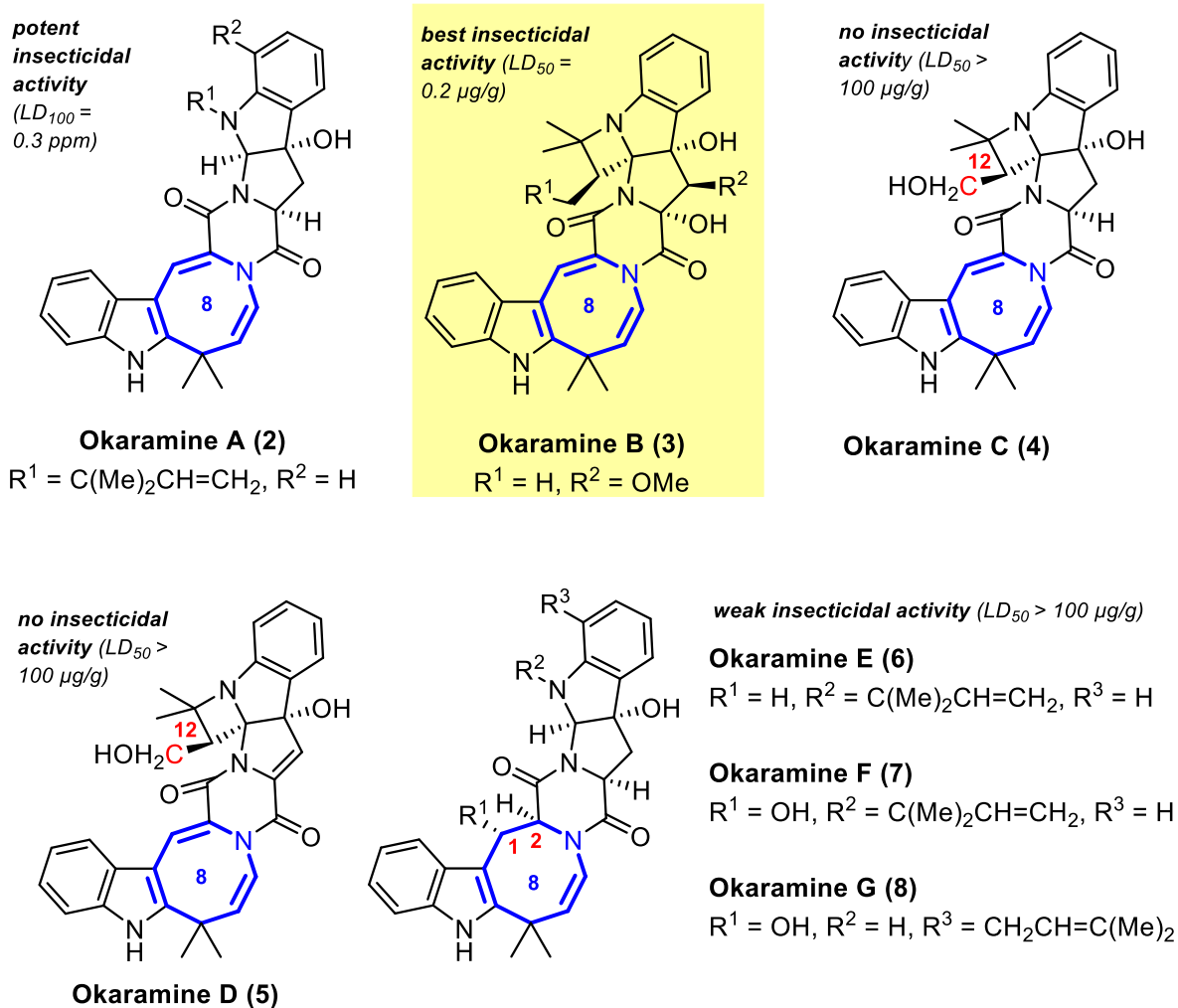


**Figure 2.1.1.2.** Structures of okaramines A-G.<sup>6</sup> The insecticidal activity of A is not directly comparable, as only the  $LD_{100}$  value in a different unit has been determined for it.<sup>6</sup>

Terpenes or isoprenoids form a highly diverse group of structurally different natural products with very widely different functionalities: from structural, as squalene **13** being a precursor for sterols (e.g. cholesterol), to functional, as in carotenoids in photosynthesis. Terpenes are found across nearly all life forms, and they are the most abundant and largest class of small-molecule natural products on Earth. Terpenes are composed of isoprene (**9**) units ( $\text{C}_5\text{H}_8$ )<sub>n</sub> so in other words, they follow the isoprene rule. Terpenes are classified according to the number of carbons into hemi- (C5), mono- (C10), sesqui- (C15), di- (C20), tri- (C30) and tetraterpenes (C40). (Figure 2.1.1.3).<sup>27</sup>

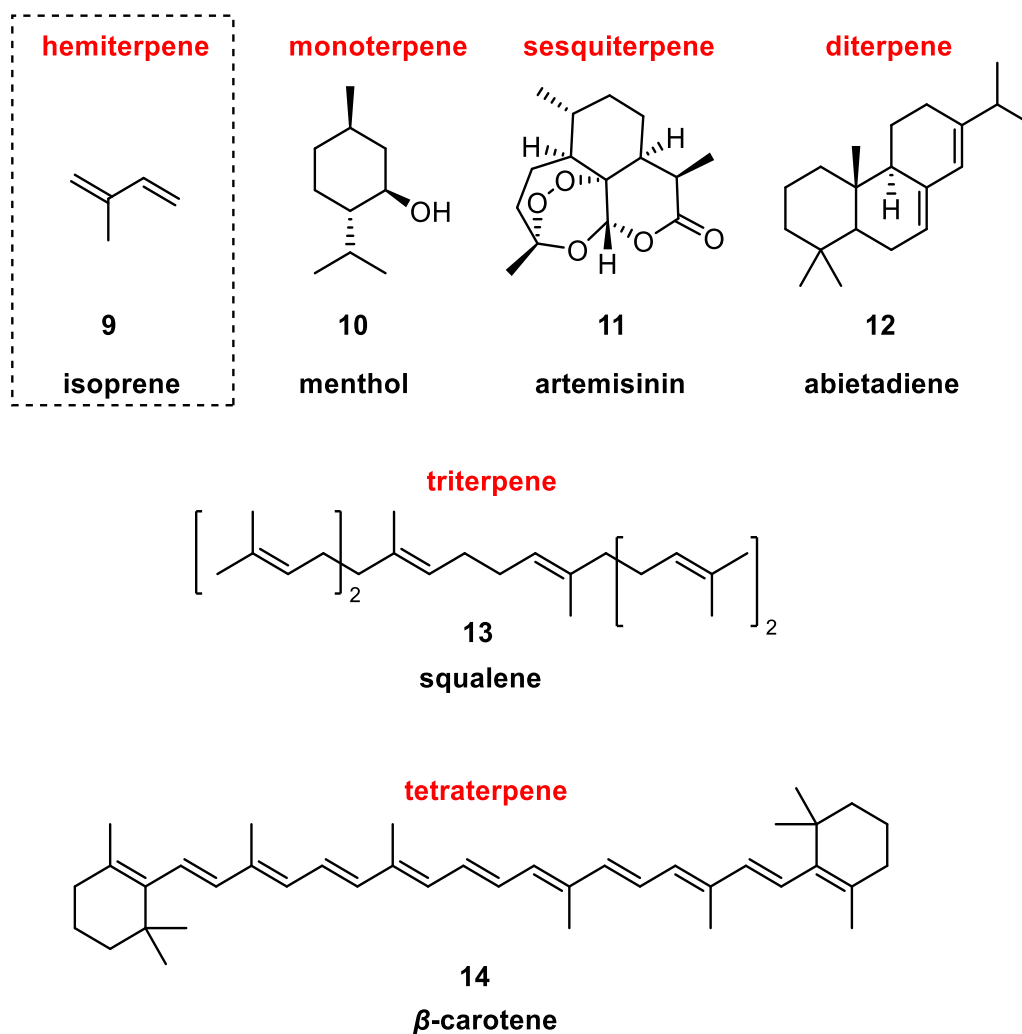
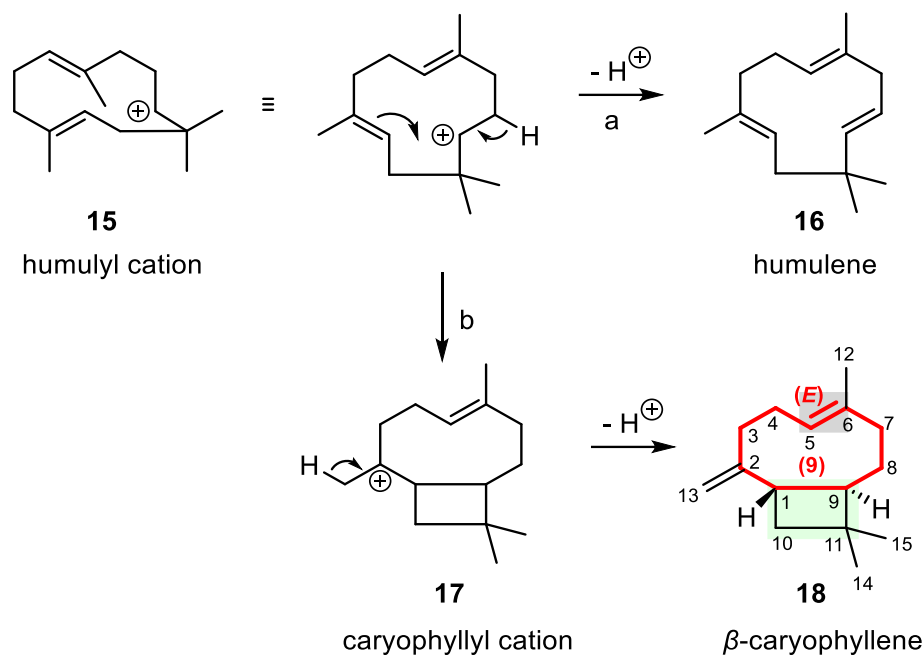


**Figure 2.1.1.3.** Isoprene unit **9** and examples of different-sized terpenes **10-14**.<sup>27</sup>

$\beta$ -caryophyllene (see Scheme 2.1.1.1) is sesquiterpene containing 15 carbons and it is found in many plants, e.g. cinnamon (*Cinnamomum zeylanicum*; Lauraceae).<sup>22,28</sup>  $\beta$ -caryophyllene has also been proposed to act as a biogenetic precursor for several other sesquiterpenes.  $\beta$ -caryophyllene is believed to be formed *via* rearrangement pathways, including transannular cyclizations. Rearrangement pathways, such as transannular cyclization, are believed to be the route for the formation of  $\beta$ -caryophyllene.<sup>29</sup>

From a biosynthetic point of view, the 11-membered carbon ring of the humulyl carbocation **15** can either remain intact and form humulene **16**, or rearrange to the caryophyllyl cation **17** containing a 9-membered ring fused to a 4-membered ring as seen in the structure of  $\beta$ -caryophyllene **18** (Scheme 2.1.1.1).<sup>22</sup> Key features of the caryophyllene structure include 4- and 9-membered rings and an (*E*)-trisubstituted alkenyl unit within the larger ring. Stereochemistry of the endocyclic C5-C6-(*E*)-alkenyl unit (highlighted in grey) is crucial and

can be controlled during synthesis. In addition, a *trans*-fused cyclobutane (highlighted in green) is a rigidifying element in the structure (see Scheme 2.1.1.1).<sup>28</sup>



**Scheme 2.1.1.1.** Rearrangement of humulyl cation **15** to  $\beta$ -caryophyllene **18** via caryophyllyl cation **17**.<sup>22</sup>

Although the ring structure of  $\beta$ -caryophyllene is rigid, Hübner *et al.*<sup>29</sup> have experimentally observed that it has three main conformations,  $\alpha\alpha$  (**19**),  $\beta\alpha$  (**20**) and  $\beta\beta$  (**21**), that rapidly interconvert in solution (Figure 2.1.1.4).<sup>29</sup>

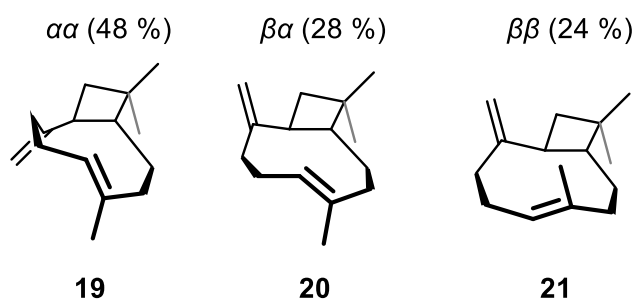


**Figure 2.1.1.4.** Three conformations of (-)- $\beta$ -caryophyllene in solution.<sup>29</sup>

An example of the synthesis of  $\beta$ -caryophyllene using a fragmentation reaction is presented in subchapter 3.1.1.



## 2.1.2 Medicinal chemistry: macrocycles and medium-sized rings

Macrocyclic natural products and their derivatives have played a significant role in pharmaceutical development. By the year 2023, natural products have provided 80-90% of the macrocyclic drugs and clinical candidates currently in use or development.<sup>4</sup> However, macrocyclic and especially medium-sized systems are under-explored in drug discovery and challenges in their synthesis contribute to their under-representation in drug libraries and drug development programs.<sup>8,10</sup>

Medium-sized rings are usually relatively rigid with specific 3D shapes. The conformational rigidity may result in improved oral bioavailability, binding ability to biological receptors, and cell permeability compared to analogous acyclic molecules or rings of other sized-ring systems.<sup>20</sup> The narrow conformational space reduces the entropy loss of binding between the ring structure and the target protein, increasing the high-affinity interaction between the macrocycle and the target protein.<sup>30</sup> Figure 2.1.2.1 shows medium-sized ring-containing structures (**22-25**) that are present in both bioactive products and therapeutically important molecules.<sup>10,31</sup>

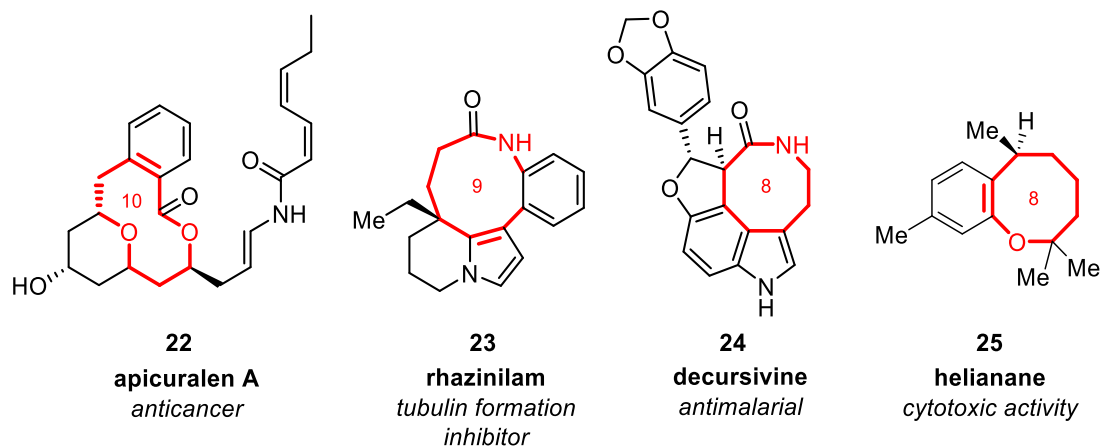


**Figure 2.1.2.1.** Bioactive medium-sized (8-10)-membered rings with therapeutic importance. The medium-sized ring is highlighted in red.<sup>10,31</sup>

The improved recognition of novel drug targets related to diseases is recognized as a critical factor for achieving success in drug discovery. Nevertheless, approximately 50 % of all targets linked to human diseases are considered "difficult to drug" using traditional small molecules, which are constrained by the chemical parameters defined by Lipinski's rule of five (Ro5).<sup>5</sup>

The Ro5 refers to the classical rules of thumb in drug discovery which states that ideal orally active compounds should not violate Lipinski's Ro5 criteria shown in Figure 2.1.2.2.<sup>32,33</sup> These physicochemical parameters are necessary for the compound to possess sufficient intestinal permeability and aqueous solubility, which are important initial steps for oral bioavailability. Whereas violation of the Ro5 is typically an indication that the compound probably has poor oral bioavailability, many compounds that pass Ro5 do not possess drug-like properties. In addition, any chemically specific structural features that clearly distinguish drugs from non-drugs are not involved in the Ro5.<sup>32</sup>

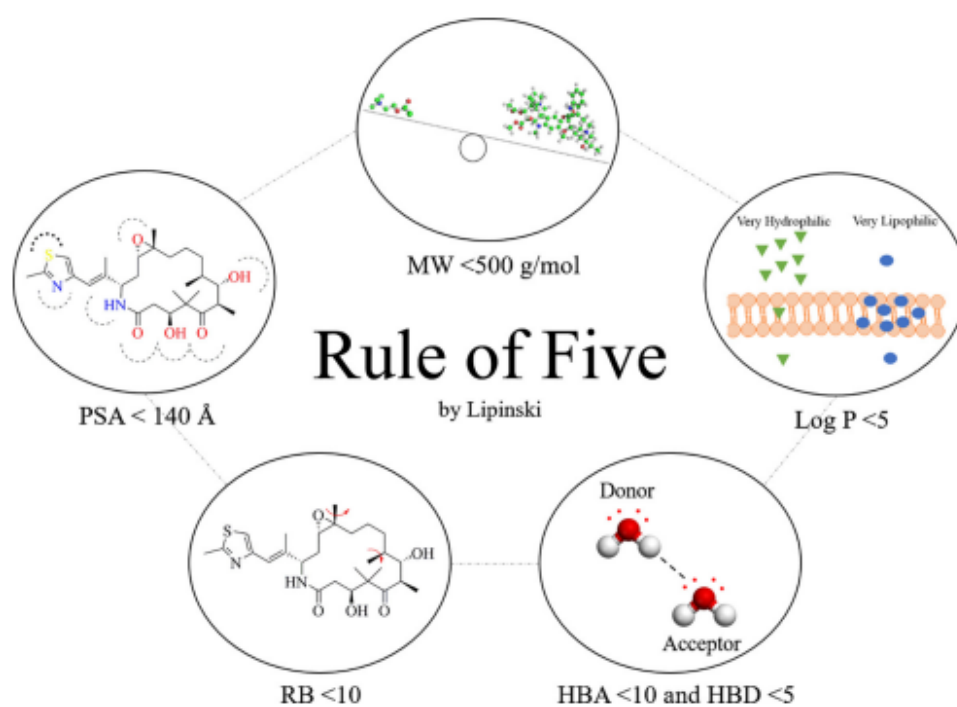


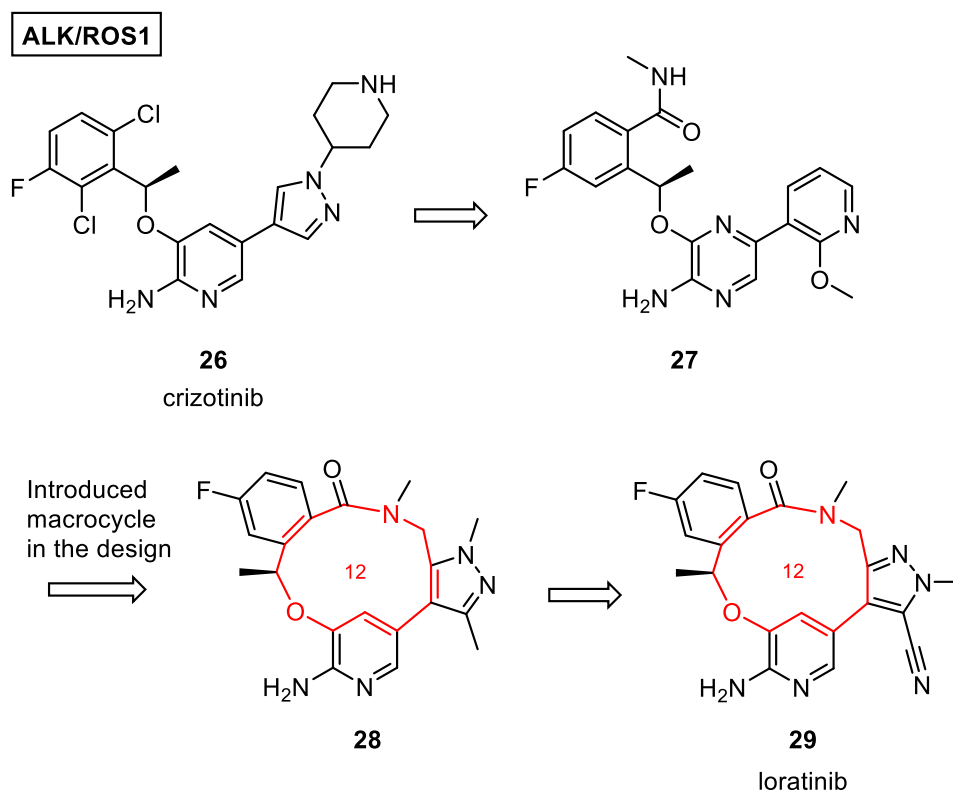
**Figure 2.1.2.2.** Scheme illustrating Lipinski's rule of five criteria: Molecular weight (MW), log P, hydrogen bond acceptor (HBA), hydrogen bond donor (HBD), rotatable bond (RB), and polar surface area (PSA).<sup>33</sup> Reprinted from *International Journal of Pharmaceutics*, 549, Chagas, C. M.; Moss, S. and Alisaraie, L., Drug metabolites and their effects on the development of adverse reactions: Revisiting Lipinski's Rule of Five, 133–149, **2018**, with permission from Elsevier.

Recent research has shown that macrocycles and other compounds beyond the Ro5 chemical space can offer enhanced opportunities for drug targets that are difficult to modulate. Beyond-rule-of-5 (bRo5) space compounds can more effectively target flat, large, and groove-shaped binding sites (e.g. in protein-protein interactions). Therefore, understanding the principles of designing and optimizing orally delivered compounds in the bRo5 chemical space is important to progress drug discovery.<sup>5</sup>

Recent research into crystal structures of drugs in the bRo5 space has also shown significant variations of their conformations resulting in notable differences in the PSA. Dynamic intramolecular hydrogen bond (IMHB) formation is an efficient way to produce "chameleonic" properties that allow a molecule to regulate its conformation, thereby better adapting to its environment. The "chameleonic" molecule can vary its polarity depending on the environment: in aqueous environment, the molecule is in a more polar conformation, while to penetrate the lipophilic cell membrane, the macrocycle hides polar groups. Restricting conformations by controlling polarity is more successful with macrocycles than with medium-sized rings, as it is easier for macrocycles to form intramolecular hydrogen bonds due to their larger size. These findings suggest that the flexibility of a compound in terms of conformation might be very important for the properties of compounds in the chemical space.<sup>5,34</sup> In conclusion, conformational flexibility helps in the design of drugs beyond the Ro5 chemical space.

Macrocycles bridge the gap between small molecules and biomacromolecules. Macrocyclic drugs have been approved since the 1940s for various diseases and they are suitable for previously mentioned "difficult-to-drug" targets, lacking defined binding pockets. In pharmaceuticals, challenges of macrocycles include synthesis complexities and oral administration issues due to stability and permeability. In addition, the synthesis and large-scale production of macrocycles is often challenging due to their structural complexity.<sup>34</sup> Macrocycles represent a valuable structural space for drug discovery providing pre-organized scaffolds for optimal binding to disease targets. Binding energy is enhanced due to entropy loss minimization caused by conformational preorganization. Reliable synthetic routes and library approaches enhance the accessibility of macrocycles and the potential for new drug discovery.<sup>34,35</sup>

Macrocycles have special structural characteristics - they differ from acyclic compounds in molecular weight, hydrogen bonding, and physicochemical properties like solubility and permeability. Many macrocycles can be orally bioavailable even though they violate Ro5. They can form additional interactions with critical residues in targets.<sup>34</sup> As an example, Zhang *et al.*<sup>34</sup> have derived the macrocyclic loratinib **29** from an earlier pharmaceutical, the acyclic crizotinib **26**. Macrocyclization in the design resulted in higher selectivity for anaplastic lymphoma kinase (ALK) proteins (see Scheme 2.1.2.1). It also exhibited strong activity against crizotinib-resistant c-ros onco gene 1 (ROS1) mutants (ROS1<sup>G2032R</sup> and ROS1<sup>G2026M</sup>).<sup>36,37</sup>



**Scheme 2.1.2.1.** Redesign of drugs: from acyclic **26** (crizotinib) to the macrocyclic ALK/ROS1 kinase inhibitor **29** (loratinib).<sup>34</sup>

In drug development, nefopam **31** is an example of a case where the design progressed from an open-chain structure to a medium-sized ring. Nefopam, also known as fenazoxine, is a cyclized analog of orphenadrine **30** (Figure 2.1.2.3).<sup>38,39</sup> The importance of nefopam in medicine is discussed in more detail in subchapter 4.2.1.

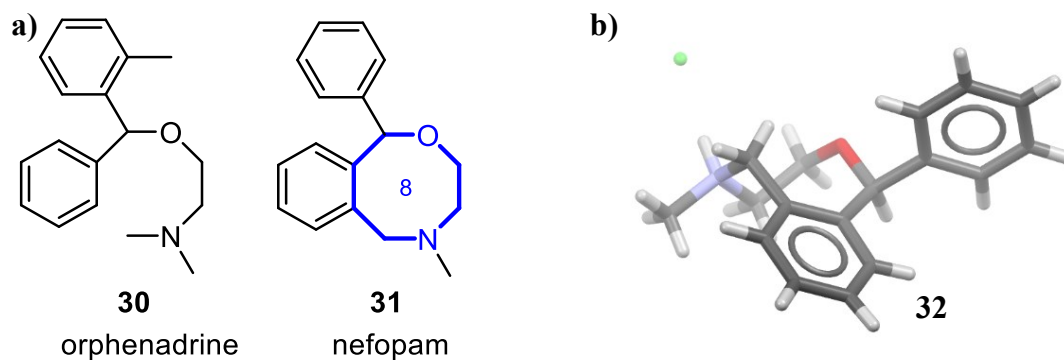
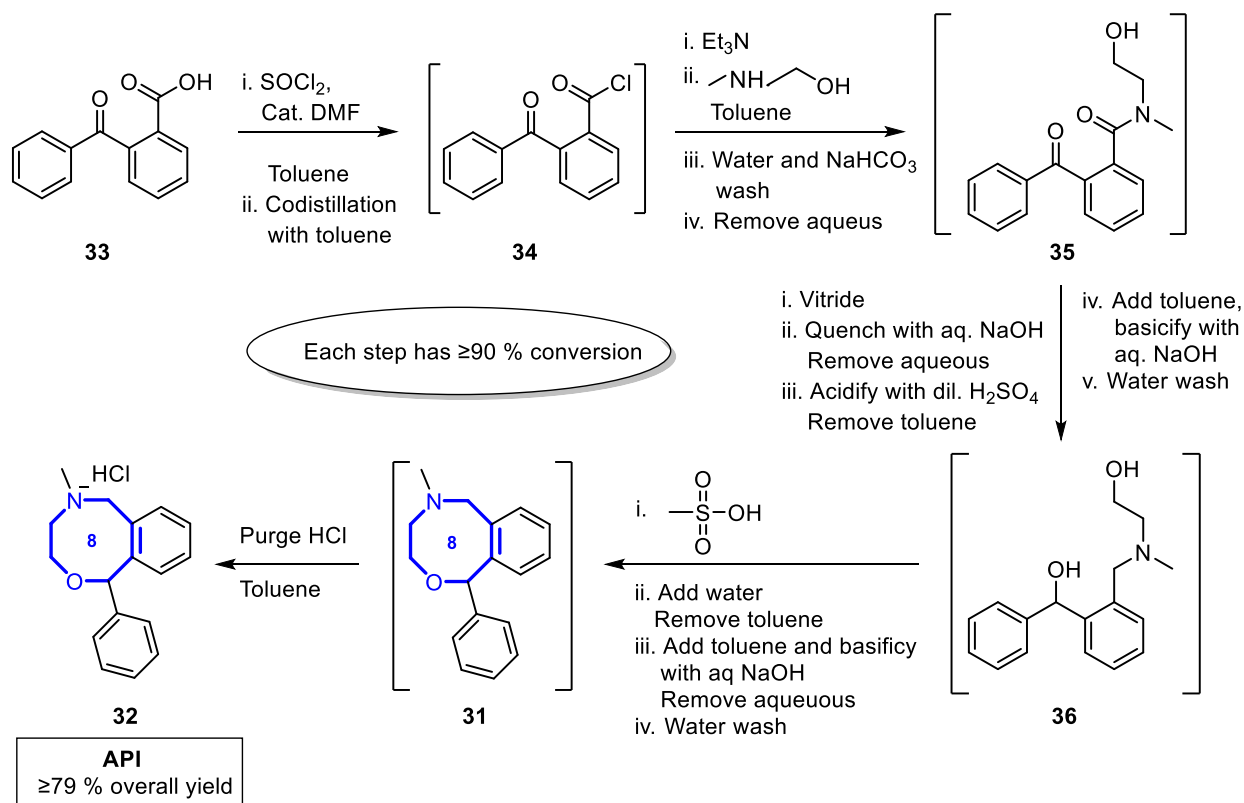


**Figure 2.1.2.3.** **a)** Structures of orphenadrine and nefopam.<sup>39</sup> **b)** The crystal structure of nefopam hydrochloride **32**, CCDC DEHSEO11.<sup>40</sup>

Interestingly, the synthesis of nefopam also proceeds from the acyclic precursor to the cyclic molecule. Bodireddy *et al.*<sup>41</sup> have reported a one-pot synthesis for nefopam hydrochloride **32** that is commercially viable and made on a multi-kilogram scale. The efficient one-pot reaction in toluene starts with the transformation of benzoylbenzoic acid (**33**) into acid chloride (**34**), which undergoes consecutive amidation (**35**), reduction (**36**), cyclization (**31**), and formation of hydrochloride salt yielding the active pharmaceutical ingredient (API) **32** ( $\geq 79\%$  overall yield and  $\geq 99.9\%$  purity), as outlined in Scheme 2.1.2.2.<sup>41</sup>



**Scheme 2.1.2.2.** Synthesis of nefopam hydrochloride (**32**) from benzoylbenzoic acid (**33**).<sup>41</sup>

This one-pot multistep synthetic strategy reported by Bodireddy and coworkers partially aligns with green chemistry principles. Another advantage of the synthetic route (Scheme 2.1.2.2) is the use of only one solvent, toluene, instead of alcoholic solvents. This allows the method to effectively avoid the formation of genotoxic impurities, which is a major concern in the pharmaceutical industry. In addition, this reduces the risk of contamination caused by multiple solvents and simplifies the procedure. The overall efficiency of the synthesis is also improved by  $\geq 90\%$  conversion at each step (Scheme 2.1.2.2).<sup>41</sup> While nefopam is relatively easy to synthesize, this is not always the case for medium-sized rings. The challenges of synthesis and possible solutions to them are discussed in more detail in the following chapters.

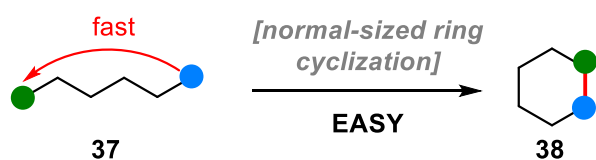
## 2.2 Challenges in synthesis

The difficulty in synthesizing medium-sized rings is perhaps the most distinguishing and best-known feature of them.<sup>1</sup> Synthesizing medium-sized rings is often challenging especially at larger scales because high-dilution cyclization methods, typically required for the synthesis, are sensitive and impractical.<sup>8,9</sup> In addition, medium-sized macrocycles are thermodynamically unstable, and for example, traditional cyclization methods face enthalpic and entropic challenges.<sup>8</sup> Forcing the acyclic starting material into a highly strained ring shape is enthalpically unfavorable. From the perspective of entropy, the competition between intermolecular polymerization reactions and intramolecular cyclization increases as the length of the molecule increases.<sup>9,42</sup>

The difficulties in synthesis typically arise from the challenge of achieving selective intramolecular coupling *via* end-to-end cyclization in forming larger rings. While cyclization reactions to form normal-sized rings such as **37** → **38** (Scheme 2.2.1a) are generally kinetically favorable and straightforward, similar cyclization reactions to produce large-sized rings **39** → **40** are usually more challenging. These attempts often encounter competing intermolecular reactions **39** → **41**, as described in Scheme 2.2.1b.<sup>9</sup>

### Cyclization vs. macrocyclization

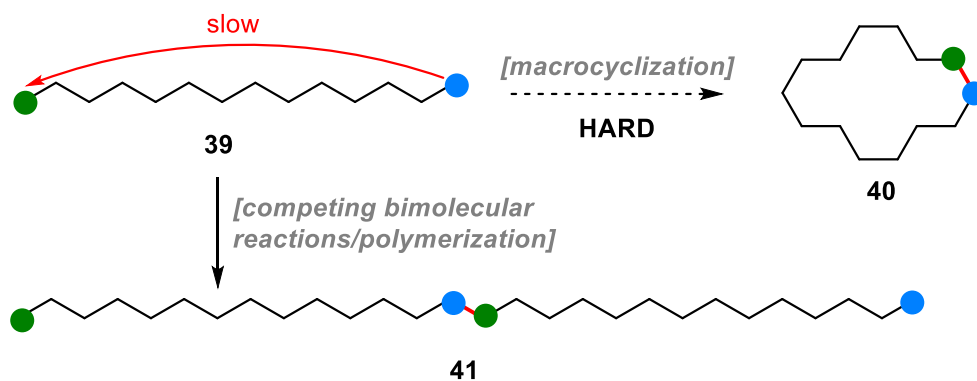
#### a) Cyclization



#### Challenges of macrocyclization

- High dilution usually needed
- Inconsistent reaction outcomes with low yields in common
- Competing intermolecular coupling/side reactions

#### b) Macrocyclization



Scheme 2.2.1. The principles of cyclization and macrocyclization.<sup>9</sup>

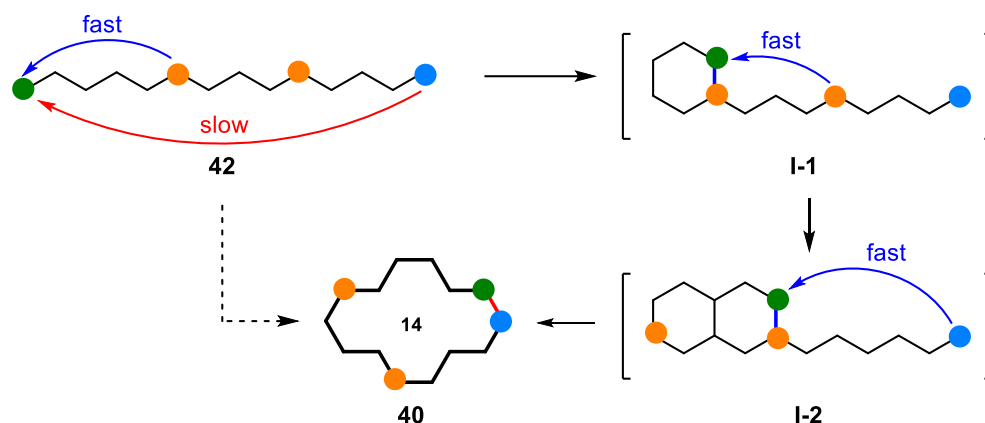
The above-mentioned competing reactions make selective intramolecular coupling difficult for larger rings.<sup>9</sup> Cyclization is a first-order reaction, unlike polymerization which is a second-order reaction if the reaction is bimolecular. Based on this result, low concentration favors the cyclization reaction, making intermolecular collisions less likely compared to intramolecular collisions.<sup>42</sup> As a result, high-dilution methods are usually needed to limit intermolecular reactions, but they rarely prevent them entirely. Moreover, the scalability and practicability of the synthesis might suffer, and high dilution tends to increase reaction times. The reaction setups are also quite complex, often requiring one or more syringe pumps.<sup>43</sup>

In the case of small and normal-sized ring structures, competitive intramolecular reactions do not occur so easily, because the entropy change caused by bond rotation is smaller than the conformational entropy change in cyclization. This is not the case for medium-sized and especially large macrocycles, as the conformers of the larger ring structure are less constrained.<sup>44</sup>

The development of new experimental methods favoring macrocyclization is an important goal in the near future. Method development would enable the scaling of reactions on an industrial scale when working above the millimolar concentration range. This would also potentially bring savings in financial costs, as the amount of solvent could be reduced. The combination of acyclic and macrocyclic stereocontrol can affect the reaction results. For this reason, the utilization and development of computational methods are also important: they enable a better understanding of the conformational properties of molecules and, utilize these results to predict the course and outcome of the macrocyclization reaction.<sup>45</sup>

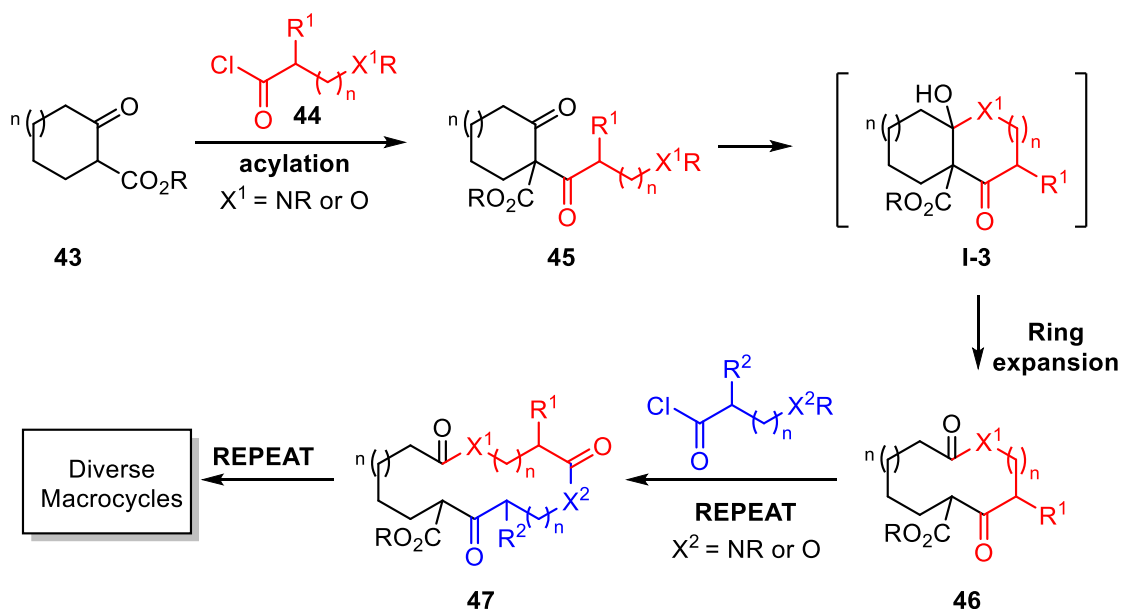
Cyclization/ring expansion cascade reactions are a general and modular approach to the synthesis of medium-sized rings and macrocycles without resorting to high dilution conditions. A key concept that distinguishes the models of the new methods is to force the cascade to occur only through the transition states of low-energy, normal-sized cyclic compounds. This is achieved by appropriately placing reactive groups within the linear precursor **42** (colored orange) so that the subsequent cyclization/ring expansion cascade can occur stepwise, e.g. **42** → **I-1** → **I-2** → **40** (Scheme 2.2.2). As a result, the kinetically prohibitive direct end-to-end cyclization that would otherwise be required to generate large rings is avoided and replaced by a process that involves smaller and surmountable steps. This replacement makes the entity much more kinetically favorable.<sup>9</sup>

## Cyclization Ring Expansion (CRE) cascade



**Scheme 2.2.2.** Cyclization Ring Expansion (CRE) cascades can make macrocyclization easier by exclusively proceeding *via* normal-sized cyclizations (intermediates **I-1** and **I-2**).<sup>9</sup>

An example of the utilization of CRE is the successive ring expansion (suRE) approach reported by Baud *et al.*<sup>8</sup>, in which smaller ring structures are expanded into larger ones (see Scheme 2.2.3). This cascade enables the formation of lactams and lactones **46** *via* a telescopic acylation/ring expansion sequence when 3- or 4-atom fragments of amino acid **43** and hydroxy acid origin **44** are inserted to form cyclic  $\beta$ -ketoesters **45**.<sup>8</sup>



**Scheme 2.2.3.** Successive ring expansion (SuRE) approach.<sup>8</sup>

Although ring expansion is a reversible reaction in principle, neither intermediates **46** nor **47** were observed and the formation of medium-sized ring products worked. A significant feature



of this approach is that the replication of the cyclic  $\beta$ -ketoester motif in the starting material to the ring-enlarged product enables sequential ring expansion (SuRE) reactions to be performed (e.g. **46**  $\rightarrow$  **47**). The method is promising: preparation of rings of any size is potentially possible by repetition of the same acylation/ring expansion procedure with various amino or hydroxy acid units on the product.<sup>8</sup>

In general, medium-sized rings fall into a difficult place synthetically because the kinetic and thermodynamic barriers to their formation are generally higher than other ring sizes. They are large enough that cyclization of a linear precursor often leads to a significant entropy loss, yet small enough to experience destabilizing transannular interactions and strain.<sup>42</sup> These significant limitations have often led to lower yields of the desired products, as illustrated in Figure 2.2.1.<sup>46</sup>

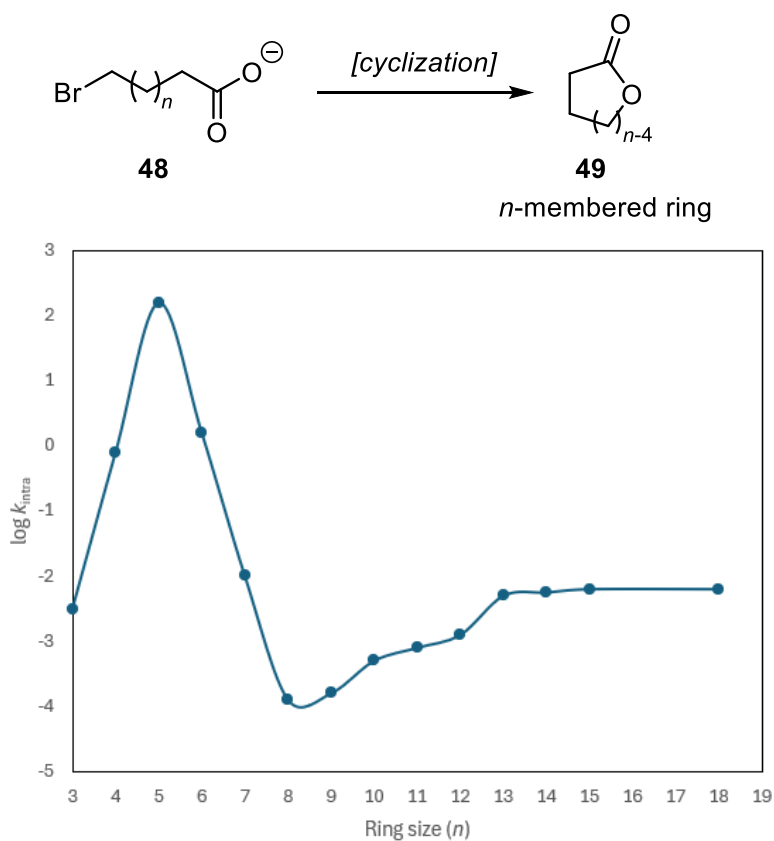


**Figure 2.2.1.** Reactivity profile of lactone (**49**) formation.<sup>42</sup> The Figure is adapted from Figure 1 of reference 42.

As can be seen from the graph (Figure 2.2.1), the rate of lactone formation significantly increases when the ring size increases from 3-membered to 5-membered. The faster rate of formation is explained, for example, by the lower Baeyer strain of the 5-membered ring, since its bond angles are closer to the ideal tetrahedral angle ( $109.5^\circ$ ). However, beyond 6-membered

rings, the rate constants drop dramatically, decreasing by a factor of a million at an 8-membered ring. The rings that are bigger than the 9-membered form more rapidly because the strain energy decreases with increasing chain length and the formation of large rings is otherwise less sensitive to chain length. The effective molarities (EM) show a common tendency for cyclization in different reactions and become similar as the ring size increases beyond medium-sized rings.<sup>42</sup>

The Illuminati-Mandolini case cited above is just one of many examples and the rate of ring formation is affected by several factors, such as the number and type of substituents. Nevertheless, the synthesis of medium-sized rings is generally more challenging than other ring sizes, and the rate of ring formation can be said to follow the trend shown in Figure 2.2.1. More examples of the challenges of synthesis and possible solutions, as well as synthetically challenging molecules, are discussed in later chapters.

## 2.3 Rigidifying elements, stereochemistry, and atropisomerism

Conformational analysis methods are needed to understand the possible isomers and their relative energies. As mentioned earlier, rigidifying elements of the ring structure decrease the number of possible conformers. The rigidifying elements can be for example endocyclic double bonds and aromatic fusions, heteroatoms, various alkyl substituents, and ester- and amide-groups (see Figure 2.3.1).

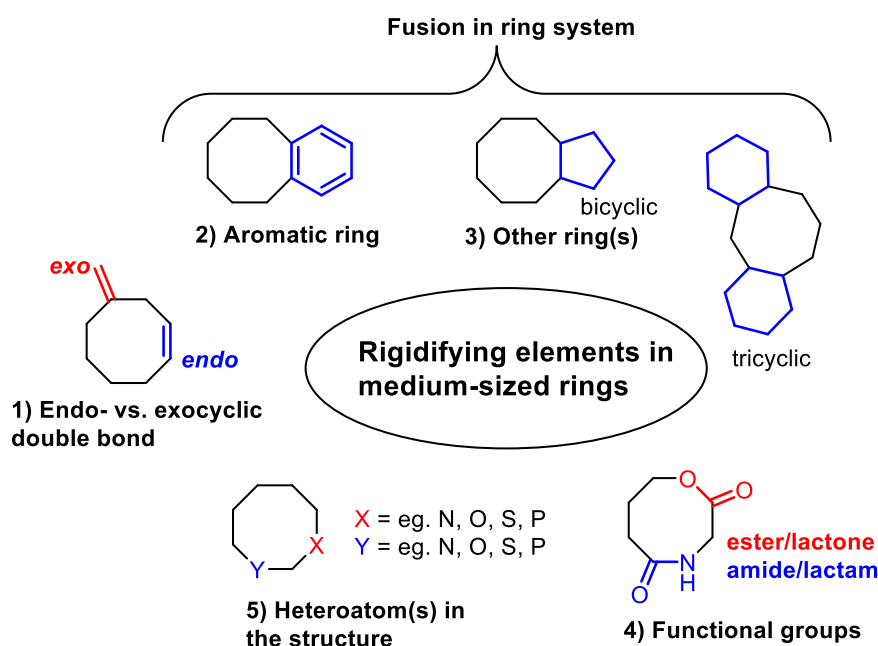


**Figure 2.3.1.** Rigidifying elements in medium-sized rings.

The presence of endocyclic double bonds **1)** restricts both puckering and pseudo-rotation in medium-sized rings, reducing the degrees of freedom of the ring thus limiting the number of possible conformations. They also restrict the free rotation of the ring, which affects the distribution of phase angles. Double bonds cause strong coupling between different phase angles, which limits the mobility of the ring.<sup>47</sup> This rigidity can help stabilize the ring structure. If there are substituents at allylic positions, those may offer additional rigidifying opportunities *via* 1,3-allylic strain.<sup>48,49</sup>

The medium-sized ring can also share bonds with an aromatic ring forming a benzo-fused system **2)**. Similarly to double bonds, aromatic bonds in the ring structure can limit conformational flexibility. Incorporating additional fused rings **3)** and functional groups **4)** can increase the rigidity of structures as well. Heteroatoms **5)** can affect electronic properties, and flexibility can be influenced *via* strategic placement of substituents.

Humilisin E (**50**), presented in more detail in the experimental part, is a highly strained system due to its 9/4/5 ring structure. It is an example of a structure containing a medium-sized ring with many rigidifying elements. Along with the ring fusion, the epoxide at C7-C8, methyl substituents at C4 and C8, and the endocyclic C3-C4-(*Z*)-olefin of the 9-membered ring rigidify the structure and create a lot of challenges in terms of synthesis (Figure 2.3.2).<sup>24</sup>

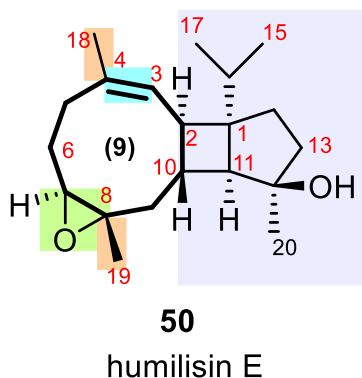


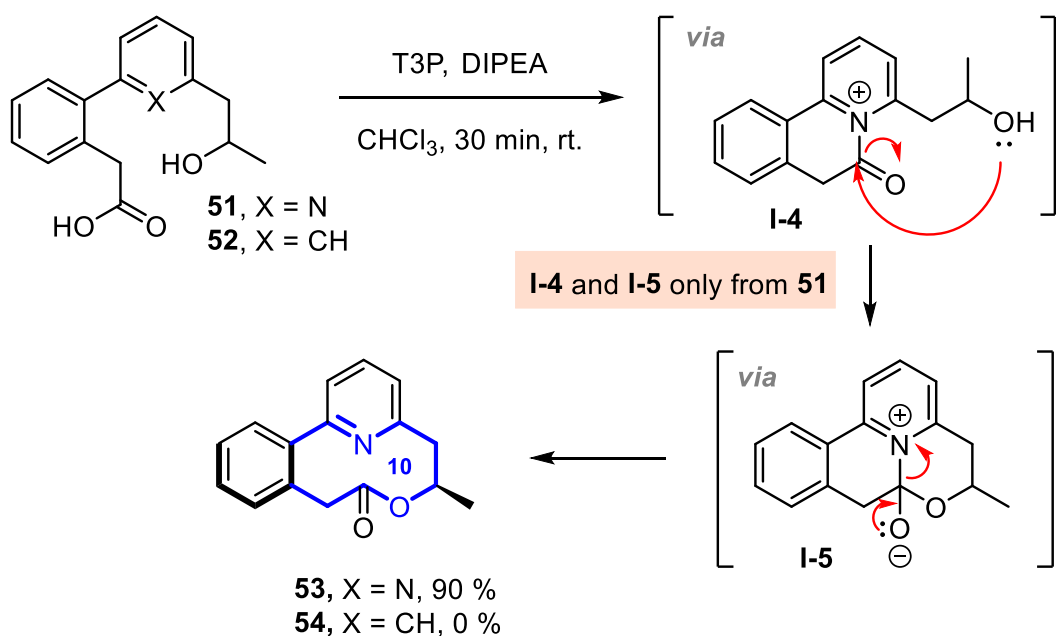
**Figure 2.3.2.** Structure of humilisin E (**50**).<sup>24</sup> The rigidifying elements of the 9-membered ring are highlighted.

Atropisomers are so-called frozen conformations, and the possibility of their appearance increases when there are more rigidifying elements in the ring structure and the ring is small enough to hinder bond rotation. Indeed, atropisomerism arises from highly restricted bond rotation, creating a chiral axis. Atropisomers can undergo time-dependent chirality inversion, and thus complicate drug development. Recognition and characterization of atropisomerism have improved in medicinal chemistry *via* the improvement of analytical and separation

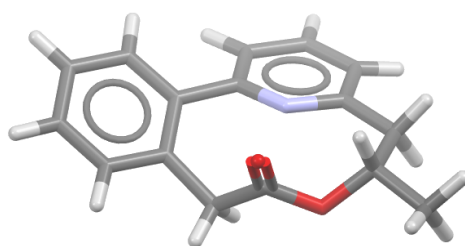
techniques. Atropisomeric drug molecules can exhibit different biological activities and pharmacokinetics. Macrocycles may also display atropisomerism due to conformational restrictions.<sup>50</sup> The ring size also matters: if the ring is too large, atropisomers interconvert too rapidly and cannot be separated.<sup>51</sup>

Zalesky *et al.*<sup>9</sup> aimed to establish a new series of CRE cascade reactions, which required ensuring the participation of the internal nucleophilic component in the cascade as planned. This was done by the control experiment (CRE strategy), shown in Scheme 2.3.1, in which the hydroxy acid **51** is converted to the 10-membered lactone **53**, probably *via* the acylpyridinium intermediate **I-4**. This reaction produces the single atropisomer **53** in 90% yield, while the analogous lactone **54** was not obtained at all. This suggests that the pyridine nitrogen is an important enabler of the cyclization of structure **51**.<sup>9</sup>

**a) CRE method: carboxylic acid activation using T3P**



**b)**



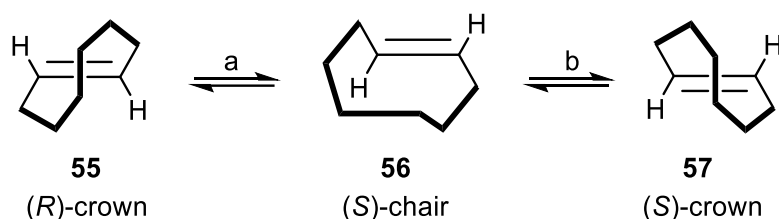
**53** (CCDC 1913413)

**Scheme 2.3.1.** a) Cyclization and ring expansion cascade synthesis of **53**.<sup>9,52</sup> b) The crystal structure of **53**.<sup>52</sup>

The principle of the CRE reaction is presented in more detail in subchapter 2.2. Lawer *et al.*<sup>52</sup> reported the realization of the above-mentioned CRE strategy in an earlier proof-of-concept study. During the procedure internal nucleophilic catalyst-mediated cyclization (**51** → **I-4**) and ring expansion cascade reactions (**I-5** → **53**) occurred when the pyridine-containing linear precursor **51** was activated with propanephosphonic acid anhydride (T3P) and *N,N*-Diisopropylethylamine (DIPEA) in chloroform. X-ray crystallographic data supported the structural and stereochemical assignment of 10-membered lactone **53**.<sup>52</sup>

Various strategies have been developed to remove the stereochemical barrier of atropisomerism, especially for molecules possessing intermediate atropisomeric stability. The first strategy is to increase the rotational barrier by making the molecules more rigid. The second strategy is to make one desired atropisomer favored in equilibrium by another stereochemical attribute. In addition, lowering the barrier to facilitate equilibration and removing the stereocenter by symmetrizing the molecule are other strategies.<sup>50</sup> Both rigidifying elements and atropisomerism constrain the structure of the molecule. Rigidity can lock conformations so that they cannot change into each other. To further illustrate the conformational space of medium-sized ring cycloalkenes, the *E-trans* cycloalkenes are discussed below.

The sufficiently short, saturated segment of *trans*-cycloalkene is forced out of the plane of the olefinic moiety, which normally constitutes the symmetry plane of the molecule. In larger *trans*-cycloalkenes, the double bond can more easily swivel through the polymethylene bridge with a resulting decrease in the racemization barrier ( $E_a$ ): *E*-cyclooctene 149 kJ·mol<sup>-1</sup>, *E*-cyclononene 83.7 kJ·mol<sup>-1</sup> and *E*-cyclodecene 10.7 kJ·mol<sup>-1</sup>.<sup>53</sup> Taking into account a molecular model of *E*-cyclooctene it is possible to conclude that the swiveling of a double bond through the polymethylene bridge does not result in the molecule converting into its enantiomer. However, the molecule inverts the configuration of the planar chiral moiety, interconverting the configuration between the chair and crown conformations of the molecule (Scheme 2.3.2). An additional conformational change is needed to turn the distorted chair conformation into a crown conformer that will be the enantiomer of the original structure.<sup>53</sup>



**Scheme 2.3.2.** Racemization of (*E*)-cyclooctene. The barrier for step **a** is 149 kJ·mol<sup>-1</sup> and for step **b** 43.3 kJ·mol<sup>-1</sup>.<sup>53</sup>

Replacing the hydrogen atoms with methyl groups in the *E*-cycloalkenes increases the racemization barrier significantly. This phenomenon is probably due to the more severe steric hindrance caused by the bulkier methyl substituents, which may greatly restrict the swiveling motion of the double bond.<sup>53</sup>

The growing demand for functionalized medium-sized rings creates the need for developing new methods of synthesis that are scalable, practical, and predictable.<sup>10</sup> The rigidifying elements affect how stereoselective the reactions are in the rings: from a stereoselective synthesis point of view: medium-sized rings and macrocycles present unique and sometimes unpredictable challenges. Although vicinal centers can be effectively controlled through internal or relative asymmetric induction, it is more challenging to establish the correct relationships between widely separated or remote asymmetric centers. Stereocontrol of remote substituents has usually been achieved using commercially available enantiopure starting material, enantiomers separated from intermediates, or the effect of asymmetric induction of enantiopure starting material.<sup>18</sup>

## 2.4 Conformational analysis

Conformational analysis is needed to determine the number of isomers and possible atropisomers but also to infer stereochemical control in synthesis, the biological effect of the drug, and binding to the target protein. It can provide a tool for solving synthetic challenges, as it helps to better understand the properties of molecules and the reasons explaining them. Molecules should not be viewed as immobile entities as suggested by molecular models.<sup>1</sup> The most general definition of conformation was coined by Barton in the middle of the 20<sup>th</sup> century: "The conformations of a molecule (of defined constitution and configuration) are those arrangements in space of the atoms of the molecule which are not superposable upon each other".<sup>54</sup> It was known by that time that rotation about a single bond might be hindered and thereby produce separable stereoisomers.<sup>55</sup> The balance of intramolecular forces determines the molecular conformation. Consequently, understanding the conformational properties of medium-sized rings is also important in better interpreting their intramolecular interactions and reactivity. Molecular conformations and their populations are influenced by different stabilizing and destabilizing interactions.<sup>2</sup>

In pharmaceutical chemistry, conformations are often compared between open-chain and ring-structured compounds - a fully open-chain system has significantly fewer conformations than ring structures. Cyclization of the ring reduces the available conformational space and adding rigidifying elements to the ring further restricts the conformational space.<sup>11,56</sup> The ring size affects the conformational populations: the number of conformations starts to drastically increase as the ring size increases. While 6-membered cycloalkanes have two well-defined conformers, chair and boat, large- and medium-sized rings have a much larger array of conformations.<sup>18</sup> The increased flexibility of these structures complicates the conformational analysis.<sup>2</sup> In conclusion, the ring size affects both the number of low-energy conformers and their relative populations. In practice, the number of conformations cannot be directly predicted, and the relative energies and structures of different conformations are typically obtained by computational methods.<sup>13</sup> Due to several low-energy conformations of medium-sized rings, the reactivity can be difficult to predict.<sup>12</sup>

The conformations of medium-sized macrocycles are formed as a sum of many factors, and several factors that influence the analysis. Such factors include, for example, non-covalent inter-ring interactions, such as hydrophobic interactions, as well as several steric interactions and ring strain effects.<sup>13</sup> Different types of strains vary according to the size of the ring. With smaller rings, the bond angles deviate more from the ideal bond angles, so such compounds are subject to bigger angular strain. In general, the ring structures tend to settle in the space where the substituents are as far apart as possible, and their shielding is minimized.<sup>1</sup>

The body of medium-sized rings is the multi-membered ring itself, and usually, several heteroatoms and substituents are also attached to it. In medium-sized rings, the transannular ring atoms are very close to each other, and there may not be sufficient space available to minimize the destabilizing interactions between the substituents in an ideal conformation.<sup>1</sup> These destabilizing interactions are often referred to as different types of strain, *i.e.* as deviations from idealized conformations, such as torsional strain (Pitzer), angular strain (Baeyer), and transannular interactions (see Figure 2.4.1). Ideal conformations minimize transannular interactions and high-energy torsional strain in simple macrocyclic structures.<sup>13,42</sup>

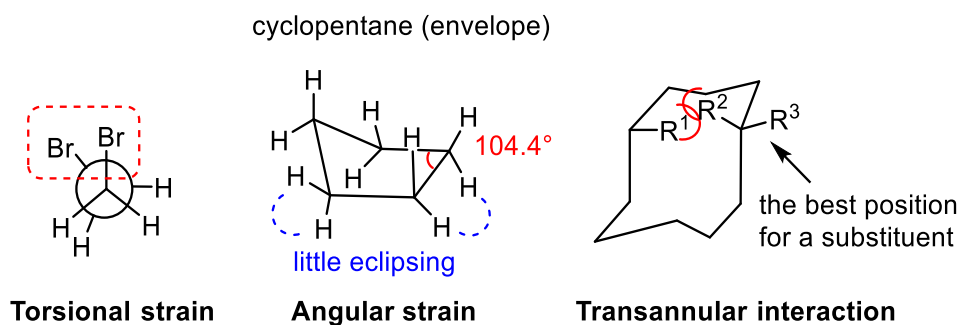


**Figure 2.4.1.** Description of Pitzer strain (torsional), Baeyer strain (angular) and transannular interaction.

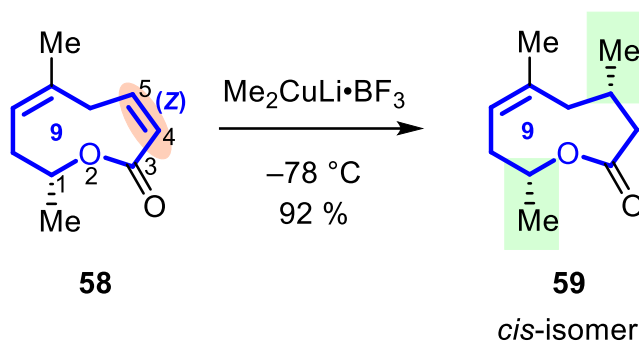
Pitzer strain (torsional strain) is caused by the imperfect staggering of bonds, causing atoms to approach each other too closely. Baeyer strain, in turn, is due to the deformation of bond angles within the ring from their ideal values.<sup>42</sup> If a methylene group is replaced with a carbonyl group or a heteroatom, it affects the conformation and the balance of intramolecular interactions in the entire ring.<sup>2</sup> It has been recognized that the replacement of two hydrogens by methyl groups at a methylene carbon accelerates the formation of small- and common-sized rings and this phenomenon is referred to as the gem-dimethyl effect (also known as Thorpe-Ingold or reactive rotamer effect).<sup>42,57</sup>

The difference in stereochemistry between two different stereoisomers affects the physical properties as well. Local steric interactions surrounding the stereocenter propagate through the ring and affect the overall flexibility of the framework and the rearrangement ability of the macrocycle in different solvents. Changing stereochemistry affects both ground state conformational preferences and the kinetic barriers controlling the conformational behavior when the solvent is changed. Relatively modest modifications in macrocycles or medium-sized rings may lead to local conformational changes around the ring and affect distal structural features. This can result in higher barriers to specific bond rotations, such as biaryl atropisomerism when the bond is part of a macrocyclic backbone. It is not well understood what kind of factors determine how such changes propagate: for example, how far bond rotations are coupled. Thus, it is difficult to predict what kind of modifications could cause major changes in conformation in remote regions of the macrocycle.<sup>13</sup>

The perception of medium-sized rings as uncontrolled, conformationally flexible, and cyclic stereocontrol-inhibiting systems changed when diastereoselectivity was observed in simple cyclic systems. When these lessons are applied, synthetically useful building blocks can be obtained. One example of this is the synthesis of the C30-C43 fragment of the marine palytoxin



by Still and Galynker<sup>58</sup> starting from lactone **58**. The reaction involves a conjugate addition of lithium dimethylcuprate to 9-membered (*Z*)-enone **58**, which gives compound **59** as a single diastereomer in 92 % yield (see Scheme 2.4.1). This is an example of the propagation effect in a reaction of a medium-sized macrocycle, where stereoselectivity can be conveyed even from a distant stereocenter: in this case, long-range stereocontrol is achieved over a distance of five atoms (Scheme 2.4.1).<sup>58,59</sup>



**Scheme 2.4.1.** Synthesis of *cis*-isomer **59**.<sup>58,59</sup>

In conclusion, the behavior and chemical reactivity of the molecules are largely guided by conformation so understanding it is very central to research.<sup>13</sup> It has long been appreciated that elucidation of the structural factors controlling the relative energies of the macrocycle conformations and kinetic barriers between them is one necessary component to the optimization of macrocycle biological activity by chemical modification.<sup>60</sup>

## 2.4.1 Methods of conformational analysis

The energy and conformation of a molecule can be determined in several different ways, which can be roughly divided into computational and experimental methods.<sup>13</sup> However, each method is incomplete in some way and may not give a true description of energy in all situations. Therefore, to obtain more reliable and accurate results, several different methods are needed in the studies. For example, while molecular mechanics methods may not be physically accurate, they can quickly provide insights into how different elements of strain contribute to the stability of the conformers.<sup>15</sup>

Spectroscopic analysis is the first step in understanding the conformational preference of the macrocycle. Experimental methods are used to resolve averages of populations. X-ray

crystallography can only present the conformation in detail in a solid phase, and the packing of crystals may greatly affect the conformation. Thus, caution is needed while making predictions about behavior in solution using these results. Unsubstituted cycloalkanes and cycloalkenes are generally unsuitable for X-ray studies, since they are either liquids at room temperature or form crystals which are poorly ordered.<sup>14</sup>

Nuclear magnetic resonance spectroscopy (NMR) is one of the common techniques employed in the study of macrocycle conformations in solutions, while modern two-dimensional techniques of NMR enable rapid resonance assignment.<sup>13</sup> Both of these above-mentioned methods offer very valuable structural information but are limited in the characterization of multi-conformational systems. A good alternative is microwave spectroscopy due to its high resolution, allowing one to unambiguously distinguish among different conformations that may be simultaneously present in the sample.<sup>2</sup>

A three-dimensional model of the molecule in a specific solvent is needed to analyze the conformation of a macrocycle. The generation of these macrocycles is done by computational methods by applying sampling algorithms exploring different conformations of the molecule and energy models assessing the stability of each particular conformation. The most successful searches return to a large and diverse set of conformers in a short period. Furthermore, they accurately identify either the lowest energy or at least a match with experimentally determined conformations. Dynamic studies must be able to have the algorithm overcome energy barriers between conformations. Often, the algorithms that result in the highest diversity of conformers have the lowest artificial barriers between conformations.<sup>13</sup>

The most common methods of performing macrocycle conformational searches utilize molecular mechanics (MM) methods, based on classical equations and parameters. The force fields used in MM are derived from experiments or quantum mechanical (QM) calculations that are combined with Monte Carlo searches using energy calculations to develop new molecule conformations. Alternatively, conformations around a starting geometry can be explored by using molecular dynamics (MD) simulations, although they are much slower and require greater computer time, especially to cross energy barriers between different conformations.<sup>13,61</sup> Quantum chemical calculations, especially those performed within the density functional theory (DFT) framework, have long served as an effective means to predict properties that experimentalists can subsequently verify. They have also provided insights at the molecular level for explaining observations from high-pressure experiments.<sup>62</sup>

Conformational analysis has been discussed in more detail in many review articles and other master's theses as well.<sup>63,64</sup> For this reason, this thesis does not delve into the topic in more detail.

## 2.4.2 Example of modern conformational analysis by DFT: nefopam

In the literature, there are relatively few examples of conformational analyses of pharmaceuticals using computational methods. This subchapter presents how modeling can be done today in a few hours on a computer. A quick demonstration of the conformational search was done by my supervisor and only the results are summarized here. A crystal structure has been previously reported for nefopam **31**.<sup>40</sup> If a crystal structure exists for a compound, it is a good starting point for conformational analysis.

To carry out the conformational analysis, first, the conformational space of nefopam was explored by MM methods using the OPLS4 force field (water as solvent). The conformational analysis was carried out using the MacroModel module (10,000 steps, Mixed torsional/low mode sampling) embedded within the Schrödinger Maestro suite of software.<sup>65</sup> The eight lowest-energy conformers obtained in the Monte Carlo conformational search were subject to DFT calculations. The geometry optimizations of the lowest energy conformers were carried out at the M06-2x/6-311G\*\* level of theory in the gas phase.<sup>66</sup> The geometry optimizations were carried out using the Jaguar software embedded within the Schrödinger Maestro.<sup>67</sup> The entire procedure took approx. 8 h. The structures of the three lowest energy conformations of nefopam obtained by the DFT method are shown in Figure 2.4.2.1.

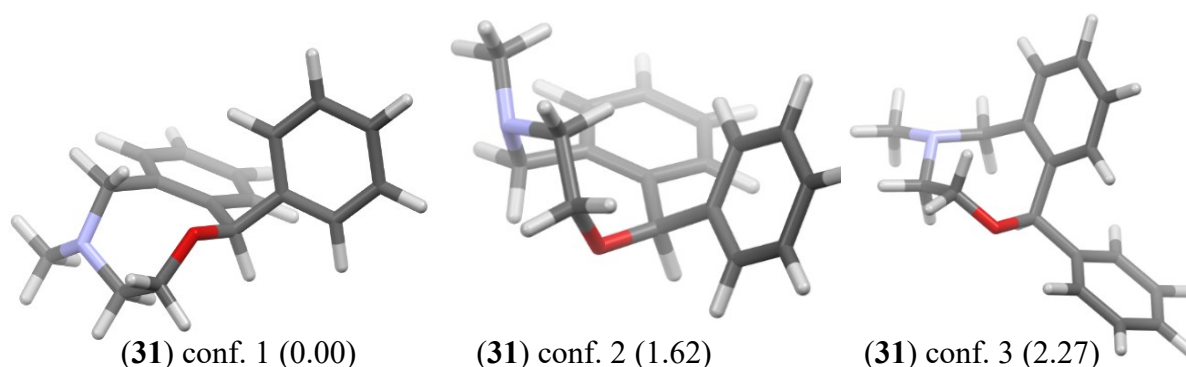


**Figure 2.4.2.1.** Three lowest energy conformations of nefopam by DFT-calculations. The computed relative stabilities shown in parentheses (in kJ/mol) refer to solution-phase electronic energies concerning the most stable form of nefopam (conf 1).

The choice of the DFT method and the basis set will obviously affect the energies of the conformers, but the methods used here are examples of typically used methods (for a related example, see ref.<sup>68</sup>). The redundant conformers were eliminated using maximum atom deviation (cutoff: 2 Å). As a result, the electronic energies in the gas phase were obtained. Based on the results, nefopam has several conformations whose energies are quite close to each other. The energy of the eight conformers is compared in Table 2.4.2.1. Computational methods are not discussed in detail, as they are beyond the scope of this thesis.

**Table 2.4.2.1.** Computed energies of different nefopam conformers

<b>Conformer</b>	<b>Gas phase energy (<math>E_h</math>)</b>	<b>Gas phase energy (kJ/mol)</b>	<b>Difference (kJ/mol) compared to conformer 1</b>
1 (lowest energy)	-789.068079	-2071698.24	0
2	-789.067462	-2071696.62	1.6
3	-789.067214	-2071695.97	2.3
4	-789.066776	-2071694.82	3.4
5	-789.066619	-2071694.41	3.8
6	-789.065383	-2071691.16	7.1
7	-789.065175	-2071690.62	7.6
8	-789.064957	-2071690.05	8.2

Computational conformational analysis could be carried out more carefully using different solvation models, other DFT methods, etc. In medicinal chemistry, computational methods can be used to predict changes that lead to better potency or higher binding affinity. For example, the identification of bioactive conformations can be easier and faster with the help of conformational analysis of ligands. Alternatively, the goal may be to reduce the affinity of the unwanted target while maintaining its affinity for the target of interest. Understanding conformations is important because flexibility (such as the number of rotatable bonds) may have a negative impact on binding and selectivity.<sup>5</sup>

### 2.4.3 Cyclooctane

Cyclooctane is the smallest medium-sized-carbocycle and it exhibits various strain types, including the previously mentioned transannular interactions and torsional strain (see Figure 2.4.3.1). As mentioned in subchapter 2.4, the ring strain significantly influences conformational stability and reactivity. Understanding the effect of strains is crucial for predicting the behavior of cyclooctane in chemical reactions and applications.<sup>1</sup>

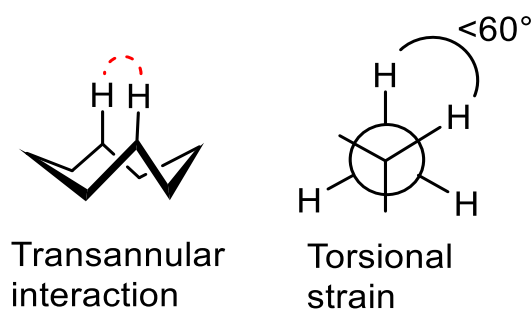


**Figure 2.4.3.1.** An example of the interactions observed in the cyclooctane ring.

For example, a diamond lattice contains a cyclic path with eight carbon atoms (Figure 2.4.3.2a). There is a high degree of strain in the ring because two pairs of hydrogens (Ha and Hb) are competing for the same position in the lattice (Figure 2.4.3.2b and 2.4.3.2c). This causes steric hindrance in a structure, being an example of transannular strain.<sup>1</sup>

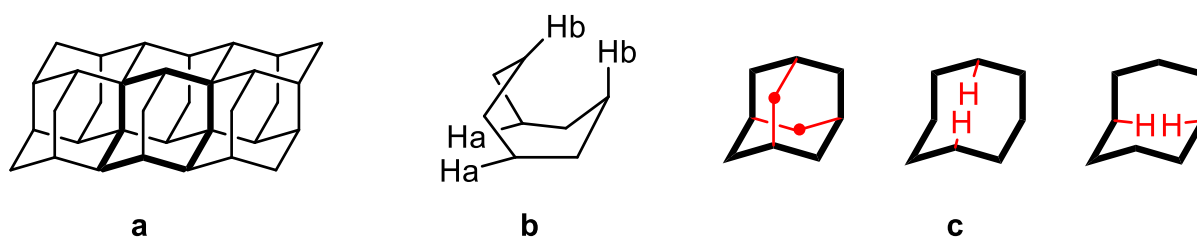


**Figure 2.4.3.2.** a) Cyclooctane as a part of the diamond lattice. b) Two hydrogen atoms causing strain by pointing “inwards” and competing for the same positions. c) An alternative representation of transannular strain in cyclooctane.<sup>1</sup>

The torsional strain occurs when the inability of the cycloalkane to adopt a staggered conformation causes the substituents to shade each other.<sup>3</sup> In medium-sized rings, it is important to minimize the transannular interactions because the ring substituents, even hydrogen atoms, easily collide with each other. However, this change occurs at the expense of strain caused by

another interaction, for example forcing the bonds to the same level which increases the torsional strain of the ring system.<sup>1</sup> The ring structure of cyclooctane leads to a range of bond angles, contributing to its overall instability.<sup>3</sup> Torsional (Pitzer) strain is related to the non-bonded interactions and steric hindrance in cyclooctane, affecting its conformational flexibility. This strain arises from eclipsing interactions between adjacent bonds, especially in the chair and boat conformations. The lowest-energy conformation, the boat-chair, still experiences torsional strain due to the eclipsing interactions in its structure.<sup>69</sup>

Medium-sized rings cannot have all the strain-inducing interactions completely eliminated in a single conformation. Thus, unsubstituted medium-sized rings lack a single well-defined conformation with low energy but instead exist in an equilibrium involving several conformations that are roughly equal in energy and separated by low-energy barriers.<sup>1</sup>

Ten conformations of cyclooctane have been identified and divided into four families (Figure 2.4.3.3). According to the conformational analysis by Zou *et al.*<sup>16</sup>, cyclooctane can undergo pseudorotation which helps to reduce Pitzer strain by allowing the molecules to explore different conformations. Within each family, conformations shift through pseudorotation, which has a low energy barrier. Conversions between different families occur by inversion, which involves a high energy barrier.<sup>1</sup>

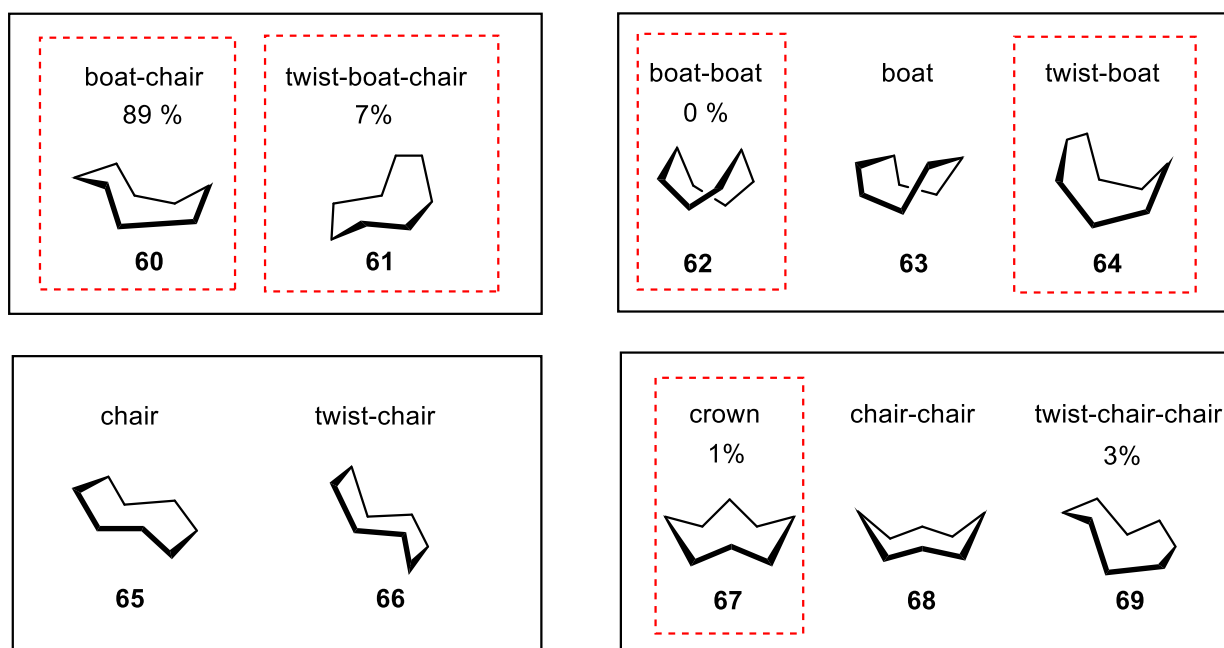


**Figure 2.4.3.3.** Conformations of cyclooctane and some of their calculated relative amounts present in the gas phase at 298 K, were determined from the calculated free energies of each conformer.<sup>1,70</sup> Minimum energy conformations of cyclooctane<sup>71</sup> are circled with a red dashed line.

Boat-boat (BB) conformation **62** is derived from a diamond lattice: it is high energy conformation and unstable. Crown (CR) conformation **67** is a low-energy conformation, but it has high torsional strain due to its symmetry. Almost an ideal bond and torsion angles can be obtained by changing the crown conformation. This would result in a conformation in which the inner ring hydrogens would be very close to each other, therefore causing a high steric strain. Stretching of opposite atoms in the crown conformation leads to a chair-chair (CC) conformation **68** while stretching the opposite bonds creates conformation **69**, a twist-chair-chair (TCC) which is slightly more stable (Figure 2.4.3.4).<sup>1</sup>

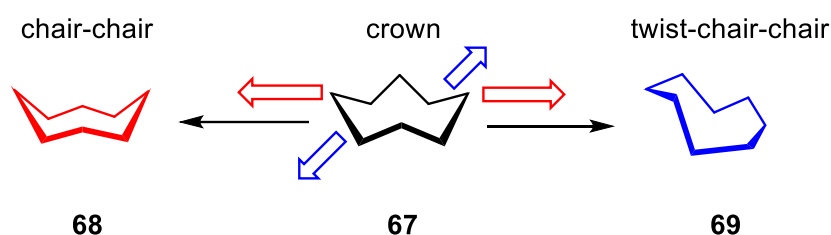


**Figure 2.4.3.4.** Formation of chair-chair and twist-chair-chair conformations of cyclooctane.<sup>1</sup>

Boat-chair (BC) conformation **60** is a hybrid between chair-chair (CC) **68** and twist-chair (TC) **66** conformations, and its energy is the lowest. Molecular dynamics simulations show that the conformational mixture of cyclooctane is temperature-dependent, with some of the conformers being favored at specific temperatures due to non-bonded interactions exerting a significant influence on the molecular packing.<sup>71</sup> *Ab initio* calculations demonstrate that the potential energy surface (PES) of cyclooctane has several minima, and the boat-chair conformer is the most stable.<sup>72</sup> The presence of non-bonded interactions affects the energy barriers between these conformers, influencing their relative populations in various environments.<sup>73</sup>

Non-bonded interactions play a crucial role in determining the structural properties of cyclooctane, affecting its conformational stability and energy landscape. Due to the spatial disposition of the atoms, these interactions largely impact the conformational diversity and stability of the molecule in its different phases. The non-bonded interactions can be attractive or repulsive, depending on the electronic configuration of the participating atoms. For cyclooctane, these interactions stabilize various conformers, such as the boat-chair and crown forms (Figure 2.4.3.3).<sup>74</sup>

Even though non-bonded interactions are essential for understanding the structural properties of cyclooctane, it is also important to consider how these interactions might change in other molecular environments and thereby potentially lead to different conformational behaviors in

related compounds. The unique properties of molecules can also lead to unexpected stability in certain environments, challenging traditional strain theories.

#### 2.4.4 *N*-Acetylbenzazocine

Rigidifying elements reduce conformational freedom compared to the unsubstituted rings. On the other hand, rigidifying elements, especially double bonds, benzene rings, and amides, also reduce the transannular interactions of the ring by removing hydrogen atoms or CH bonds from the ring.<sup>4,5</sup> When the structure has rigidifying elements, a more precise classification of the conformations is challenging (cf. cyclooctane). The analysis must then be done on a case-by-case basis using computational methods.<sup>75</sup> Hassner *et al.*<sup>75</sup> have studied the conformational behavior of acylated hexahydrobenzazocines (**70-76**) that are benzo-fused 8-membered *N*-heterocycles (see Figure 2.4.4.1).<sup>75</sup>

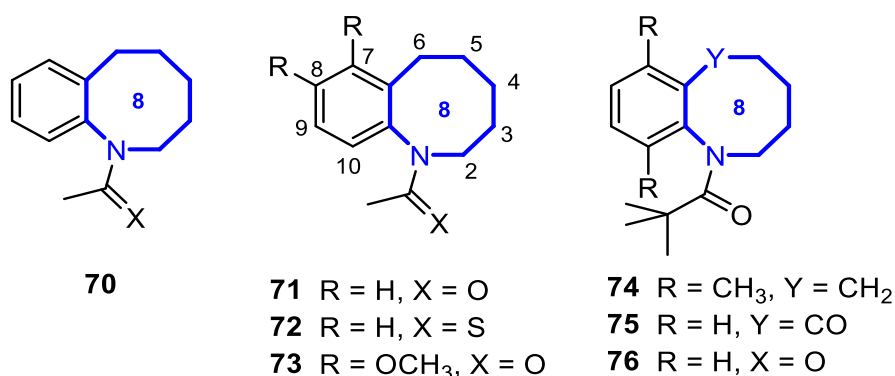


**Figure 2.4.4.1.** Structure of acylated hexahydrobenzazocines.<sup>75</sup>

These results strongly suggest that the <sup>1</sup>H NMR spectrum reflects two or more rapidly interconverting conformers (for each of the amide rotamers) at rt. To investigate this result, Hassner *et al.*<sup>75</sup> performed molecular mechanics calculations for amide **71** (Figure 2.4.4.1.) using the GMMX subroutine of PCModel, which conducts a random search for low-energy conformers. The geometries and energies of the latter were optimized with the MM3 force field.<sup>75</sup>

The results provided two conformations of the 8-membered ring separated in energy by 0.32 kcal·mol<sup>-1</sup>. In each of the two conformers, the nitrogen atom (N) and carbons C2, C5, and C6 are almost coplanar. However, in conformer A, carbon C3 is on the  $\alpha$ -side of this plane while C4 is on the  $\beta$ -side. On the contrary, the positions are reversed in conformer B (Figure



2.4.4.2). Further, weighted averages of the predicted  $^3J_{HH}$  coupling constants for the two conformers (weights of 0.6 for A and 0.4 for B) closely mimic the experimental vicinal coupling constants. These calculations for  $\Delta G_0$  align well with experimental data, as a K ratio of 0.6:0.4 = 1.5 corresponds to an energy difference of 0.24 kcal·mol<sup>-1</sup> at rt.<sup>75</sup>

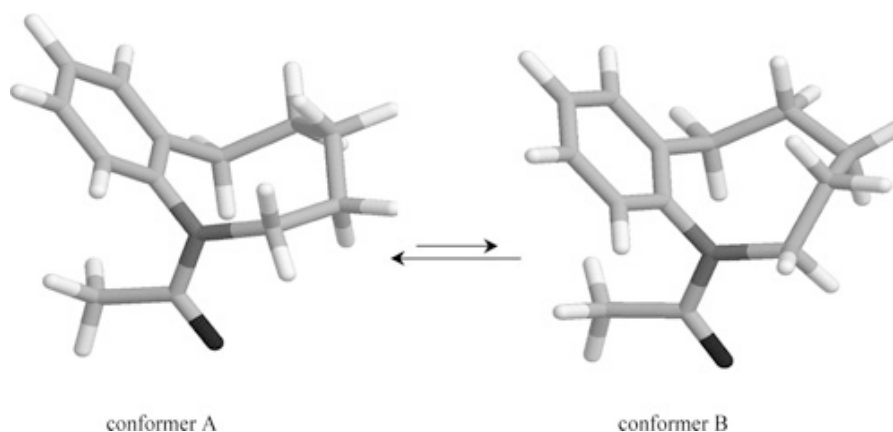


**Figure 2.4.4.2.** Calculated conformations of *N*-Acetylbenzazocine **71**.<sup>75</sup> Reproduced with permission from Hassner, A.; Amit, B.; Marks, V. and Gottlieb, H. E., On the Conformation of 8-Membered Ring Heterocycles – Dynamic and Static Conformational Analysis of Acylated Hexahydrobenzazocines, *European Journal of Organic Chemistry*, **2006**, 1256–1261, published by John Wiley and Sons, <https://creativecommons.org/licenses/by-nc-nd/4.0/>.

Careful analysis of vicinal proton-proton coupling constants and molecular mechanics calculations suggested that these compounds exist as a rapidly equilibrating mixture of octacycle conformational isomers at ambient temperature. The conclusion was further confirmed by recording the <sup>13</sup>C spectra of the parent compound **71** at low, below –90 °C, temperatures in CDCl<sub>2</sub>F (Figure 2.4.4.3). Below –70 °C, numerous lines broaden substantially and then split into two unequal peaks in a 2.8:1 ratio at  $\delta = 22.56$  and 19.81 for the major and minor isomer acetyl methyl groups, respectively  $\Delta G_0 = 0.33$  kcal·mol<sup>-1</sup> at –112.5 °C). Line shape analysis at –92.4 °C gave a major-to-minor rate constant of 150 s<sup>-1</sup>, corresponding to an activation barrier of 8.6 kcal·mol<sup>-1</sup>.<sup>75</sup>

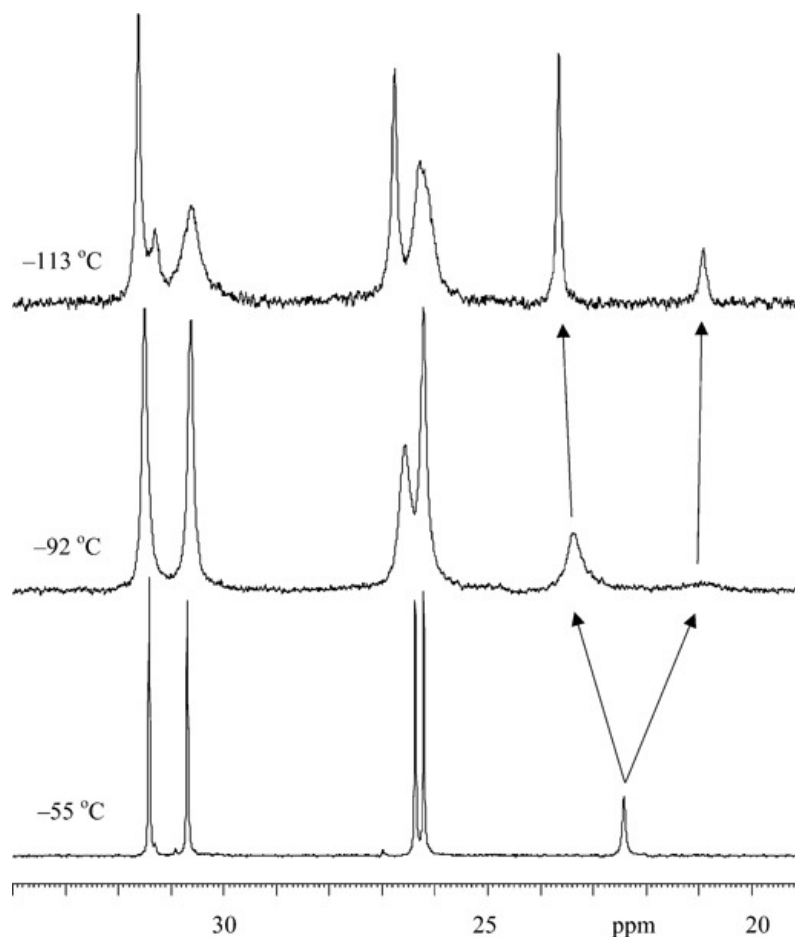


**Figure 2.4.4.3.**  $^{13}\text{C}$  spectra of *N*-Acetylbenzazocine **71** in  $\text{CDCl}_2\text{F}$  show significant line broadening at low temperatures. The acetyl  $\text{CH}_3$  resonance at  $\delta = 22$  ppm splits into two unequally intense peaks corresponding to the two 8-membered ring conformational isomers (Figure 2.3.4.2).<sup>75</sup> Reproduced with permission from Hassner, A.; Amit, B.; Marks, V. and Gottlieb, H. E., On the Conformation of 8-Membered Ring Heterocycles – Dynamic and Static Conformational Analysis of Acylated Hexahydrobenzazocines, *European Journal of Organic Chemistry*, **2006**, 1256–1261, published by John Wiley and Sons, <https://creativecommons.org/licenses/by-nc-nd/4.0/>.

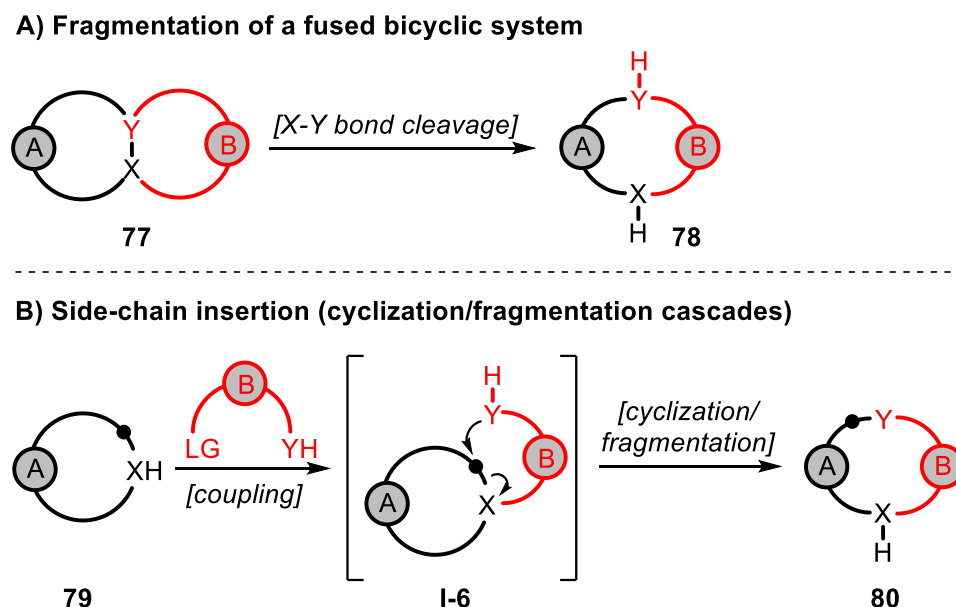
### 3 Synthetic methods for medium-sized rings

As mentioned in Chapter 2, medium-sized rings are very challenging synthesis targets due to their strained ring structures. However, different medium-sized rings are part of many interesting natural substances and pharmaceuticals, which has increased both the need and interest in exploring new and functional synthesis strategies. Compared to smaller rings, one interesting feature of medium-sized rings is that they can also contain an endocyclic double bond in the *trans* configuration in addition to the *cis* configuration.<sup>76</sup>

This chapter presents various synthetic strategies that have been used to stereoselectively synthesize medium-sized rings. This chapter focuses on 8- and especially 9-membered medium-sized rings, as these ring sizes are the most challenging to synthesize (illustration in Scheme 2.2.1 in subchapter 2.2). Methods that apply to these ring sizes could probably be extended to 10- and 11-membered rings as well.

### 3.1 Ring expansion reactions

In the ring expansion reaction, as the name suggests, two or more fused ring structures are expanded into larger rings by breaking the bridging bonds between them (see Scheme 3.1.1).



**Scheme 3.1.1.** Fragmentation-type ring expansion reactions.<sup>77</sup>

C-H functionalization has become one of the main focuses of organic chemistry, as C-H bonds are found in almost all organic compounds. Following C-H functionalization, the resulting functional group handles can be used for ring expansion reactions to prepare medium-sized rings which are attractive but challenging targets of synthesis. They are not subject to the rigidity of small-sized rings but also lack the flexibility of macrocycles or linear compounds.<sup>12</sup>

Understanding thermodynamic challenges becomes important in creating novel strategies for medium-sized ring construction. One methodology for preparing medium-sized rings is to "grow" them into the target size *via* ring expansion reactions, thereby avoiding medium-sized

transition states and the kinetic challenges of direct cyclization methods (Figure 3.1.1). However, for such approaches to succeed, the reaction must have a thermodynamic driving force favoring the rearrangement. Since converting normal- into medium-sized rings is thermodynamically "uphill," an exergonic ring expansion requires compensating for the thermodynamic cost *via* other means.<sup>10,78</sup>

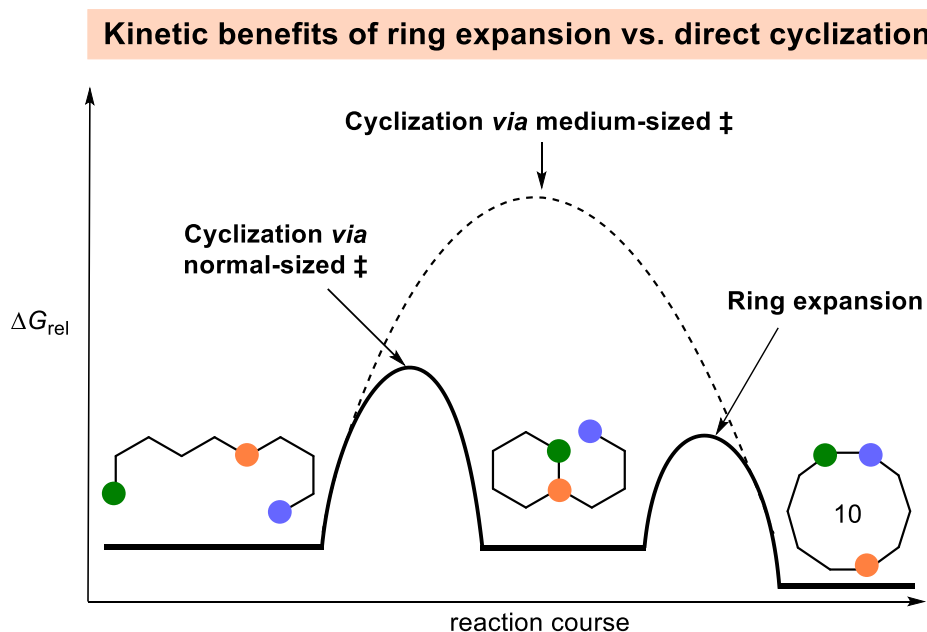


**Figure 3.1.1.** Kinetic benefits of ring expansion compared to direct cyclization.<sup>10</sup>

The facilitation of this lower-energy pathway enables medium-sized ring transition states to be circumvented and would likely decrease side reactions to obviate the necessity for impractical high dilution or pseudo-high dilution conditions usually indispensable in medium-sized ring and macrocycle cyclizations.<sup>52</sup> These methods also have diverse functionalization allowing for the incorporation of various functional groups and substituents.<sup>17</sup>

Expansion of smaller ring systems typically offers a very attractive alternative in the construction of larger ring compounds because it negates the cumbersome end-to-end cyclization step that complicates the traditional approaches.<sup>8</sup> Making a fused 6,5 system is generally quite easy. Stereochemistry and 6-ring conformation are precisely defined<sup>1</sup>, which leads to good stereocontrol in the product as well. The ring-opening reaction is also very selective because the structure was originally rigidified.

Ring expansion methods can also be integrated with other synthetic methods, providing unprecedented routes for the synthesis of complex molecules. This integration may lead to the identification of bioactive compounds that can target previously undruggable targets. This is a

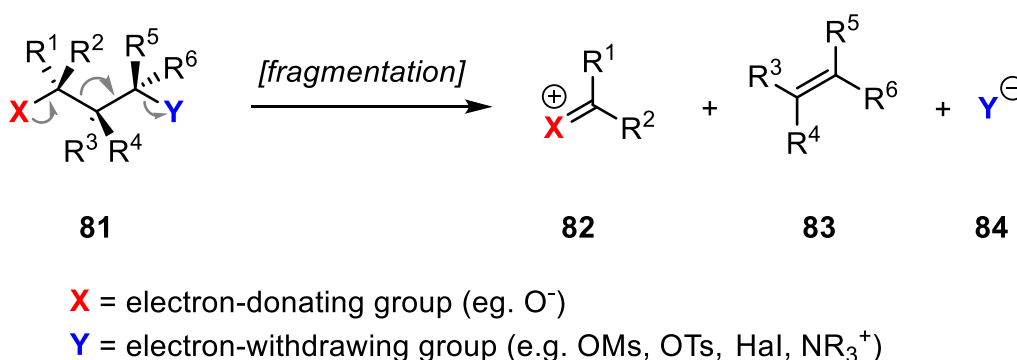
significant feature, among others, for the discovery of new drugs and pharmacological effects, which in turn advances medicine.<sup>17</sup>

### 3.1.1 Fragmentation reactions

Most ring-expansion reactions occur upon fragmentation of fused bicyclic compounds. Classical head-to-tail cyclizations of linear precursors usually suffer from poor predictability and low scalability. The synthesis of fused bicyclic compounds as intermediates for ring-expansion reactions simply necessitates the formation of 5- to 7-membered rings in cyclization reactions. Numerous precedents exist for the formation of this kind of rings, so synthesis planning is generally facile.<sup>78</sup>

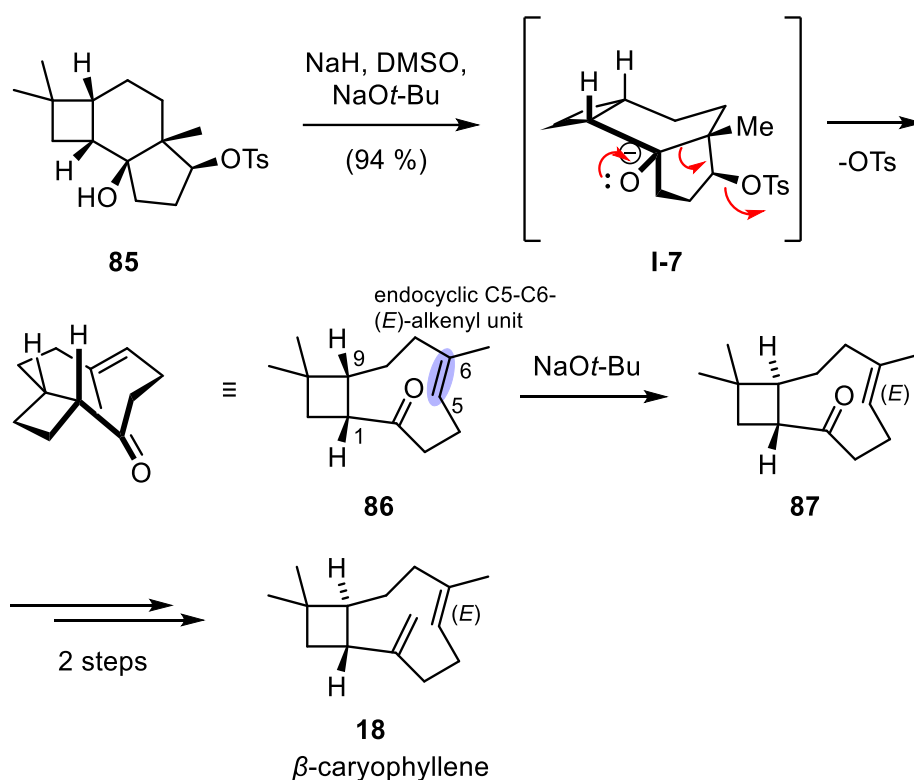
Grob fragmentation is perhaps the most famous method for the synthesis of 9-membered carbocycles.<sup>78</sup> The method offers several key advantages: first, it is stereospecific concerning the stereochemistry of the leaving group, allowing both *cis* and *trans* cyclic olefins to be formed from diastereomeric starting materials. Second, the stereochemistry of alkoxide does not impact the stereoselectivity of the fragmentation. Fragmentation reactions are widely used in natural product synthesis, as they proceed under mild conditions with very good yields. Further development is still needed, especially for synthesizing the necessary bicyclic precursor. This is because molecules derived from organisms (e.g. plants) are very complex and diverse.<sup>79</sup>

During an elimination-type Grob fragmentation reaction, a molecule of type **81** breaks into three fragments (**82-84**) through heterolytic cleavage (Scheme 3.1.1.1). The reaction is irreversible and the choice of leaving group  $Y^-$  (**84**) defines the thermodynamic driving force for the reaction. This force makes Grob fragmentation a valuable tool for overcoming the high ring strains associated with the formation of medium-sized carbocyclic rings.<sup>78,80</sup>



**Scheme 3.1.1.1.** Grob fragmentation of 1,3-diheterosubstituted compounds **81**.<sup>78</sup>

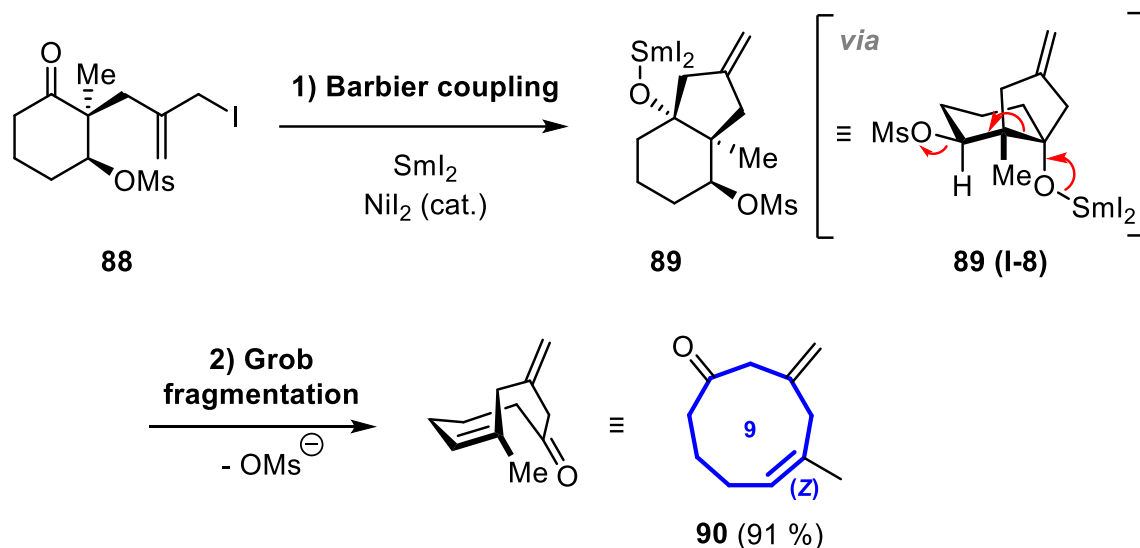
A bicyclic molecule with two fused rings is often used as the starting material for fragmentation. The bridging bond is then broken by fragmentation, resulting in the formation of one larger ring. The Corey group successfully synthesized  $\beta$ -caryophyllene in 1963 by this kind of fragmentation reaction using sodium hydride-promoted ring expansion.<sup>28</sup> This discovery was a significant milestone as  $\beta$ -caryophyllene was the first reported natural product containing a 9-membered carbocyclic ring. The cyclononane ring containing an endocyclic C5-C6-(*E*)-alkenyl unit (highlighted in purple) was constructed *via* a sodium hydride-promoted ring expansion of the bicyclic 5,6-ring system **85** (monotosylated 1,3-diol). The base treatment of **86** produced (*E*)-olefin **87**, which was elaborated into  $\beta$ -caryophyllene **18** (see Scheme 3.1.1.2).<sup>78</sup>



**Scheme 3.1.1.2.** Synthetic route for  $\beta$ -caryophyllene presented by Corey *et al.*<sup>28,78</sup>

Grob fragmentation has recently been applied in cascade reactions for efficient synthesis. The 8-, 9-, and 10-membered rings were accessed through a samarium diiodide-mediated cyclization/ fragmentation cascade of simple iodocycloalkanones **88** reported by Molander and co-workers. Samarium(III)alkoxide **89** is formed by intramolecular cyclization of  $\delta$ -iodo ketone **88** in the domino reaction combining a Barbier-type coupling reaction with fragmentation. First, an intramolecular Barbier reaction occurs between the iodoalkyl chain and a ketone in **88** to form a bicyclic alkoxide **89**. Alkoxide **89** is further fragmented to afford the corresponding

cyclononene **90** (Scheme 3.1.1.3). The isolated olefin **90** showed the (*Z*)-selectivity, making the ring expansion stereoselective.<sup>79</sup>



**Scheme 3.1.1.3.** Molander's cyclization/fragmentation cascade.<sup>79</sup>

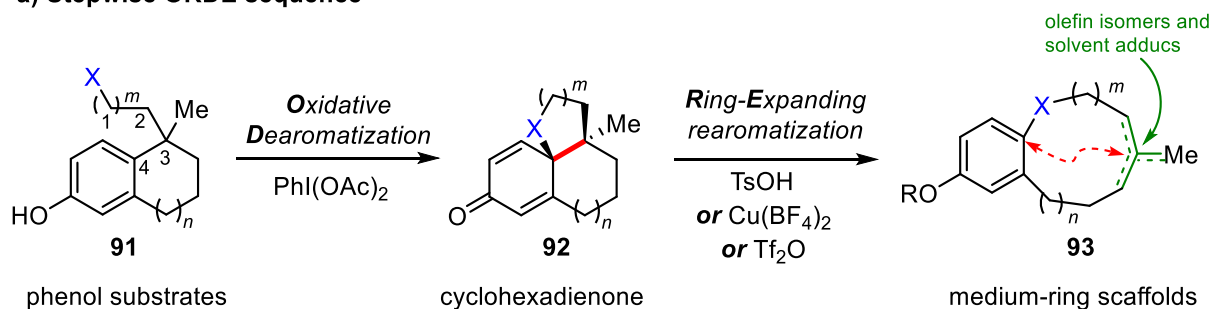
$\text{SmI}_2$  is a mild reductive coupling agent that was suitable for the reaction sequence for multiple reasons: first, the cyclization takes place in mild conditions, and the reaction is likely highly diastereoselective. Second, the cyclized product readily undergoes the fragmentation reaction under the reaction conditions.<sup>81</sup> In general, most of the  $\text{SmI}_2$ -promoted reactions are neutral, so the reductive cyclization likely occurs before the elimination of the leaving group. However, the method requires an iodoallyl chain and the main limitation of the method is the required length of the iodoalkyl chain.<sup>79</sup>

Conventional cyclization methods are substrate-dependent and have low cyclization rates. New synthetic approaches, particularly ring expansion, are being developed to access medium-sized rings.<sup>21</sup> If the medium-sized ring is fused to an aromatic ring system, alternative ring expansion reactions based on the reactivity of aromatic rings are possible. Phenols or anilines can be oxidatively functionalized at C4 to give intermediate quinonoid species which can then be rearomatized. A biomimetic ring expansion approach, as known oxidative dearomatization-ring expansion (ODRE) reaction, could provide flexible and efficient access to benzannulated medium-sized ring scaffolds (Scheme 3.1.1.4a). It offers improvements to traditional ring expansion, as the method aims to avoid competing pathways and adapt to different functional groups.<sup>11</sup>

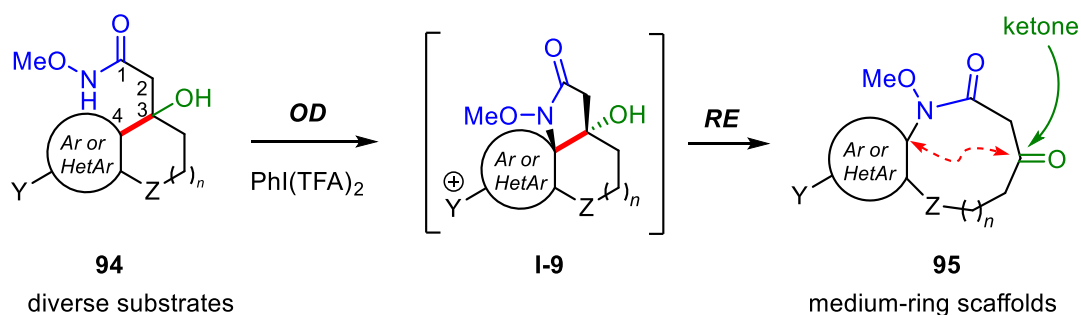
As a synthetic method, biomimetic ring expansion is functionally simple, straightforward, and scalable. In addition, for example, the position of double bonds in the products could be

proactively changed. On the other hand, the applicability of the reaction is limited because only phenol substrates are allowed (Scheme 3.1.1.4a).<sup>11</sup> A novel tandem ODRE reaction is introduced for medium-ring lactams by Guney *et al.*<sup>21</sup> (Scheme 3.1.1.4b). This new strategy allows a broader substrate use and direct ring expansion from reactive intermediates.<sup>21</sup>

**a) Stepwise ORDE sequence**



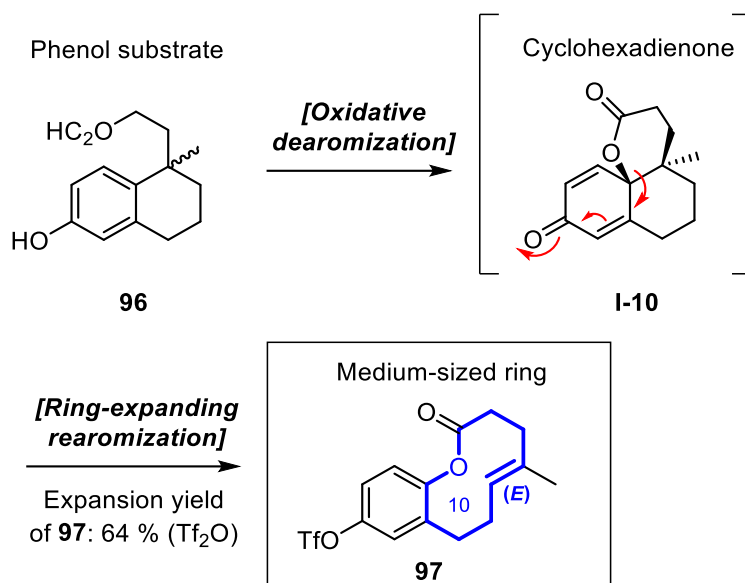
**b) Tandem ORDE reaction**



**Scheme 3.1.1.4.** ODRE approaches for the synthesis of medium-sized rings. **a)** Stepwise ODRE sequence is limited to phenol substrates providing mixtures of products. **b)** Tandem ODRE reaction provides medium-ring scaffolds **95** from bicyclic substrates **94**.<sup>21</sup>

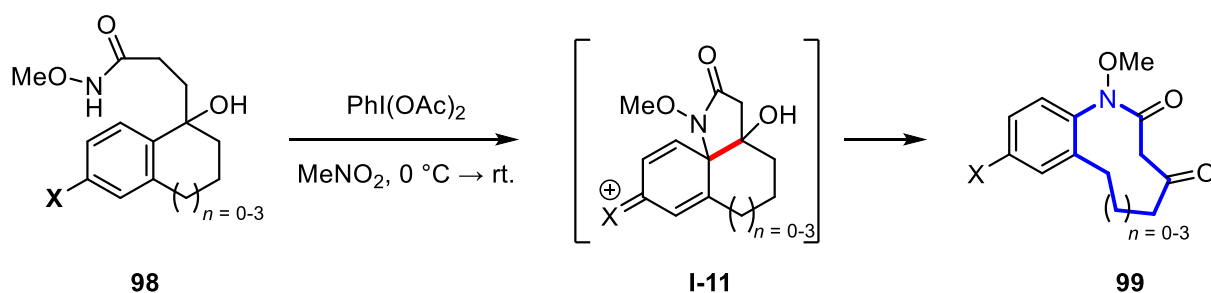
This biomimetic ODRE-strategy, presented by Bauer *et al.*<sup>11</sup>, enabled the synthesis of a first-generation library of structurally diverse benzannulated medium-sized rings. The strategy is based on the dearomatization/rearomatization sequence, which begins with the dearomatization of bicyclic phenol **96**. The ring expanding rearomatization of cyclohexadienone **I-10** leads to the formation of benzannulated medium-sized ring **97** (see Scheme 3.1.1.5).<sup>11</sup> In other words, the aromaticity of the structure is dearomatized and restored during the sequence. The example shown in Scheme 3.1.1.5 leads to the stereoselective formation of **97**, a 10-membered ring containing an *E*-alkene. This example was interesting as it was related to the humilisin E, presented in the experimental part, in which the (*E*)-stereocontrol in the rigid 9-membered ring has been challenging.





**Scheme 3.1.1.5.** Biomimetic ODRE approach for the synthesis of benzannulated medium-sized rings.<sup>11</sup>

In order to improve the diversity beyond phenolic substrates, an alternative umpolung strategy uses an electron-rich aromatic ring in **98** to directly attack an electrophilic side chain, generating an accessible cationic tricyclic intermediate **I-11** with the possibility for direct expansion *via* the domino process. Further, the introduction of tertiary alcohol into the substrate also controls the course of reaction toward the ketone product **99** instead of the pathway of competition for termination and providing a handle for further diversification. This approach further expands the substrate scope to enable the synthesis of pivotal medium-ring products, like aryl ethers and heteroaromatic derivatives (Scheme 3.1.1.6).<sup>17</sup> The tandem ODRE reaction provides access to diverse benzannulated medium-ring lactams. Tandem cyclization/ring expansion methods offer greater efficiency and flexibility than direct cyclization.<sup>21</sup>

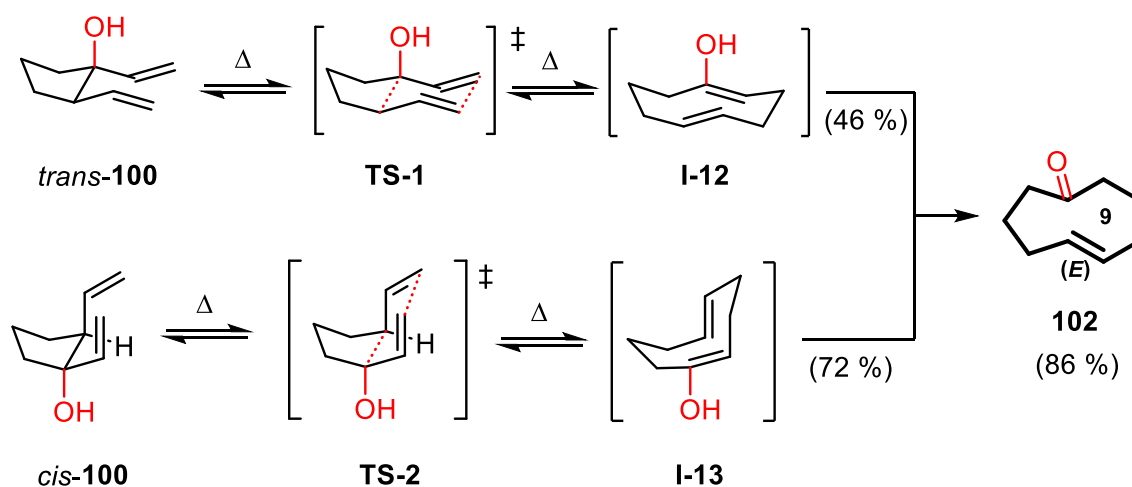


**Scheme 3.1.1.6.** Tandem ORDE reaction that provides access to benzannulated medium-ring lactams **99**.<sup>17</sup>

### 3.1.2 Pericyclic ring-expansion reactions

Sigmatropic rearrangements have been extensively studied for synthesizing medium-sized rings, including 9-membered carbocycles. Key reactions include pinacol rearrangement, semi-pinacol rearrangement, Tiffeneau-Demjanov rearrangement, and homologation reactions involving diazo compounds.<sup>78</sup> In recent years Tiffeneau-Demjanov rearrangement has had limited application for 9-membered carbocycles due to its harsh reaction conditions. In contrast, the semi-pinacol rearrangement is synthetically more useful and can be performed under milder conditions using various Lewis acids at low temperatures<sup>82</sup>, allowing for a broader range of functional group tolerance.<sup>78</sup>

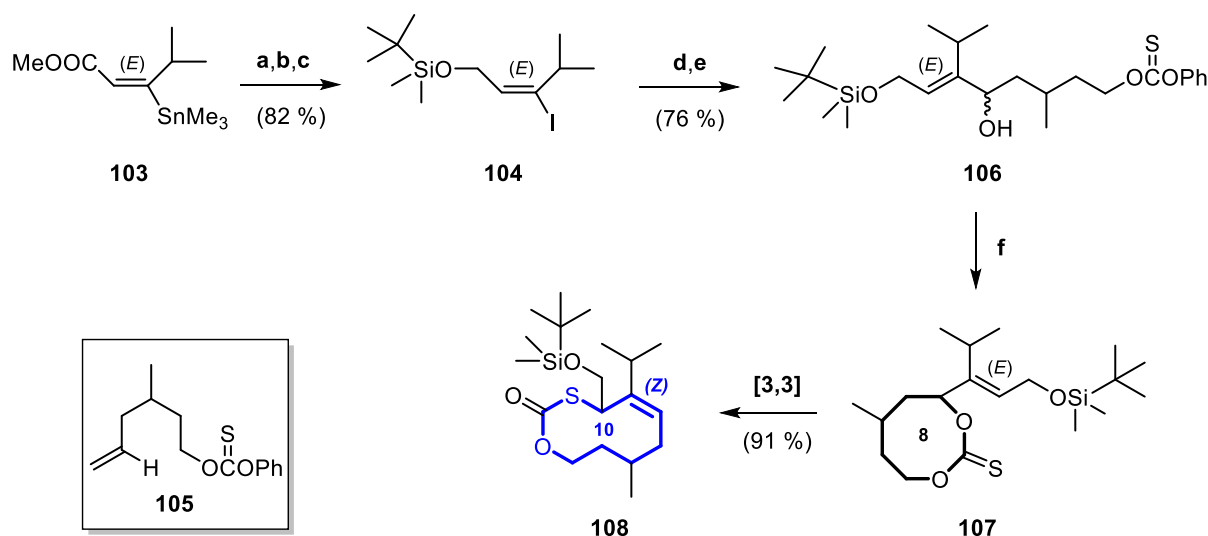
The [3,3]-sigmatropic rearrangements, particularly the oxy-Cope and Claisen rearrangements, are favored for synthesizing 9-membered carbocycles.<sup>78</sup> These reactions are noted for their broad applicability and irreversibility, primarily due to the formation of a more stable C=O double bond.<sup>83</sup> The oxy-Cope rearrangement can be executed thermally or *via* anionic rearrangement, the latter providing advantages such as increased reaction rates and functional group tolerance.<sup>78</sup> The oxy-Cope rearrangement was first utilized for 9-membered carbocycles by Kato *et al.*<sup>84</sup> in 1980. When heated at 220 °C, the 81:19 mixture of the *trans*-**100** and *cis*-**100** isomers gave (*E*)-5-cyclononen-1-one **102** in good yield as a single isomer (Scheme 3.1.2.1). The (*E*)-stereoselectivity of this reaction can be explained by the chair-like transition-state structures depicted in Scheme 3.1.2.1.



**Scheme 3.1.2.1.** Thermal oxy-Cope rearrangement of *trans*-**100** and *cis*-**100** yielding cyclononenone **102** *via* TS-1 and I-12 (for *trans*-**100**) and TS-2 and I-13 (for *cis*-**100**).<sup>78</sup>

In conclusion, this study showed that thermal activation and anionic conditions can yield specific isomers in good yields, demonstrating the effectiveness of this method in synthesizing complex structures. The reaction was later carried out as an anionic oxy-Cope rearrangement by treating *trans*-**100** with potassium hydride at 0 °C to give the ring-expanded product **102** in 86 % yield.<sup>85</sup>

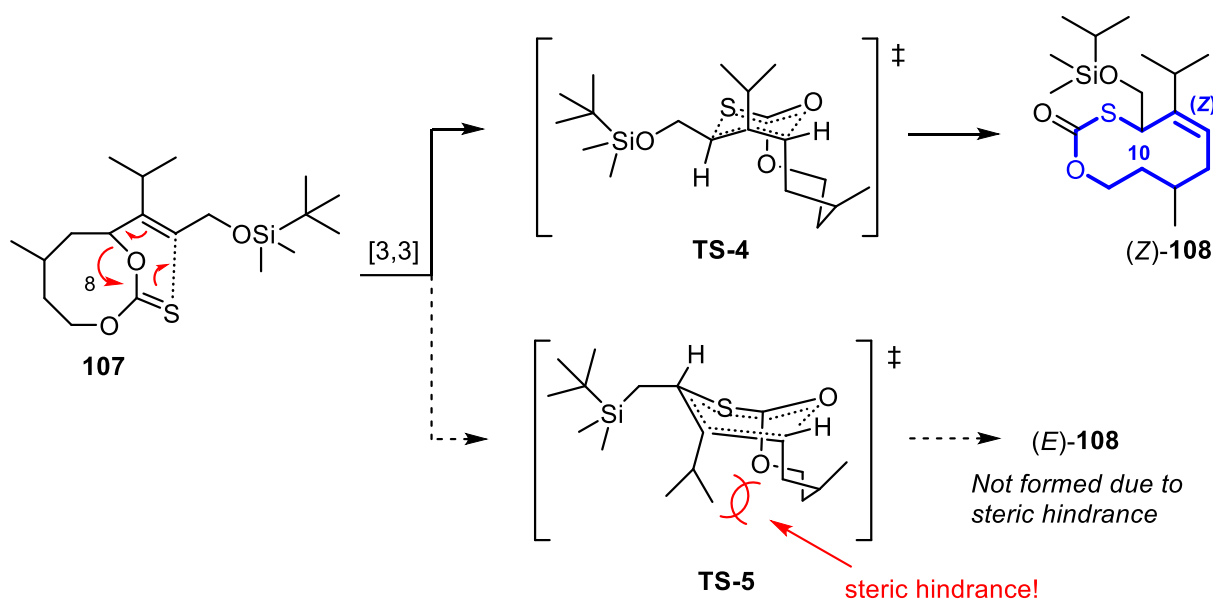
[3,3]-Sigmatropic ring expansion reactions have also succeeded in synthesizing e.g. 10-membered rings stereoselectively: a notable example is the synthesis of yellow scale pheromone published by Harusawa *et al.*<sup>86</sup> The 10-membered thiolcarbonate **108** required for this synthesis was stereoselectively prepared by [3,3]-sigmatropic ring expansion of 8-membered monothionocarbonate **107** (see Scheme 3.1.2.2).<sup>86</sup> The synthesis begins with the conversion of (*E*)-Vinyltin **103** to vinyl iodide **104** by DIBAL reduction, silyl protection, and iodine treatment. Lithium-halogen exchange in step d is followed by the addition of aldehyde **105**, which then affords diol monothionocarbonate **106**. The reaction performed for **106** (step f) proceeded to completion immediately *via* [3,3]-sigmatropic ring expansion to give 8-membered thionecarbonate **107** (Scheme 3.1.2.2). Routine work-up and silica-gel purification yielded compound **108** as a diastereomeric mixture in 91 % yield.



**Scheme 3.1.2.2.** [3,3]-sigmatropic ring expansion of monothionocarbonate **107** yielding thiolcarbonate **108**. **a)** DIBAL (3.0 equiv), pentane, -45 °C; **b)** TBDMSOTf (1.05 equiv), Pyridine, 0 °C; **c)** I<sub>2</sub>, Et<sub>2</sub>O, 0 °C → rt.; **d)** *t*-BuLi, Et<sub>2</sub>O, -72 °C; **e)** **105**, -72 °C; **f)** (TMS)<sub>2</sub>NLi (1.1 equiv), THF, rt.<sup>86</sup>

Decoupling and NOE-difference analyses of the <sup>1</sup>H-NMR spectrum were used to confirm the (*Z*)-stereochemistry of **108**. The exclusive formation of the (*Z*)-isomer in the rearrangement of

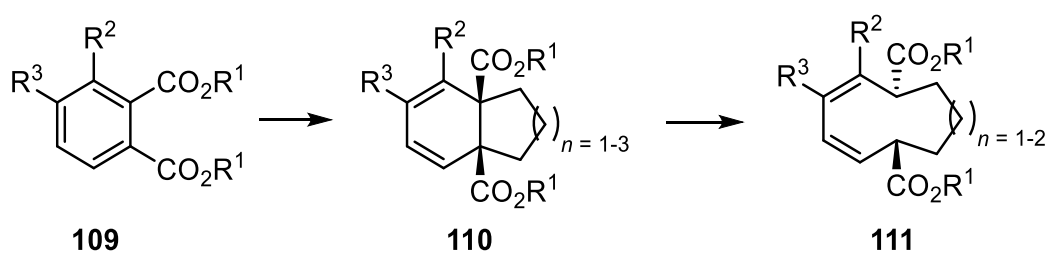
**107** can be explained in terms of transition states: the structure has a conformational preference for the chair-like transition state (**TS-4**) as it is sterically less hindered. A more crowded boat-like transition state (**TS-5**) would in turn lead to the (*E*)-isomer (see Scheme 3.1.2.3).<sup>86</sup>



**Scheme 3.1.2.3.** Explanation for the (*Z*)-stereochemistry of the 10-membered ring (**108**).<sup>86</sup>

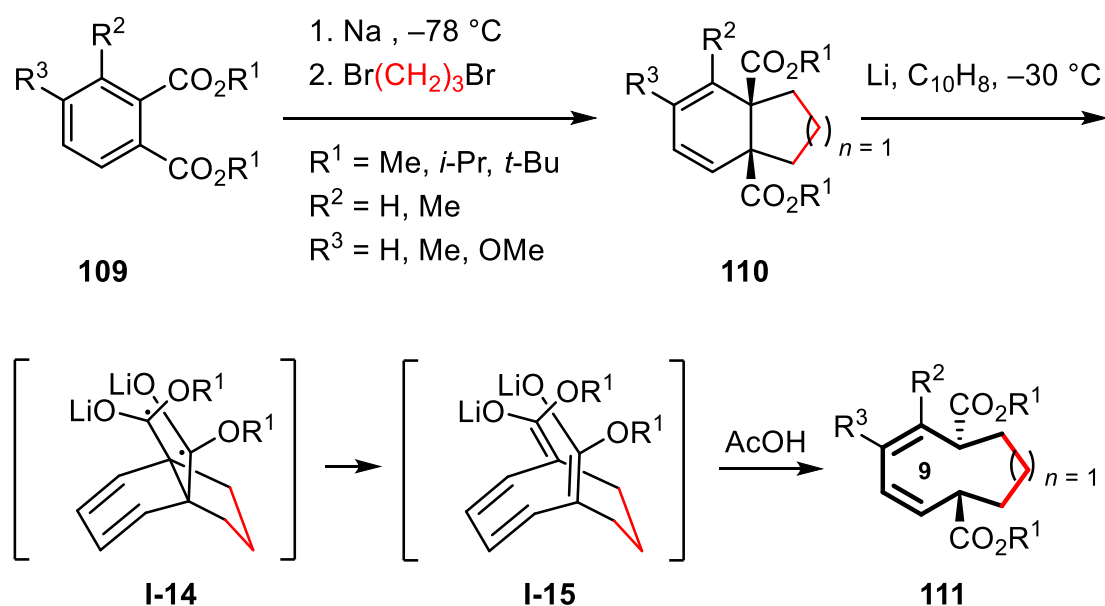
### 3.1.3 Acyloin condensation followed by ring expansion

Prado *et al.*<sup>87</sup> have described a two-step stereoselective procedure for synthesizing 9- and 10-membered carbocycles where the aromaticity of the ring is eliminated. In the process, dialkyl phthalates **109** are converted into [6,*n*]-fused bicyclo systems **110** via dearomatization/cyclization ( $n = 5,6,7$ ). After that, bond cleavage reactions are carried out for these bicyclo systems, converting them into cyclonona- and cyclodecadienes **111** (see Scheme 3.1.3.1).<sup>87</sup> In other words, the method utilizes the strategy presented in subchapter 2.2, where the smaller ring that was first manufactured is expanded into a larger one.



**Scheme 3.1.3.1.** A simplified description of the two-step synthesis for 9- and 10-membered rings developed by Prado *et al.*<sup>87</sup>

In the first step, phthalates **109** are reduced with sodium metal, followed by alkylation with 1,3-dibromo propane which acts as an electrophile. The resulting fused bicyclic system **110** is then subjected to stereoselective ring-opening by treatment with lithium in THF at  $-30\text{ }^{\circ}\text{C}$  to afford *bis*-enolate intermediate **I-15**. Naphthale ( $\text{C}_{10}\text{H}_8$ ) enables complete conversion by acting as an electron carrier. The enolate **I-15** probably formed from the intermediate dianion diradical **I-14** by bond cleavage and stereoselective protonation with acetic acid yielded the 9-membered carbocyclic diene **111** (see Scheme 3.1.3.2).<sup>78,87</sup>

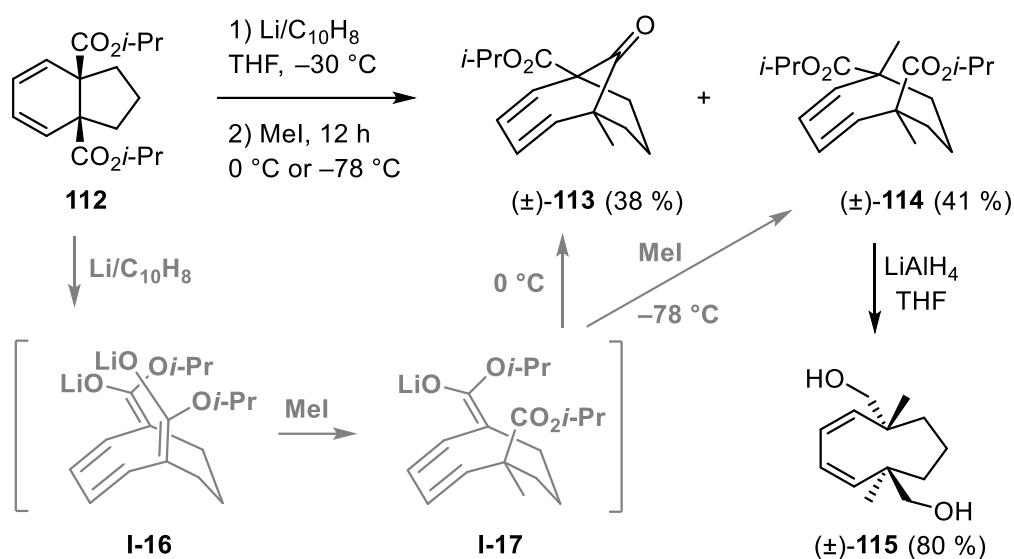


**Scheme 3.1.3.2.** Synthesis of carbocycle **111** via stereoselective reductive ring opening.<sup>78</sup>

Previous work involved a one-step dearomatization–annulation protocol with toxic and high-cost organotin compounds. Therefore, reaction conditions were sought that required only substoichiometric (catalytic) amounts of tin reagents. The new approach of Prado and coworkers aimed to develop simpler methods using inexpensive starting materials. It avoided hazardous reagents by generating *bis*-enolates **I-15** from phthalates **109**. Initial investigations revealed that these compounds undergo bond-cleavage reactions under reductive conditions. Sodium was a more effective reductant than lithium for desired product yields. However, the yields varied based on the substituents on the aromatic ring, with isopropyl (*i*-Pr) esters providing better yields compared to methyl or *tert*-butyl groups.<sup>88</sup>

The best-yielding fused bicyclic system **110** was obtained when  $n = 1$ ,  $\text{R}^1 = i\text{-Pr}$  and  $\text{R}^2 = \text{R}^3 = \text{H}$ . After the ring opening, the monoalkylation of intermediate *bis*-enolate **I-16** gives monoenolate **I-17**. Bicyclic structure **113** is formed by Dieckmann condensation and

dimethylcyclononene **114** via methylation of **I-17**. The selectivity of the reaction was steered by temperature: **114** was the major product (6:1 ratio of **114** and **113**) at  $-78\text{ }^{\circ}\text{C}$ , while bicyclic product **113** was favored at  $0\text{ }^{\circ}\text{C}$  (4:1 of **113** and **114**, see Scheme 3.1.3.3). This result indicates that the reaction conditions can be optimized for desired outcomes. Finally,  $\text{LiAlH}_4$  reduction of nonadiene **114** yielded diol **115** (80 %). *Trans*-stereochemistry of the stereocenters in **114** was determined by X-ray diffraction analysis of **115** (see Scheme 3.1.3.3).<sup>78,87</sup>



Scheme 3.1.3.3. Stereoselective ring-opening/alkylation.<sup>87</sup>

### 3.2 Cyclization reactions of acyclic precursors

Based on the study by Illuminati and Mandolini<sup>42</sup>, direct cyclization reactions are more challenging causing lower yields. Various challenges, such as transannular strain and limited degrees of freedom, complicate the synthesis of medium-sized rings by direct cyclization methods. Ring-expansion reactions efficiently alleviate high ring strain in building 9-membered carbocycles.<sup>17</sup> However, complex fused polycyclic substrates prone to difficult synthesis are often needed. Alternatively, forming 9-membered carbocycles from acyclic precursors allows a simpler retrosynthetic disconnection of the C–C bond.<sup>78</sup> Medium-sized rings can be directly formed by, for example, copper and gold-catalyzed cyclization reactions. In many instances, these are only one-step reactions from acyclic starting materials which improves the atom economy.<sup>89</sup>

Internal nucleophilic catalysts can be employed in cyclization, which allows the process to be much more practical for medium-sized lactones and lactams. Lawer *et al.*<sup>52</sup> researched cyclization reactions that operated *via* kinetically favorable 'normal' sized cyclic transition states, avoiding the high-dilution conditions typically required for medium-sized ring cyclization. This approach should also help minimize the side reactions and avoid the often impracticable high-dilution or pseudo-high-dilution conditions usually required for medium-sized ring and macrocycle cyclizations in conventional conditions.<sup>52</sup>

In medium-sized rings, cyclization reactions effectively create many bonds and stereogenic centers in a single step, avoiding the synthetic difficulties brought on by strained intermediates and regioselectivity problems that frequently arise in ring-expansion reactions. Rhodium-catalyzed intramolecular dipolar cycloadditions have produced highly functionalized products with exact control over stereochemistry.<sup>90</sup>

Several different alternatives have been developed for macrocyclization, of which ring-closing metathesis (RCM), macrolactonization, and -lactamization are the most common. In addition, radical cyclizations, cycloadditions, and transannular reactions are examples of widely used methods.<sup>91</sup> In the following subchapters, selected examples of RCM and radical cyclization are presented. These methods enabled successful stereoselective syntheses of medium-sized rings containing other functional groups and/or rigidifying elements are presented. Finally, Taxol® is presented as a case study. The synthesis of the medium-sized ring of Taxol® is difficult due to its exceptionally rigid structure, but the comparison between different approaches is possible due to the extensive amount of research.

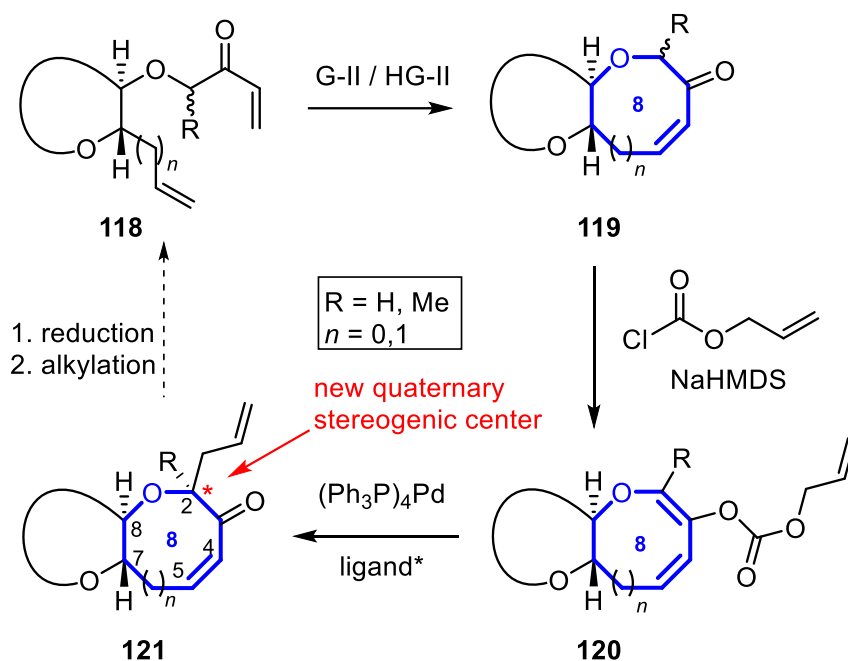
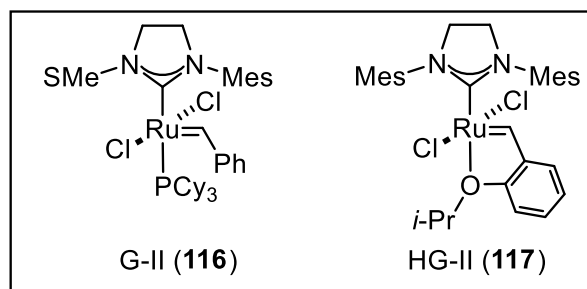
### 3.2.1 Ring-closing metathesis (RCM)

Besides cross-coupling reactions, RCM is one of the most common direct annulation methods. Researchers are still interested in developing catalytic annulation reactions to obtain medium-sized rings even though various options have been tried to be utilized in the synthesis of medium-sized ring structures.<sup>19</sup> One advantage of RCM is the use of simple starting materials. However, factors related to enthalpy and entropy easily become a challenge for the strategy.<sup>42</sup> In addition, precious noble metals such as ruthenium and palladium are required as catalysts in RCM.<sup>19</sup>

Skardon-Duncan *et al.*<sup>92</sup> have developed novel strategies for rapid and stereoselective preparation of medium-sized cyclic ethers which are highly functionalized. These methods are being applied to the efficient construction of the fused polycyclic ether frameworks through iterative ring assembly. Encouraged by the successive fragment coupling reactions, the group examined the Tsuji–Trost allylation reaction as a general approach for synthesizing 7- and 8-membered cyclic ether building blocks that are fully functionalized. This strategy also facilitates the preparation of fused polycyclic ether arrays *via* iterative cyclic ether formation as shown in Scheme 3.2.1.1.<sup>92</sup>

The first step of the plan is ring-closing metathesis of enone **118**, by using either Grubbs second-generation catalyst G-II (**116**) or Hoveyda–Grubbs second-generation catalyst HG-II (**117**). The cyclic enone **119** is then elaborated to allylic enol carbonate **120** by base treatment and allyl chloroformate. Finally, C-allylated product **121** is subsequently formed from **120** by using a stereoselective Tsuji–Trost allylation reaction and chiral palladium complex (see Scheme 3.2.1.1). In other words, the reaction is a palladium-catalyzed allylation reaction in which the ligand directs the stereochemistry of the new quaternary stereogenic center. Further reduction of carbonyl followed by functionalization would enable the repetition of the RCM and allylation sequence, permitting the iterative construction of the target polycyclic ether framework.<sup>92</sup>





**Scheme 3.2.1.1.** Iterative and stereoselective construction of fused polyethers.<sup>92</sup>

In conclusion, new substrates for Tsuji–Trost allylation have been prepared for further exploration. High diastereocontrol favored *cis* relationships between the allyl substituent at C2 and the substituent at C7/C8 in cases when catalyst control was matched to substrate control.<sup>92</sup>

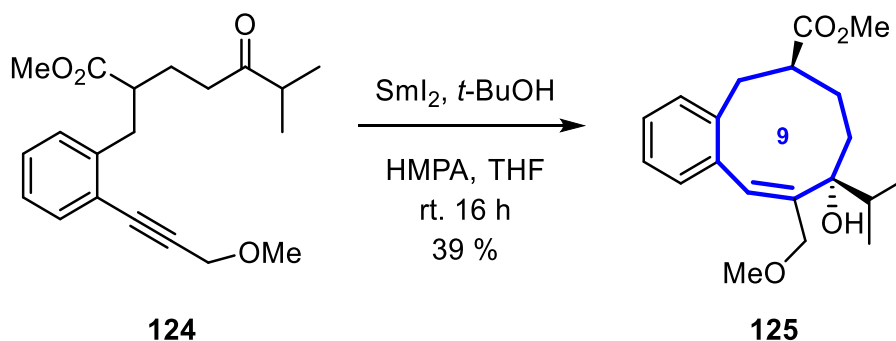
### 3.2.2 Samarium(II)-promoted cyclizations

Samarium(II)iodide was used as a reducing agent for the first time in 1980 and it has recently become a popular reagent in the synthesis of medium-sized carbocycles.<sup>93</sup> The Reissig group<sup>94</sup> has illustrated that medium-sized benzannulated carbocycles can be effectively constructed by samarium(II)iodide-induced radical cyclization. Diastereomeric  $\delta$ -ketoester **122** is a highly substituted precursor that undergoes a 9-*endo-trig* cyclization affording cyclononane derivative **123** in moderate yield but with excellent stereoselectivity (Scheme 3.2.2.1).<sup>94</sup>



**Scheme 3.2.2.1.** Samarium diiodide-induced *9-endo-trig* cyclizations of isopropenyl-substituted cyclic  $\delta$ -ketoester **122**.<sup>94</sup>

The  $\delta$ -ketoester **124** has been synthesized by Sonogashira coupling<sup>95</sup> of **7** with 3-methoxyprop-1-yne in pursuit of related alkynyl-substituted compounds. In the synthesis,  $\text{SmI}_2$ -promoted *9-endo-dig* cyclization affords the cyclononenol derivative **125** in moderate yield (Scheme 3.2.2.2). This approach is a valuable way to access medium-sized rings bearing an allylic alcohol function, thus offering many alternatives for subsequent functionalization.<sup>94</sup>



**Scheme 3.2.2.2.** Samarium diiodide-Induced *9-endo-dig* cyclization of 3-Methoxypropynyl-substituted  $\delta$ -ketoester **124**.<sup>94</sup>

This approach of  $\text{SmI}_2$ -induced radical cyclizations is particularly appealing because of the functional group compatibility of the substrates and the ease of access to starting materials from simple and inexpensive building blocks, allowing for wide variation. Further research is nevertheless needed to continue to investigate the scope of the method, its limitations, and even stereoselectivity factors that may affect it.

### 3.2.3 Case study: Taxol®

Taxol® is a famous natural taxane diterpenoid and an important anticancer medicine.<sup>96</sup> It has many structural features and one of them is a highly functionalized 8-membered ring in a very complex setting (highlighted in blue in Figure 3.2.3.1).<sup>96,97</sup> This subchapter presents possible synthesis strategies for Taxol®, focusing on the key synthesis step which is closing an 8-membered ring. Taxol® as a medicine is discussed in more detail in subchapter 4.1.1.

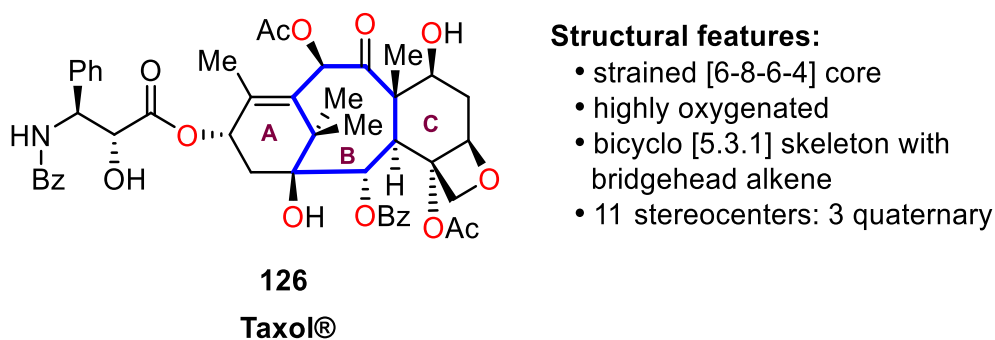


**Figure 3.2.3.1.** The structure of Taxol® and its structural features.<sup>96</sup>

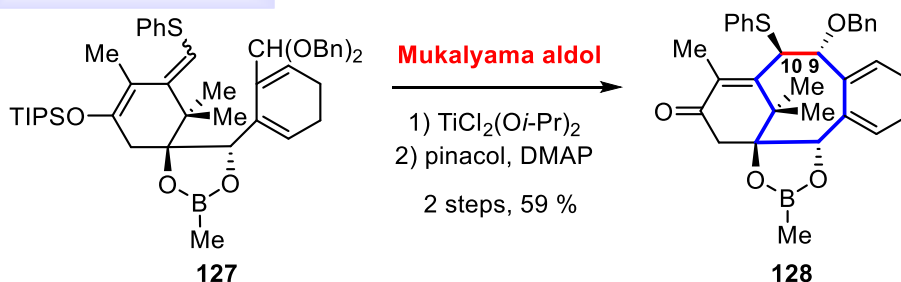
The conformations of the 8-membered ring of Taxol® are strongly dependent on the nature of the substituents. The flexibility of the 8-membered ring creates difficulties in predicting and controlling reactivity and stability for vicinal functional groups. Taxol® has attracted significant interest in more than 40 synthetic chemistry groups, which has led to significant total syntheses and formal syntheses.<sup>96</sup> The synthesis of Taxol® has been discussed in several review articles: for example, in the review article published by Min *et al.*<sup>98</sup>, 63 model studies have been presented for the 8-membered Taxol® ring. Although the synthesis of Taxol® was long considered impossible due to its complex structure, no fewer than 13 successful total syntheses have been presented.<sup>98</sup> As mentioned, this subchapter focuses on the 8-membered ring of Taxol, presenting a few selected case studies for it.

The major issues in the synthesis of taxanes are focused on two main points: the construction of a highly strained tricarboxylic structure, and the stereocontrol over multiple asymmetric centers.<sup>97</sup> The 8-membered ring has traditionally been considered one of the most difficult to construct due to unfavorable entropy, destabilizing transannular interactions, and bond angle deformations.<sup>99</sup> The formation of the 8-membered ring has also emerged as a major challenge in the synthesis of Taxol®. In the most used strategies, the 8-membered ring is closed at the top of the plane structure by making a top part disconnection either to the C9-C10 bond (Kuwajima,

1998)<sup>97</sup> or to the C10-C11 bond (Danishefsky, 1995)<sup>100</sup>. It is noteworthy that efficient Grob-type fragmentation (Wender, 1997)<sup>101</sup> and type II Intramolecular Diels-Alder (IMDA) reaction (Baran, 2020)<sup>102</sup> have also been used for the formation of A and B rings. Examples of these previously executed Taxol® syntheses are compiled in Scheme 3.2.3.1.<sup>96</sup>

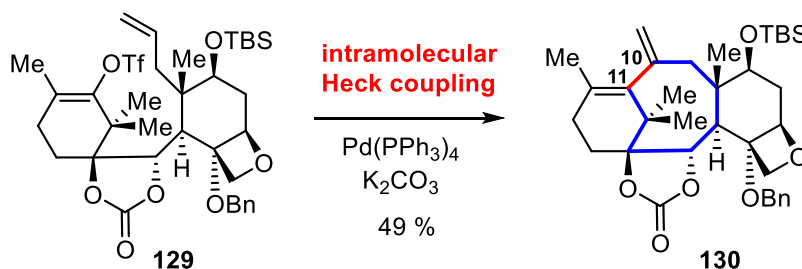
### Kuwajima (1998)

cyclization at C9-C10



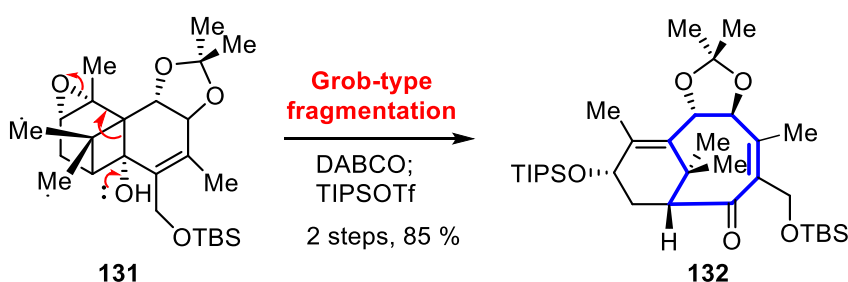
### Danishefsky (1995)

cyclization at C10-C11



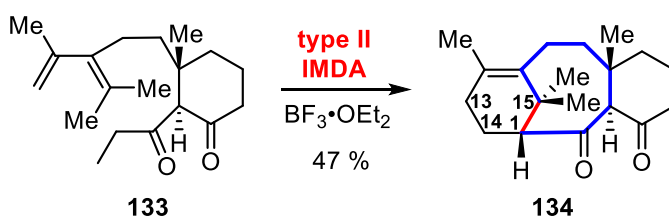
### Wender (1997)

Grob-type fragmentation



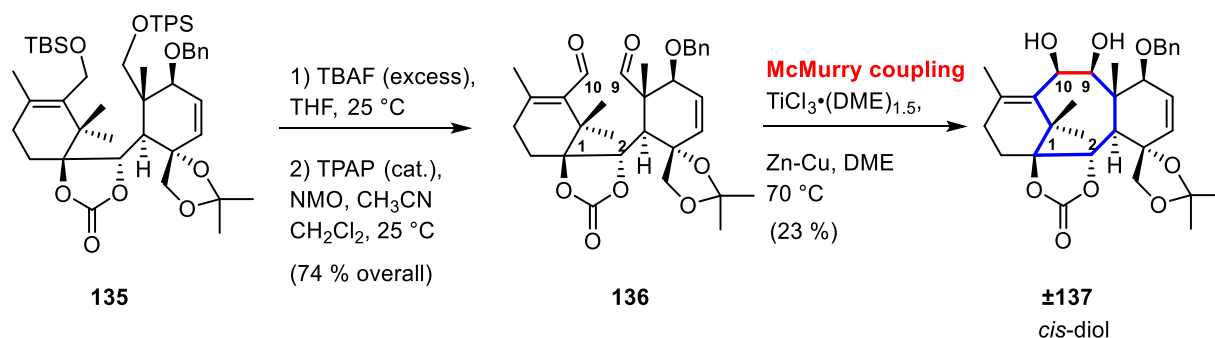
### Baran (2020)

type II Intramolecular Diels-Alder



**Scheme 3.2.3.1.** Summary of some previous syntheses of the 8-membered ring of Taxol®.<sup>96</sup>

Nicolaou's pioneering synthesis was the first synthesis developed for Taxol®, and it has inspired researchers over the years. A critical step in the synthesis was reached when both silicon-protecting groups were successfully removed from carbonate **135** using excess *tetra-n*-butylammonium fluoride (TBAF). As a result, the resulting diol could be oxidized to the key intermediate **136** (see Scheme 3.2.3.2).<sup>99</sup> A Ti<sup>0</sup>-mediated pinacol coupling, also known as the McMurry coupling reaction, appeared particularly attractive. After several systematic studies, it was found that when dialdehyde **136** in dimethyl ether (DME) was added with a syringe pump to a 70 °C solution of TiCl<sub>3</sub>•(DME)<sub>1.5</sub> (11 equivalents) and Zn-Cu couple (26 equivalents) in DME, the *cis*-diol ( $\pm$ 29) was obtained in 23 % yield (see Scheme 3.2.3.2). Although the yield for the crucial cyclization step was modest (23 %), it was encouraging that the congested taxane carbon framework could be assembled through the direct closure of the 8-membered ring.<sup>99</sup>

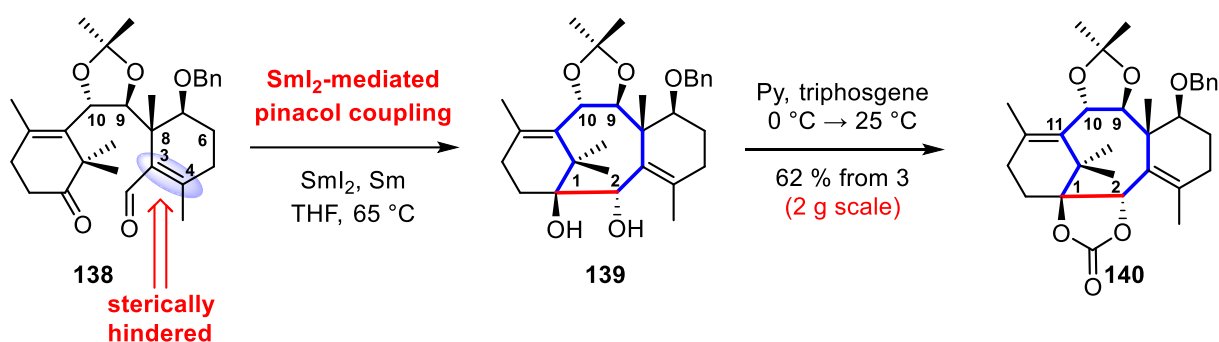


**Scheme 3.2.3.2.** The formation of key intermediate **136** and the closure of 8-membered ring of Taxol® by McMurry coupling reaction.<sup>99</sup>

The 5-membered cyclic carbonate ring of Taxol® is a valuable structural feature that connects the vicinal oxygen atoms attached to carbons C1 and C2. Based on the analysis of molecular models of compound **136**, this cyclic protecting group might have a favorable effect on the pinacol coupling reaction, as it restricts the rotational freedom of the backbone. In other words, this cyclic protecting group, connecting the oxygen atoms at C1 and C2, favors conformational adaptation. The successful closure of the 8-membered ring allowed the assembly of the congested taxane carbon framework, which was an encouraging result despite the modest yield of the cyclization step (23 %).<sup>99</sup>

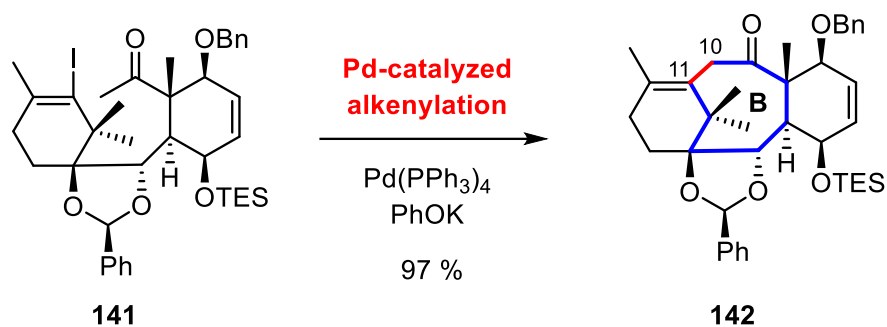
Hu *et al.*<sup>96</sup> have reported an asymmetric total synthesis of Taxol® using a compact approach *via* 19 isolated intermediates. The 8-membered ring of Taxol® is efficiently constructed by a diastereoselective intramolecular SmI<sub>2</sub>-mediated pinacol coupling that formed the C1–C2 bond

(see Scheme 3.2.3.3). This was the first time that closure of the synthetically challenging 8-membered ring *via* C1–C2 bond formation was reported.<sup>96</sup> The optimized conditions for the SmI<sub>2</sub>-mediated pinacol coupling of compound **138** were found after extensive research. The most optimal result was obtained when compound **138** was added as a 0.1 M THF solution to preheated SmI<sub>2</sub>/Sm in THF at 65 °C. The addition was performed dropwise using a syringe pump. In this 0.1 mmol scale, compound **140** was obtained as a single diastereomer in 64 % yield. As scaled up to 2 g, the one-pot method yielded **140** in 62 % yield. High temperature (65 °C) was found to be favorable for the SmI<sub>2</sub>-mediated pinacol coupling reaction, as it made it easier to overcome the high rotational energy barrier of the C10–C11 bond (Scheme 3.2.3.3).<sup>96</sup>



**Scheme 3.2.3.3.** Illustration of C1-C2 bond formation in **140** by intramolecular and diastereoselective SmI<sub>2</sub>-mediated pinacol coupling.<sup>96</sup>

The intramolecular Heck coupling in Danishefsky's synthesis, presented in Scheme 3.2.3.1, formed the desired C10–C11 bond closing the 8-membered ring, but the method was rather poor yielding (49 %). Another, significantly higher-yielding example of the C10–C11 bond formation has been disclosed in Nakada's formal synthesis in 2015, reported by Min *et al.*<sup>98</sup> In the synthesis, the 8-membered carbocycle **142** was successfully prepared with 97 % yield. Bond formation C10–C11 installs the B ring utilizing Pd-catalyzed alkenylation (see Scheme 3.2.3.4). Although this cyclization proceeds in exceptional yield, further functionalization of the 8-membered ring is still necessary after this reaction.<sup>98</sup>



**Scheme 3.2.3.4.** Illustration of C10-C11 bond formation and B ring installation utilizing Pd-catalyzed alkenylation.<sup>98</sup>

In conclusion, the ability to carry out reactions on a larger scale with better yields indicates progress in the field. Of the examples presented in this subsection, the synthetic strategy of Nakada and coworkers seems to be very promising: 48% improvement in yield is significant compared to Danishefsky's synthetic strategy. The use of diastereoselective reactions has also improved the efficiency of the synthesis. The ability to control stereochemistry during the formation of intermediates is critical for the successful synthesis of the complex structure of Taxol.

#### 4 Medium-sized rings in pharmaceuticals and natural products

This chapter focuses on natural substances that have been shown to have medical significance. The applications of drug-like macrocycles are becoming an exciting area of medicinal chemistry, with recent examples showing how macrocyclization can enhance biological and physicochemical properties.<sup>103</sup> Macrocycles have more conformations than compounds containing smaller rings, which is why conformational constraints in open-chain starting materials may help in their synthesis. The large number of conformations also makes it difficult to predict the strategy and tactics used for macrocyclization. Examples of the utilization of conformational control in macrocyclization have also been presented in the literature.<sup>45</sup>

Cyclic frameworks enhance binding affinity, bioavailability, selectivity, and metabolic stability compared to linear structures.<sup>45</sup> Aliphatic 5- and 6-membered rings are more prevalent in approved pharmaceuticals compared to medium-sized rings that are absent among the top 200 brand-name and generic drugs.<sup>11</sup> The research has pointed out that naturally occurring molecules might act as templates for developing new pharmaceutical compounds.<sup>7</sup> Medium-

sized, 8-12 membered (hetero)cyclic compounds remain poorly exploited in drug design but have been shown to have medical relevance.<sup>10</sup> For example relatively under-investigated category of 8-membered azasultams has promised capabilities for improving anticancer efficacy, which motivated the authors to formulate an innovative synthetic approach for these compounds.<sup>7</sup>

Although natural product macrocycles and their synthetic derivatives have been clinically valuable, there seems to be a growing interest in the expansion of macrocyclic scaffolds in drug development to target more challenging therapeutic areas.<sup>103</sup> Natural-product small-molecule libraries are crucial for drug discovery due to their structural diversity. Diversity-oriented synthesis (DOS) is a key strategy for constructing diverse small-molecule libraries. Future research should explore uncharted chemical spaces to discover unique bioactive compounds. Integrating ring-expansion reactions with emerging synthetic methods could lead to new therapeutic agents.<sup>17</sup>

Recent advances in the synthesis and application of 8-membered carbo- and heterocycles have led to the approval of several pharmaceuticals, including notable examples like paclitaxel (**126**)<sup>96,104</sup> and xevinapant (**143**)<sup>105</sup> (Figure 4.1). These compounds will be discussed in more detail in the following subchapters.

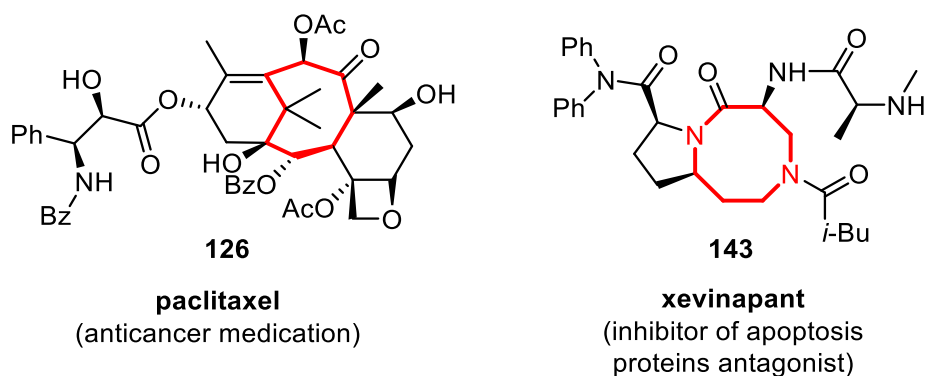


**Figure 4.1.** The structures of paclitaxel<sup>96,104</sup> and xevinapant<sup>105</sup>.



## 4.1 Carbocycles

As can be seen from the challenges of synthesis, carbocycles are challenging to synthesize. They require multiple substituents to be incorporated into their structure to satisfy Lipinski's rule of five (presented in subchapter 2.1.2). Heterocycles, on the other hand, require less functionalization, as Ro5 is filled by the X groups embedded in the ring (see Figure 4.1.1). In this case, some of the heteroatoms are already hydrogen bond donors and acceptors, which reduces the need for other functionalities to fulfill the Ro5 conditions.

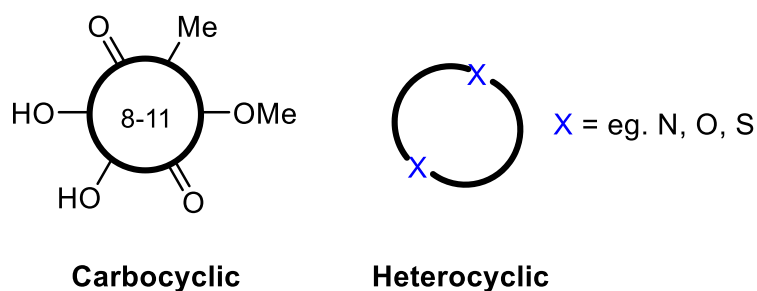


**Figure 4.1.1.** The structure of carbocyclic vs. heterocyclic drug candidate. Fulfilling the Ro5 rules requires dense functionalization of the carbocycles, while the heterocycles are already functionalized with hydrogen bond donor and/or acceptor groups.

### 4.1.1 Paclitaxel

Taxol®, as a generic name of paclitaxel (PTX), is a beneficial chemotherapeutic agent derived from the *Taxus* species. PTX was identified by Dr. Jonathan L. Hartwell in the 1960s but clinical trials did not begin until 1984. The high demand for Taxol® caused significant depletion of its natural supply, so synthesis methods had to be developed; these eventually turned out to be too cumbersome and costly. Despite its commercial success, Taxol® does face some competition with alternative formulations and high production costs, though it is still a standard treatment among various cancers.<sup>104</sup>

As mentioned in subchapter 3.2.3, Taxol® **126** is an example of a very heavily substituted terpenoid with an 8-membered carbocyclic ring (Figure 4.1.1.1). The Food and Drug Administration (FDA) approved Taxol® officially as a potential anticancer drug in 1998 and nowadays it belongs to the most widely used chemotherapeutic agents in the therapy of cancers.

Since the antitumoral activity was discovered, more than one million patients have been treated with Taxol®, making it as one of the most widely administered antitumoral drugs.<sup>96,104</sup>

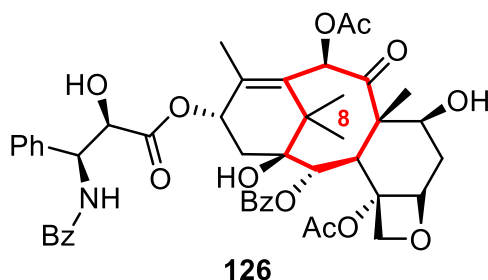


**Figure 4.1.1.1.** Structure of Taxol® **126**.<sup>96</sup>

A major challenge in anti-cancer therapy is developing drugs that can specifically target tumor cells. Taxol® is called a microtubule targeting agent (MTA) as it causes cell death by binding to tubulin and inhibits the microtubules' disassembly. PTX-treated cells are detained in the G2/M phase, preventing progression through the cell cycle and leading to cell death. This sequence of events is called mitotic arrest (Figure 4.1.1.2a). Some cells also undergo premature mitotic exit called "mitotic slippage", which is a factor that greatly reduces the effectiveness of the drug. Taxol® activates metabolic apoptosis, causing cell death also in the tumor (Figure 4.1.1.2b). Apoptosis has been suggested to be associated with the activation of the transcription factor p53, which is involved in the progression of several tumors. PTX has also been shown to increase ROS and the overexpression of endoplasmic reticulum (ER) stress-related genes and proteins in osteosarcoma cells. Increased ROS production is due to  $\text{Ca}^{2+}$  overload and mitochondrial damage.<sup>104</sup>

Additionally, a recent study has shown that in canine mammary gland tumor cells, PTX reduces the expression of the anti-apoptotic protein B-cell Leukemia 2 (Bcl-2) and increases the expression of the pro-apoptotic protein Bcl-2-associated X protein (BAX).<sup>106</sup> It has also been demonstrated that PTX interferes with the toll-like receptor 4 (TLR4) inflammatory pathway (Figure 4.1.1.2c). The dysregulation of TLR4 triggers the MyD88 pathways resulting in the activation pro-oncogenic signals, for example nuclear factor kappa-light-chain-enhancer of activated B cells (NFκB). This pathway is very important in cellular defense, and it is also implicated in decreasing the antitumor efficacy of PTX.<sup>104</sup>

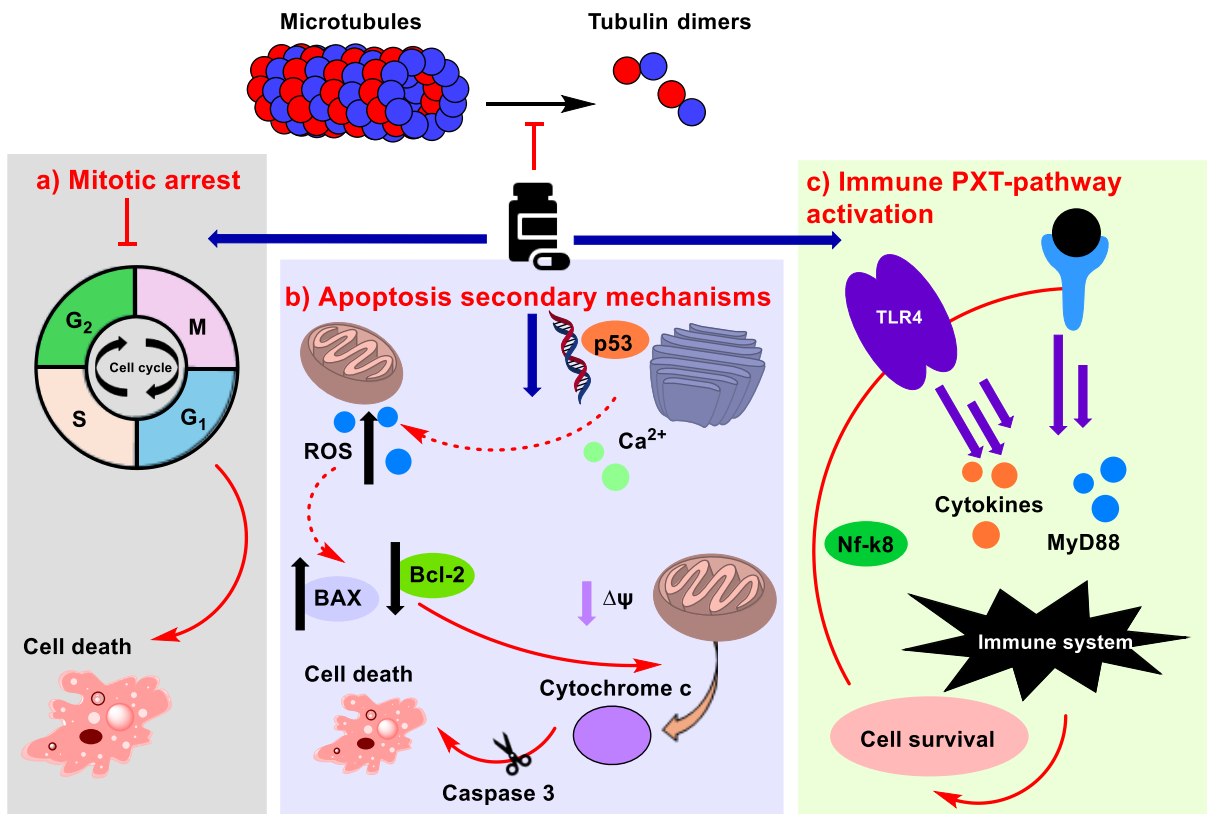


**Figure 4.1.1.2.** Proposed paclitaxel mechanisms of action in cancer cells. Suggested mechanisms are marked with discontinuous lines.<sup>104</sup>

Despite its generalized use, Taxol® presents several drawbacks. Among them, an environmentally friendly production process by microorganisms is required because of unsustainable and expensive production. The bioavailability of Taxol® should be increased without affecting the health of patients, and resistance phenomena should be reduced in a high percentage of cells treated with paclitaxel. Low water solubility is one of the major limitations of PTX, which complicates its drug delivery. The problem has been attempted to be solved, for example using Cremophor EL (CrEL), a non-ionic heterogeneous surfactant for poorly soluble drugs. However, their use was associated with adverse effects, such as anaphylactoid hypersensitivity reactions and aggregation of erythrocytes, which prompted the search for safer alternatives. New formulations, including nanoparticle-based systems like albumin-based nanoparticles (e.g. Abraxane®) and liposomes (e.g., Lipusu®), have shown improved efficacy and reduced side effects compared to traditional Taxol®.<sup>104,107</sup>

In conclusion, much progress has been made in understanding the PTX pathway, although it is still unclear. While Taxol® remains a vital tool in cancer treatment, its production challenges and the mechanisms of resistance require ongoing research and innovations. Ongoing research

aims to enhance oral bioavailability and develop targeted delivery systems to improve therapeutic outcomes. This would provide important answers and open new doors for future research and drug development.<sup>104</sup>

#### 4.1.2 HIV protease inhibitors

HIV protease inhibitors have been one of the key strategies of human immunodeficiency virus (HIV) treatment; hence, the search for potent yet affordable inhibitors with good oral bioavailability is constant. Even though various HIV protease inhibitors have shown promising results in enzyme inhibition and exhibited *in vitro* anti-viral activity, the most candidates identified so far are peptide-derived compounds. Unfortunately, compounds belonging to this class often possess unfavorable pharmacokinetic properties, like poor oral bioavailability, fast excretion, and complications of their synthesis.<sup>20,108</sup>

HIV protein inhibitors were studied in a screening program by a pharmaceutical company Pharmacia & Upjohn. The company was interested in what kind of changes would be observed in the structure-activity relationship (SAR) of the cycloalkyl ring as a result of various structural changes, such as saturation of the 5,6-double bond or substitution of the phenyl ring. The work built on earlier findings that flagged 4-hydroxycoumarins (e.g. **144** in Figure 4.1.2.1a) as key scaffolds and enabled the development of a wide series of cycloalkylpyranones. Synthesis of cycloalkylpyranones included replacing the rigid benzene ring of the coumarins with various-sized cycloalkyl rings that are conformationally flexible. This replacement assessed their effects on binding affinity (see Figure 4.1.2.1b). Based on the results, it was evident that the ideal size for the cycloalkyl ring is eight as the cycloalkyl derivative **145d** showed over a 10-fold increase in activity compared to the lead structure **144**.<sup>108</sup>

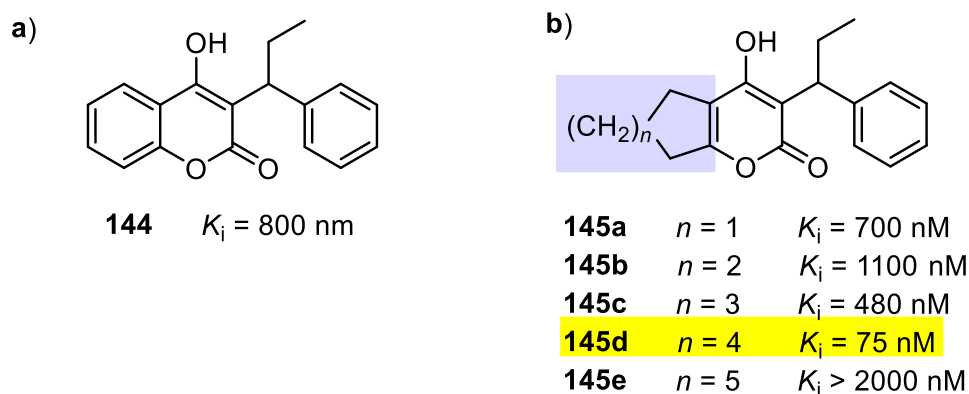


**Figure 4.1.2.1.** a) Structure of 4-hydroxycoumarin **144**. b) Structures of hydroxycoumarins **145a-e** with the benzene ring replaced. Description of the effect of ring size on the  $K_i$  value, which indicates the binding affinity between the inhibitor and the protease. A smaller  $K_i$  tells about higher binding affinity, meaning that less ligand is required to inhibit the activity of its binding partner.<sup>108</sup>

Examination of the inhibitor-protease complexes has shown that the pyrone ring acts as a pharmacophore by establishing the key hydrogen bonding at the active site. X-ray crystal structures obtained from the complex of both **145c** and **145d** with HIV protease showed that the cycloalkyl ring folds into the S1 pocket of the protease (Figure 4.1.2.2). The crystal structures indicated that the S1 region is more filled for the cyclooctyl ring compared to the cycloheptyl ring.<sup>20,108</sup>

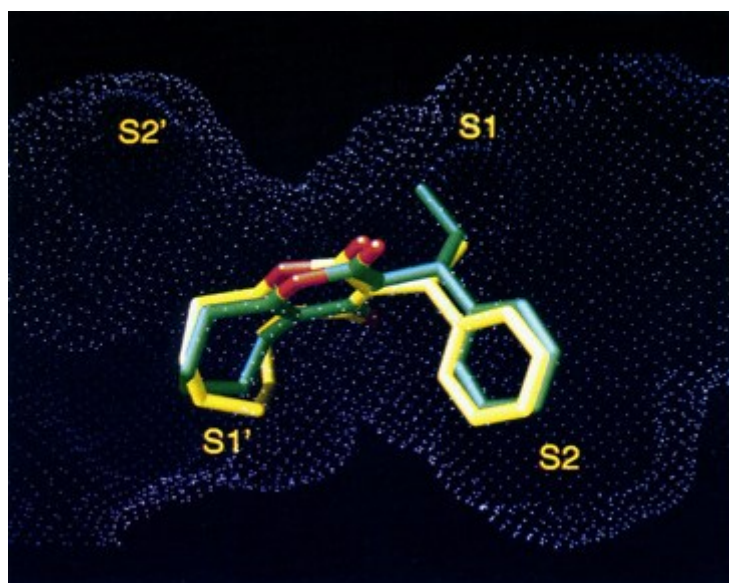
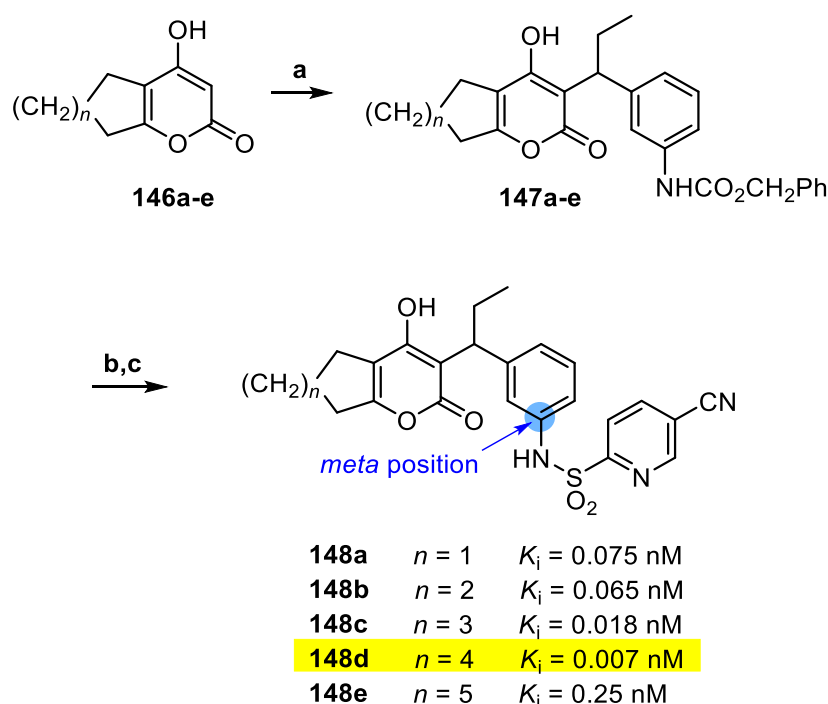


**Figure 4.1.2.2.** The X-ray crystal structure of **145c** (depicted in green) in complex with HIV-2 protease is contrasted with the X-ray crystal structure of the inhibitor **145d** (illustrated in yellow). The surface of the enzyme, represented by white dots, corresponds to its complexation with inhibitor **145d**. In both cases, the medium-sized ring of the cycloalkyl fits into the S1' pocket of the enzyme.<sup>20</sup> Reprinted with permission from Romines, K. R.; Watenpugh, K. D.; Tomich, P. K.; Howe, W. J.; Morris, J. K.; Lovasz, K. D.; Mulichak, A. M.; Finzel, B. C. and Lynn, J. C., Use of Medium-Sized Cycloalkyl Rings To Enhance Secondary Binding: Discovery of a New Class of Human Immunodeficiency Virus (HIV) Protease Inhibitors, *J. Med. Chem.*, **1995**, 38, 1884–1891.

Copyright (2024) American Chemical Society.

Previous studies have shown that substitution at the *meta*-position of the phenyl ring enables the substituents to reach the S3' pocket thereby enhancing the enzyme binding affinity. Notably, incorporating the arylsulfonamide substituent at this position has often resulted in potent enzyme inhibitory activity as well as significant antiviral activity. The effect of this *meta*-substitution on the optimal cycloalkyl ring size was investigated in the study.<sup>109</sup>

Cycloalkylpyranones bearing sulfonamide substituent were prepared by a three-step synthesis starting from known cycloalkylpyranones **146a-e** (see Scheme 4.1.2.1). The presence of sulfonamide at the *meta* position significantly increased the enzyme binding affinity of these analogs (**148a-e**) over the unsubstituted series (**145a-e** presented above). The optimal size of the cycloalkyl rings was not altered, with 7- and 8-membered derivatives **148c**, and **148d** being the most potent ones. The 8-membered ring analog **148d**, unlike the other compounds in series **148**, also showed good antiviral activity in H9 cells infected with HIV-1 (The median effective dose, ED<sub>50</sub> = 2.6 μM).<sup>108</sup>



**Scheme 4.1.2.1.** a) 3-EtCH(OH)C<sub>6</sub>H<sub>4</sub> NHCO<sub>2</sub>CH<sub>2</sub>Ph, *p*-TsOH; b) Pd/C, cyclohexene; c) 4-cyano-2-pyridinesulfonyl chloride, pyridine, CH<sub>2</sub>Cl<sub>2</sub>.<sup>108</sup>

In contrast to the *meta* substitution of sulfonamide, saturation of the 5,6 double bond shifted the optimum size of the cycloalkyl ring from eight to six, having a significant impact on the SAR in the cycloalkyl ring. Reduced binding affinity was observed for these saturated products, which was concluded to be due to greater hydrophobic interactions between the cyclooctyl ring

of the **145d** structure and the S1 pocket of the enzyme compared to the cyclohexyl of structure **149**, the one with the best binding affinity in the saturated series (see Figure 4.1.2.3).<sup>108</sup>

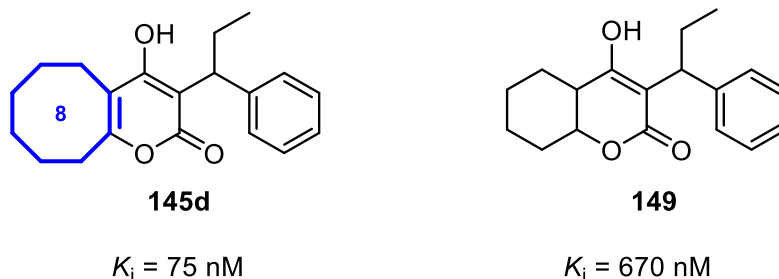


**Figure 4.1.2.3.** Comparison between the structures of the most potent compound from the unsaturated (**145d**) and saturated (**149**) series.<sup>108</sup>

In conclusion, the research investigated the effectiveness of trisubstituted cycloalkylpyranones as HIV protease inhibitors. It focused on optimizing the cycloalkyl ring size and understanding the effects of structural modifications on enzyme binding affinity, thus paving the way for future research to explore other modifications. In the future, attention should be paid to studying the mechanisms underlying the observed antiviral effect, which will also enable the development of compounds with improved bioavailability and efficacy.

## 4.2 Heterocycles

It is not surprising that drug design of medium-sized containing heteroatoms has been more successful than that of fully carbocyclic rings, and these designs have already made their way into pharmaceuticals (e.g. nefopam). As discussed in the introduction of Chapter 4, heteroatoms in the ring help to fulfill various requirements for drugs (such as Ro5) more easily compared to carbocycles. The following subsections discuss the medical significance of two compounds containing heterocyclic medium-sized rings, nefopam and xevinapant. The last subsection presents a case study of SMAC mimetics, which are promising candidates for anticancer therapeutics by enhancing apoptosis in cancer cells.

### 4.2.1 Nefopam

Opioids, non-steroidal anti-inflammatory drugs (NSAIDs), and paracetamol are common analgesics for pain management. However, these analgesics have significant side effects limiting their clinical use. Multimodal analgesia aims to reduce opioid dosage and side effects by combining drugs.<sup>38,39</sup>

Nefopam **31** (Figure 4.2.1.1) is an interesting pharmaceutical containing an 8-membered heterocyclic ring which was originally developed as an antidepressant. It is derived from orphenadrine **30** (Figure 4.2.1.1) which possesses both antimuscarinic and noradrenaline sensitizing activity. Earlier studies postulated that modification of orphenadrine, by cyclization of the alkyl amino side chain, might yield a compound with reduced antimuscarinic activity. This structural modification was expected to retain much of the noradrenaline-sensitizing actions of the parent molecule but devoid of the atropine-like side effects commonly encountered in tricyclic antidepressants. This has turned out to be true: the antimuscarinic activity was thirty times greater with orphenadrine compared to fenoxide as tested using the isolated guinea-pig ileum. The decrease in antimuscarinic activity is probably due to the steric restriction that the ring closure imposes on the nitrogen atom of the fenoxide molecule.<sup>39</sup>

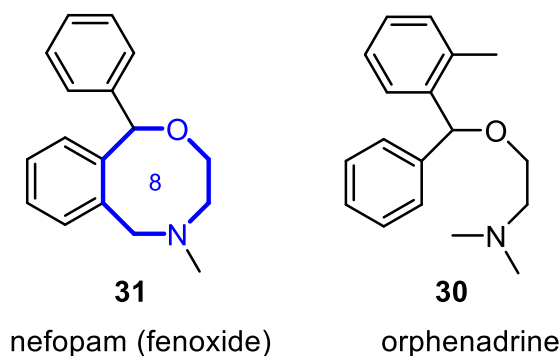


**Figure 4.2.1.1.** Structures of nefopam **31** and orphenadrine **30**.<sup>39</sup>

Nefopam is a promising non-opioid analgesic with unique properties: it does not bind to opioid receptors and lacks respiratory depression effects.<sup>38</sup> Nefopam hydrochloride is widely used in most European countries to this day as an analgesic due to its non-opiate and non-steroidal effects. Opioids and other analgesics also cause more painful side effects compared to nefopam. Incompetence of respiratory depression and superiority to aspirin are also advantages of nefopam.<sup>41</sup>



The analgesic action of nefopam involves inhibiting serotonin, norepinephrine, and dopamine reuptake. It also modulates glutamatergic pathways, reducing hyperalgesia. Previous studies have indicated that nefopam has a morphine-sparing effect post-surgery.<sup>38</sup> Combining nefopam with opioids shows enhanced analgesic effects and reduced consumption. The efficacy of nefopam varies with surgical context and pain modality: it has been clinically used for the treatment of mild to moderate postoperative pain. Combining nefopam with NSAIDs and paracetamol shows promise for improved analgesia. Further research is still needed to optimize nefopam's clinical applications and combinations.<sup>38,39</sup>

#### **4.2.2 X-linked inhibitor of apoptosis protein (XIAP) and xevinapant**

Cancer of the head and neck regions is a major health concern worldwide, being the eighth most prevalent cancer with over 878,000 new incidences and 444,000 deaths reported in 2020. More than 90% of these cancers are represented by squamous cell carcinoma of the head and neck (SCCHN), with most patients being diagnosed at locally advanced (LA) stages, with excessive poor prognosis and high recurrence rates. The standards in current treatment have not significantly changed in two decades, which brings urgency to the development of new treatment options.<sup>7,105</sup>

One of the major contributors to local and distant cancer recurrence is treatment resistance, in large part because of the ability of tumor cells to evade apoptosis through mechanisms that enable them to survive the cell death that generally would be induced by the anticancer therapies. This occurrence often correlates with overexpression of inhibitors of apoptosis protein IAPs, including X-linked IAP (XIAP) and cellular IAP 1 and 2 (cIAP1/2). Generally, IAPs are the second mitochondria-derived activator of caspase (SMAC) mimetics. These proteins inhibit the caspase activity and the activation of the proapoptotic complexes at tumor necrosis factor (TNF) receptors (see Figure 4.2.2.1). Caspases are proteins that play a key role in the apoptotic process. This disruption allows apoptosis to be restored in cancer cells, making them more susceptible to anticancer drugs. Moreover, cIAP1/2 acts as an activator of both canonical and noncanonical NF $\kappa$ B signaling, thus possibly influencing immune signaling and apoptosis.<sup>7,105</sup>

As a result, IAPs play an important role in the regulation of apoptosis. Overexpression of IAPs is usually followed by increased survival of tumor cells against treatment-induced apoptosis in various cancers, including SCCHN.<sup>105</sup>

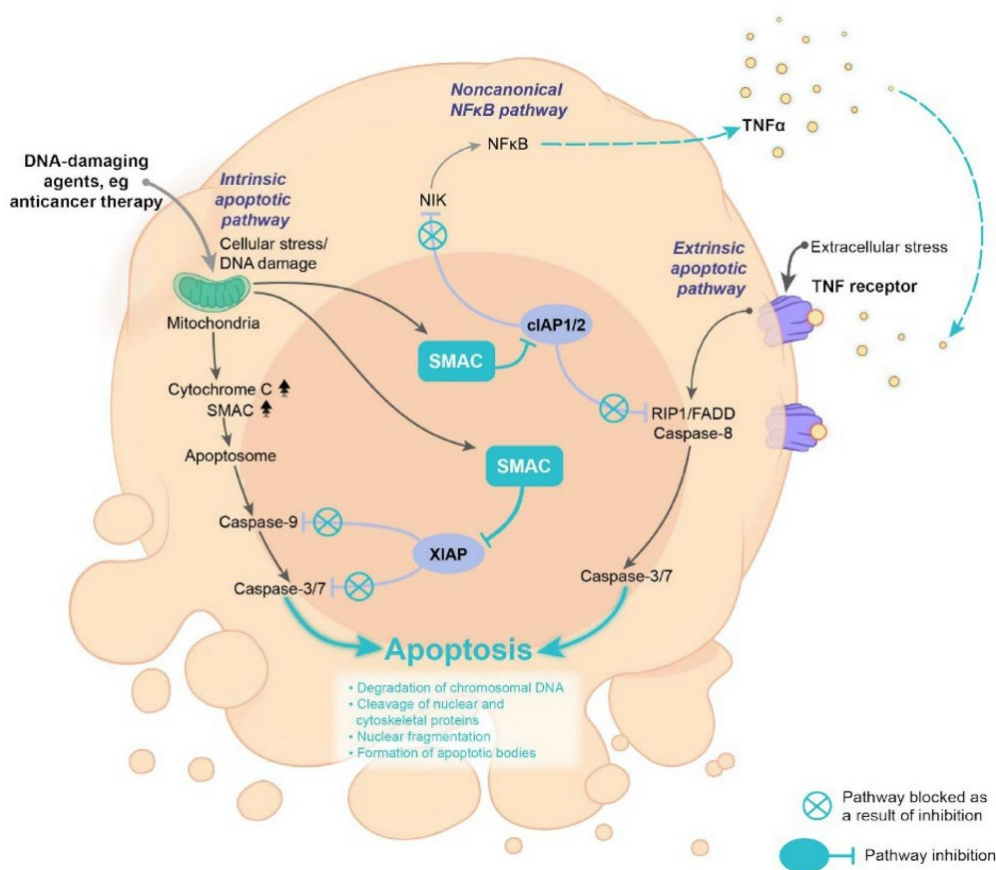


**Figure 4.2.2.1.** The second mitochondria-derived activator of caspase promotes apoptosis *via* the inhibition of IAPs. A proapoptotic stimulus triggers the release of SMAC from mitochondria into the cytosol. Inhibition of XIAP and cIAP1/2 allows for the activation of the caspase cascade, promoting downstream apoptotic signaling and the production of inflammatory cytokines *via* NFκB pathway.<sup>110</sup> Reprinted from *Cancer Treatment Reviews*, 113, Ferris, R. L.; Harrington, K.; Schoenfeld, J. D.; Tahara, M.; Esdar, C.; Salmio, S.; Schroeder, A. and Bourhis, J., Inhibiting the inhibitors: Development of the IAP inhibitor xevinapant for the treatment of locally advanced squamous cell carcinoma of the head and neck, **2023**, with permission from Elsevier.

<https://creativecommons.org/licenses/by/4.0/>

Xevinapant **143** (Figure 4.2.2.2) is known as the first IAP inhibitor, reducing the treatment resistance of cancer cells and thus enhancing the sensitivity for treatment. It has received the Food and Drug Administration (FDA) breakthrough therapy designation, especially for carcinomas that were previously untreated. Xevinapant acts as a SMAC mimetic, an oral small-molecule IAP inhibitor with efficient target protein inhibition of XIAP and cIAP1/2. In consequence, xevinapant can effectively enhance apoptosis in cancer cells.<sup>7,110</sup>

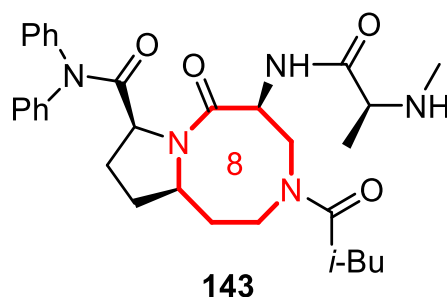


**Figure 4.2.2.2.** Structure of xevinapant **143**.<sup>7</sup>

The 8-membered ring structure of xevinapant likely contributes to its ability to fit into the binding sites of IAPs. This structural compatibility increases the probability of effective interactions with target proteins, which is crucial for its inhibitory effect. It has demonstrated a proapoptotic effect by restoring sensitivity to apoptosis in cancer cells, thereby increasing the potency of conventional anticancer therapies, such as radio- and chemotherapy. To date, this agent has demonstrated activity in the clinical setting in terms of improving treatment outcomes for patients with locally advanced SCCHN by facilitating an improved response to combined chemoradiotherapy.<sup>105</sup>

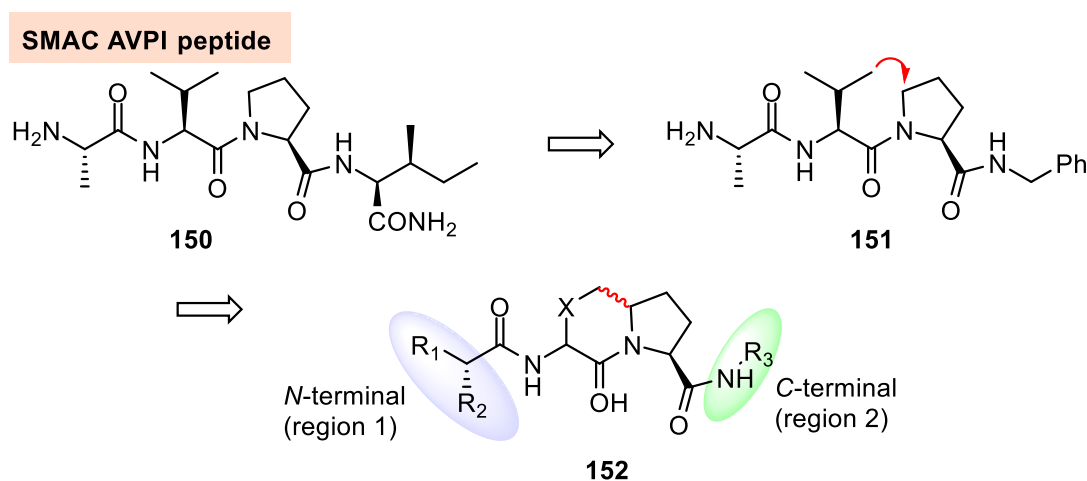
Four IAP inhibitors, including xevinapant, have previously been under investigation in clinical trials in SCCHN. Among these inhibitors, xevinapant is the most advanced in clinical development and to date the only IAP inhibitor to have demonstrated antitumor activity. It has shown synergistic effects with chemotherapy and radiotherapy in preclinical studies: preclinical data for xevinapant supported a strong rationale to move forward with IAP inhibition in combination with either chemoradiotherapy (CRT) or radiotherapy alone in locally advanced squamous cell carcinoma of the head and neck.<sup>110,111</sup> In general, IAP inhibitors represent a promising therapeutic class due to their role in treatment resistance. Most IAP inhibitors are still in early clinical development or have been discontinued despite the recent advances in research causing an urgent need for novel treatment options.<sup>110</sup>

In conclusion, endogenous antagonist proteins are molecules that inhibit the activity of IAPs. One example is SMAC mimetics, which are released from mitochondria in response to the internal stress caused by anticancer treatment. This ultimately leads to apoptosis in the manner of the reaction sequence shown in Figure 4.2.1.1. The following subchapter presents research related to SMAC mimetics.

### 4.2.3 SMAC mimetics

The study by Sun *et al.*<sup>112</sup> aimed to develop potent SMAC mimetics that could serve as promising new candidates for anticancer therapeutics by targeting XIAP (X-linked inhibitor of apoptosis protein) and enhancing apoptosis in cancer cells. Apoptosis is essential for development and homeostasis in multicellular organisms. Targeting apoptosis regulators can help to overcome cancer cell resistance. XIAP is an effective apoptosis inhibitor that is highly expressed in many tumors. It contributes to cancer cell resistance against various anticancer drugs.<sup>112,113</sup>

The approach by Sun *et al.*<sup>112</sup> was supported by earlier findings demonstrating that SMAC-derived peptides with the AVPI (Ala1-Val2-Pro3-Ile4) binding motif conjugated to a carrier peptide for intracellular delivery, have shown that for example the antitumor activity of various chemotherapeutic agents can be enhanced by these compounds both *in vivo* and *in vitro*. Although these peptides are useful reagents for proof-of-concept studies, they are unsuitable as drug candidates because they possess highly limited/weak cellular activity and presumably poor stability *in vivo*. To overcome these challenges, several research groups have focused on designing peptidic and non-peptidic small-molecule SMAC mimetics. The goal of this effort is to create more drug-like molecules that could potentially be developed into a new class of anticancer drugs.<sup>111,112</sup> Sun and coworkers did comprehensive structure-activity relationship (SAR) studies of *N*- and *C*-terminal regions of bicyclic and conformationally constrained SMAC peptide mimetics (see Scheme 4.2.2.1). These studies were made to understand how different structural changes in SMAC mimetics affected their binding affinities to the XIAP BIR3 (baculoviral IAP repeat) domain and their efficacy in inhibiting cancer cell growth.<sup>112</sup>

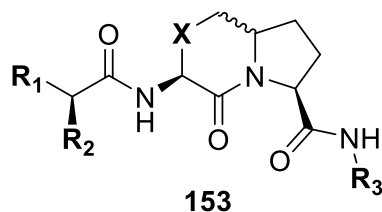


**Scheme 4.2.3.1.** Design of SMAC peptide mimetics.<sup>112</sup>

The size of the rings in SMAC mimetics plays a crucial role in determining their binding affinity, potency, and overall effectiveness as inhibitors of the XIAP. Table 4.2.3.1 shows that increasing ring size decreases the binding constant. When comparing, for example, a 6-ring to an 8-ring (compound **154** vs. **155**), the binding is found to improve more than 100 times.<sup>112</sup>

The size of the rings also affects hydrophobic interactions with the target protein. Larger rings may provide more extensive contact with hydrophobic pockets in XIAP, enhancing binding. For example, the 8-membered ring in compound **156** illustrated extensive contact with Trp323, which is crucial for its binding affinity.<sup>112</sup>

**Table 4.2.3.1.** Some examples of conformationally constrained bicyclic SMAC mimetics and their binding affinities to XIAP BIR3



Compound	X	R <sub>1</sub>	R <sub>2</sub>	R <sub>3</sub>	XIAP BIR3 K <sub>i</sub> (μM)
<b>154</b>	CH <sub>2</sub>	Me	NH <sub>2</sub>		2.33 ± 0.68
<b>155</b>	(CH <sub>2</sub> ) <sub>3</sub>	Me	NH <sub>2</sub>		0.014 ± 0.003
<b>156</b>	(CH <sub>2</sub> ) <sub>3</sub>	Et	MeNH		0.067 ± 0.018
<b>157</b>	CH <sub>2</sub>	Me	NH <sub>2</sub>	Bn	4.47
<b>158</b>					>100
<b>159</b>	(CH <sub>2</sub> ) <sub>3</sub>	Me	MeNH		0.026 ± 0.005
<b>160</b>	(CH <sub>2</sub> ) <sub>3</sub>	Me	MeNH		0.014 ± 0.005
<b>161</b>	(CH <sub>2</sub> ) <sub>3</sub>	Me	MeNH		0.274 ± 0.037

As can be seen from the table, replacing the benzyl group of compound **157** with a diphenyl methyl group resulted in a more than two-fold decrease in the  $K_i$  value of compound **154**. This result supports the hypothesis by Sun and others, that the carbonyl group might affect the binding ability of SMAC to XIAP by reducing the entropy loss associated with binding by controlling the orientation of the hydrophobic side chain (Ile4).<sup>112</sup>

In addition to ring size, stereochemistry was found to affect the inhibitory constant. For instance, the introduction of a [6,5] bicyclic lactam core structure was explored, and it was found that the stereochemistry at the ring fusion significantly affects binding. For example, compound **157**, with *S*-configuration, showed a  $K_i$  value of 4.47  $\mu\text{M}$ , while compound **158**, with an *R*-configuration, exhibited no appreciable binding (Figure 4.2.3.1).<sup>112</sup>

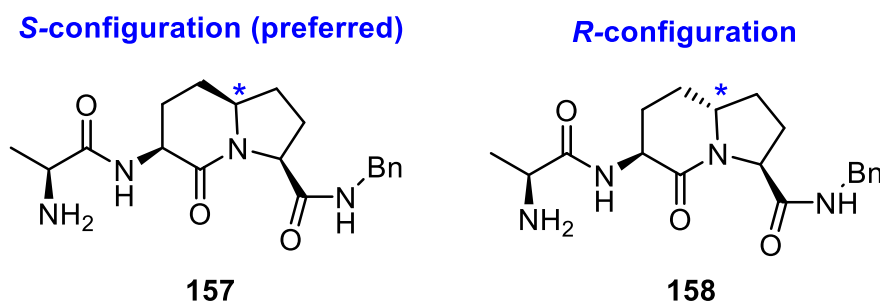


**Figure 4.2.3.1.** Conformations of SMAC mimetics **157** and **158**.<sup>112</sup>

Based on the results, the best binding ability was achieved when the R2 group was a primary amino group ( $\text{NH}_2$ ): replacement with an *N*-methyl amino group resulted in a 2-3-fold decrease in binding ability (**155** vs. **159**). Binding ability was reduced by up to 20-800-fold when the primary amino group was replaced by an *N,N*-dimethyl amino, a cyclic tertiary amino or a hydroxyl group.<sup>112</sup>

The effect of the R3 group as a controller and orientation restrictor of the phenyl group was also investigated, as this could affect the binding affinity. As a result, compounds **160** and **161**, which are stereoisomers of each other and in which the second fused ring restricted the conformation of the phenyl group, were synthesized (see Figure 4.2.3.2). In contrast to the previously presented example, the *R* configuration of the amine turned out to be the preferred one for the chiral center: the  $K_i$  value of the *R* form (14 nM) was approximately 15 times lower than that of the *S* form (207 nM).<sup>112,114</sup>

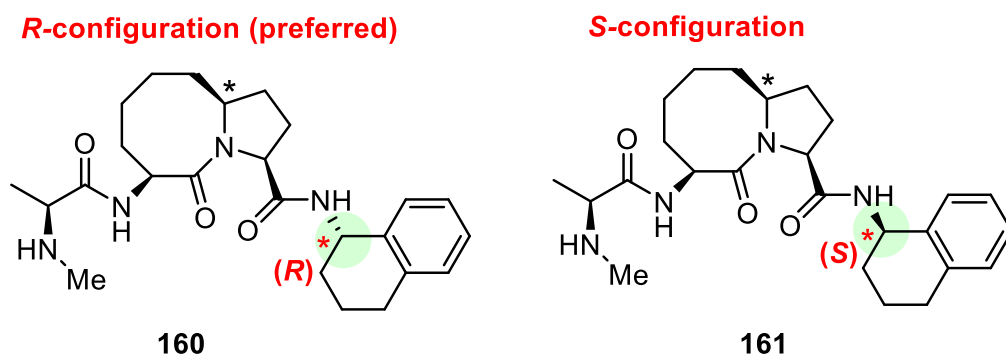


**Figure 4.2.3.2.** Conformations of SMAC mimetics **160** and **161**.<sup>112</sup>

In conclusion, the inhibitors of apoptosis (IAPs) and their emerging role in cancer studies presented in this subchapter provided new and important insights about SAR SMAC mimetics. Compounds such as **156**, **159**, and **160** were found to be potent and cell-permeable, effectively binding to XIAP BIR3. These SMAC mimetics inhibited cancer cell growth and induced apoptosis. The crystal structure of compound **156** provided insights for further optimization and overall, the structural data helps to guide further design of potent SMAC mimetics revealing the effect of the conformation on the overall interaction with the protein. It can be said that SMAC mimetics are promising lead compounds for developing new anticancer drugs which in turn may open new doors for cancer treatment.

## 5 Conclusions of the literature review

Medium-sized rings are cyclic compounds containing 8-11 atoms, whose structure is typically quite strained. Transannular interactions are characteristic intramolecular interactions resulting from destabilizing interactions caused by collisions between substituents. Conformational analysis is an important tool for inferring stereochemical control, determining the number of isomers/atropisomers, and assessing, for example, binding to the target protein.

The thermodynamic and kinetic challenge associated with the synthesis of strained medium-sized rings is generally very difficult to overcome. This challenge has forced researchers to invent creative solutions and new strategies for the synthesis of medium-sized rings. Strategies for accessing medium-sized carbocycles can be roughly classified into ring-expansion/-contraction and cyclization reactions. Grob fragmentation is an example of a ring-expansion reaction that has enabled the stereocontrolled synthesis of medium-sized rings with good yield.  $\beta$ -caryophyllene, possibly one of the most famous 9-membered natural products, has been successfully synthesized by Grob fragmentation, and as a compound, it has attracted much interest for decades. The [3,3]-sigmatropic rearrangements and acyloin condensation followed by ring expansion are also examples of the utilization of ring expansion in the synthesis of medium-sized macrocycles.

Another well-known alternative for synthesizing medium-sized rings is the cyclization of various acyclic precursors. Illuminati and Mandolini noted in their research in the 1980s that direct cyclization reactions are challenging, resulting in lower yields. This observation proved to be correct when examining the yields of samarium(II)-promoted radical cyclizations, which were only 39% and 46% for the examples presented in this thesis. On the other hand, the cyclization-ring expansion (CRE) cascade has been shown to offer kinetic advantages over direct cyclization: it occurs through low-energy transition states, thus avoiding high-energy intermediate ring transition states. As a result, side reactions and high dilution conditions, typical for intermediate rings, are also likely to be avoided.

The backbone of several interesting drug molecules contains a rigid medium-sized ring. Examples of this kind of molecule are nefopam, which acts as an antidepressant, and xevinapant, which acts as an inhibitor of apoptosis proteins antagonist. However, compounds containing medium-sized rings are under-explored in drug discovery and the challenges in their synthesis lead to their underrepresentation in drug libraries and drug development programs. For example, traditional cyclization-based approaches are highly substrate-dependent, and



unfavorable transannular interactions cause their lowest cyclization rates compared to other ring sizes.

Future research should focus on integrating medium-sized ring systems into functional frameworks and studying their interactions in different environments. This kind of effort would increase understanding of the structure of medium-sized rings and provide opportunities to optimize their properties, for example for industrial and pharmaceutical applications.

In terms of molecular design, the ring structure can be rigidified with various substituents and functionalities which may enable, for example, better stereocontrol when the structure acts as a precursor molecule in further reactions. Examples of rigidifying functionalities include aromatic rings, amides, and alkenyl groups. With alkenes, there is an additional challenge to access the alkenes in good *E* or *Z* stereoselectivity. In the experimental part of this thesis, a photo-Cope rearrangement was explored as a potential new method to address this issue, and the results are described in the following chapters. Carbon chains with defined *E/Z* stereochemistry could be useful as rigidifying elements in the preparation of medium-sized macrocycles. The aim of the experimental part of this master's degree was to prepare such a carbon frame that is suitable for cyclization into a medium-sized ring.

**EXPERIMENTAL PART**

## 6 Introduction

The experimental part of this master's thesis focuses on the problem identified in the Pihko group on the synthesis of medium-sized rings, in particular, the 9-membered unsaturated ring system of humilisin E. (Figure 6.1). Synthesis strategies for synthesizing molecules of the humilisin family have not yet been developed, as they have been isolated quite recently. As mentioned in subchapter 2.1.1, humilisin E belongs to the diterpenoids. Its tricyclic tetradecahydrocyclopenta[3',4']cyclobuta[1',2':4,5]cyclonona[1,2-b]oxirene ring system is unusual for diterpenoids and the multiple functionalities of the ring system make humilisin E an interesting target for total synthesis.<sup>24</sup> However, building a rigid 9-membered ring with good (*E*)-stereocontrol is challenging from a synthesis point of view. The stereoselective synthesis of (*E*)-trisubstituted alkenes is still challenging even in acyclic systems. In 2024, the Pihko group<sup>115</sup> published a synthetic strategy for accessing humilisin E (**1**) *via* the corresponding (*Z,E*)-diene, so-called “pre-diene” (**2**) (Figure 6.1). The synthesis of pre-diene requires access to at least one acyclic precursor with a stereodefined trisubstituted alkene.

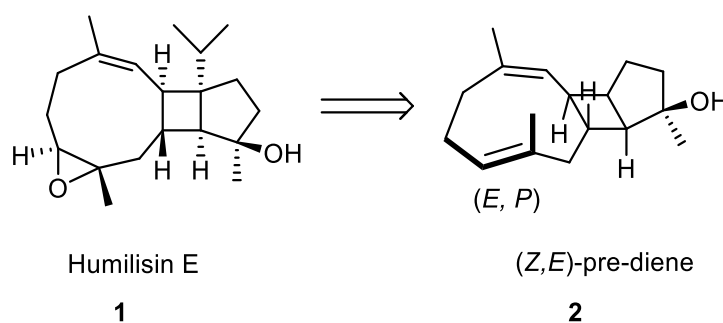


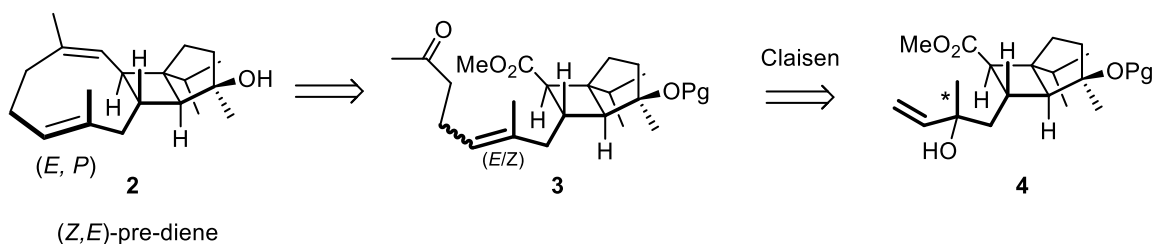
**Figure 6.1.** The structures of humilisin E **1** and pre-diene **2**. Note! For clarity, compounds are numbered separately in the experimental part of the thesis.

A convenient method to access trisubstituted alkenes in the middle of the carbon chain is using different Claisen rearrangement variants. A characteristic feature of the Claisen rearrangement is the migration of the allyl moiety in a [3,3]-sigmatropic shift, resulting in the formation of a new substituted alkenyl functionality.<sup>116</sup>

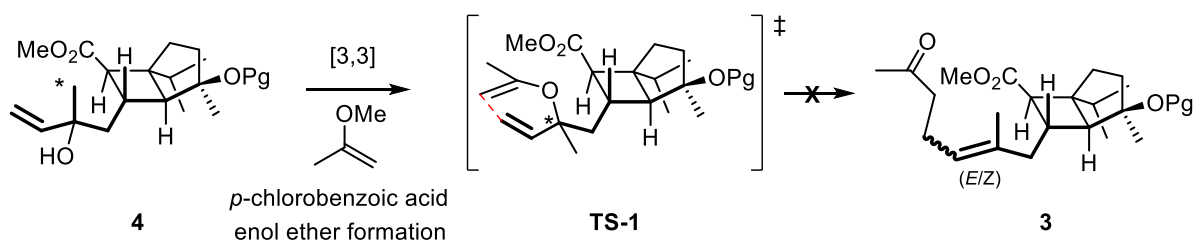
In the humilisin E project, an attempted Claisen rearrangement failed to provide a trisubstituted alkene precursor **3** (Scheme 6.1a/b). Previously, similar ketone Claisen rearrangements were reported in the group by Bruce *et al.*<sup>117</sup> In this study, linalool, a tertiary alcohol, was a viable substrate (51 % yield, 60:40 *E:Z* selectivity), but the more hindered substrates failed to react.

Claisen rearrangements with tertiary alcohol-derived enol ethers are known to be slow, and they are typically non-stereoselective.<sup>118</sup> Presumably, when starting materials with bulky substituents are used, the pseudoaxial positioning of substituents during the rearrangement process often results in products lacking stereochemical control.<sup>116,118</sup> Presumably, the reason for the lack of stereoselectivity in the Claisen rearrangement results from the alkyl chain ending up in a pseudoaxial position in the transition states (see Scheme 6.1c).

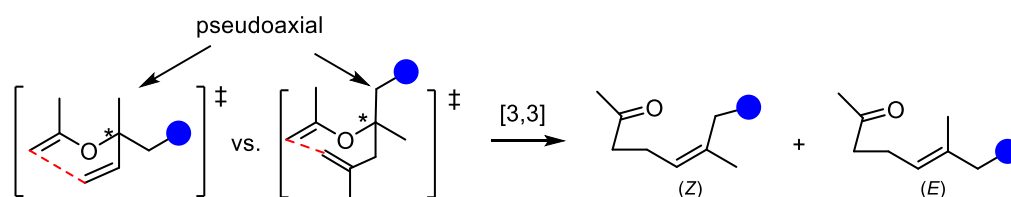
**a) Retrosynthetic analysis of 2 via intermediate 3**



**b) Verma & Pihko, unpublished**



**c) Even if the Claisen rearrangement proceeds, it is not stereoselective with tertiary alcohols**

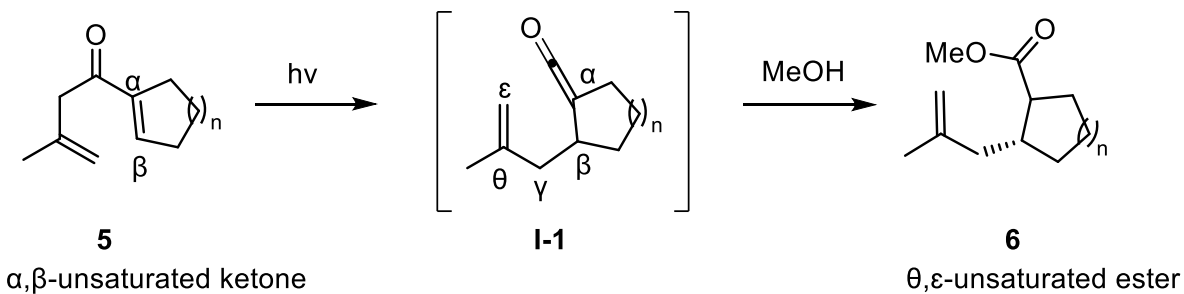


**Scheme 6.1.** Retrosynthetic scheme for the formation of (*Z, E*)-pre-diene **2** (a), unpublished results for Claisen rearrangement of tertiary alcohols (b), and an explanation for the non-stereoselectivity of the Claisen rearrangement with tertiary alcohols (c).<sup>117</sup>

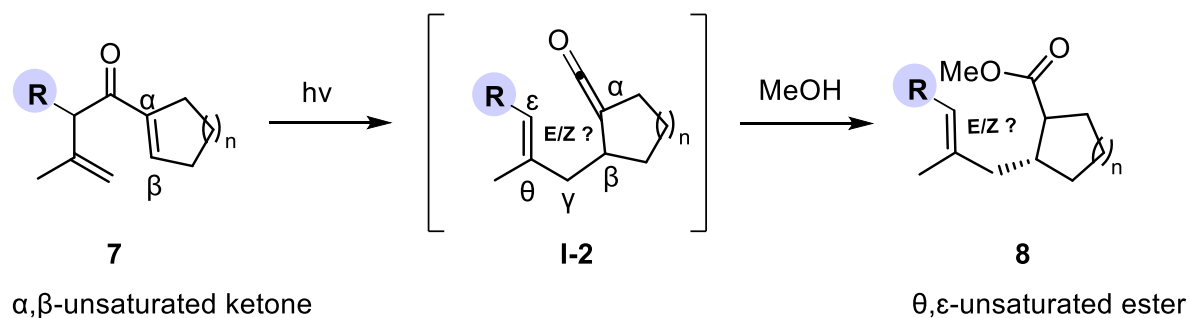
As described above, Claisen rearrangement with tertiary alcohol is known to be sluggish and non-stereoselective. Other alternative methods are needed since Claisen rearrangement does not afford trisubstituted alkenes in the middle of the chain. One alternative could be the photochemical methods tested in this experimental part. In 1973, Agosta and Smith<sup>119</sup> published

a photochemical variant of the Cope rearrangement that converted cyclic unsaturated dienone **5** to the corresponding unsaturated ester **6** via the ketene intermediate **I-2** (Scheme 6.2a). However, variants (**7**) that would lead to trisubstituted alkenes (**8**) were not tested in this study, and consequently, no information was available on the effect of substituents on (*Z/E*)-selectivity (Scheme 6.2b).

**a) 1973 Agosta & Smith precedent**



**b) Extension to trisubstituted alkenes**

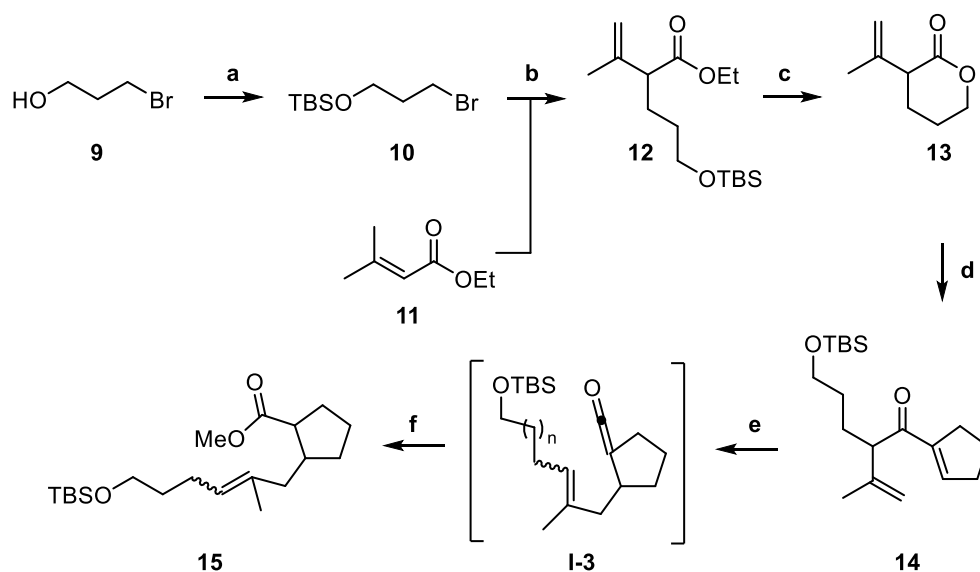


**Scheme 6.2.** Photochemical Cope rearrangement reported by Agosta & Smith<sup>119</sup> (**a**) and unexamined extension to trisubstituted alkenes (**b**).

In other words, an alternative method to the Claisen rearrangement was studied in this experimental part. Photo-Cope rearrangement reactions were an interesting research topic, as there is no information available on the stereoselectivity when variant **7**, leading to a trisubstituted alkene **8**, is used. In addition, it was also unknown whether the reaction would tolerate substituents at all, so these became interesting research questions for the experimental part of the project.

## 7 Work plan

The initial synthetic route outlined for the preparation of model dienone **14** and the planned photochemical experiments towards trisubstituted alkene **15** is shown in Scheme 7.1. However, the original plan had to be modified as problems appeared along the way. According to the original plan, the synthesis would start with the protection of 3-bromo-1-propanol **9**. After this step, the idea was to prepare ethyl ester **12** by performing alkylation reaction between TBS-protected bromoalcohol **10** and enoate **11**. The alkylation product would undergo desilylation and cyclization, resulting in the formation of lactone **13**. Dienone **14** could be formed from the lactone *via* the addition of cyclopentenyllithium or the corresponding Grignard reagent. The Shapiro reaction would be used to produce the vinyl lithium species required for this step. The final step, photo-Cope reaction, is used for converting the unsaturated dienone **14** to the corresponding unsaturated ester **15** *via* the ketene intermediate **I-3** (see Scheme 7.1).

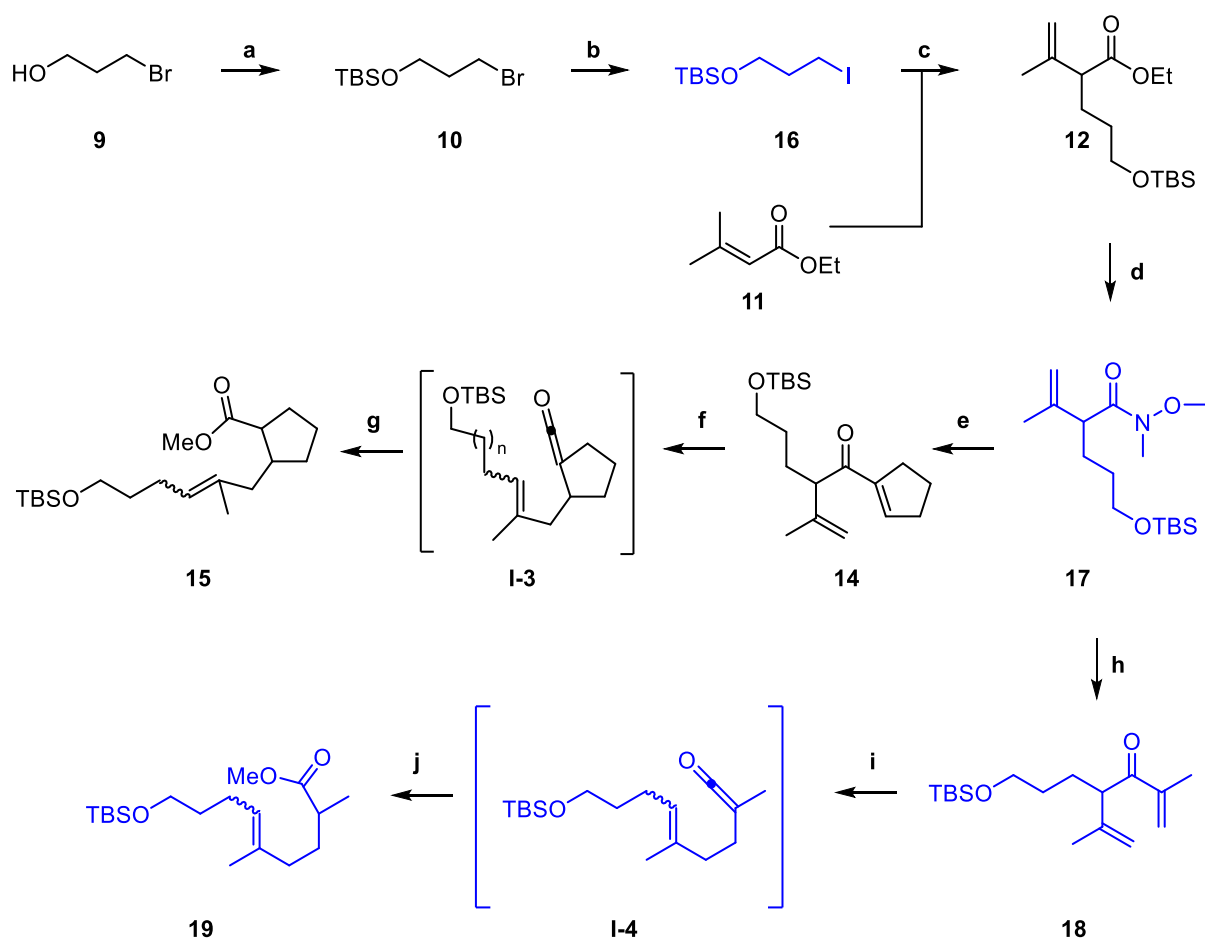


**Scheme 7.1.** The original synthesis plan. **a)** TBS, imidazole, THF, rt.; **b)** LDA, THF,  $-78\text{ }^{\circ}\text{C} \rightarrow \text{rt.}$ ; **c)**  $\text{H}^+$ , TMSOEt, rt.  $\rightarrow 60\text{-}80\text{ }^{\circ}\text{C}$ ; **d)** 1-Cyclopentenyllithium, PgX, rt.  $\rightarrow -78\text{ }^{\circ}\text{C}$ ; **e)** and **f)** MeOH,  $h\nu$ , rt.

The first change to the original plan was made when the alkylation of enoate **11** with TBS-protected bromoalcohol **9** failed to provide an alkylated ester **12**. Based on the previously performed test alkylation of enoate **11** with ethyl iodide, the alkylation with iodide was successful and the substitution product was selectively formed. Thus, the first change was the replacement of the halogen in the TBS-protected bromoalcohol **10** from Br to I with the

Finkelstein reaction. The second and biggest change was to prepare the corresponding Weinreb amide **17** (see Scheme 7.02) directly from ethyl ester **12** without silyl deprotection. This change was made because the lactone **13** was very unstable and highly polymerizable, and it could not be isolated from the reaction mixture in pure form. In addition to cyclopentenylketone **14**, isopropenyl ketone **18** was used as a second starting material for photochemical reactions. The reaction was expected to produce an acyclic trisubstituted alkene **19** *via* an intermediate **I-4**.

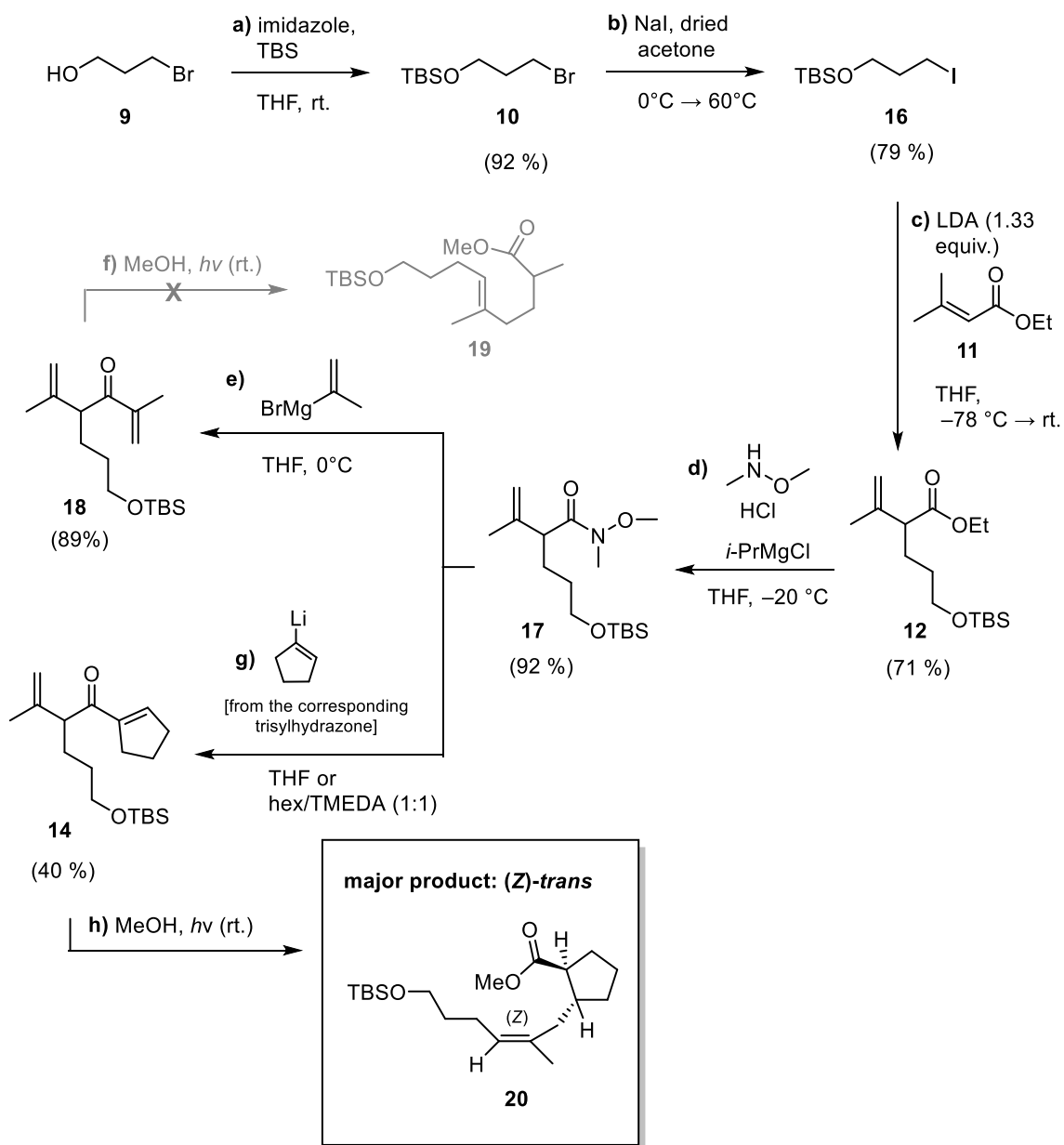
An alternative synthesis plan is shown in Scheme 7.2 and significant changes compared to the original plan are highlighted in blue.



**Scheme 7.2.** The alternative synthesis plan. **a)** TBS, imidazole, THF, rt.; **b)** NaI, acetone, 60 °C; **c)** LDA, THF, -78 °C → rt.; **d)** *i*-PrMgCl, CH<sub>3</sub>ONHCH<sub>3</sub> · HCl, THF, -20 °C; **e)** 1-cyclopentenyllithium, THF or Hex/TMEDA (1:1), rt. → -78 °C; **f)** and **g)** MeOH, *hν*, rt.; **h)** *i*-PrMgBr, THF, 0 °C, **i)** and **j)** MeOH, *hν*, rt.

## 8 Execution of work plan

The revised synthesis of trisubstituted alkene **20** and its progress are shown in Scheme 8.1. The Photo-Cope reaction performed on cyclopentenyl ketone **14** produced a mixture of four different isomers, and the major product was determined to be the (*Z*)-*trans* alkene **20** shown in Scheme 8.1. The photo-Cope reaction performed on isopropenyl ketone **18** failed to provide ketone **19**, so this experiment (step f) is shaded gray.

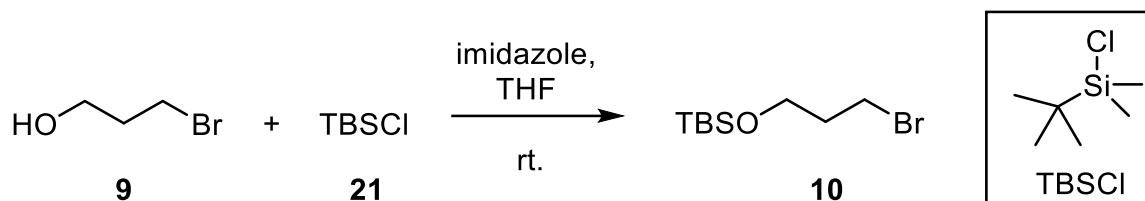


**Scheme 8.1.** Accomplished synthesis route for (*Z*)-*trans* alkene **20**.



## 8.1 TBS protection of 3-bromo-1-propanol

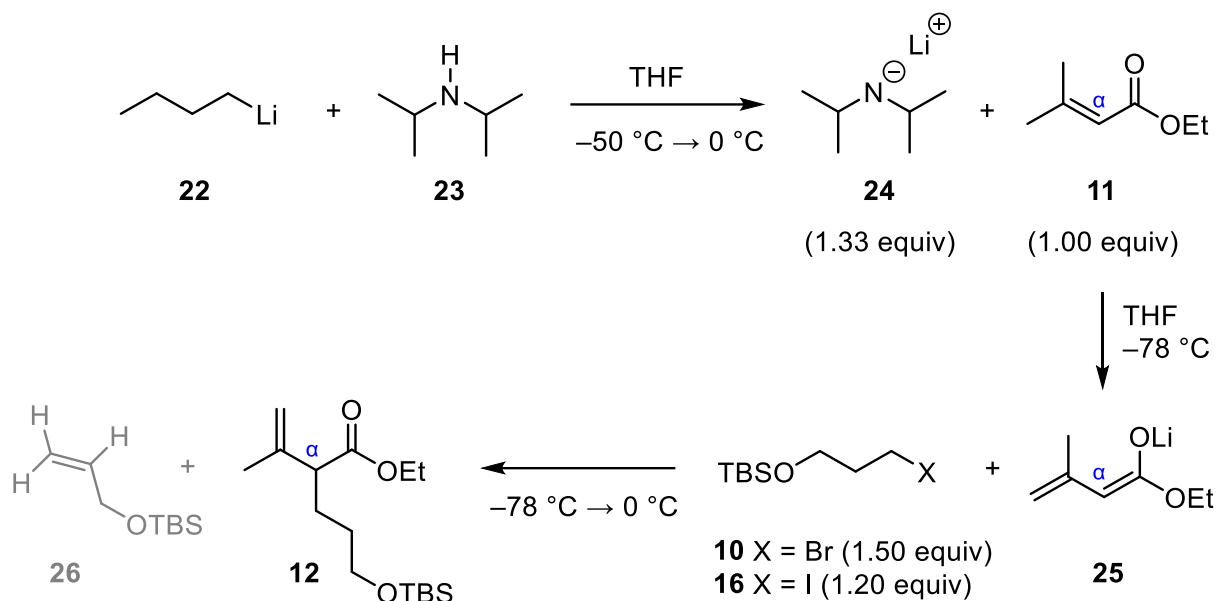
The first step of the synthesis was the addition of TBSCl protecting group **21** to 3-bromo-1-propanol **9** (see Scheme 8.1.1). TBS-protected bromoalcohol **10** was successfully produced earlier in the short research project (KEMS9800) *via* silylation of 3-bromo-1-propanol **9**, and the reaction was optimized in the experimental part of this thesis. TBS protection was selected due to the bulk structure of the TBSCl-group, which provides significant stability to protected alcohol. Thus, the compound withstands different reaction conditions and is more suitable for complex synthesis routes. In addition, the larger size of the TBSCl-group, compared to for example smaller silyl ethers, partly prevents unwanted reactions.<sup>120</sup> The reaction was performed in conditions previously reported in the literature.<sup>121</sup> Based on TLC analysis, the reaction proceeded to completion and was mostly uneventful. During the short research project, it was found that purification of the reaction significantly reduces the yield. Because of this result, it was decided to continue with a slightly impure product and do the purification in a later reaction step.



**Scheme 8.1.1.** The synthesis of TBS-protected bromoalcohol **10**.

## 8.2 Alkylation reaction

Next came one of the most critical but also challenging steps of the synthesis plan, *i.e.* the alpha alkylation of ethyl ester **11** with TBS-protected halide (Scheme 8.2.1). The alkylation reaction was carried out by adapting the procedure found in the literature for 2-ethyl-3-methylbut-3-en-1-ol.<sup>122</sup> The alkylation step consisted of two reactions: LDA was first prepared by deprotonating di-isopropyl amine (**23**) using *n*-BuLi (**22**) at  $-50\text{ }^{\circ}\text{C}$ . After that, LDA **24** deprotonated the ester **11** giving the dienolate (**25**) as an intermediate. Finally, the halide (**10** or **16**) was added dropwise to the reaction mixture at  $-78\text{ }^{\circ}\text{C}$ . The alkylation reaction was optimized during my short research project (see summary in Table 8.2.1) and the optimized procedure was used in this work for scale-up.

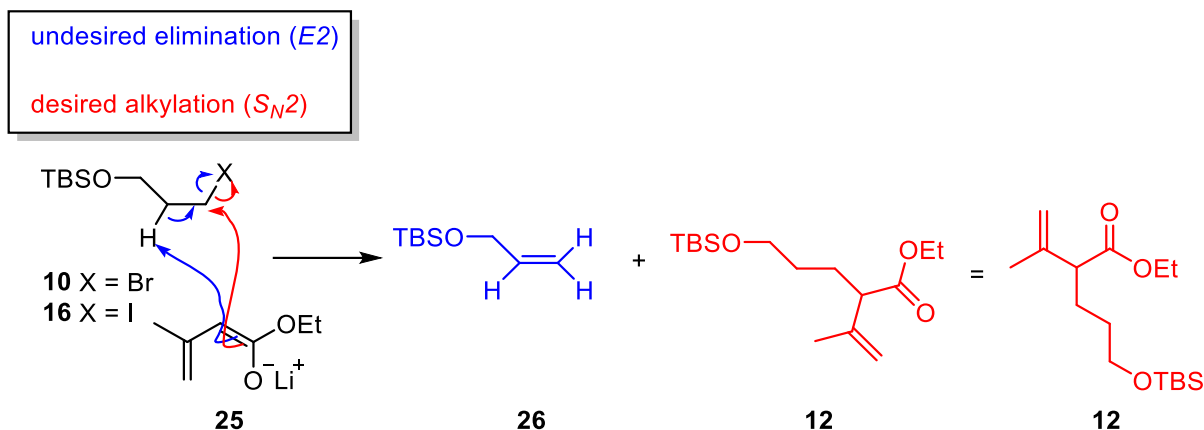


**Scheme 8.2.1.** Synthesis of alkylated ester **12**.

**Table 8.2.1.** Optimization of the synthesis of alkylated ester **12**

Experiment	X	Scale (g)	Equiv (11)	Equiv (24)	Reaction time in total (h)	Product(s)
1	Br	1.00	1.50	1.20	5	<b>12:26</b> (1:1)
2	I	0.30	1.33	1.20	5	<b>12</b>

As previously described in my short research project report, the alkylation reaction with bromide **10** at a 7.8 mmol scale was only partially successful. The desired alkylation product **12** was formed, but the selectivity of the reaction was compromised by a competing elimination reaction, resulting in the formation of alkylated ester **12** and unwanted allyl ether **26** in ca. 1:1 ratio based on crude  $^1\text{H}$  NMR. In other words, roughly half of the alkylation agent was lost *via* competing elimination. However, the control experiment performed in a short research project with ester **11** and ethyl iodide (EtI) under the same conditions was fully selective and the alkylation product **12** was isolated with 85 % yield. This result suggested that changing the halogen-leaving group from Br to I might suppress the competing elimination (see Scheme 8.2.2). The result contrasts with the computationally derived trend in which conversion to iodide accelerates elimination ( $E2$ ) more than substitution ( $S_N2$ ).<sup>123</sup>



**Scheme 8.2.2.** Mechanisms for elimination ( $E2$ ) and substitution ( $S_N2$ ) reactions.

Based on the result of the control experiment, it was decided to perform halogen exchange by Finkelstein reaction (presented in subchapter 8.3). Alkylated ester **12** could be isolated since the alkylation with TBS-protected iodine alcohol **16** was completely selective. Alkylation experiments with iodide on a larger scale are presented in Table 8.2.2. Based on TLC analysis, the iodide **16** was not completely consumed even though the first experiment was continued overnight. The poor yield of the first experiment was caused by the failure of purification due to the too short column and the silica layer.

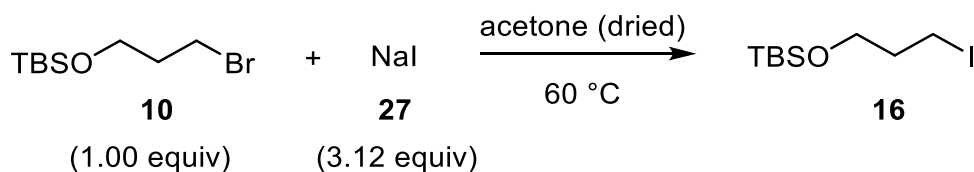
**Table 8.2.2.** Scaling up the alkylation reaction

Experiment	X	Scale (g)	Equiv ( <b>11</b> )	Equiv ( <b>24</b> )	Reaction time in total (h)	Product (yield)
1	I	1.13	1.33	1.20	22	<b>12</b> (49 %)
2	I	1.63	1.33	1.20	5	<b>12</b> (71 %)

The halogen exchange from bromine to iodine facilitates alkylation due to chemical properties that make iodine a better leaving group.<sup>123</sup> The iodide ion ( $I^-$ ) is bigger and less electronegative compared to the bromide ion ( $Br^-$ ). A better-leaving group, in this case,  $I^-$  stabilizes the negative charge more effectively after leaving the molecule. This behavior is caused by its larger size and lower charge density. There have not been (many) studies explaining the improvement in selectivity in the past, so there is no definitive knowledge of the reasons for it.

### 8.3 Finkelstein reaction

To obtain the iodide **16** required for the alkylation (see subchapter 8.2 above), halogen exchange was performed using conditions previously reported in the literature.<sup>124</sup> TBS-protected iodoalcohol **16** was afforded in my short research project, but the halide exchange reaction was optimized in this study. The halogen exchange reaction was carried out with sodium iodide **27** as presented in Scheme 8.3.1. In practice, the reaction appeared to proceed to completion by TLC analysis in all cases when an excess of sodium iodide was used, and the **16** was successfully purified. This type of reaction usually produces no impurities, and in this case, the same observation was made. Although the reaction yield was good (~80 %), it could be better when compared to the 93 % yield reported in the literature. A small amount of **10** remained in the mixed fraction, as it was difficult to distinguish **10** and **16** from each other due to the almost identical  $R_f$  value.



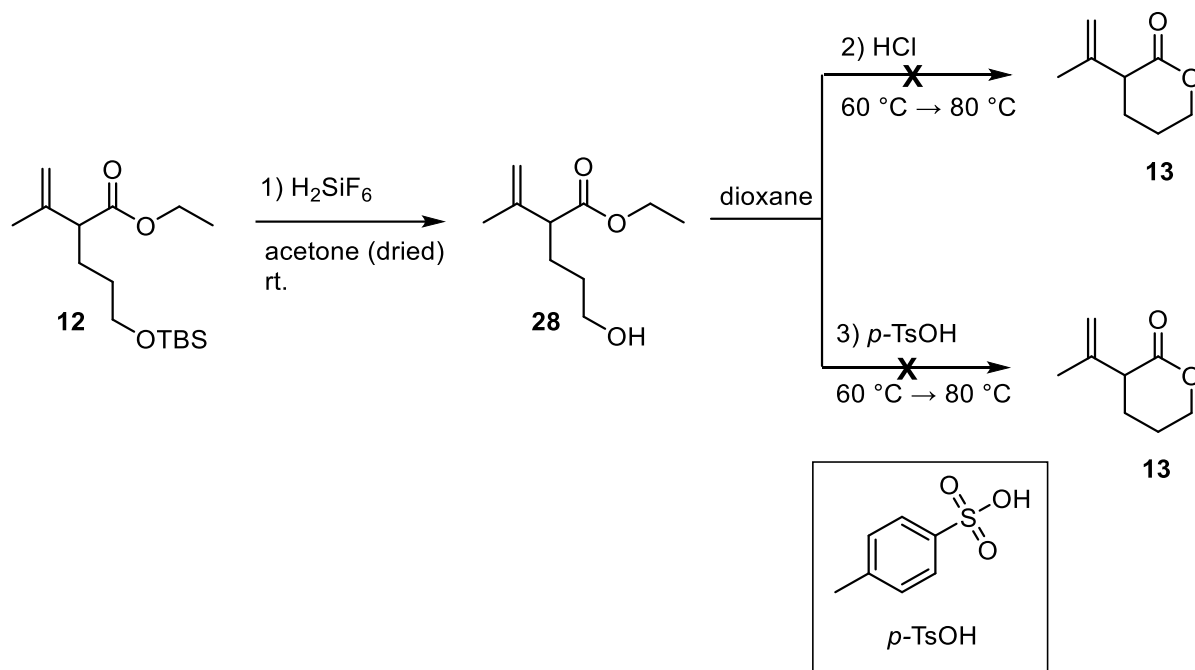
**Scheme 8.3.1.** Synthesis of TBS-protected iodoalcohol **16**.

### 8.4 Deprotection and lactonization attempts

The next step was the removal of the TBS-group and preparation of the lactone **13** from the alkylated ester **12**. No procedure for lactonization of this kind has been reported in the literature, so it was decided to perform the test experiments on a vial scale using a heat block. Acidic conditions were used in the reactions, as (very) basic conditions would cause the lactone to open and hydrolyze to the carboxylate ion. Dioxane was chosen as the co-solvent, because for example methanol would cause the formation of methyl ester instead of lactone, and ether would prevent mixing. In both experiments, a complex mixture of different products was formed. Based on the broad peaks of the <sup>1</sup>H NMR spectrum, polymerization had occurred.

Based on the first experiment, hexafluorosilicic acid (H<sub>2</sub>SiF<sub>6</sub>) effectively removed the TBS-protection group, but cyclization did not take place and consequently, lactone **13** was not formed. This behavior can be explained by the fact that H<sub>2</sub>SiF<sub>6</sub> is not a very strong acid. After

H<sub>2</sub>SiF<sub>6</sub>-promoted desilylation and workup, the crude alcohol **28** was dissolved in dioxane and divided into two vials. Either 0.5 equiv HCl (aq) or *p*-TsOH were added (see Scheme 8.4.1 and Table 8.4.1). To promote the desired cyclization, the reactions were heated first to 60 °C and then to 80 °C. However, the cyclization failed to provide lactone **13** based on <sup>1</sup>H NMR spectra.



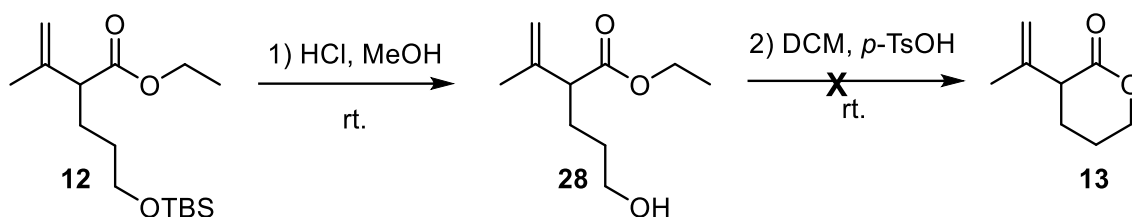
**Scheme 8.4.1.** Lactonization reactions with H<sub>2</sub>SiF<sub>6</sub> in dried acetone and aq. HCl or *p*-TsOH in dioxane.

**Table 8.4.1.** Conditions of the reactions that are presented in Scheme 8.4.1

Experiment	Scale (mg)	Reaction time, lactonization (h)	Reaction time, cyclization (h)	Yield ( <b>13</b> )
1	50	3	-	-
2 / 3	27	-	4	-

In the next test experiment, HCl (0.5 equiv) in dioxane was used, but this experimental setup did not lead to the formation of lactone **13** either. Alternatively, one-pot desilylation and cyclization were also attempted with aq. HCl in MeOH and *p*-TsOH in DCM (see Scheme 8.4.2 and Table 8.4.2).<sup>125,126</sup> Based on TLC analysis, the desilylation proceeded to completion in the first experiment, but a small amount of alcohol **28** remained unreacted in the cyclization reaction. In this experiment, the crude product was a complex mixture of polymers as well. An

attempt to purify the crude product after the *p*-TsOH/DCM test also failed to provide the lactone **13** in pure form.



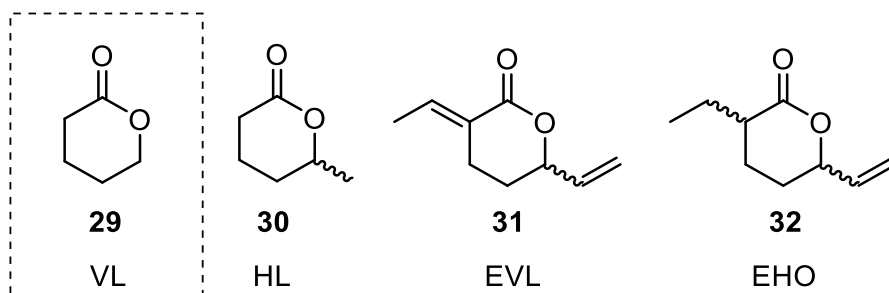
**Scheme 8.4.2.** Lactonization reactions with aq. HCl in MeOH and *p*-TsOH in DCM.

**Table 8.4.2.** Conditions of the reaction that are presented in Scheme 8.4.2

Experiment	Scale (mg)	Reaction time, lactonization (min)	Reaction time, cyclization (h)	Yield ( <b>13</b> )
1	50	70	2	-
2	100	70	2.5	-

In both experiments, the desilylation succeeded but the cyclization did not. Based on the lit.<sup>127</sup>, ring-opening polymerization (ROP) together with chain polymerization, might have occurred. Six-membered lactones are known to be prone to polymerization.<sup>127</sup> Although 6-membered rings do not usually show significant strain, the presence of substituents can affect their reactivity and vulnerability to polymerization.

Duparc *et al.*<sup>128</sup> discovered in their study that substituents on the  $\delta$ -valerolactone VL (**29**) ring (Figure 8.4.1) significantly affect monomer polymerizability, regardless of the catalyst or operating conditions. Furthermore, based on thermodynamic studies,  $\delta$ -hexalactone HL (**30**) has a much higher reactivity (polymerization rate) in mass or solution than analogous 5-alkyl- $\delta$ -valerolactones, e.g. 2-ethylidene-6-hepten-5-olide EVL (**31**) and 2-ethylheptane-5-olide EHO (**32**), with longer alkyl substituents (Figure 8.4.1).<sup>128</sup>



**30** polymerizes easily, **31** and **32** are relatively stable

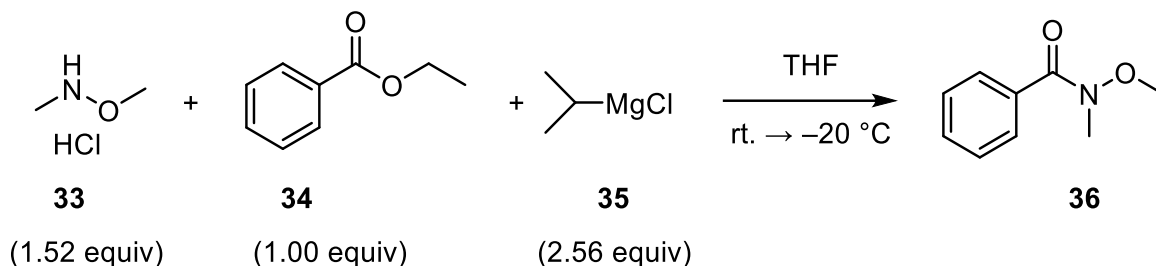
**Figure 8.4.1.** 6-membered ring (substituted)  $\delta$ -valerolactones.

In summary, 6-membered lactones tend to decompose and/or polymerize easily. Deeper analysis of the responsible factor(s) for the decomposition of lactones was not possible at this time. For example, too harsh reaction conditions might expose itself to polymerization, which is why cyclization could have also been tested in milder conditions. To save time, these experiments were not done and another way of making the ketone was planned. The most potential option was to make the corresponding Weinreb amide **17** from alkylated ester **12**. This reaction could be used to prepare the cyclopentenyl ketone **14** directly without removing the silyl protection.

## 8.5 Weinreb amide synthesis

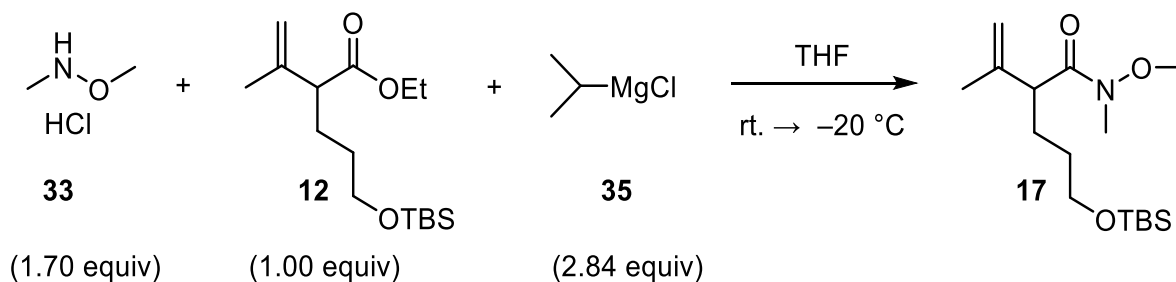
In the next step, Weinreb amide **17** was prepared by the reaction between *N,O*-dimethylhydroxylamine hydrochloride **33**, isopropyl magnesium chloride (*i*-PrMgCl) **35**, and alkylated ester **12**. *N*-methoxy-*N*-methylamides, also known as Weinreb amides, have become common in the conversion of esters to ketones.<sup>129</sup> They are versatile synthetic precursors and effective acylating agents in organic synthesis. Weinreb amides can be synthesized from lactones, carboxylic acids, and esters through various synthetic routes.<sup>130</sup>

In a preliminary experiment, the quality of *i*-PrMgCl solution **35** was checked by using ethyl benzoate **34** instead of the alkylated ester **12** (see Scheme 8.5.1). This experiment afforded the desired *N*-methoxy-*N*-methylbenzamide **36** (102 % mass balance, with 2 mol% EtOAc remaining in the product).



**Scheme 8.5.1.** Test experiment for the Weinreb amide synthesis.

After the successful test experiment, the actual Weinreb amide synthesis was carried out, using the reaction conditions presented in the literature.<sup>131</sup> In the reaction, nucleophilic acyl substitution of alkylated ester **12** with **33** produced the desired Weinreb amide **37** (see Scheme 8.5.2). Based on the TLC analysis, the ester **12** was not completely consumed in 1.5 hours. However, the major product in the crude reaction mixture was the desired Weinreb amide **17** (92 % yield), and the crude product was used in the next step without further purification.

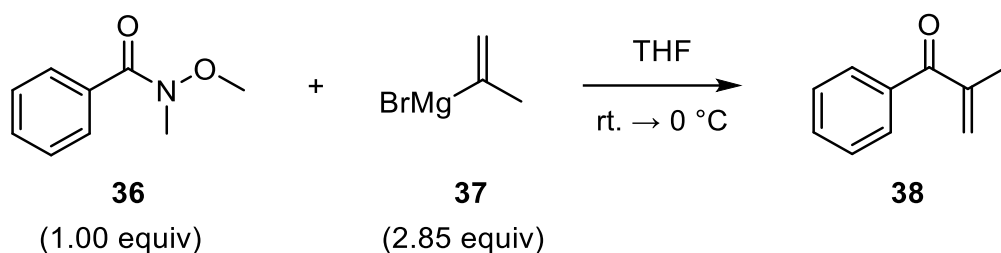


**Scheme 8.5.2.** Synthesis of Weinreb amide **17**.

## 8.6 Weinreb ketone synthesis

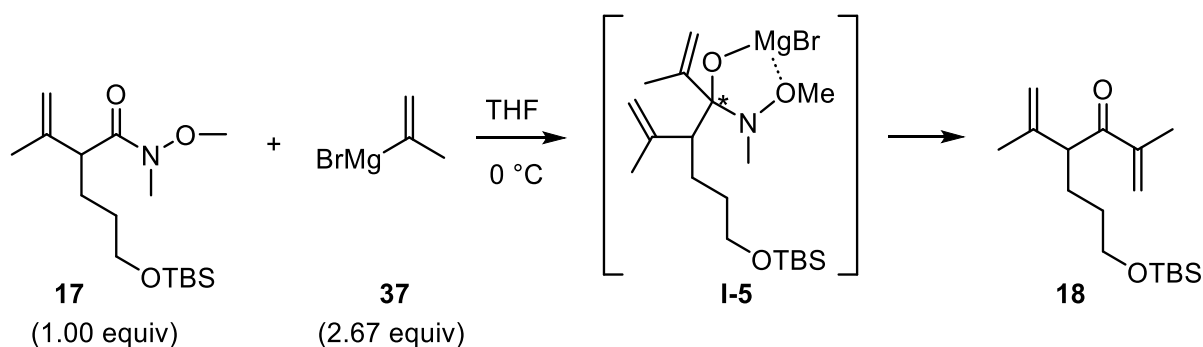
To prepare the second substrate **18** for the photo-Cope experiments, the commercially available isopropenyl magnesium bromide (*i*-PrMgBr) **37** was used as a nucleophile. Before using the reagent with the Weinreb amide **17**, the quality of **37** was tested by carrying out a test experiment with *N*-methoxy-*N*-methylamides **36** (see Scheme 8.6.1) which afforded the desired enone **38** (146 % mass balance with THF remaining in the product).





**Scheme 8.6.1.** Synthesis of test experiment for *i*-PrMgBr **37**.

Weinreb enone substrate **18** was prepared by the Grignard reaction between isopropenylmagnesium bromide **37** and Weinreb amide **17** (see Scheme 8.6.2). First in the Weinreb ketone synthesis, the Grignard reagent **37** reacts as a nucleophile at the carbonyl carbon of the Weinreb amide **17**, forming a tetrahedral intermediate during **I-5**. This intermediate is stabilized by chelation from the methoxy group present in the Weinreb amide and the isopropenyl ketone **18** forms during the workup.



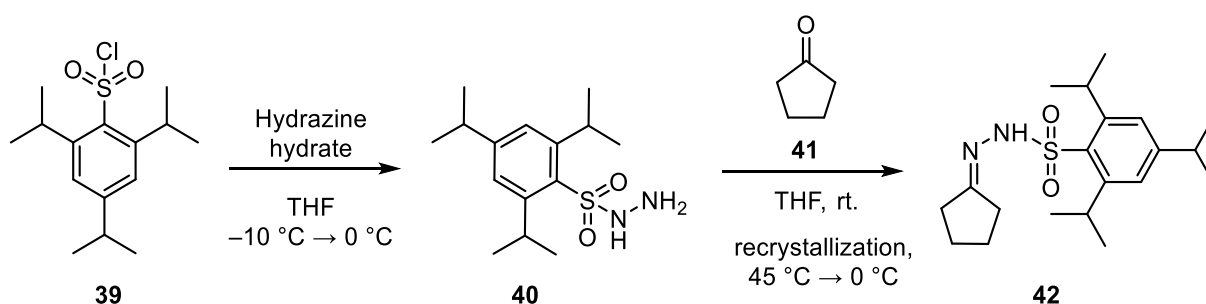
**Scheme 8.6.2.** Synthesis of isopropenyl ketone **18**. The stereogenic center is marked with an asterisk in **I-5**.

In practice, the Weinreb ketone synthesis was carried out by adding **37** to a cooled (0 °C) reaction mixture. The reaction proceeded to completion in 1 h. The purification of the product failed at the first time, as the product decomposed and radical polymerization occurred. This experiment suggested that the desired isopropenyl ketone **18** is easily degradable and/or polymerizable. Therefore, in the second experiment, a small amount of BHT was added to the fractions containing the product as a stabilizer. Presumably, this allowed purification to succeed the second time. In addition, the concentration of the fractions was done more carefully at a lower temperature (30 °C) and higher pressure (approx. 100 bar), as it was concluded that the ketone is also easily volatile.

## 8.7 Shapiro reaction

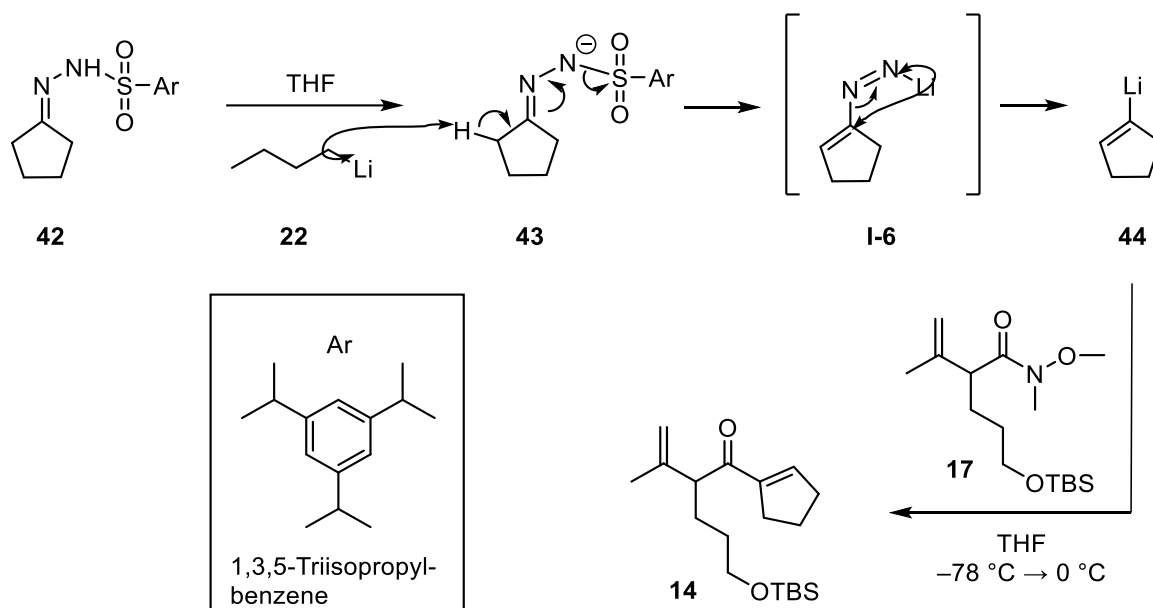
The Shapiro reaction was another critical step of the synthesis plan, as it would provide the primary substrate for the photochemical experiments bearing the cyclopentenyl ketone unit. The Shapiro reaction was chosen as a method because cyclopentenyl halides, precursors to the requisite cyclopentenyl organometallic species, are not commercially available. In addition, a corresponding example of the use of the Shapiro reaction was found in the literature.<sup>132</sup>

The first step of the Shapiro reaction was the formation of tosylhydrazone **42** from hydrazide **40**. This reaction was achieved by treating the carbonyl compound **41** with tosylhydrazide **40** in THF.<sup>133</sup> Tosylhydrazide, on the other hand, was prepared by the reaction between 2,4,6-triisopropylbenzenesulfonyl chloride **39** and hydrazine hydrate in THF (see Scheme 8.7.1).<sup>134</sup> The isopropyl groups are necessary in the ring structure, otherwise there would be a risk of lithiation occurring from the aromatic ring.<sup>135</sup>



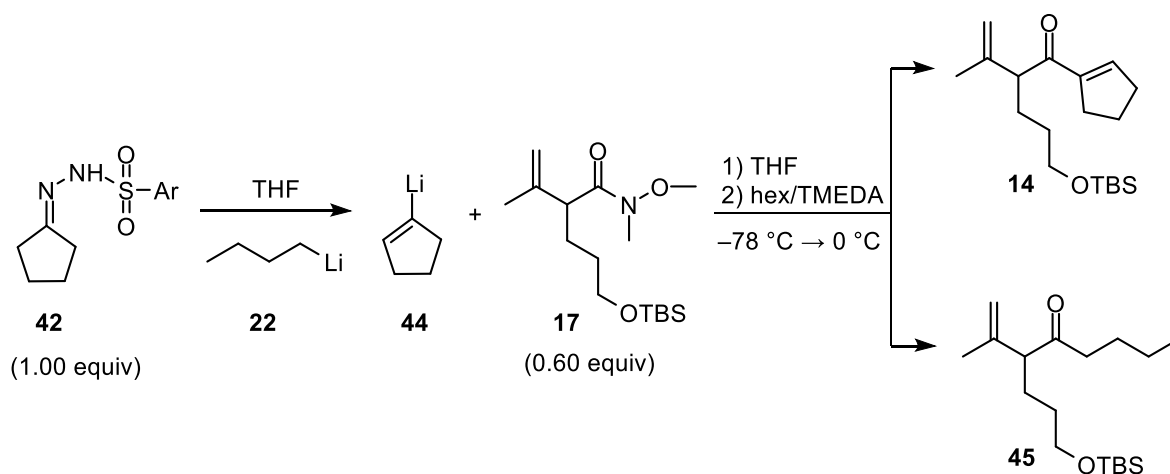
**Scheme 8.7.1.** Formation of tosylhydrazone **42**.

In the Shapiro reaction, tosylhydrazone **42** was treated with *n*-BuLi **22** which acts as a strong base deprotonating the hydrazone and generating a dianion intermediate **43**. After deprotonation, an elimination reaction occurred, and the tosylate group departed leading to the formation of a vinylolithium intermediate (in **I-6**) which is crucial to the double bond formation. In stage **I-6**, nitrogen gas was also produced which was observed as bubbling. Finally, the vinyl lithium **44** was treated with Weinreb amide **17** (see Scheme 8.7.2).



**Scheme 8.7.2.** Mechanism for the synthesis of cyclopentenyl ketone **14**. In the Scheme Ar = 1,3,5-triisopropylbenzene.

To assay the efficiency of the cyclopentenyllithium formation, two preliminary test experiments were carried out where tosylhydrazone **42** was reacted with *n*-BuLi **22** and *N*-methoxy-*N*-methylbenzamide **36** or benzaldehyde. The first experiment with **36** failed, possibly due to adventitious moisture in it. However, the second experiment, with benzaldehyde as the test electrophile, gave a promising result.  $^1\text{H}$  NMR analysis of the crude reaction mixture indicated the presence of a desired product, but most of the signals in the  $^1\text{H}$  NMR spectrum came from side products. The Shapiro reaction with the actual substrate is presented in Scheme 8.7.3 and Table 8.7.1 summarizes the experiments.



**Scheme 8.7.3.** Summary of Shapiro reaction.

**Table 8.7.1.** Reaction conditions and results of Shapiro reactions

Experiment	Solvent	Scale (mg)	Reaction time (h)	Yield of 14 (%)	Yield of 45 (%)	Other products
1	THF	600	3.5	38	34	x*
2	Hex/TMEDA (1:1)	500	3.0	40	44	no

\* More polar spot on TLC, structure is unknown

In the first Shapiro experiment, the starting materials were fully consumed as judged by TLC. Three major product spots were observed on TLC, and these products were successfully isolated and analyzed by NMR. Based on  $^1\text{H}$ ,  $^{13}\text{C}$ , HH-COSY, HSQC-edited, and IR measurements, the first two eluting products were identified as the desired cyclopentenyl ketone **14** and the undesired butyl ketone **45**. A third product was isolated, but its structure remained unknown.

For the second Shapiro experiment, it was decided to change the solvent from THF to a 1:1 mixture of hexane and TMEDA, in an attempt to suppress the formation of butyl ketone.<sup>136</sup> The second experiment also proceeded to completion and the crude reaction mixture was successfully purified. TLC analysis of the second experiment was similar to the TLC of the first experiment, but the spot corresponding to the third, more polar (side)product appeared missing. The overall yield of the second experiment was slightly better than the first (40 % vs. 38 %), but on the other hand, 10 % more unwanted butyl ketone **45** was also formed. In summary, it can be said that in both cases the yield was moderate, unwanted side reaction(s) occurred, and solvent change had no significant effect on yield.

Although the Shapiro reaction was simple and fairly straightforward, it also produced butyl ketone **45** as an unwanted byproduct. To circumvent this problem, an alternative could be the use of *sec*-BuLi instead of *n*-BuLi as the lithiating reagent. The branched structure of *sec*-BuLi renders it effectively a stronger base. However, fresh *sec*-BuLi was not available at this time, and for this reason, this base was not used in this project. Alternatively, an incorrect titration result of *n*-BuLi could also explain the formation of butyl ketone because an excess of *n*-BuLi would have reacted directly with a Weinreb amide **17**. Since the Shapiro reaction was challenging to optimize, other methods such as Barton vinyl iodide synthesis<sup>137</sup> were considered to form cyclopentenyl lithium **14**. However, due to a lack of time, the original plan was followed.

## 8.8 Photo-Cope Rearrangement

The photo-Cope rearrangement reactions were explored with the enone substrates **14** and **18** (Figure 8.8.1).

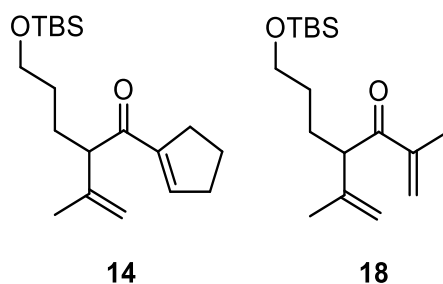
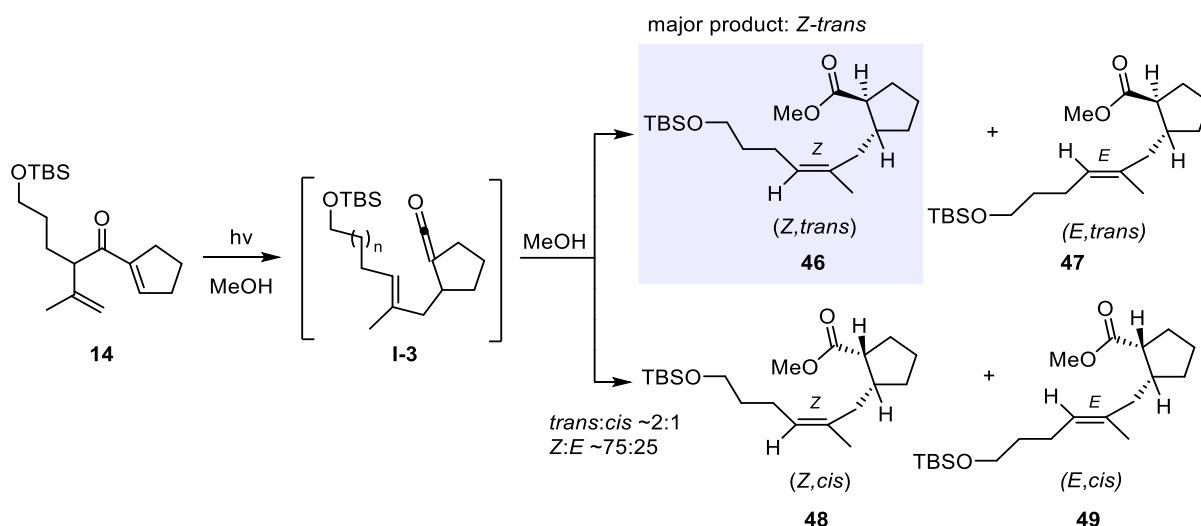


**Figure 8.8.1.** Starting materials for the photo-Cope rearrangement.

Irradiation of isopropenyl ketone **18** for 2 hours did not lead to the occurrence of the photo-Cope reaction and only the starting material **18** was recovered. On the other hand, irradiation of the cyclic unsaturated dienone, cyclopentenyl ketone **14**, led to the photo-Cope rearrangement and the formation of four isomers of the unsaturated ester **15** via the ketene intermediate **I-3** (see Scheme 8.8.1). Further details of the reactions are presented in Table 8.8.1.

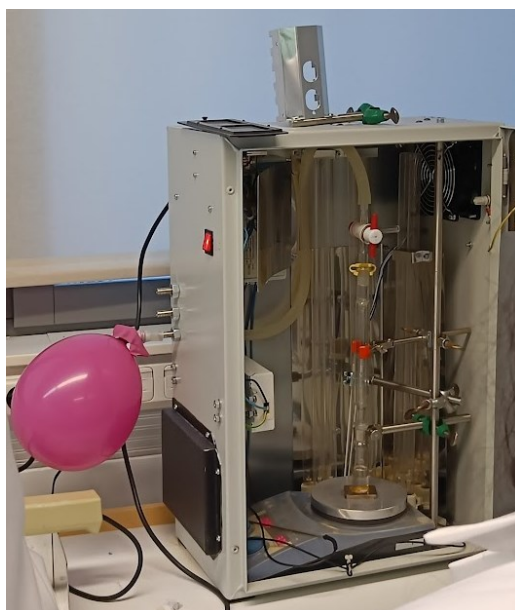


**Scheme 8.8.1.** Photo-Cope rearrangement for cyclopentenyl ketone **14**.

**Table 8.8.1.** Reaction conditions and results of the photo-Cope experiments of **14**

Experiment	Amount of <b>14</b> (mg)	Solvent (mL)	Irradiation time (min)	<b>14</b> left (%)	Product (mg)	Notes
1	16.2	12	90	5.4	122.4	Weighing/ taring error
2	28.2	18	65	11	99.8	Weighing/ taring error
3	17.5	15	65	30	25.3  (145 % mass balance)	Grease in the product

Experimentally, the reactions were carried out in a quartz flask at ca. 5.4 mM concentration in MeOH. The progress of the reaction was analyzed by TLC. The reaction mixtures were irradiated under Ar at rt. in a photoreactor (Figure 8.8.2). No external cooling was used during the experiments and the emission wavelength was 253.4 nm (TUV PL-L 60W/4P HO 1CT/25 lamps).

**Figure 8.8.2.** The equipment for photochemical reactions.

In the case of dienone **14** the reactions proceeded to completion as judged by TLC, but the  $R_f$  value of the final product **15** (mixture of **46**, **47**, **48**, and **49**) was almost identical compared to dienone **14**. However, dienone **14** was colored red with vanillin, differing from the light blue color of **15**. These differences allowed these compounds to be distinguished on the TLC plate. The reaction time of approx. an hour was not necessarily enough, because in the first experiment, the irradiation time was the longest and there was comparatively the least amount of starting material left. However, the product distribution remained very similar in all photo-Cope experiments, based on the  $^1\text{H}$  NMR integrals of the  $\text{OCH}_3$  peaks.

Although the photo-Cope reactions with cyclopentenyl ketone **14** appeared to proceed to completion without appreciable side product formation, the true yields could not be determined reliably. Enone **14** is volatile, and evacuation of the quartz flask was not possible, resulting in weighing or taring errors when transferring the substrate to the photochemical flask. However, the literature precedent<sup>119</sup> suggests that the photochemical Cope rearrangement, as well as conversion to the methyl ester, are essentially quantitative reactions. The key question was whether the reactions were (*E/Z*) selective, and this will be discussed below.

Purification was successful by column chromatography with an  $\text{Et}_2\text{O}$ /pentane gradient run. However, a splitting of the methyl peak of the methyl ester ( $\text{OCH}_3$ ) was observed in the  $^1\text{H}$  NMR spectrum, which indicated a mixture of several isomers. Based on the four  $\text{OCH}_3$  peaks, the isolated product was a mixture of four isomers: **46**, **47**, **48**, and **49** (see Figure 8.8.3).

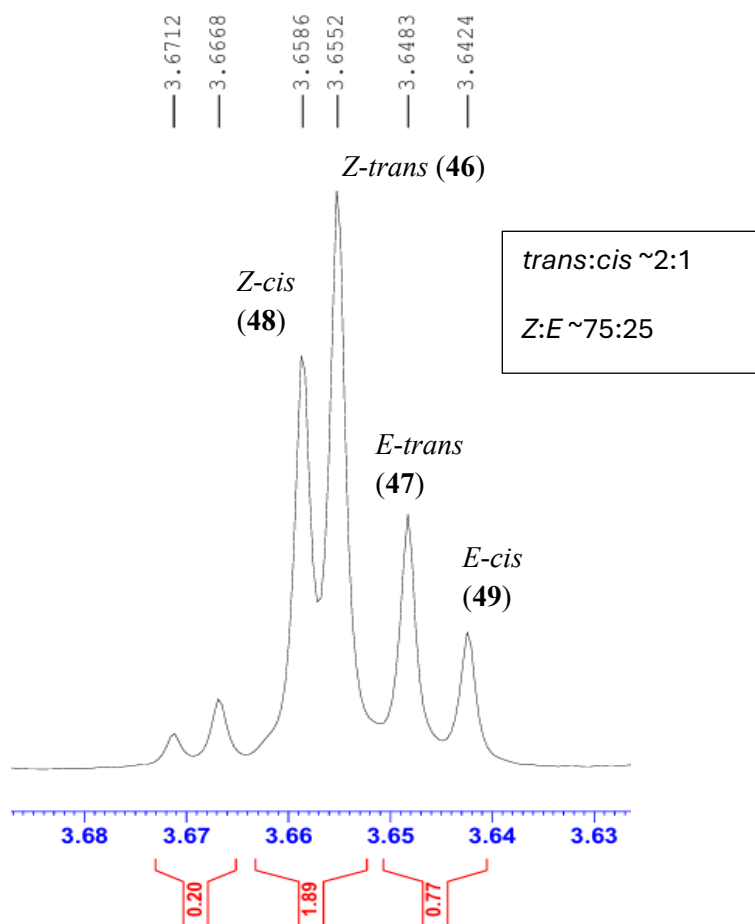


**Figure 8.8.3.** Methyl peaks of four isomers of **15** (tentative assignment). The figure is taken from Appendix 35.

The stereochemistries were confirmed using 1D-NOE experiments and various 2D techniques: HH-COSY, NOESY, and HSQC-edited. For example, HH-COSY helped to determine the spin systems in the molecule and HSQC-edited was useful in assigning the key signals and identifying the carbon-hydrogen connections. *Cis*- and *trans*-products were formed in an estimated ratio of 2:1, which also corresponds to the results presented in the literature<sup>119</sup>. Importantly, Agosta and Smith<sup>119</sup> were able to separate the *trans* and *cis* isomeric esters in their study. Based on their reported <sup>1</sup>H NMR data and their assignment, herein the chemical shifts of the alpha proton (H2) of the *trans* isomer (see numbering Figure 8.8.4) can be assumed to be smaller as well. Accordingly, the tentative ratio of *trans/cis* isomers is based on integrals of the <sup>1</sup>H NMR peaks at 2.84 ppm (*cis*) and 2.34 ppm (*trans*), as seen in Figure 8.8.4.



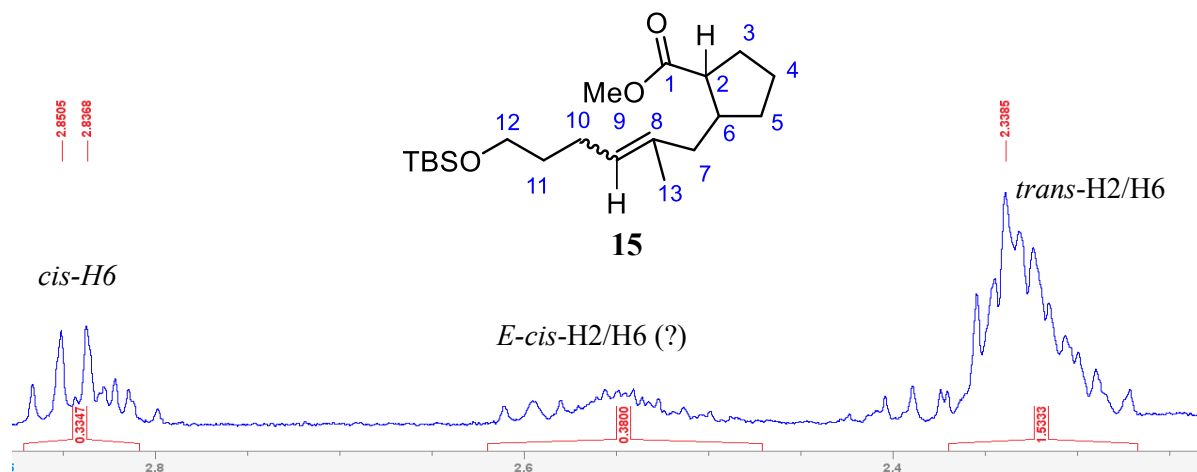


**Figure 8.8.4.** Tentative assignment of the peaks of *cis/trans*-isomers.

The stereochemistry was determined by selectively irradiating the H9-proton in 1D NOE experiments. In these experiments, NOE interactions with protons H2/H6, H10, H11, H12, and H13 were revealed (Figure 8.8.5). This information helped to determine the relative stereochemistry of product **15** as (*Z*).

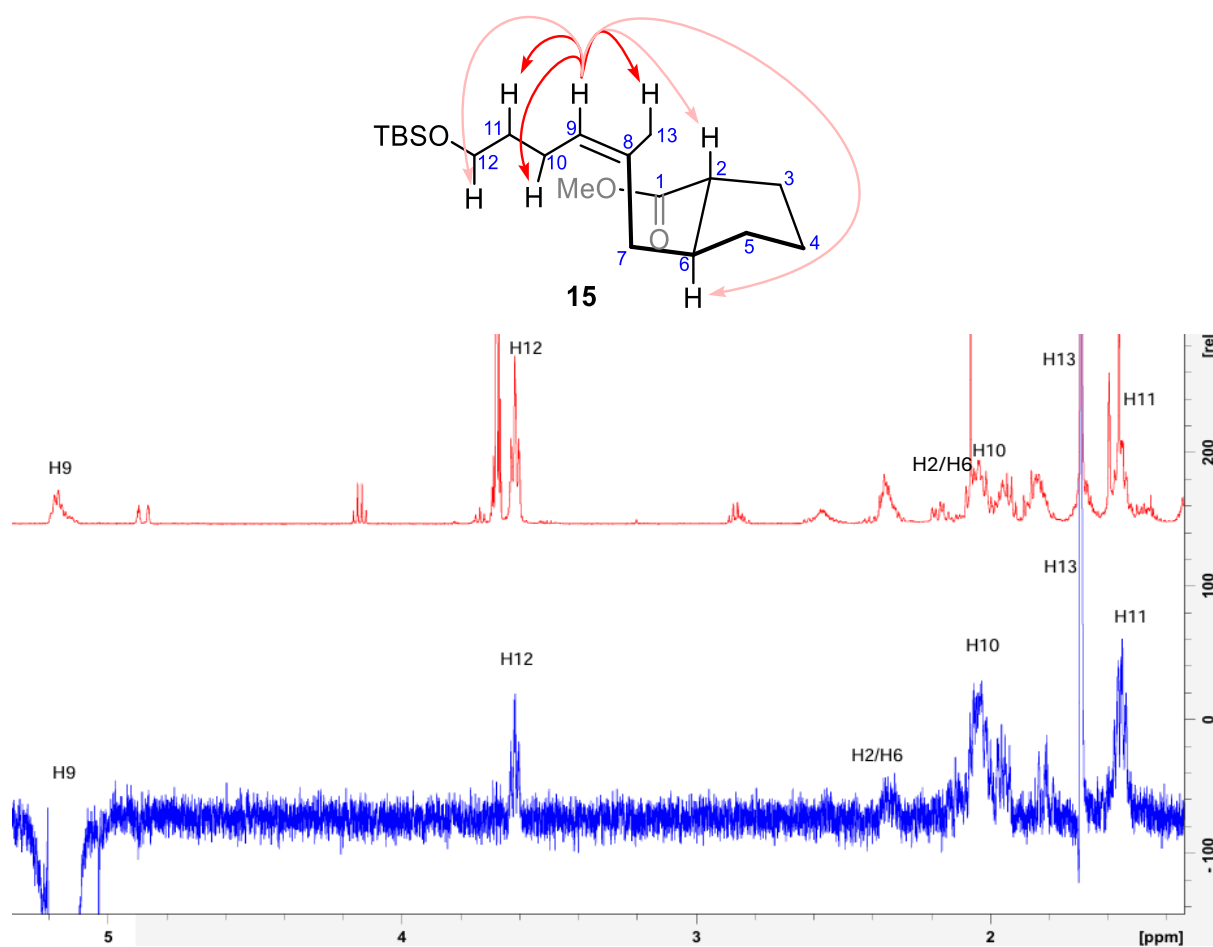
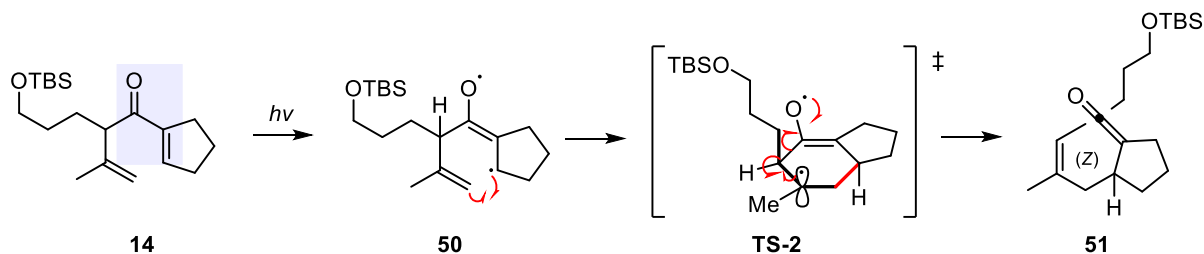


**Figure 8.8.5.** 1D-NOE with H9 irradiated.

The formation of *Z*-isomer as the major product can be rationalized using the model presented in Scheme 8.8.2. The alkyl chain ends up pseudo-axial because of the allylic strain caused by a methyl group and a double bond.



**Scheme 8.8.2.** Formation of the *Z*-isomer **51** from the diradical **50** via **TS-2**.

In conclusion, the photochemical reaction was rapid (completed in approx. 1 h) and the conversion was good: in the most successful reactions, only approx. 5 % of the starting material remained. In addition, the product was easy to isolate. However, the stereoselectivity remained weak and the desired *E*-isomer could not be isolated pure. The reaction as such is not a very good method for the selective preparation of trisubstituted alkenes. Cooling the reaction and using other substrates could have been tried to improve the stereoselectivity.

The failure of isopropenyl ketone **18** to undergo the photo-Cope sequence can be rationalized as follows. According to the literature<sup>138</sup>, **18** as an acyclic  $\alpha\beta$ -unsaturated ketone undergoes photoisomerization unlike cyclic  $\alpha\beta$ -unsaturated ketones that undergo 1,3- and 1,2-photorearrangement from excited singlet state (1,3) and triplet state (1,2).<sup>138</sup> The difference in behavior can be explained by the "free rotor" effect available to acyclic ketones, which allows energy to be dissipated *via* geometric isomerization rather than rearrangement. The olefinic system of cyclic ketones is constrained, causing the "free rotor" effect to be inoperative. In this case, the formation of cyclopropyl ketones by acyl transfer becomes important.<sup>138</sup>

## 9 Conclusions

The key research question of this thesis was to test whether trisubstituted alkenes can be produced stereoselectively by using photochemical activation. Synthesis of trisubstituted alkenes in a stereoselective manner could be used to access medium-sized rings or macrocycles containing alkenyl groups as rigidifying elements. In this experimental part, such a method,

photo-Cope reaction, was successfully explored, so the goal was reached in this regard. The photochemical reaction could be successfully used with cyclopentenyl ketone **14** as the substrate, giving *Z-trans*-isomer as a major product. However, the analysis was complicated by the fact that the ketene intermediate (during **I-3**) gave a mixture of diastereomers during the methanolysis step, resulting in the formation of four different stereoisomers, *Z-trans* (**46**), *Z-cis* (**48**), *E-trans* (**47**) and *E-cis* (**49**) with tentative 3:1 *Z:E* selectivity and 2:1 *trans:cis* selectivity. Thus, the synthesis route did not offer a direct solution for stereoselectively making trisubstituted alkenes. Finding a solution to the stereoselectivity issue would require improving the selectivity and repeating the experiment with different substrates. If time allowed, an attempt could have been made to separate the isomers by decanting the TBS and methyl ester with NaOH and performing macrocyclization, which would have allowed them to be identified more precisely. The next step would be to consider a completely different way to prepare the *E*-isomer.

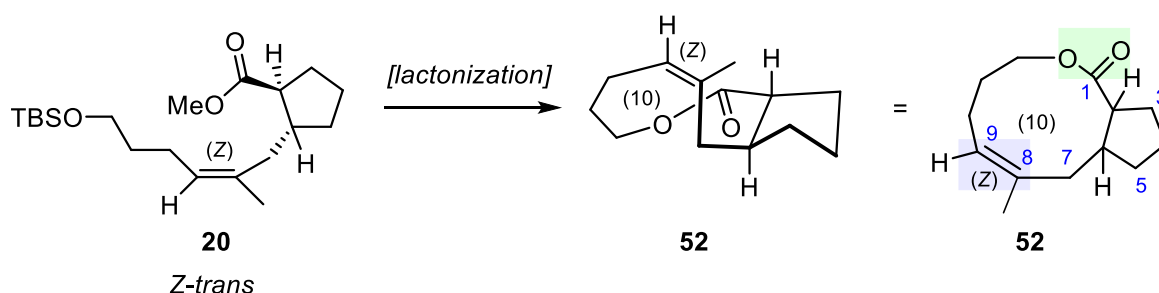
In terms of the synthesis of the photo-Cope precursor, the crucial factor was the success of the alkylation and Shapiro reactions, because they enabled the synthesis of the carbon backbone of the starting material **14** for the photo-Cope experiments, which were the crucial part of the experimental part. Rearrangement reactions are generally useful in the synthesis of carbon frameworks, but they still present challenges. For photo-Cope experiments, two enone substrates **14** and **18** were synthesized. As mentioned before, the photo-Cope rearrangement was successful for **14** which led to the formation of trisubstituted alkene(s). The result provided new information about the effect of substituent on (*Z/E*)-selectivity and this information can be applied in the planning of possible future reactions, including the ongoing humilisin E-project in the Pihko group.

Apart from the selectivity issues in the last step, the synthesis route was mostly functional and could be scaled up. Overall, the synthesis was straightforward, and the substrates were easy to prepare. However, the sensitive volatility of intermediate products, especially alkylation product **12**, was a challenge during the synthesis. In addition, the sensitive polymerization of the lactone led to changes that extended the original synthesis plan. However, making the Weinreb amide **17** directly from the ethyl ester worked and the amide was a stable compound, facilitating the following reactions. However, the enone **18** polymerized easily, like the lactone, making its purification difficult.

Some steps such as the Shapiro reaction, would also require careful optimization due to the mediocre yield and formation of the butyl ketone by-product. Instead of the Shapiro reaction, e.g. Barton vinyl iodide synthesis<sup>137</sup> could be tried to make cyclopentenyl ketone **14**. In

addition, optimizing the photo-Cope reaction would have required more time. Epimerization could have been attempted for the reaction mixture of four isomers, but based on the lit.<sup>119</sup> this experiment would not have improved the mixture ratio much. In addition, the epimerization lasts five days according to Agosta and Smith<sup>119</sup> so the experiment was not performed also due to the time limit of the project.

If there had been more time, the macrocyclization reaction leading to the ring closure would have been attempted (see Scheme 9.1.1). In this case, the desired product would have been a 10-membered macrocycle **52**, in which the rigidifying elements are an ester group (highlighted in green) and an endocyclic *Z* double bond (highlighted in purple) presented in Scheme 9.1.1.



**Scheme 9.1.1.** Macrocyclization of *Z,trans* isomer **20** to 10-membered heterocycle **52**.

## 10 Experimental methods

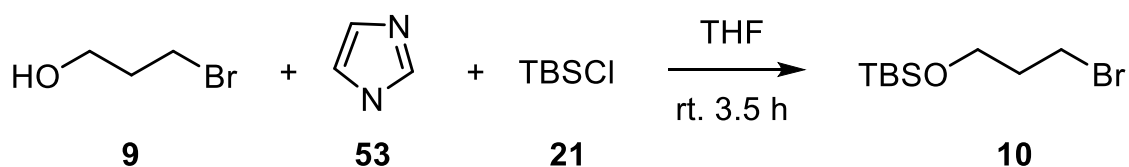
All reactions of the experimental part were carried out under an argon atmosphere in oven-dried (120 °C) glassware. Dry solvents were taken from the MBraun SPS-800 solvent drying system unless otherwise noted. Diisopropylamide was distilled over a potassium hydroxide pellet and stored over molecular sieves at room temperature. The titration of *n*-BuLi was done before each use and due to its pyrophoric nature, its processing was conducted very carefully with air and moisture-sensitive techniques. Other solvents and reagents were used as obtained from the supplier unless otherwise noted. Concentration was conducted with Buchi R-II Rotavapor using a 30-40 °C bath.

Merck silica gel F254 (200-400 mesh) plates were used for TLC monitoring of reactions and calculation of  $R_f$  values. TLC plates were stained with potassium permanganate solution (4 g  $\text{KMnO}_4$ , 30 g  $\text{K}_2\text{CO}_3$ , 7.5 mL 1M NaOH, 450 mL  $\text{H}_2\text{O}$ ) or vanillin (6 g vanillin, 5 mL conc.

H<sub>2</sub>SO<sub>4</sub>, 3 mL glacial acetic acid, 250 mL EtOH. The products were purified by flash chromatography with Merck silica gel 60 (230–400 mesh) silica.

The NMR measurements were recorded in CDCl<sub>3</sub> or DMSO on Bruker Avance III 300 MHz or 500 MHz spectrometers at 30 °C. Peak shifts were reported in ppm relative to the deuterated solvent shift. IR spectra were measured with a Bruker Tensor 27 FTIR spectrometer. The melting points (mp) of the solid products were determined in open capillaries using the Bibby-Stuart Scientific SMP3 melting point apparatus. The high-resolution mass spectrometric data of the unknown compounds were measured using Agilent Technologies 6560 Ion Mobility ESI-Q-TOF LC/MS mass spectrometer.

### 10.1 (3-bromopropoxy)(*tert*-butyl)dimethylsilane



3-bromo-1-propanol **9** (1.95 mL, 21.51 mmol, 1.00 equiv) was slowly added to a mixture of imidazole **53** (1.61 g, 23.60 mmol, 1.09 equiv) and THF (10 mL) at rt. A solution of TBSCl **21** (3.00 g, 19.91 mmol, 0.92 equiv) in THF (10 mL) was added dropwise over 10 minutes during which time a white precipitate formed. The resulting mixture was stirred overnight. Et<sub>2</sub>O (30 mL) and water (20 mL) were added, and the mixture was transferred to a separatory funnel. The layers were separated, and the aqueous phase was extracted with Et<sub>2</sub>O (3 x 20 mL). The combined organic layers were washed with brine, dried (Na<sub>2</sub>SO<sub>4</sub>), filtered, and concentrated. Crude <sup>1</sup>H NMR analysis of the residue indicated the presence of unreacted **9**. The crude mixture was dissolved in THF (6 mL) and more imidazole (401.7 mg,) and TBSCl **21** (901.3 mg) in THF (7 mL) were added. The reaction mixture was stirred for 2 h at rt. Et<sub>2</sub>O (30 mL) and water (20 mL) were added, the phases were separated, and the aqueous phase was extracted with Et<sub>2</sub>O (4 x 20 mL). The combined organic layers were washed with brine (20 mL), dried (Na<sub>2</sub>SO<sub>4</sub>), filtered, and concentrated to give the TBS-protected alcohol **10** as a volatile colorless liquid. <sup>1</sup>H NMR spectrum of **10** indicated that further purification was not necessary.

Yield: 5.02 g, 92 %

$R_f$  (Et<sub>2</sub>O:pentane 3:7): 0.95

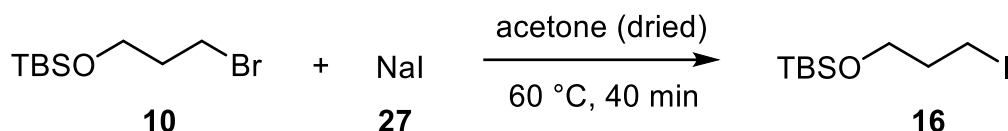
IR (film): 2953, 2929, 2856, 1471, 1253, 1099, 1061, 940, 833, 775 cm<sup>-1</sup>

<sup>1</sup>H NMR (300 MHz, CDCl<sub>3</sub>):  $\delta$  3.74 (t, 2H,  $J$  = 5.7 Hz), 3.51 (t, 2H,  $J$  = 6.5 Hz), 2.08–1.99 (m, 2H), 0.90 (s, 9H), 0.07 (s, 6H)

<sup>13</sup>C NMR (75 MHz, CDCl<sub>3</sub>):  $\delta$  60.6, 35.7, 30.8, 26.1, 18.4, -5.2

The IR and NMR spectra correspond to the values presented in the literature.<sup>121,139,140</sup>

## 10.2 1-iodo-3-(*tert*-butyldimethylsilyloxy)propane



Sodium iodide **27** (6.24 g, 0.042 mol, 3.12 equiv) was slowly added to a solution of TBS-protected halide **10** (3.38 g, 0.042 mol, 1.00 equiv) and molecular sieve-dried acetone (20 mL). The reaction mixture was heated at 60 °C. After 40 minutes, the reaction was judged to be complete by TLC analysis (eluent: 25% EtOAc/hex). The solution was diluted with Et<sub>2</sub>O (30 mL) and the solid was removed by filtration. The solvent was evaporated, and the oily residue was purified by column chromatography (silica gel, linear gradient 0-5 % EtOAc/hexanes) to give iodine **16** as a colorless oil.

Yield: 3.20 g, 79 %

$R_f$  (25 % Et<sub>2</sub>O/hex): 0.36

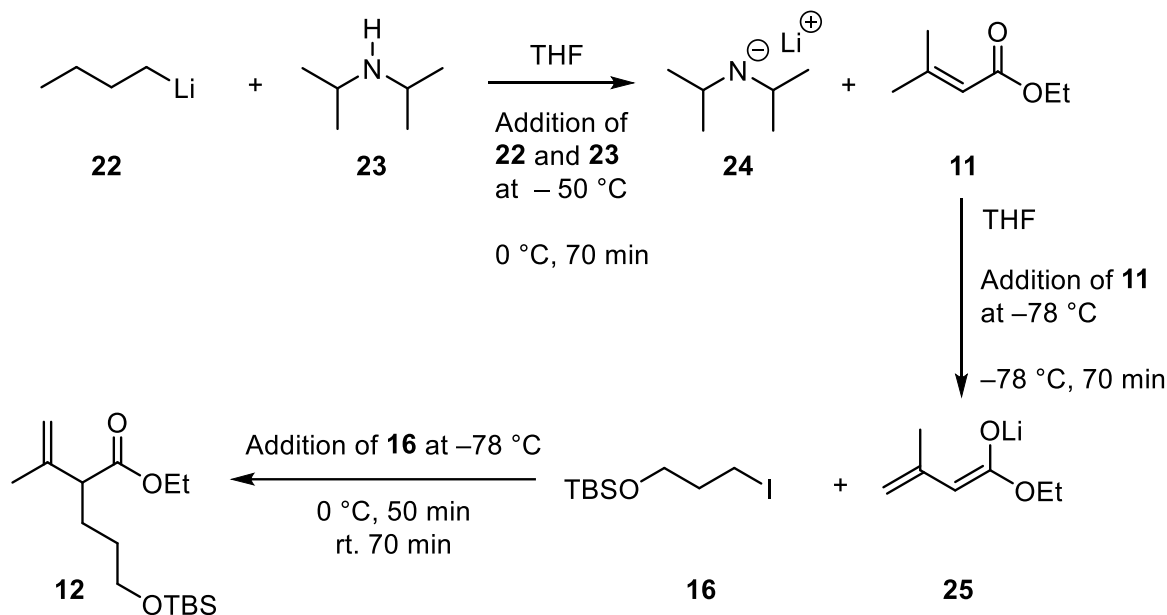
IR (film): 2953, 2928, 2894, 2856, 1470, 1424, 1384, 1360, 1253, 1180, 1137, 1096, 1051, 1006, 831, 812, 774, 714, 662, 605, 516 cm<sup>-1</sup>

<sup>1</sup>H NMR (300 MHz, CDCl<sub>3</sub>):  $\delta$  3.67 (t,  $J$  = 5.7 Hz, 2H), 3.28 (t,  $J$  = 6.7 Hz, 2H), 2.04-1.97 (m, 2H), 0.90 (s, 9H), 0.07 (s, 6H)

<sup>13</sup>C NMR (75 MHz, CDCl<sub>3</sub>):  $\delta$  62.5, 36.4, 26.1, 3.7, -5.2

The IR and NMR spectra correspond to the values presented in the literature.<sup>124,140</sup>

### 10.3 ethyl-5-((*tert*-butyldimethylsilyloxy)-2-(prop-1-en-2-yl)pentanoate



A solution of LDA **24** was prepared by adding 7.93 mL of *n*-BuLi **22** (16.89 mmol, 2.13 M, 1.00 equiv) dropwise to the solution of di-isopropylamine **23** (2.62 mL, 18.58 mmol, 1.10 equiv) and THF (8.96 mL) at -50 °C. A color change from transparent to yellow was observed during the addition of *n*-BuLi. The resulting solution was warmed to 0 °C in an ice bath and stirred for 70 min. A solution of ethyl ester **11** (1.77 mL, 12.72 mmol, 1.00 equiv) and THF (8 mL) was prepared in a separate flask. The LDA solution was cooled to -78 °C and ester **11** in THF was added dropwise. The resulting clear solution was stirred for 70 min and after that, iodide **16** (3.52 mL, 15.24 mmol, 1.20 equiv) was added dropwise. The resulting solution was warmed to 0 °C in an ice bath and stirred for 50 min. The ice bath was removed, and the mixture was stirred at rt. for 70 min.

At this stage, iodide **6** was completely consumed by TLC analysis. Sat. aq. NH<sub>4</sub>Cl (20 mL) was added, the phases were separated, and the aqueous phase was extracted with Et<sub>2</sub>O (3 x 20 mL). The combined organic layers were washed with sat. aq. NaHCO<sub>3</sub> (20 mL) and brine (20 mL), dried with Na<sub>2</sub>SO<sub>4</sub>, filtered, and concentrated. The crude product was purified by column chromatography (silica gel, linear gradient 0–5% EtOAc/hexanes) to give alkylated ester **12** as a colorless oil.

Yield: 2.7 g, 71 %

$R_f$  (10 % Et<sub>2</sub>O/hex): 0.84

IR (film): 2953, 2930, 2888, 2857, 1733, 1646, 1472, 1463, 1447, 1368, 1252, 1157, 1095, 1031, 1006, 895, 834, 774, 661 cm<sup>-1</sup>

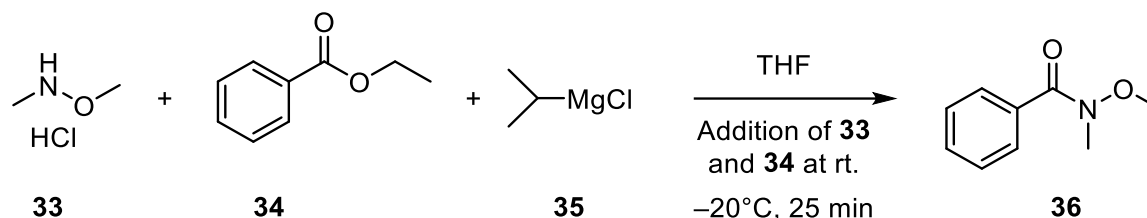
<sup>1</sup>H NMR (300 MHz, CDCl<sub>3</sub>):  $\delta$  4.89 (s, 2H), 4.14 (q,  $J$  = 7.1 Hz, 2H), 3.61 (td,  $J$  = 2.4 Hz, 0.03 Hz, 2H), 3.0 (t,  $J$  = 7.7 Hz, 1H), 1.74 (s, 3H), 1.89-1.59 (m, 4H), 1.54-1.46 (m, 3H), 0.89 (s, 11 H), 0.04 (s, 7H)

Grease was also observed in the <sup>1</sup>H NMR spectrum: 1.27-1.22 (m, 6H), 0.89 (s)

<sup>13</sup>C NMR (75 MHz, CDCl<sub>3</sub>):  $\delta$  142.7, 113.8, 62.9, 60.5, 53.0, 30.7, 26.6, 26.0, 20.2, 18.4, 14.3, -5.2

HRMS (ESI+):  $m/z$  [M+Na]<sup>+</sup> calculated for [C<sub>16</sub>H<sub>32</sub>O<sub>3</sub>SiNa]<sup>+</sup> 300.2121, found 300.2125,  $\Delta$  = 0.4 mDa

#### 10.4 *N*-methoxy-*N*-methylbenzamide



*N,O*-dimethyl hydroxylamine hydrochloride **33** (1.48 g, 15.6 mmol, 1.52 equiv) was dissolved in THF (20 mL) at rt. Ethyl benzoate **34** (1.43 mL, 10 mmol, 1.00 equiv) was slowly added to the solution. The resulting suspension was cooled to -20 °C and *i*-PrMgCl **35** (12.8 mL of a 2.0 M solution in THF, 25.6 mmol, 2.56 equiv) was added dropwise over 3 minutes. After 25 minutes, the reaction was judged nearly complete by TLC analysis. An estimated conversion to the product was approx. 95 % and sat. aq. NH<sub>4</sub>Cl (20 mL) was added. THF was evaporated, the phases were separated, and the aqueous phase was extracted with EtOAc (3 x 25 mL). The combined organic layers were washed with brine, dried (Na<sub>2</sub>SO<sub>4</sub>), and concentrated to give amide **36** as a colorless oil. The yield was distorted by e.g. ethyl acetate and a small amount of starting material remaining in the reaction mixture.



Yield: 1.67 g, 102 % mass balance (83 % purity)

$R_f$  (20 % EtOAc/hex): 0.18

IR(ATR): 2970, 2935, 1637, 1447, 1413, 1377, 1275, 1212, 977, 787, 704  $\text{cm}^{-1}$

$^1\text{H}$  NMR (300 MHz,  $\text{CDCl}_3$ ):  $\delta$  7.67 (d,  $J = 7.4$  Hz, 2H), 7.43 – 7.40 (m, 3H), 3.56 (s, 3H), 3.36 (s, 3H).

Ca. 2 mol % of EtOAc was also observed in the  $^1\text{H}$  NMR spectrum: 4.12 (q,  $\text{CH}_2$ ), 2.04 (s,  $\text{CH}_3\text{CO}$ ) 1.23 (t,  $\text{CH}_3$ )

Ca. 15 mol % of ethyl benzoate **34** was also observed in the  $^1\text{H}$  NMR spectrum: 7.55 (t,  $J = 7.9$  Hz), 4.38 (q,  $J = 7.1$  Hz), 1.40 (t,  $J = 7.1$  Hz)<sup>141</sup>

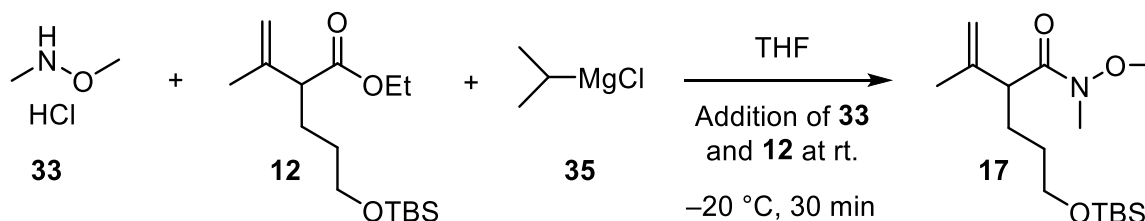
$^{13}\text{C}$  NMR (75 MHz,  $\text{CDCl}_3$ ):  $\delta$  170.1, 134.3, 130.7, 128.3, 128.1, 61.1, 33.9

EtOAc was also observed in the  $^{13}\text{C}$  NMR spectrum: 14.3

Ethyl benzoate **34** was also observed in the  $^{13}\text{C}$  NMR spectrum: 132.9, 129.7.<sup>141</sup>

$^1\text{H}$  NMR and  $^{13}\text{C}$  NMR spectra correspond to the values reported in the literature.<sup>142,143</sup> The values of the IR spectrum also correspond to the values reported in the literature.<sup>144</sup>

### 10.5 5-((*tert*-butyldimethylsilyloxy)-*N*-methoxy-*N*-methyl-2-(prop-1-en-2-yl)pentanamide



*N,O*-dimethyl hydroxylamine hydrochloride **33** (497.0 mg, 5.1 mmol, 1.70 equiv) was dissolved in THF (5 mL) at rt. To this solution, ester **12** (902.8 mg, 3.0 mmol, 1.00 equiv) in THF (3 mL) was slowly added by a syringe. The resulting suspension was cooled to  $-20\text{ }^\circ\text{C}$  and *i*-PrMgCl **35** (4.26 mL of a 2.0 M solution in THF, 8.53 mmol, 2.84 equiv) was added dropwise over 2 minutes to cooled ( $-20\text{ }^\circ\text{C}$ ) suspension. After 30 minutes, the reaction was judged nearly complete by TLC analysis. Sat. aq.  $\text{NH}_4\text{Cl}$  (10 mL) was added, the phases were

separated, and the aqueous phase was extracted with Et<sub>2</sub>O (3 x 20 mL). The combined organic layers were washed with brine, dried (Na<sub>2</sub>SO<sub>4</sub>), and concentrated to give amide **18** as a colorless oil.

Yield: 961.3 mg, 92 % (75 % purity)

R<sub>f</sub> (10 % Et<sub>2</sub>O/hex): 0.12

IR(ATR): 2953, 2930, 2887, 2857, 1664, 1377, 1253, 1097, 1000, 893, 834, 774, cm<sup>-1</sup>

<sup>1</sup>H NMR (300 MHz, CDCl<sub>3</sub>): δ 4.88 (s, 1H), 4.85 (s, 1H), 3.67 (s, 3H), 3.63-3.58 (m, 2H), 3.47 (t, *J* = 4.2 Hz, 1H), 3.18 (s, 3H), 1.76 (s, 3H), 1.72-1.63 (m, 2H), 1.51-1.45 (m, 2H), 0.89 (s, 9H), 0.04 (s, 6H)

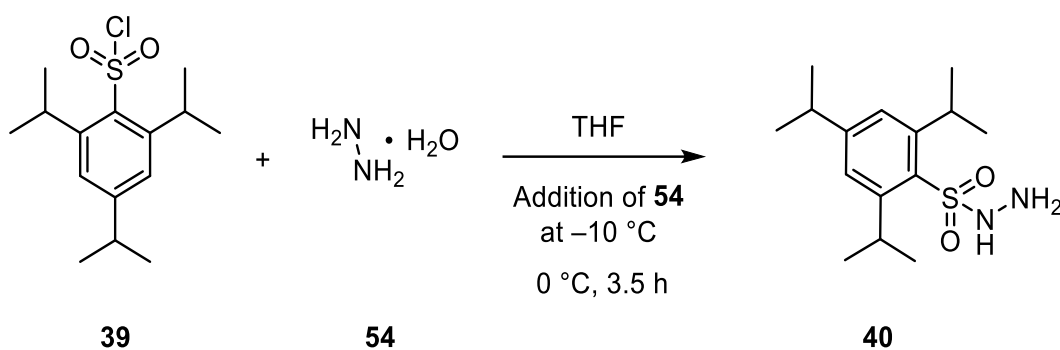
Ca. 17 mol% of THF was also observed in the <sup>1</sup>H NMR spectrum: 3.76 – 3.71 (m), 1.86-1.78 (m)

<sup>13</sup>C NMR (75 MHz, CDCl<sub>3</sub>): δ 143.8, 113.3, 63.1, 61.4, 48.7, 32.5, 31.0, 27.1, 26.1, 20.7, 18.5, -5.2

THF was also observed in the <sup>13</sup>C NMR spectrum: 68.1, 25.8

HRMS (ESI<sup>+</sup>): *m/z* [M+H]<sup>+</sup> calculated for [C<sub>16</sub>H<sub>33</sub>NO<sub>3</sub>SiH]<sup>+</sup> 315.223, found 315.2228, Δ = 0.2 mDa.

## 10.6 2,4,6-Triisopropylbenzenesulfonyl hydrazide



2,4,6-triisopropylbenzenesulfonyl chloride **39** (5.02 g, 16.57 mmol, 1.00 equiv) was dissolved in THF (25 mL) in rt. The solution was cooled to -10 °C and hydrazine hydrate **54** (2.29 mL, 36.16 mmol, 2.19 equiv) was added dropwise over 10 min. The reaction mixture was warmed

to 0 °C and stirred for 3.5 h until a white precipitate was formed. Based on TLC analysis, the reaction proceeded to completion. Water (3 mL) was added dropwise until the precipitate was dissolved. Et<sub>2</sub>O (20 mL) was added, and the aqueous layer was removed and extracted with Et<sub>2</sub>O (3 x 30 mL). The combined organic layers were washed with brine (3 x 25 mL), dried (Na<sub>2</sub>SO<sub>4</sub>), and filtered through Celite. The concentration of filtrate was done in vacuo at 20 °C. Hexane (75 mL) was added and the formed precipitate was collected by filtration and washed thoroughly with hexane to give hydrazide **40** as a white solid.

Yield: 3.90 g, 79 %

*R<sub>f</sub>* (20 % EtOAc/hex): 0.33

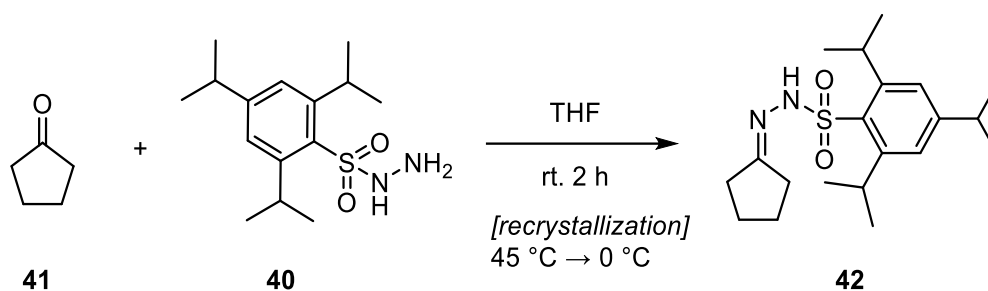
mp 128-132 °C (lit.<sup>134</sup> mp 118-120 °C)

IR (ATR): 3168, 2957, 2930, 2868, 1601, 1461, 1427, 1362, 1320, 1149, 884, 653, 555 cm<sup>-1</sup>

<sup>1</sup>H NMR (300 MHz, CDCl<sub>3</sub>): δ 7.3 (s, 2H), 7.0 (s, 1H), 4.2 (sept, *J* = 6.1 Hz, 4H), 2.9 (m, 1H), 1.2 (m, 30H, includes residual water signal)

The IR and NMR spectra correspond to the values presented in the literature.<sup>134</sup>

## 10.7 Cyclopentanone (2,4,6-Triisopropylbenzenesulfonyl)hydrazone



TPSH **40** (3.73 g, 12.48 mmol, 1.00 equiv) was added to a solution of cyclopentanone **41** (1.11 mL, 12.48 mmol, 1.00 equiv) in THF (28 mL) at rt. After two hours, the reaction was judged to be complete by TLC analysis and the product was a yellow liquid. Methanol was warmed to 45 °C, THF was removed under vacuum and the residual solid was dissolved in warm methanol. The recrystallization continued by cooling the mixture at 0 °C in an ice bath for 1 h. The pure hydrazone **42** was collected as a white solid by suction filtration and drying under vacuum.

Yield: 2.52 g, 55 %

$R_f$  (20 % EtOAc/hex): 0.4

mp 145-148 °C dec (lit.<sup>145</sup> mp 133-134 °C)

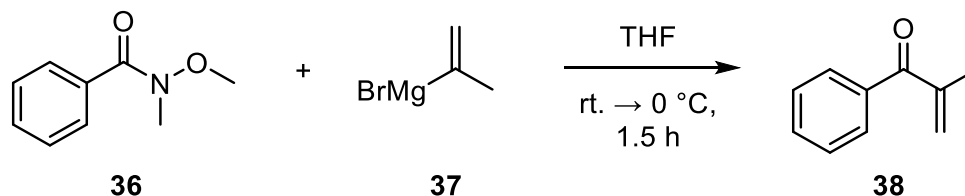
IR (ATR): 3223, 3164, 2958, 2868, 1599, 1461, 1428, 1383, 1365, 1311, 1298, 1165, 1153, 1029, 958, 923, 884, 765, 635, 546  $\text{cm}^{-1}$

$^1\text{H}$  NMR (300 MHz,  $\text{CDCl}_3$ ):  $\delta$  7.17 (s, 2H), 6.96 (s, 1H), 4.24 (quint,  $J = 6.87$  Hz, 2H), 2.90 (quint,  $J = 6.51$  Hz, 1H), 2.34 (t,  $J = 7.23$  Hz, 2H), 2.14 (t,  $J = 7.29$  Hz, 2H), 1.87–1.69 (m, 4H), 1.26 (dd,  $J = 6.72, 2.46$  Hz, 18 H)

$^{13}\text{C}$  NMR (75 MHz,  $\text{CDCl}_3$ ):  $\delta$  207.0, 153.3, 151.5, 131.7, 124.0, 38.5, 34.3, 33.5, 31.0, 30.1, 24.9, 23.7, 23.4 (two extra signals appeared at 27.6, 25.5 ppm)

The IR and NMR spectra correspond to the values presented in the literature.<sup>133,145</sup>

### 10.8 2-methyl-1-phenylprop-2-en-1-one



Amide **36** (233.3 mg, 1.41 mmol, 1.00 equiv) was dissolved in THF (3 mL) in rt. The solution was cooled to 0 °C and *i*-PrMgBr **37** (7.3 mL, 3.65 mmol, 2.58 equiv) was added dropwise over 5 min to a solution. According to TLC, the reaction went to completion at 1.5 h. Sat. aq.  $\text{NH}_4\text{Cl}$  (6 mL) was added, the phases were separated, and the aqueous phase was extracted with  $\text{Et}_2\text{O}$  (3 x 20 mL). The combined organic layers were washed with brine (30 mL), dried ( $\text{Na}_2\text{SO}_4$ ), filtered, and concentrated at 30 °C to give a colorless liquid. Based on the crude  $^1\text{H}$  NMR, the desired aromatic ketone **38** had formed.

Yield: 258.2 mg, 146 % mass balance

$R_f$  (20 % EtOAc/hex): 0.82

IR (ATR): 2959,2925,1653, 1597, 1447, 1330, 1198, 1175, 1015, 978, 931, 901, 752, 708, 692, 609  $\text{cm}^{-1}$

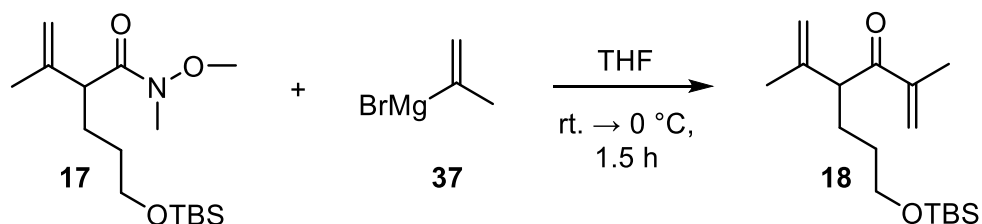
$^1\text{H}$  NMR (300 MHz,  $\text{CDCl}_3$ ):  $\delta$  7.73 (d,  $J = 7.4$  Hz, 2H), 7.53 (t,  $J = 7.1$  Hz, 1H), 7.43 (t,  $J = 7.1$  Hz, 2H), 5.91 (s, 1H), 5.62 (s, 1H), 2.08 (s, 3H)

THF was also observed in the  $^1\text{H}$  NMR spectrum: 3.74 (m), 1.85 (m)

$^{13}\text{C}$  NMR (75 MHz,  $\text{CDCl}_3$ ):  $\delta$  144.0, 138.0, 132.1, 129.6, 128.3, 127.1, 18.8

The IR and NMR spectra corresponded to the values presented in the literature presented in the literature.<sup>146,147</sup> The formation of a keto carbon signal at approx. 198 ppm would have probably required a longer measurement time or a more concentrated sample.

### 10.9 7-((*tert*-butyldimethylsilyl)oxy)-2-methyl-4-(prop-1-en-2-yl)hept-1-en-3-one



Weinreb amide **17** (224.9 mg, 0.71 mmol, 1.00 equiv) was dissolved in THF (3.5 mL) in rt. The solution was cooled to 0 °C and *i*-PrMgBr **37** (3.8 mL, 1.90 mmol, 2.67 equiv) was added dropwise over 3 min to a solution. According to TLC, the reaction went to completion at 1.5 h. Sat. aq.  $\text{NH}_4\text{Cl}$  (5 mL) was added, the phases were separated, and the aqueous layer was extracted with  $\text{Et}_2\text{O}$  (3 x 25 mL). The combined organic layers were washed with brine (30 mL), dried ( $\text{Na}_2\text{SO}_4$ ), filtered, and concentrated at 30 °C to give a colorless liquid. Based on the crude  $^1\text{H}$  NMR, the desired isopropenyl ketone **18** had formed. The residue was purified by column chromatography (silica gel, linear gradient 10-15 %  $\text{Et}_2\text{O}$ /pentane) to give isopropenyl ketone **18** as a colorless oil.

Note: Based on the observed decomposition of the previous batch, ketone **18** appears to be readily degradable/polymerizable. Therefore, a small amount of BHT stabilizer was added to the fractions containing the product (1 mg of BHT/1 ml of  $\text{Et}_2\text{O}$ ).

Yield: 168 mg, 89 %

$R_f$  (20 % EtOAc/hex): 0.92

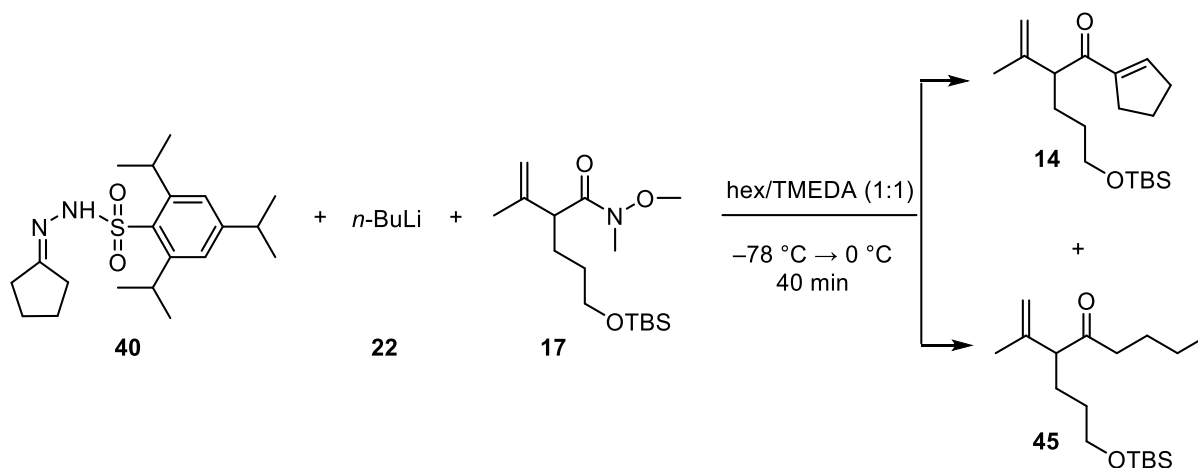
IR (ATR): 2927, 2854, 1676, 1641, 1450, 1376, 1253, 1098, 893, 774  $\text{cm}^{-1}$

$^1\text{H}$  NMR (300 MHz,  $\text{CDCl}_3$ ):  $\delta$  6.00 (s, 1H), 5.72 (s, 1H), 4.89 (s, 1H), 4.81 (s, 1H), 3.81 (t,  $J = 7.0$  Hz, 1H), 3.60 (t,  $J = 6.4$  Hz, 2H), 1.87 (s, 3H), 1.84-1.74 (m, 1H), 1.67 (s, 3H), 1.48-1.41 (m, 2H), 1.32-1.21 (m, 1H), 0.89 (s, 9H), 0.04 (s, 6H)

$^{13}\text{C}$  NMR (75 MHz,  $\text{CDCl}_3$ ):  $\delta$  202.2, 144.6, 143.9, 124.4, 114.1, 63.2, 53.9, 30.9, 30.5, 26.8, 26.1, 20.2, 18.5, -5.2

HRMS (ESI+):  $m/z$   $[\text{M}+\text{Na}]^+$  calculated for  $[\text{C}_{17}\text{H}_{33}\text{O}_2\text{SiNa}]^+$  296.2172, found 296.2163,  $\Delta = 0.9$  mDa.

### 10.10 5-((*tert*-butyldimethylsilyl)oxy)-1-(cyclopent-1-en-1-yl)-2-(prop-1-en-2-yl)pentan-1-one



TPSH **40** (496.7 mg, 1.36 mmol, 1.00 equiv) was dissolved in 1:1 hex/TMEDA solution (6 mL). The resulting solution was cooled to  $-78\text{ }^\circ\text{C}$  and  $n\text{-BuLi}$  **22** (1.76 mL, 3.15 mmol, 2.31 equiv) was added dropwise over 3 min, resulting in a color change from yellowish to dark red. After 70 minutes, the cooling bath was replaced by an ice bath, and stirring was continued for 20 min during which time gas evolution was observed and the color changed from brown to orange. The solution was cooled back to  $-78\text{ }^\circ\text{C}$ . Weinreb amide **17** (258 mg, 0.82 mmol, 0.60 equiv) in 6 ml hex/TMEDA (1:1) solution was added dropwise and the reaction mixture was stirred for 40 min at  $-78\text{ }^\circ\text{C}$  and for 15 min at  $0\text{ }^\circ\text{C}$  in an ice bath. At this stage, amide **17** was completely consumed according to TLC analysis. Sat. aq.  $\text{NH}_4\text{Cl}$  (8 mL) was added, the phases were separated, and the aqueous phase was extracted with  $\text{Et}_2\text{O}$  (3 x 25 mL). The combined organic layers were successively washed with  $\text{KHSO}_4$  (50 mL), aq.  $\text{HCl}$  (10 mL),  $\text{H}_2\text{O}$  (10 mL),

and NaHCO<sub>3</sub> (10 mL) (Note 1). The extracts were dried with Na<sub>2</sub>SO<sub>4</sub>, filtered, and concentrated (Note 2). The crude was purified by column chromatography (silica gel, linear gradient 2-6 % Et<sub>2</sub>O/pentane) to give butyl ketone **45** (196 mg, 44 %), followed by cyclopentenyl ketone **14** (178 mg, 40 %).

Note 1: KHSO<sub>4</sub> and finally a strong acid (HCl) were used in the extraction to get rid of TMEDA. The acid washes were important because TMEDA could co-extract with the desired product, complicating the purification process.

Note 2: Some solids and precipitates were formed during the concentration.

#### Characterization of **14**:

Yield: 178 mg, 40 %

*R<sub>f</sub>* (20 % EtOAc/hex): 0.79

IR (ATR): 2953, 2928, 2857, 1666, 1614, 1493, 1471, 1452, 1253, 1168, 1098, 1034, 1007, 836, 775, 696, 542 cm<sup>-1</sup>

<sup>1</sup>H NMR (300 MHz, CDCl<sub>3</sub>): δ 6.79 (s, 1H), 4.86 (d, 2H), 3.71 (t, *J* = 7.2 Hz, 1H), 3.60 (t, *J* = 5.9 Hz, 2H), 2.56-2.52 (m, 4H), 1.96-1.84 (m, 2H), 1.67 (s, 3H), 1.48-1.28 (m, 4H), 1.34-1.18 (m, 10H), 0.89 (s, 19H), 0.04 (s, 6H).

*n*-hexane was also observed in the <sup>1</sup>H NMR spectrum: 1.27 (m), 0.89 (t)

Grease and impurities were also observed in the <sup>1</sup>H NMR spectrum (multiplets at δ 1.34-1.18, 0.89). Integral 19 at 0.89 also refers to a silyl impurity, which can be caused by e.g. a small amount of remaining butyl ketone.

<sup>13</sup>C NMR (75 MHz, CDCl<sub>3</sub>): δ 199.0, 145.6, 144.1, 143.4, 113.9, 63.2, 55.9, 34.1, 31.1, 30.9, 26.5, 26.1, 22.8, 22.5, 20.1, 18.5, 14.2, -5.1

HRMS (ESI<sup>+</sup>): *m/z* [M+H]<sup>+</sup> calculated for [C<sub>19</sub>H<sub>34</sub>O<sub>2</sub>SiH]<sup>+</sup> 322.2328, found 322.2323, Δ = 0.5 mDa.

#### Characterization of **45**:

Yield: 196 mg, 44 %

$R_f$  (20 % EtOAc/hex): 0.84

IR (ATR): 2955, 2930, 2858, 1714, 1463, 1254, 1100, 1007, 836, 775, 696  $\text{cm}^{-1}$

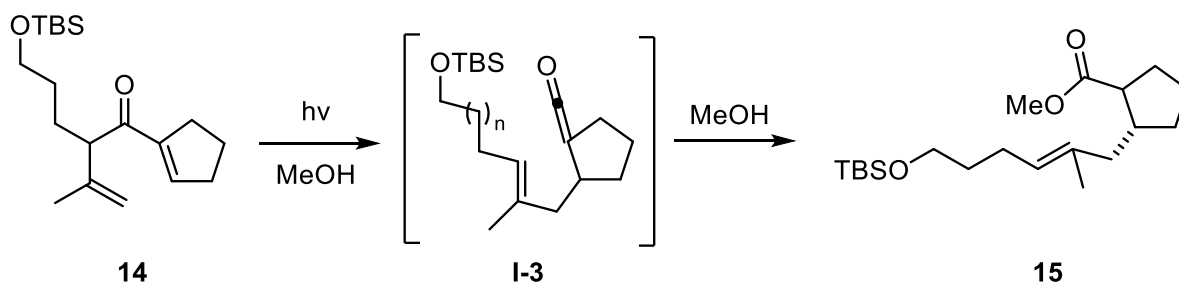
$^1\text{H}$  NMR (300 MHz,  $\text{CDCl}_3$ ):  $\delta$  4.92 (d, 2H), 3.59 (t,  $J = 5.9$  Hz, 2H), 3.15 (t,  $J = 7.2$  Hz, 1H), 2.55-2.44 (td,  $J = 7.4, 16.9$ , 1H), 2.41-2.31 (td,  $J = 7.3, 16.9$ , 1H) 1.82-1.24 (m, 12H), 0.89 (s, 12H), 0.04 (s, 6H).

Ca. 2 mol% of BHT was also observed in the  $^1\text{H}$  NMR spectrum: 2.27 (s)

Integral 12 at 0.89 refers to a silyl impurity, which can be caused by e.g. a small amount of remaining cyclopentenyl ketone.

HRMS (ESI+):  $m/z$   $[\text{M}+\text{Na}]^+$  calculated for  $[\text{C}_{19}\text{H}_{34}\text{O}_2\text{SiH}]^+$  312.2485, found 312.2486,  $\Delta = 0.1$  mDa.

### 10.11 methyl (2*R*)-2-((*Z*)-6-((*tert*-butyldimethylsilyl)oxy)-2-methylhex-2-en-1-yl)cyclopentane-1-carboxylate



Cyclopentenyl ketone **14** (17.50 mg, 54.25  $\mu\text{mol}$ , 1.00 equiv) was dissolved in 15 mL of HPLC grade MeOH and transferred to a photo-reactor flask. The reaction mixture was irradiated for 65 min and during that time dienone **14** was completely consumed by TLC analysis. The reaction mixture was poured into a separatory funnel and pentane (40 mL) and water (20 mL) were added. The layers were separated, and the organic layer was washed with water (10 mL) and brine (10 mL). The extracts were dried with  $\text{Na}_2\text{SO}_4$ , filtered, and concentrated. The crude was purified by column chromatography (silica gel, linear gradient 5-6 %  $\text{Et}_2\text{O}$ /pentane) to give **15** as a colorless oil. As previously noted, the isolated product **15** turned out to be a mixture of four different isomers.

Yield: 25.3 mg, 145 % mass balance



$R_f$  (20 % EtOAc/hex): 0.83

IR (ATR): 2951, 2928, 2856, 1735, 1435, 1361, 1252, 1160, 1097, 1036, 1006, 834, 773, 698, 662  $\text{cm}^{-1}$

$^1\text{H}$  NMR (300 MHz,  $\text{CDCl}_3$ ):  $\delta$  5.17-5.08 (m, 1H), 3.66-3.64 (4 x s, 0.7, 1.0, 0.5, 0.2 H, total 3H), 3.59 (overlapping triplets,  $J = 6.5$  Hz, 2H), 2.87-2.80 (m, 0.4H, *cis*), 2.35-2.27 (m, 2H), 2.18-2.14 (dd, 0.5H), 2.06-1.89 (m, 4H), 1.86-1.78 (m, 2H), 1.67 (brs, 3H), 1.56-1.53 (m, 2H), 1.32-1.15 (m, 9H, obscured by grease), 0.88 (s, 9H, obscured by grease and silyl impurities), 0.04 (s, 6H)

$^{13}\text{C}$  NMR (75 MHz,  $\text{CDCl}_3$ ):  $\delta$  (major isomer **46**) 177.2, 134.4, 126.4, 62.9, 51.3, 50.0, 42.8, 37.1, 34.3, 33.1, 30.6, 24.4, 23.6, 22.5, 14.2, -5.2 (tentative assignment)

In addition, the following peaks were observed for the minor isomers.

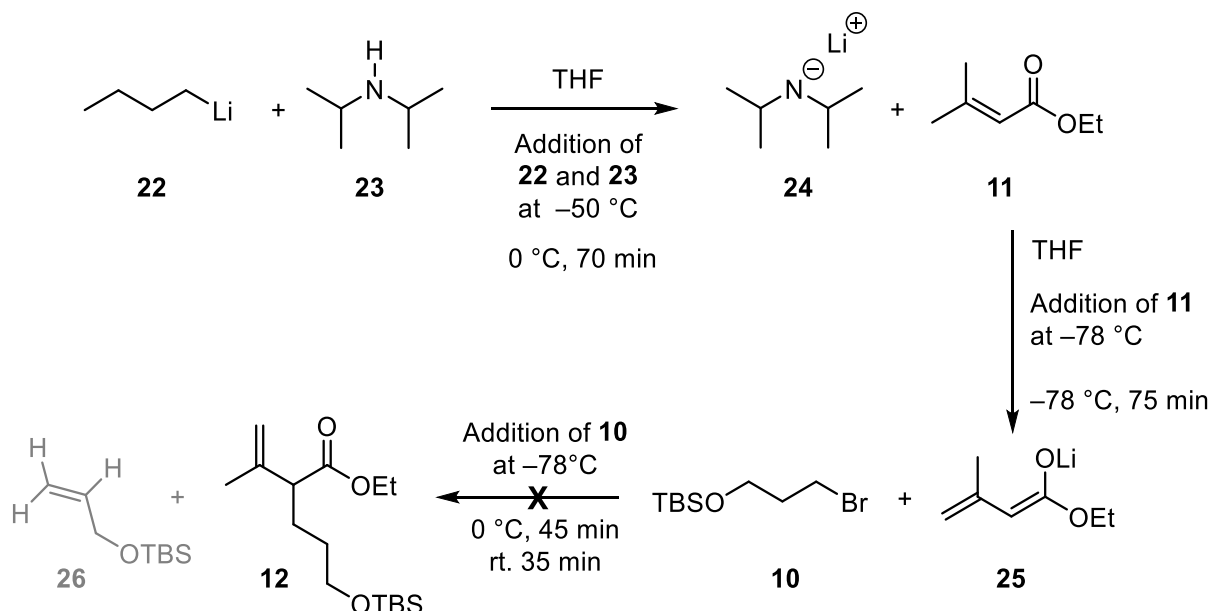
$^{13}\text{C}$  NMR (75 MHz,  $\text{CDCl}_3$ ):  $\delta$  (minor isomers **47**, **48**, **49**) 175.8, 126.1, 63.0, 51.6, 50.2, 48.0, 45.8, 42.1, 41.7, 41.0, 33.3, 32.6, 32.5, 32.3, 30.3, 29.8, 27.9, 15.4 (tentative assignment)

Grease and impurities were also observed in the  $^{13}\text{C}$  NMR spectrum: 26.1, 18.5

HRMS (ESI+):  $m/z$   $[\text{M}+\text{H}]^+$  calculated for  $[\text{C}_{20}\text{H}_{38}\text{O}_3\text{SiH}]^+$  354.259, found 354.2584,  $\Delta = 0.6$  mDa.

## 10.12 Attempted reactions

### 10.12.1 ethyl-5-((*tert*-butyldimethylsilyl)oxy)-2-(prop-1-en-2-yl)pentanoate

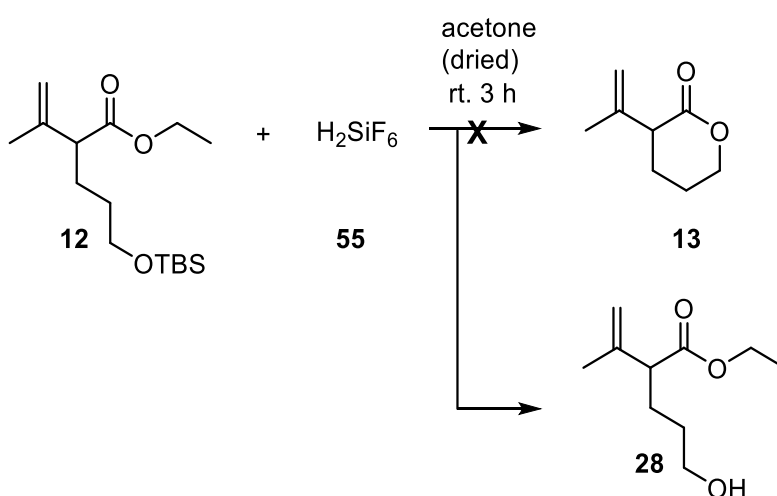


A solution of LDA **24** was prepared by adding 5.84 mL of *n*-BuLi **22** (9.34 mmol, 1.60 M, 1.00 equiv) dropwise to the solution of di-isopropylamine **23** (1.45 mL, 10.28 mmol, 1.10 equiv) and THF (3.51 mL) at  $-50\text{ }^{\circ}\text{C}$ . A color change from transparent to yellow was observed during the addition of *n*-BuLi. The resulting solution was warmed to  $0\text{ }^{\circ}\text{C}$  in an ice bath and stirred for 75 min. A solution of ethyl ester **11** (1.08 mL, 7.80 mmol, 1.00 equiv) and THF (5 mL) was prepared in a separate flask. The LDA solution was cooled to  $-78\text{ }^{\circ}\text{C}$  and ester **11** in THF was added dropwise over 4 min during which time the color of the solution changed from white to colorless. The resulting solution was stirred for 90 min and after that, bromine **10** (2.71 mL, 11.70 mmol, 1.50 equiv) was added dropwise and during that, the color changed from bright to orange. The resulting solution was warmed to  $0\text{ }^{\circ}\text{C}$  in an ice bath and stirred for 45 min. The ice bath was removed, and the mixture was stirred at rt. for 30 min.

At this stage, bromine **10** was not completely consumed by TLC analysis (15 % Et<sub>2</sub>O/hex). Sat. aq. KHSO<sub>4</sub> (15 mL) was added, and THF was evaporated with rotavapor. The phases were separated, and the aqueous phase was extracted with Et<sub>2</sub>O (5 x 20 mL). The combined organic layers were dried (Na<sub>2</sub>SO<sub>4</sub>), filtered, and concentrated. Based on the <sup>1</sup>H crude NMR, the reaction produced the desired alkylation product **12** and elimination product **26** in an approximate 1:1 ratio.

### 10.12.2 3-(prop-1-en-2-yl)tetrahydro-2H-pyran-2-one

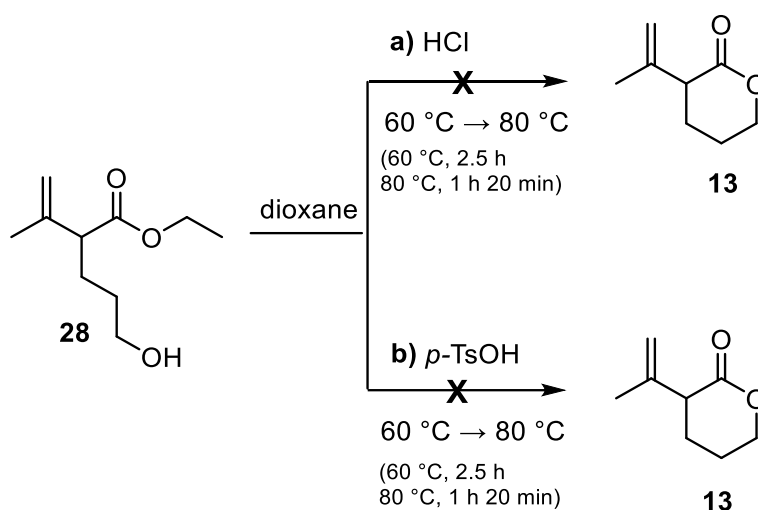
#### Attempt 1)



Alkylated ester **12** (61.1 mg, 0.20 mmol, 1.00 equiv) and dried acetone (1.1 mL) were added to the vial at rt. Hexafluorosilicic acid **55** (27 mL, 0.083 mmol, 34 %, 0.41 equiv) was carefully added with a glass syringe to the vial. After three hours, the reaction was judged to be complete

by TLC analysis (30 % Et<sub>2</sub>O/pentane). NaHCO<sub>3</sub>, reaction mixture, and Et<sub>2</sub>O were added to the separating funnel. The phases were separated, and the aqueous phase was extracted with Et<sub>2</sub>O (4 x 20 mL). The combined organic layers were dried (Na<sub>2</sub>SO<sub>4</sub>), filtered, and concentrated. Based on the <sup>1</sup>H crude NMR, the desilylation of the alkylated ester **12** was successful, leading to the formation of alcohol **28**. Thus, the reaction was continued: crude (54.9 mg) was dissolved in dioxane (2 mL) in a flask and the solution was divided into two vials.

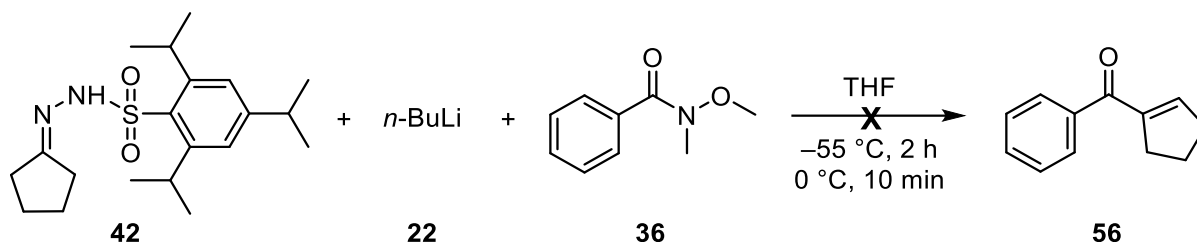
### Attempt 2)



Half of the mixture of alcohol **28** (27.45 mg, 0.15 mmol, 1.00 equiv) and dioxane (1 mL) (from attempt 1) and HCl (4.90  $\mu$ l, 0.074 mmol, 37 %, 0.49 equiv) were added to the first vial (**a**). The other half of the alcohol **28** (27.45 mg, 0.15 mmol, 1.00 equiv) in dioxane (1 mL) and *p*-TsOH (15.58 mg, 0.090 mmol, 0.61 equiv) were added to the second vial (**b**). The reaction mixtures were stirred and heated in a heat block at 60 °C for 2.5 h. At this stage, alcohol **6** was not completely consumed based on TLC analysis (10 % MeOH/DCM), so the stirring was continued for 80 minutes at 80 °C.

In both experiments, NaHCO<sub>3</sub>, reaction mixtures, and Et<sub>2</sub>O were added to the separating funnels. The phases were separated, and the aqueous phases were extracted with Et<sub>2</sub>O (4 x 20 mL). The combined organic layers were dried (Na<sub>2</sub>SO<sub>4</sub>), filtered, and concentrated. Based on the <sup>1</sup>H crude NMR a lot of dioxane was left and the peaks were very broad and inaccurate. Polymerization had probably taken place in reactions and mostly polyester had been formed instead of the desired lactone **13**. As previously noted in subchapter 8.4, this *kind* of behavior is very typical for 6-membered lactones.

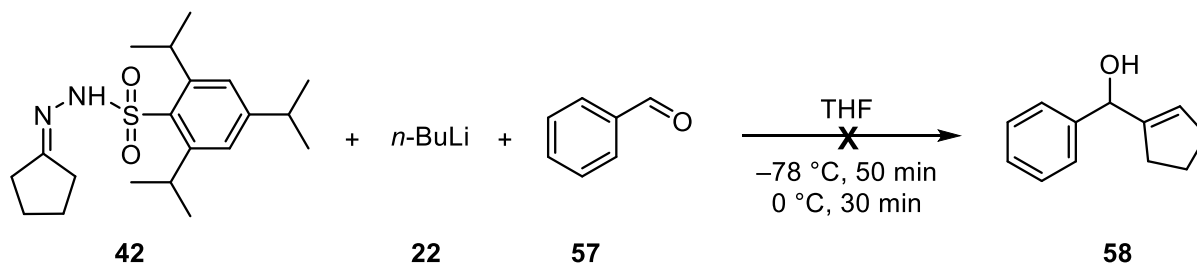
### 10.12.3 1-Cyclopenten-1-ylphenylmethanone



TPSH **42** (403.4 mg, 1.11 mmol, 1.00 equiv) was dissolved in THF (5 mL) in rt. The solution was cooled to  $-55\text{ }^{\circ}\text{C}$  and  $n\text{-BuLi}$  **22** (1.25 mL, 2.23 mmol, 2.01 equiv) was added dropwise over 5 min to a solution. The color changed from colorless to orange and stirring continued for 2 hours. Amide **36** was azeotropically dried, followed by the dissolution of amide (0.12 mL, 800.99  $\mu\text{mol}$ , 0.73 equiv) in THF (1 mL). The solution of **42** in THF was warmed to  $0\text{ }^{\circ}\text{C}$  and the solution of **36** in THF was added dropwise. After 10 minutes of stirring, the reaction was judged to be complete by TLC analysis (eluent: 20 % EtOAc/hex).

Sat. aq.  $\text{NH}_4\text{Cl}$  (6 mL) was added, the phases were separated, and the aqueous phase was extracted with  $\text{Et}_2\text{O}$  (4 x 20 mL). The combined organic layers were washed with  $\text{H}_2\text{O}$  (2 x 15 mL), 1 N HCl (15 mL), and  $\text{H}_2\text{O}$  (2 x 15 mL). The solution was dried ( $\text{Na}_2\text{SO}_4$ ), filtered, and concentrated. Based on the  $^1\text{H}$  NMR of crude, none of the desired product **56** had formed as only signals from the amide **36** were detected. This indicates that vinyl lithium did not form, or it did not react long enough with amide **36**. Neither nitrogen evolution nor color change to brown was observed during stirring at  $0\text{ }^{\circ}\text{C}$ , so the formation of vinyl lithium likely failed.

### 10.12.4 1-(hydroxy(phenyl)methyl)-1-cyclopentene

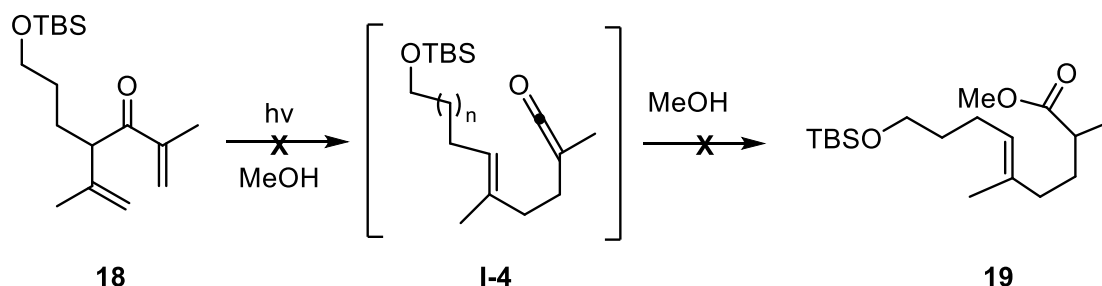


TPSH **42** (405.9 mg, 1.11 mmol, 1.00 equiv) was dissolved in THF (5 mL) in rt. The solution was cooled to  $-78\text{ }^{\circ}\text{C}$  and  $n\text{-BuLi}$  **22** (1.25 mL, 2.23 mmol, 2.01 equiv) was added dropwise over 5 min to a solution. The color changed from colorless to orange and stirring was continued

for 50 min. The solution was warmed to 0 °C and stirring was continued for 30 min. The solution was cooled back to -78 °C and benzaldehyde **57** (82  $\mu$ L, 811.35  $\mu$ mol, 0.73 equiv) was added dropwise. The cooling bath was replaced by an ice bath and stirring was continued for 45 minutes. At this stage, the reaction was judged to be complete by TLC analysis (eluent: 20 % EtOAc/hex).

Sat. aq.  $\text{NH}_4\text{Cl}$  (8 mL) was added, the phases were separated, and the aqueous phase was extracted with  $\text{Et}_2\text{O}$  (3 x 20 mL). The combined organic layers were washed with  $\text{NaHCO}_3$  (2 x 15 mL) and brine (25 mL). The solution was dried ( $\text{Na}_2\text{SO}_4$ ), filtered, and concentrated. The  $^1\text{H}$  NMR of the crude product indicated that some product had formed but a significant part of the signals were caused by byproducts.

#### 10.12.5 methyl (2R)-2-((Z)-6-((tert-butyldimethylsilyl)oxy)-2-methylhex-2-en-1-yl)cyclopentane-1-carboxylate



Isopropenyl ketone **18** (48.6 mg, 163.9  $\mu$ mol, 1.0 equiv) was dissolved in HPLC grade methanol (18 mL) and transferred to a photo-reactor flask. The solution was irradiated for 2.5 h, after which time the reaction was not complete according to TLC (20 % EtOAc/hex). The solution was poured into a separatory funnel and pentane (40 mL) and water (35 mL) were added. The layers were separated, and the organic layer was washed with water (15 mL) and brine (15 mL). The organic layer was dried ( $\text{Na}_2\text{SO}_4$ ), filtered, and concentrated. Only isopropenyl ketone **18** was observed in the  $^1\text{H}$  NMR spectrum of the crude product. The desired product **19** was not formed in the reaction at all. This can be rationalized by the "free rotor" effect, introduced at the end of subchapter 8.8, which allows energy dissipation through geometric isomerization rather than rearrangement in the case of acyclic ketones (like ketone **16**).<sup>138</sup>

## References

1. Dragojlovic, V., Conformational analysis of cycloalkanes, *ChemTexts*, **2015**, *1*, 14.
2. Burevschi, E.; Peña, I. and Eugenia Sanz, M., Medium-sized rings: conformational preferences in cyclooctanone driven by transannular repulsive interactions, *Physical Chemistry Chemical Physics*, **2019**, *21*, 4331–4338.
3. Fitzgerald, J. P., Cyclooctane conformational analysis via mechanical and computational models, *J. Chem. Educ.*, **1993**, *70*, 988.
4. Garcia Jimenez, D.; Poongavanam, V. and Kihlberg, J., Macrocycles in Drug Discovery—Learning from the Past for the Future, *J. Med. Chem.*, **2023**, *66*, 5377–5396.
5. Rossi Sebastiano, M.; Doak, B. C.; Backlund, M.; Poongavanam, V.; Over, B.; Ermondi, G.; Caron, G.; Matsson, P. and Kihlberg, J., Impact of Dynamically Exposed Polarity on Permeability and Solubility of Chameleonic Drugs Beyond the Rule of 5, *J. Med. Chem.*, **2018**, *61*, 4189–4202.
6. Lee, S. and Sperry, J., Isolation and biological activity of azocine and azocane alkaloids, *Bioorg. Med. Chem.*, **2022**, *54*, 116560.
7. Posternak, H. V.; Semoshkina, O. D.; Hys, V. Y.; Milokhov, D. S.; Virych, P. A.; Shishkina, S. V.; Volovenko, Y. M. and Dobrydnev, A. V., Expedient synthesis of 8-membered azasultams: A combined synthetic, DFT, and in vitro study, *Tetrahedron Chem*, **2024**, *11*, 100085.
8. Baud, L. G.; Manning, M. A.; Arkless, H. L.; Stephens, T. C. and Unsworth, W. P., Ring-Expansion Approach to Medium-Sized Lactams and Analysis of Their Medicinal Lead-Like Properties, *Chem. – Eur. J.*, **2017**, *23*, 2225–2230.
9. Zalessky, I.; Wootton, J. M.; Tam, J. K. F.; Spurling, D. E.; Glover-Humphreys, W. C.; Donald, J. R.; Orukotan, W. E.; Duff, L. C.; Knapper, B. J.; Whitwood, A. C.; Tanner, T. F. N.; Miah, A. H.; Lynam, J. M. and Unsworth, W. P., A Modular Strategy for the Synthesis of Macrocycles and Medium-Sized Rings via Cyclization/Ring Expansion Cascade Reactions, *J. Am. Chem. Soc.*, **2024**, *146*, 5702–5711.
10. Clarke, A. K. and Unsworth, W. P., A happy medium: the synthesis of medicinally important medium-sized rings via ring expansion, *Chem. Sci.*, **2020**, *11*, 2876–2881.
11. Bauer, R. A.; Wenderski, T. A. and Tan, D. S., Biomimetic diversity-oriented synthesis of benzannulated medium rings via ring expansion, *Nat. Chem. Biol.*, **2013**, *9*, 21–9.
12. Zhao, C.; Ye, Z.; Ma, Z.; Wildman, S. A.; Blaszczyk, S. A.; Hu, L.; Guizei, I. A. and Tang, W., A general strategy for diversifying complex natural products to polycyclic scaffolds with medium-sized rings, *Nat. Commun.*, **2019**, *10*, 4015.
13. Appavoo, S. D.; Huh, S.; Diaz, D. B. and Yudin, A. K., Conformational Control of Macrocycles by Remote Structural Modification, *Chem. Rev.*, **2019**, *119*, 9724–9752.
14. Dunitz, J. D., Conformations of medium rings, *Pure Appl. Chem.*, **1971**, *25*, 495–508.
15. Engler, E. M.; Andose, J. D. and Schleyer, P. V. R., Critical evaluation of molecular mechanics, *J. Am. Chem. Soc.*, **1973**, *95*, 8005–8025.

16. Zou, W.; Tao, Y. and Kraka, E., Systematic description of molecular deformations with Cremer–Pople puckering and deformation coordinates utilizing analytic derivatives: Applied to cycloheptane, cyclooctane, and cyclo[18]carbon, *J. Chem. Phys.*, **2020**, *152*, 154107.
17. Lee, H.; Kim, J. and Koh, M., Medium-Sized Ring Expansion Strategies: Enhancing Small-Molecule Library Development, *Molecules*, **2024**, *29*, 1562.
18. Still, W. C. and Galynker, I., Chemical consequences of conformation in macrocyclic compounds: An effective approach to remote asymmetric induction, *Tetrahedron*, **1981**, *37*, 3981–3996.
19. Zhao, Z.; Popov, S.; Lee, W.; Burch, J. E.; Delgadillo, D. A.; Kim, L. J.; Shahgholi, M.; Lebrón-Acosta, N.; Houk, K. N. and Nelson, H. M., Accessing Medium-Sized Rings via Vinyl Carbocation Intermediates, *Org. Lett.*, **2024**, *26*, 1000–1005.
20. Romines, K. R.; Watenpaugh, K. D.; Tomich, P. K.; Howe, W. J.; Morris, J. K.; Lovasz, K. D.; Mulichak, A. M.; Finzel, B. C. and Lynn, J. C., Use of Medium-Sized Cycloalkyl Rings To Enhance Secondary Binding: Discovery of a New Class of Human Immunodeficiency Virus (HIV) Protease Inhibitors, *J. Med. Chem.*, **1995**, *38*, 1884–1891.
21. Guney, T.; Wenderski, T. A.; Boudreau, M. W. and Tan, D. S., Synthesis of Benzannulated Medium-ring Lactams via a Tandem Oxidative Dearomatization-Ring Expansion Reaction, *Chem. – Eur. J.*, **2018**, *24*, 13150–13157.
22. Dewick, P. M., *Medicinal Natural Products: A Biosynthetic Approach*, Verlag Helvetica Chimica Acta - Zürich, **2002**.
23. Hesse, M., *Alkaloids: Nature's Curse Or Blessing?*, John Wiley & Sons, **2002**.
24. Sun, L.-L.; Li, W.-S.; Li, J.; Zhang, H.-Y.; Yao, L.-G.; Luo, H.; Guo, Y.-W. and Li, X.-W., Uncommon Diterpenoids from the South China Sea Soft Coral *Sinularia humilis* and Their Stereochemistry, *J. Org. Chem.*, **2021**, *86*, 3367–3376.
25. Forte, B.; Malgesini, B.; Piutti, C.; Quartieri, F.; Scolaro, A. and Papeo, G., A Submarine Journey: The Pyrrole-Imidazole Alkaloids, *Marine Drugs*, **2009**, *7*, 705–753.
26. Hayashi, H.; Takiuchi, K.; Murao, S. and Arai, M., Structure and Insecticidal Activity of New Indole Alkaloids, Okaramines A and B, from *Penicillium simplicissimum* AK-40, *Agric. Biol. Chem.*, **1989**, *53*, 461–469.
27. Oldfield, E. and Lin, F.-Y., Terpene Biosynthesis: Modularity Rules, *Angew. Chem. Int. Ed.*, **2012**, *51*, 1124–1137.
28. Corey, E. J.; Mitra, R. B. and Uda, Hisashi., Total Synthesis of d,l-Caryophyllene and d,l-Isocaryophyllene, *J. Am. Chem. Soc.*, **1964**, *86*, 485–492.
29. Hübner, M.; Rissom, B. and Fitjer, L., Conformation and Dynamics of (–)-β-Caryophyllene, *Helv. Chim. Acta*, **1997**, *80*, 1972–1982.
30. Yudin, A. K., Macrocycles: lessons from the distant past, recent developments, and future directions, *Chem. Sci.*, **2014**, *6*, 30–49.

31. Reyes, R. L.; Iwai, T. and Sawamura, M., Construction of Medium-Sized Rings by Gold Catalysis, *Chem. Rev.*, **2021**, *121*, 8926–8947.
32. Lipinski, C. A., Lead- and drug-like compounds: the rule-of-five revolution, *Drug Discovery Today: Technol*, **2004**, *1*, 337–341.
33. Chagas, C. M.; Moss, S. and Alisaraie, L., Drug metabolites and their effects on the development of adverse reactions: Revisiting Lipinski's Rule of Five, *Int. J. Pharm. (Amsterdam, Neth.)*, **2018**, *549*, 133–149.
34. Zhang, C.; Liu, F.; Zhang, Y. and Song, C., Macrocycles and macrocyclization in anticancer drug discovery: Important pieces of the puzzle, *Eur. J. Med. Chem.*, **2024**, *268*, 116234.
35. Driggers, E. M.; Hale, S. P.; Lee, J. and Terrett, N. K., The exploration of macrocycles for drug discovery -- an underexploited structural class, *Nat Rev. Drug Discovery*, **2008**, *7*, 608–24.
36. Johnson, T. W.; Richardson, P. F.; Bailey, S.; Brooun, A.; Burke, B. J.; Collins, M. R.; Cui, J. J.; Deal, J. G.; Deng, Y.-L.; Dinh, D.; Engstrom, L. D.; He, M.; Hoffman, J.; Hoffman, R. L.; Huang, Q.; Kania, R. S.; Kath, J. C.; Lam, H.; Lam, J. L.; Le, P. T.; Lingardo, L.; Liu, W.; McTigue, M.; Palmer, C. L.; Sach, N. W.; Smeal, T.; Smith, G. L.; Stewart, A. E.; Timofeevski, S.; Zhu, H.; Zhu, J.; Zou, H. Y. and Edwards, M. P., Discovery of (10R)-7-Amino-12-fluoro-2,10,16-trimethyl-15-oxo-10,15,16,17-tetrahydro-2H-8,4-(metheno)pyrazolo[4,3-h][2,5,11]-benzoxadiazacyclotetradecine-3-carbonitrile (PF-06463922), a Macrocyclic Inhibitor of Anaplastic Lymphoma Kinase (ALK) and c-ros Oncogene 1 (ROS1) with Preclinical Brain Exposure and Broad-Spectrum Potency against ALK-Resistant Mutations, *J. Med. Chem.*, **2014**, *57*, 4720–4744.
37. Zou, H. Y.; Li, Q.; Engstrom, L. D.; West, M.; Appleman, V.; Wong, K. A.; McTigue, M.; Deng, Y.-L.; Liu, W.; Brooun, A.; Timofeevski, S.; McDonnell, S. R. P.; Jiang, P.; Falk, M. D.; Lappin, P. B.; Affolter, T.; Nichols, T.; Hu, W.; Lam, J.; Johnson, T. W.; Smeal, T.; Charest, A. and Fantin, V. R., PF-06463922 is a potent and selective next-generation ROS1/ALK inhibitor capable of blocking crizotinib-resistant ROS1 mutations, *Proc. Natl. Acad. Sci.*, **2015**, *112*, 3493–3498.
38. Girard, P.; Chauvin, M. and Verleye, M., Nefopam analgesia and its role in multimodal analgesia: A review of preclinical and clinical studies, *Clin. Exp. Pharmacol. Physiol.*, **2016**, *43*, 3–12.
39. Bassett, J. R.; Cairncross, K. D.; Hacket, N. B. and Story, M., Studies on the peripheral pharmacology of fenazoxine, a potential antidepressant drug, *Br. J. Pharmacol.*, **1969**, *37*, 69.
40. Glaser, R.; Frenking, G.; Loew, G. H.; Donnell, D.; Cohen, S. and Agranat, I., Solid-state stereochemistry of nefopam hydrochloride, a benzoxazocine analgesic drug, *J. Chem. Soc., Perkin Trans. 2*, **1989**, 113–122.
41. Bodireddy, M. R.; Krishnaiah, K.; Babu, P. K.; Bitra, C.; Gajula, M. R. and Kumar, P., Old is Gold? Nefopam Hydrochloride, a Non-opioid and Non-steroidal Analgesic Drug and Its Practical One-Pot Synthesis in a Single Solvent for Large-Scale Production, *Org. Process Res. Dev.*, **2017**, *21*, 1745–1751.



42. Illuminati, G. and Mandolini, L., Ring closure reactions of bifunctional chain molecules, *Acc. Chem. Res.*, **1981**, *14*, 95–102.
43. White, C. J. and Yudin, A. K., Contemporary strategies for peptide macrocyclization, *Nat. Chem.*, **2011**, *3*, 509–24.
44. DeTar, D. F. and Luthra, N. P., Quantitative evaluation of steric effects in SN2 ring closure reactions, *J. Am. Chem. Soc.*, **1980**, *102*, 4505–4512.
45. Martí-Centelles, V.; Pandey, M. D.; Burguete, M. I. and Luis, S. V., Macrocyclization Reactions: The Importance of Conformational, Configurational, and Template-Induced Preorganization, *Chem. Rev.*, **2015**, *115*, 8736–8834.
46. Majhi, T. P.; Achari, B. and Chattopadhyay, P., Advances in the synthesis and biological perspectives of benzannulated medium ring heterocycles, *Heterocycles*, **2007**, *71*, 1011–1052.
47. Chan, L.; Hutchison, G. R. and Morris, G. M., Understanding Ring Puckering in Small Molecules and Cyclic Peptides, *J. Chem. Inf. Model.*, **2021**, *61*, 743–755.
48. Hoffmann, R. W., Allylic 1,3-strain as a controlling factor in stereoselective transformations, *Chem. Rev.*, **1989**, *89*, 1841–1860.
49. Zhao, H.; Brånalt, J.; Perry, M. and Tyrchan, C., The Role of Allylic Strain for Conformational Control in Medicinal Chemistry, *J. Med. Chem.*, **2023**, *66*, 7730–7755.
50. Glunz, P. W., Recent encounters with atropisomerism in drug discovery, *Bioorg. Med. Chem. Lett.*, **2018**, *28*, 53–60.
51. Van Den Berge, E.; Pospíšil, J.; Trieu-Van, T.; Collard, L. and Robiette, R., Planar Chirality of Imidazole-Containing Macrocycles – Understanding and Tuning Atropisomerism, *Eur. J. Org. Chem.*, **2011**, *2011*, 6649–6655.
52. Lawer, A.; Rossi-Ashton, J. A.; Stephens, T. C.; Challis, B. J.; Epton, R. G.; Lynam, J. M. and Unsworth, W. P., Internal Nucleophilic Catalyst Mediated Cyclisation/Ring Expansion Cascades for the Synthesis of Medium-Sized Lactones and Lactams, *Angew. Chem. Int. Ed.*, **2019**, *58*, 13942–13947.
53. Eliel, E. L. and Wilen, S. H., *Stereochemistry of Organic Compounds*, John Wiley & Sons, **1994**.
54. Barton, D. H. *The Principles of Conformational Analysis*. Nobel Lecture, December 11, **1969**. (<https://www.nobelprize.org/uploads/2018/06/barton-lecture.pdf>, accessed 09.12.2024)
55. Mazzanti, A. and Casarini, D., Recent trends in conformational analysis, *Wiley Interdiscip. Rev.: Comput. Mol. Sci.*, **2012**, *2*, 613–641.
56. Toniolo, C., Conformationally restricted peptides through short-range cyclizations, *Int. J. Pept. Protein Res.*, **1990**, *35*, 287–300.
57. Jung, M. E. and Piizzi, G., gem-Disubstituent Effect: Theoretical Basis and Synthetic Applications, *Chem. Rev.*, **2005**, *105*, 1735–1766.

58. Still, W. C. and Galynker, I., Stereospecific synthesis of the C30-C43 segment of palytoxin by macrocyclically controlled remote asymmetric induction, *J. Am. Chem. Soc.*, **1982**, *104*, 1774–1776.
59. Carreira, E. M. and Kvaerno, L., *Classics in stereoselective synthesis*, Weinheim [Germany]: Wiley-VCH, **2009**.
60. Ovchinnikov, Yu. A. and Ivanov, V. T., Conformational states and biological activity of cyclic peptides, *Tetrahedron*, **1975**, *31*, 2177–2209.
61. Lewis-Atwell, T.; Townsend, P. A. and Grayson, M. N., Comparisons of different force fields in conformational analysis and searching of organic molecules: A review, *Tetrahedron*, **2021**, *79*, 131865.
62. Napiórkowska, E.; Milcarz, K. and Szeleszczuk, Ł., Review of Applications of Density Functional Theory (DFT) Quantum Mechanical Calculations to Study the High-Pressure Polymorphs of Organic Crystalline Materials, *Int. J. Mol. Sci.*, **2023**, *24*, 14155.
63. Bursch, M.; Mewes, J.-M.; Hansen, A. and Grimme, S., Best-Practice DFT Protocols for Basic Molecular Computational Chemistry, *Angew. Chem. Int. Ed.*, **2022**, *61*, e202205735.
64. Rolig, A., 9-renkaiset terpenoidit : humilisiini E:n syklopentaaniytimen synteesi. M.Sc thesis, University of Jyväskylä, **2023**. <https://jyx.jyu.fi/handle/123456789/87799> (accessed 09.12.2024)
65. Schrödinger Release Notes - Release 2023-3, <https://www.schrodinger.com/life-science/download/release-notes/release-2023-3/> (14.11.2024).
66. Zhao, Y. and Truhlar, D. G., The M06 suite of density functionals for main group thermochemistry, thermochemical kinetics, noncovalent interactions, excited states, and transition elements: two new functionals and systematic testing of four M06 functionals and 12 other functionals, *Theor. Chem. Acc.*, **2008**, *119*, 525–525.
67. Bochevarov, A. D.; Harder, E.; Hughes, T. F.; Greenwood, J. R.; Braden, D. A.; Philipp, D. M.; Rinaldo, D.; Halls, M. D.; Zhang, J. and Friesner, R. A., Jaguar: A high-performance quantum chemistry software program with strengths in life and materials sciences, *Int. J. Quantum Chem.*, **2013**, *113*, 2110–2142.
68. Neuvonen, A. J.; Noutsias, D.; Topić, F.; Rissanen, K.; Földes, T.; Pápai, I. and Pihko, P. M., Dynamic Refolding of Ion-Pair Catalysts in Response to Different Anions, *J. Org. Chem.*, **2019**, *84*, 15009–15019.
69. Ivanov, P. M. and Ōsawa, E., Remarks on the analysis of torsional energy surfaces of cycloheptane and cyclooctane by molecular mechanics, *J. Comput. Chem.*, **1984**, *5*, 307–313.
70. Wiberg, K. B., The C7–C10 Cycloalkanes Revisited, *J. Org. Chem.*, **2003**, *68*, 9322–9329.
71. Bharadwaj, R. K., Conformational properties of cyclooctane: a molecular dynamics simulation study, *Molecular Physics*, **2000**, *98*, 211–218.

72. Rocha, W. R.; Pliego Jr., J. R.; Resende, S. M.; Dos Santos, H. F.; De Oliveira, M. A. and De Almeida, W. B., Ab initio conformational analysis of cyclooctane molecule, *J. Comput. Chem.*, **1998**, *19*, 524–534.
73. Zuccarello, F.; Buemi, G. ja Favini, G., Conformational energies of cyclenes, *J. Mol. Struct.*, **1973**, *18*, 295–302.
74. Lee, I.-C., MO Studies on configuration and Conformation (VI). FMO Interpretation of Nonbonded Interactions, *Bull. Korean Chem. Soc.*, **1980**, *1*, 4–10.
75. Hassner, A.; Amit, B.; Marks, V. and Gottlieb, H. E., On the Conformation of 8-Membered Ring Heterocycles – Dynamic and Static Conformational Analysis of Acylated Hexahydrobenzazocines, *Eur. J. Org. Chem.*, **2006**, *2006*, 1256–1261.
76. Nasipuri, D., *Stereochemistry of Organic Compounds: Principles and Applications*, 4th ed.; New Academic Science, **2012**.
77. Donald, J. R. and Unsworth, W. P., Ring-Expansion Reactions in the Synthesis of Macrocycles and Medium-Sized Rings, *Chem. – Eur. J.*, **2017**, *23*, 8780–8799.
78. Huber, T.; Wildermuth, R. E. and Magauer, T., 9-Membered Carbocycles: Strategies and Tactics for their Synthesis, *Chem. – Eur. J.*, **2018**, *24*, 12107–12120.
79. Molander, G. A.; Huérou, Y. L. and Brown, G. A., Sequenced Reactions with Samarium(II) Iodide. Sequential Intramolecular Barbier Cyclization/Grob Fragmentation for the Synthesis of Medium-Sized Carbocycles, *J. Org. Chem.*, **2001**, *66*, 4511–4516.
80. Grob, C. A., Mechanisms and Stereochemistry of Heterolytic Fragmentation, *Angew. Chem. Int. Ed. in English*, **1969**, *8*, 535–546.
81. Molander, G. A., Application of lanthanide reagents in organic synthesis, *Chem. Rev.*, **1992**, *92*, 29–68.
82. Snape, T. J., Recent advances in the semi-pinacol rearrangement of  $\alpha$ -hydroxy epoxides and related compounds, *Chem. Soc. Rev.*, **2007**, *36*, 1823–1842.
83. Paquette, L. A., Stereocontrolled Construction of Complex Cyclic Ketones via Oxy-Cope Rearrangement, *Angew. Chem. Int. Ed. in English*, **1990**, *29*, 609–626.
84. Kato, T.; Kondo, H.; Nishino, M.; Tanaka, M.; Hata, G. and Miyake, A., A Facile Synthesis of 1,2-Divinylcycloalkanols and Their Behavior in the Oxy-Cope Rearrangement, *Bull. Chem. Soc. Jpn.*, **1980**, *53*, 2958–2961.
85. Tomooka, K.; Ezawa, T.; Inoue, H.; Uehara, K. and Igawa, K., Dynamic chirality of (E)-5-cyclononen-1-one and its enolate, *J. Am. Chem. Soc.*, **2011**, *133*, 1754–1756.
86. Harusawa, S.; Osaki, H.; Takemura, S.; Yoneda, R. and Kurihara, T., [3,3]Sigmatropic ring expansion of cyclic thionocarbonates. 5. Stereoselective synthesis of the yellow scale pheromone, *Tetrahedron Lett.*, **1992**, *33*, 2543–2546.
87. Prado, G.; Veiga, A. X.; Fernández-Nieto, F.; Paleo, M. R. and Sardina, F. J., A Two-Step, Stereoselective Synthesis of Nine- and Ten-Membered Carbocycles from Phthalates, *Org. Lett.*, **2015**, *17*, 2054–2057.

88. Pérez-Vázquez, J.; Veiga, A. X.; Prado, G.; Sardina, F. J. and Paleo, M. R., Enantioselective Annulation Reactions of Bisenolates Prepared Through Dearomatization Reactions of Aromatic and Heteroaromatic Diesters, *Eur. J. Org. Chem.*, **2012**, 2012, 975–987.
89. Wang, N.; Xu, H.-J.; Li, T.; Ye, L.-W. and Zhou, B., Copper-Catalyzed [2 + 2] Cyclization/Ring Expansion of Ene-Ynamides: Construction of Medium- and Large-Sized Rings, *Org. Lett.*, **2024**, 26, 3861–3866.
90. Bao-Long, H.; Wong, J. J.; Na, L.; Yong-Qiang, W.; Houk, K. N. and Chuang-Chuang, L., Facile generation of bridged medium-sized polycyclic systems by rhodium-catalysed intramolecular (3+2) dipolar cycloadditions, *Nature Communications*, **2021**, 12, 5239.
91. Saridakis, I.; Kaiser, D. and Maulide, N., Unconventional Macrocyclizations in Natural Product Synthesis, *ACS Cent. Sci.*, **2020**, 6, 1869–1889.
92. Skardon-Duncan, J.; Sparenberg, M.; Bayle, A.; Alexander, S. and Clark, J. S., Stereoselective Synthesis of Medium-Sized Cyclic Ethers by Sequential Ring-Closing Metathesis and Tsuji–Troost Allylation, *Org. Lett.*, **2018**, 20, 2782–2786.
93. Girard, P.; Namy, J. L. and Kagan, H. B., Divalent lanthanide derivatives in organic synthesis. 1. Mild preparation of samarium iodide and ytterbium iodide and their use as reducing or coupling agents, *J. Am. Chem. Soc.*, **1980**, 102, 2693–2698.
94. Saadi, J.; Lentz, D. and Reissig, H.-U., Medium-Sized Carbocycles by Samarium Diiodide-Induced Carbonyl–Alkene Cyclizations, *Org. Lett.*, **2009**, 11, 3334–3337.
95. Molander, G. A. and Rivero, M. R., Suzuki Cross-Coupling Reactions of Potassium Alkenyltrifluoroborates, *Org. Lett.*, **2002**, 4, 107–109.
96. Hu, Y.-J.; Gu, C.-C.; Wang, X.-F.; Min, L. and Li, C.-C., Asymmetric Total Synthesis of Taxol, *J. Am. Chem. Soc.*, **2021**, 143, 17862–17870.
97. Morihira, K.; Hara, R.; Kawahara, S.; Nishimori, T.; Nakamura, N.; Kusama, H. and Kuwajima, I., Enantioselective Total Synthesis of Taxol, *J. Am. Chem. Soc.*, **1998**, 120, 12980–12981.
98. Min, L.; Han, J.-C.; Zhang, W.; Gu, C.-C.; Zou, Y.-P. and Li, C.-C., Strategies and Lessons Learned from Total Synthesis of Taxol, *Chem. Rev.*, **2023**, 123, 4934–4971.
99. Nicolaou, K. C. and Sorensen, E. J., *Classics in total synthesis I: targets, strategies, methods*, VCH, **1996**.
100. Danishefsky, S. J.; Masters, J. J.; Young, W. B.; Link, J. T.; Snyder, L. B.; Magee, T. V.; Jung, D. K.; Isaacs, R. C. A.; Bornmann, W. G.; Alaimo, C. A.; Coburn, C. A. and Di Grandi, M. J., Total Synthesis of Baccatin III and Taxol, *J. Am. Chem. Soc.*, **1996**, 118, 2843–2859.
101. Wender, P. A.; Badham, N. F.; Conway, S. P.; Floreancig, P. E.; Glass, T. E.; Gränicher, C.; Houze, J. B.; Jänichen, J.; Lee, D.; Marquess, D. G.; McGrane, P. L.; Meng, W.; Mucciario, T. P.; Mühlebach, M.; Natchus, M. G.; Paulsen, H.; Rawlins, D. B.; Satkofsky, J.; Shuker, A. J.; Sutton, J. C.; Taylor, R. E. and Tomooka, K., The Pinene Path to Taxanes. 5. Stereocontrolled Synthesis of a Versatile Taxane Precursor, *J. Am. Chem. Soc.*, **1997**, 119, 2755–2756.

102. Kanda, Y.; Ishihara, Y.; Wilde, N. C. and Baran, P. S., Two-Phase Total Synthesis of Taxanes: Tactics and Strategies, *J. Org. Chem.*, **2020**, *85*, 10293–10320.
103. Mallinson, J. and Collins, I., Macrocycles in new drug discovery, *Future Med. Chem.*, **2012**, *4*, 1409–1438.
104. Gallego-Jara, J.; Lozano-Terol, G.; Sola-Martínez, R. A.; Cánovas-Díaz, M. and de Diego Puente, T., A Compressive Review about Taxol®: History and Future Challenges, *Molecules*, **2020**, *25*, 5986.
105. Tao, Y.; Sun, X.-S.; Pointreau, Y.; Tourneau, C. L.; Sire, C.; Kaminsky, M.-C.; Coutte, A.; Alfonsi, M.; Calderon, B.; Boisselier, P.; Martin, L.; Miroir, J.; Ramee, J.-F.; Delord, J.-P.; Clatot, F.; Rolland, F.; Villa, J.; Magne, N.; Elicin, O.; Gherga, E.; Nguyen, F.; Lafond, C.; Bera, G.; Calugaru, V.; Geoffrois, L.; Chauffert, B.; Damstrup, L.; Crompton, P.; Ennaji, A.; Gollmer, K.; Nauwelaerts, H. and Bourhis, J., Extended follow-up of a phase 2 trial of xevinapant plus chemoradiotherapy in high-risk locally advanced squamous cell carcinoma of the head and neck: a randomised clinical trial, *Eur. J. Cancer*, **2023**, *183*, 24–37.
106. Ren, X.; Zhao, B.; Chang, H.; Xiao, M.; Wu, Y. and Liu, Y., Paclitaxel suppresses proliferation and induces apoptosis through regulation of ROS and the AKT/MAPK signaling pathway in canine mammary gland tumor cells, *Mol. Med. Rep.*, **2018**, *17*, 8289–8299.
107. Gelderblom, H.; Verweij, J.; Nooter, K. and Sparreboom, A., Cremophor EL: the drawbacks and advantages of vehicle selection for drug formulation, *Eur. J. Cancer*, **2001**, *37*, 1590–1598.
108. Romines, K. R.; Morris, J. K.; Howe, W. J.; Tomich, P. K.; Horng, M.-M.; Chong, K.-T.; Hinshaw, R. R.; Anderson, D. J.; Strohbach, J. W.; Turner, S. R. and Mizens, S. A., Cycloalkylpyranones and Cycloalkyldihydropyrones as HIV Protease Inhibitors: Exploring the Impact of Ring Size on Structure–Activity Relationships, *J. Med. Chem.*, **1996**, *39*, 4125–4130.
109. Romines, K. R.; Watenpaugh, K. D.; Howe, W. J.; Tomich, P. K.; Lovasz, K. D.; Morris, J. K.; Janakiraman, M. N.; Lynn, J. C. and Horng, M.-M., Structure-Based Design of Nonpeptidic HIV Protease Inhibitors from a Cyclooctylpyranone Lead Structure, *J. Med. Chem.*, **1995**, *38*, 4463–4473.
110. Ferris, R. L.; Harrington, K.; Schoenfeld, J. D.; Tahara, M.; Esdar, C.; Salmio, S.; Schroeder, A. and Bourhis, J., Inhibiting the inhibitors: Development of the IAP inhibitor xevinapant for the treatment of locally advanced squamous cell carcinoma of the head and neck, *Cancer Treat. Rev.*, **2023**, *113*, 102492.
111. Arnt, C. R.; Chiorean, M. V.; Heldebrant, M. P.; Gores, G. J. and Kaufmann, S. H., Synthetic Smac/DIABLO Peptides Enhance the Effects of Chemotherapeutic Agents by Binding XIAP and cIAP1 *in Situ* \*, *J. Biol. Chem.*, **2002**, *277*, 44236–44243.
112. Sun, H.; Stuckey, J. A.; Nikolovska-Coleska, Z.; Qin, D.; Meagher, J. L.; Qiu, S.; Lu, J.; Yang, C.-Y.; Saito, N. G. and Wang, S., Structure-Based Design, Synthesis, Evaluation, and Crystallographic Studies of Conformationally Constrained Smac Mimetics as Inhibitors of the X-linked Inhibitor of Apoptosis Protein (XIAP), *J. Med. Chem.*, **2008**, *51*, 7169–7180.

113. LaCasse, E. C.; Baird, S.; Korneluk, R. G. and MacKenzie, A. E., The inhibitors of apoptosis (IAPs) and their emerging role in cancer, *Oncogene*, **1998**, *17*, 3247–3259.
114. Oost, T. K.; Sun, C.; Armstrong, R. C.; Al-Assaad, A.-S.; Betz, S. F.; Deckwerth, T. L.; Ding, H.; Elmore, S. W.; Meadows, R. P.; Olejniczak, E. T.; Oleksijew, A.; Oltersdorf, T.; Rosenberg, S. H.; Shoemaker, A. R.; Tomaselli, K. J.; Zou, H. and Fesik, S. W., Discovery of Potent Antagonists of the Antiapoptotic Protein XIAP for the Treatment of Cancer, *J. Med. Chem.*, **2004**, *47*, 4417–4426.
115. Verma, P.; Pallerla, R. R.; Rolig, A. and Pihko, P. M., Humilisin E: Strategy for the Synthesis and Access to the Functionalized Bicyclic Core, *J. Org. Chem.*, **2024**, *89*, 6987–6990.
116. Liu, Y.; Liu, X. and Feng, X., Recent advances in metal-catalysed asymmetric sigmatropic rearrangements, *Chem. Sci.*, **2022**, *13*, 12290–12308.
117. Bruce, V. K.; Farshadfar, K.; Rolig, A.; Laasonen, K. and Pihko, P. M., Aliphatic Ketone Claisen Rearrangement: Troubleshooting the Transesterification Step by Identifying a Stable Acid Catalyst, *Chem. – Eur. J.*, **2024**, *30*, e202402371.
118. Belardi, J. K. and Micalizio, G. C., Conversion of Allylic Alcohols to Stereodefined Trisubstituted Alkenes: A Complementary Process to the Claisen Rearrangement, *J. Am. Chem. Soc.*, **2008**, *130*, 16870–16872.
119. Smith, A. B. and Agosta, W. C., Photochemical reactions of 1-cyclopentenyl and 1-cyclohexenyl ketones, *J. Am. Chem. Soc.*, **1973**, *95*, 1961–1968.
120. Corey, E. J. and Venkateswarlu, A., Protection of hydroxyl groups as tert-butyltrimethylsilyl derivatives, *J. Am. Chem. Soc.*, **1972**, *94*, 6190–6191.
121. Bandarage, U. K.; Fang, X.; Garvey, D. S.; Letts, L. G.; Schroeder, J. D. and Tam, S. W., Nitrosated and nitrosylated cyclooxygenase-2 inhibitors, compositions and methods of use, US 6649629 B2, **2003**.
122. Hirayama, Y.; Okuzumi, K.; Masubuti, H.; Uekusa, H.; Girault, J.-P. and Fujimoto, Y., Stereochemical Assignment of C-24 and C-25 of Amarasterone A, a Putative Biosynthetic Intermediate of Cyasterone, *J. Org. Chem.*, **2014**, *79*, 5471–5477.
123. Yang, L.; Zhang, J.; Xie, J.; Ma, X.; Zhang, L.; Zhao, C. and Hase, W. L., Competing E2 and SN2 Mechanisms for the F<sup>-</sup> + CH<sub>3</sub>CH<sub>2</sub>I Reaction, *J. Phys. Chem. A*, **2017**, *121*, 1078–1085.
124. Schneider, M.; Richter, M. J. R. and Carreira, E. M., Total Synthesis of (–)-Mitrephorone A Enabled by Stereoselective Nitrile Oxide Cycloaddition and Tetrasubstituted Olefin Synthesis, *J. Am. Chem. Soc.*, **2020**, *142*, 17802–17809
125. Cunico, R. F. and Bedell, L., The triisopropylsilyl group as a hydroxyl-protecting function, *J. Org. Chem.*, **1980**, *45*, 4797–4798.
126. Botubol-Ares, J. M.; Durán-Peña, M. J.; Hernández-Galán, R.; Collado, I. G.; Harwood, L. M. and Macías-Sánchez, A. J., Diastereoselective and enantioselective preparation of nor-mevaldic acid surrogates through desymmetrisation methodology. Enantioselective synthesis of (+) and (–) nor-mevalonic lactones, *Tetrahedron*, **2015**, *71*, 7531–7538.

127. Nuyken, O. and Pask, S. D., Ring-Opening Polymerization—An Introductory Review, *Polymers*, **2013**, *5*, 361–403.
128. Hardouin Duparc, V.; Shakaroun, R. M.; Slawinski, M.; Carpentier, J.-F. and Guillaume, S. M., Ring-opening (co)polymerization of six-membered substituted  $\delta$ -valerolactones with alkali metal alkoxides, *Eur. Polym. J.*, **2020**, *134*, 109858.
129. Williams, J. M.; Jobson, R. B.; Yasuda, N.; Marchesini, G.; Dolling, U.-H. and Grabowski, E. J. J., A new general method for preparation of *N*-methoxy-*N*-methylamides. Application in direct conversion of an ester to a ketone, *Tetrahedron Lett.*, **1995**, *36*, 5461–5464.
130. Lee, J. I. and Park, H., Synthetic Approaches to *N*-Methoxy-*N*-methylamides, *Bull. Korean. Chem. Soc.*, **2021**, *42*, 1001–1013.
131. Blackaby, W. P.; Huscroft, I. T.; Keown, L. E.; Lewis, R. T.; Raubo, P. A.; Street, L. J.; Thomson, C. G. and Thomson, J., Therapeutic Agents, WO 2006134341 A1, **2006**.
132. Fu, X.-F.; Xiang, Y. and Yu, Z.-X., RhI-Catalyzed Benzo/[7+1] Cycloaddition of Cyclopropyl-Benzocyclobutenes and CO by Merging Thermal and Metal-Catalyzed C–C Bond Cleavages, *Chem. – Eur. J.*, **2015**, *21*, 4242–4246.
133. Engel, P. S. and Culotta, A. M., Photolysis of azoalkanes. Reactions and kinetics of the 1-cyclopropylcyclopentane-1,3-diyl biradical and the 1-cyclopropylcyclopentyl radical, *J. Am. Chem. Soc.*, **1991**, *113*, 2686–2696.
134. Pattabiraman, V. R.; Stymiest, J. L.; Derksen, D. J.; Martin, N. I. and Vederas, J. C., Multiple On-Resin Olefin Metathesis to Form Ring-Expanded Analogues of the Lantibiotic Peptide, Lacticin 3147 A2, *Org. Lett.*, **2007**, *9*, 699–702.
135. Domańska-Babul, W.; Baranowska, K. and Pikies, J., Synthesis and Properties of Diisopropylamino Derivatives of Diphosphanes and Triphosphanes: The X-Ray Structure of (iPr<sub>2</sub>N)<sub>2</sub>P–P(SiMe<sub>3</sub>)<sub>2</sub>, *Phosphorus, Sulfur, and Silicon and the Related Elements*, **2009**, *184*, 936–941.
136. Bernstein, M. P.; Romesberg, F. E.; Fuller, D. J.; Harrison, A. T.; Collum, D. B.; Liu, Q. Y. and Williard, P. G., Structure and reactivity of lithium diisopropylamide in the presence of *N,N,N',N'*-tetramethylethylenediamine, *J. Am. Chem. Soc.*, **1992**, *114*, 5100–5110.
137. Barton, D. H. R.; O'Brien, R. E. and Sternhell, S., 88. A new reaction of hydrazones, *J. Chem. Soc.*, **1962**, 470–476.
138. Lam, C. and Mellor, J. M., Influence of a proximate 1,3-diene upon the photoreactivity of some  $\alpha\beta$ -unsaturated ketones, *J. Chem. Soc., Perkin Trans. 2*, **1975**, 519–522.
139. Chou, C.-H.; Wu, C.-Y.; Chen, C.-L.; Zhou, J.-Q.; Kao, Y.-C.; Chen, H.-Y. and Lin, P.-C., In vivo monitoring of carbonic anhydrase expression during the growth of larval zebrafish: a new environment-sensitive fluorophore for responsive turn-on fluorescence, *Chem. Commun.*, **2020**, *56*, 11307–11310.
140. Thompson, C. M.; Quinn, C. A. and Hergenrother, P. J., Total Synthesis and Cytoprotective Properties of Dykellic Acid, *J. Med. Chem.*, **2009**, *52*, 117–125.

141. Tang, S.; Shen, Q.; He, P.; Li, J.; Yang, J.; Si, X.; Xia, J.; Han, Y.; Li, Z.; Liu, C. and Gui, Q.-W., Synthesis of esters from 2-phenylimidazo[1,2-a]pyridines using visible light, *Tetrahedron*, **2023**, *131*, 133140.
142. Bourboula, A.; Mountanea, O. G.; Krasakis, G.; Mantzourani, C.; Kokotou, M. G.; Kokotos, C. G. and Kokotos, G., A Photochemical Protocol for the Synthesis of Weinreb and Morpholine Amides from Carboxylic Acids, *Eur. J. Org. Chem.*, **2023**, *26*, e202300008.
143. Marcos-Atanes, D.; Vidal, C.; Navo, C. D.; Peccati, F.; Jiménez-Osés, G. and Mascareñas, J. L., Iridium-Catalyzed ortho-Selective Borylation of Aromatic Amides Enabled by 5-Trifluoromethylated Bipyridine Ligands, *Angew. Chem. Int. Ed.*, **2023**, *62*, e202214510.
144. Phetcharawetch, J.; Betterley, N. M.; Soorukram, D.; Pohmakotr, M.; Reutrakul, V. and Kuhakarn, C., Synthesis of Difluoromethyl Ketones from Weinreb Amides, and Tandem Addition/Cyclization of o-Alkynylaryl Weinreb Amides, *Eur. J. Org. Chem.*, **2017**, *2017*, 6840–6850.
145. Baba, T.; Avasthi, K. and Suzuki, A., The Reaction of Organoboranes with Lithium Salts of Trisylhydrazones of Cycloalkanones Followed by Treatment with Iodine, *Bull. Chem. Soc. Jpn.*, **1983**, *56*, 1571–1572.
146. Liu, Y.; Zhan, X.; Ji, P.; Xu, J.; Liu, Q.; Luo, W.; Chen, T. and Guo, C., Transition metal-free C(sp<sup>3</sup>)–H bond coupling among three methyl groups, *Chem. Commun.*, **2017**, *53*, 5346–5349.
147. Yang, J.; Chen, S.; Zhou, H.; Wu, C.; Ma, B. and Xiao, J., Cobalt-Catalyzed  $\alpha$ -Methoxymethylation and Aminomethylation of Ketones with Methanol as a C1 Source, *Org. Lett.*, **2018**, *20*, 6774–6779.



## Appendices

APPENDIX 1:  $^1\text{H}$  NMR spectrum of TBS-protected bromoalcohol **10**

APPENDIX 2:  $^{13}\text{C}$  NMR spectrum of TBS-protected bromoalcohol **10**

APPENDIX 3: IR spectrum of TBS-protected bromoalcohol **10**

APPENDIX 4:  $^1\text{H}$  NMR spectrum of TBS-protected iodine alcohol **16**

APPENDIX 5:  $^{13}\text{C}$  NMR spectrum of TBS-protected iodine alcohol **16**

APPENDIX 6: IR spectrum of TBS-protected iodine alcohol **16**

APPENDIX 7:  $^1\text{H}$  NMR spectrum of alkylation product **12**

APPENDIX 8:  $^{13}\text{C}$  NMR spectrum of alkylation product **12**

APPENDIX 9: IR spectrum of alkylation product **12**

APPENDIX 10: HH-COSY spectrum of alkylation product **12**

APPENDIX 11:  $^1\text{H}$  NMR spectrum of amide **36**

APPENDIX 12:  $^{13}\text{C}$  NMR spectrum of amide **36**

APPENDIX 13: IR spectrum of aromatic amide **36**

APPENDIX 14:  $^1\text{H}$  NMR spectrum of Weinreb amide **17**

APPENDIX 15:  $^{13}\text{C}$  NMR spectrum of Weinreb amide **17**

APPENDIX 16: IR spectrum of Weinreb amide **17**

APPENDIX 17:  $^1\text{H}$  NMR spectrum of trisyl hydrazide **40**

APPENDIX 18: IR spectrum of trisyl hydrazide **40**

APPENDIX 19:  $^1\text{H}$  NMR spectrum of trisylhydrazone **42**

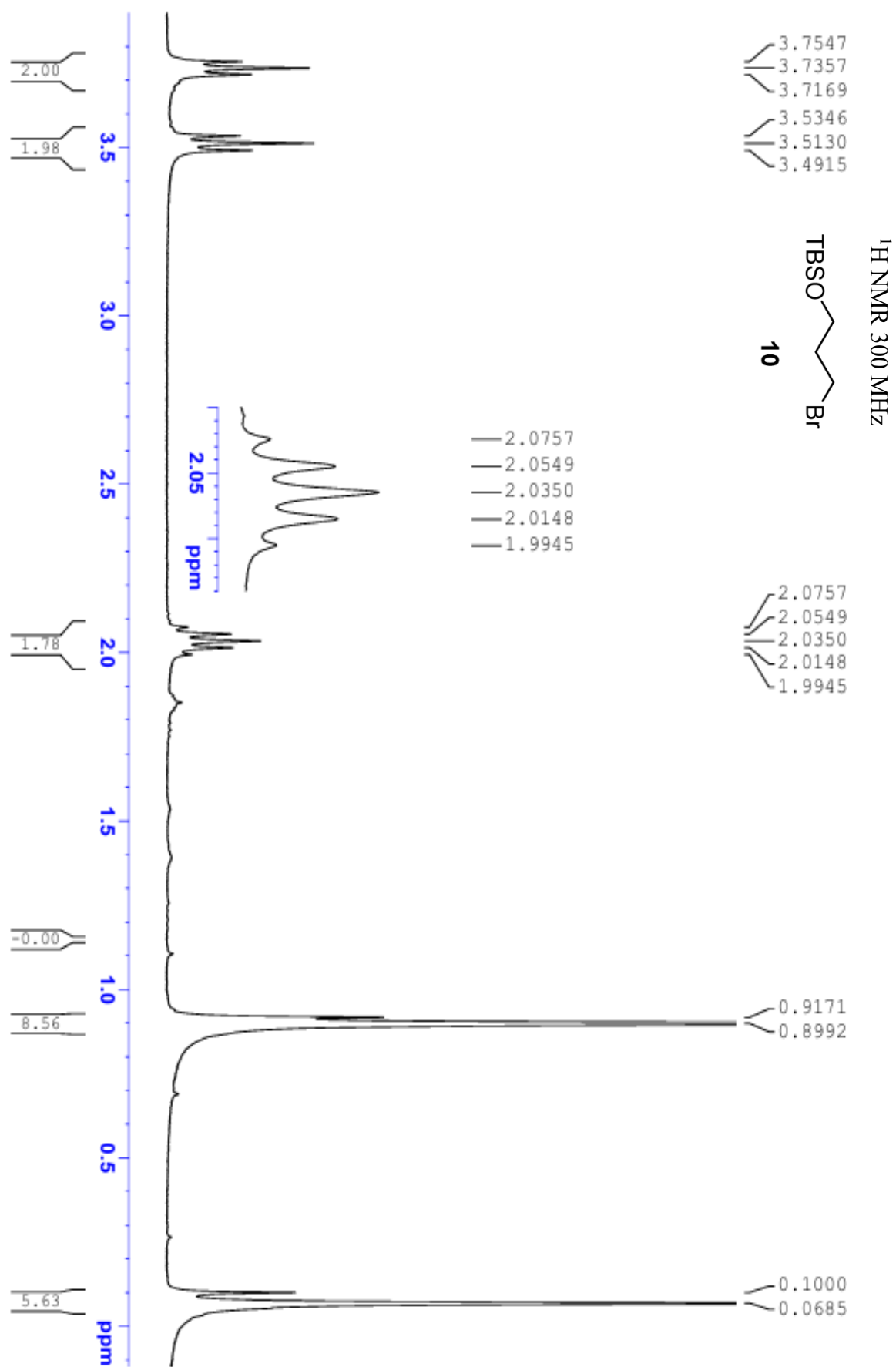
APPENDIX 20:  $^{13}\text{C}$  NMR spectrum of trisylhydrazone **42**

APPENDIX 21: IR spectrum of trisylhydrazone **42**

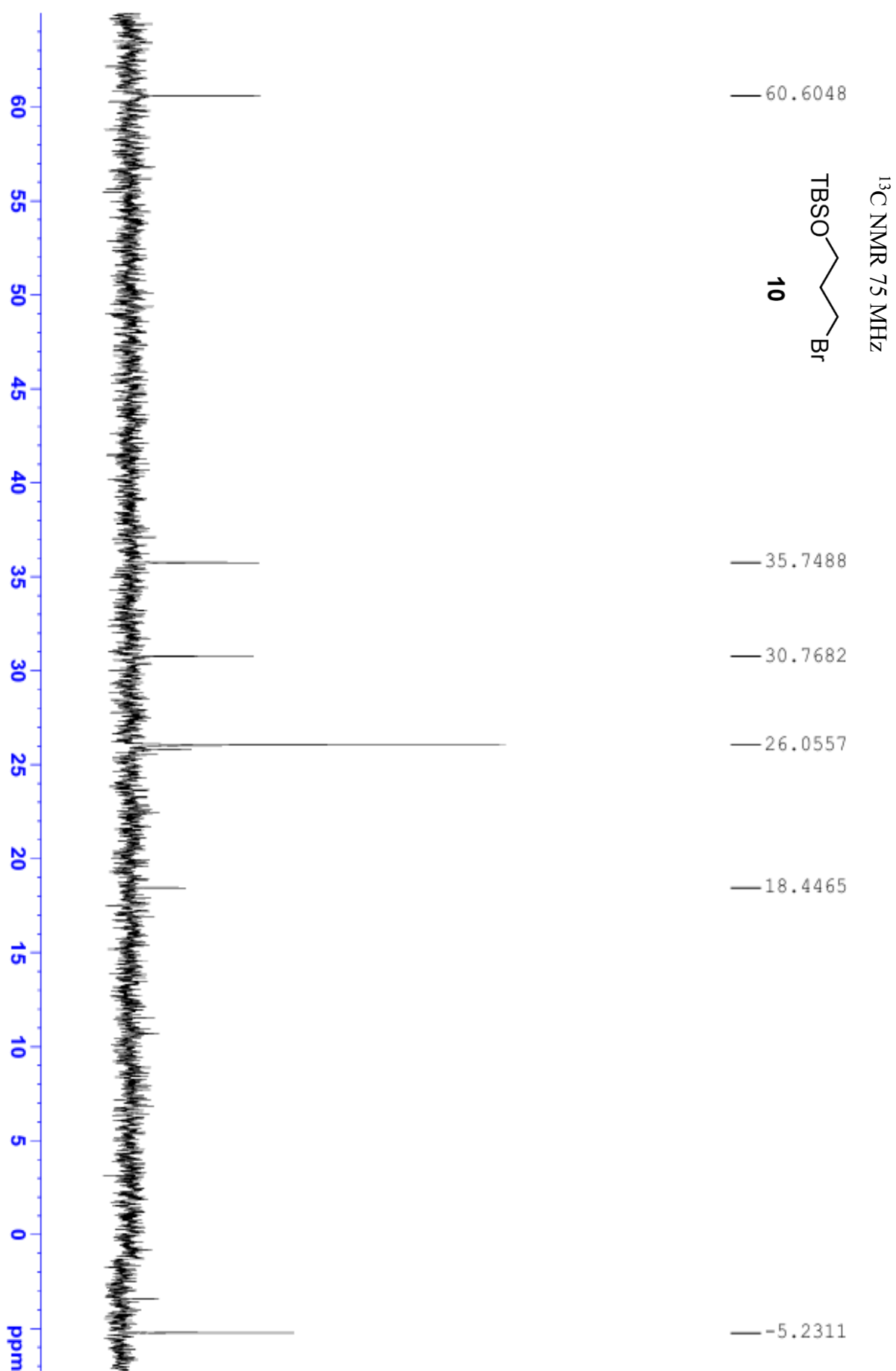
APPENDIX 22:  $^1\text{H}$  NMR spectrum of aromatic ketone **38**

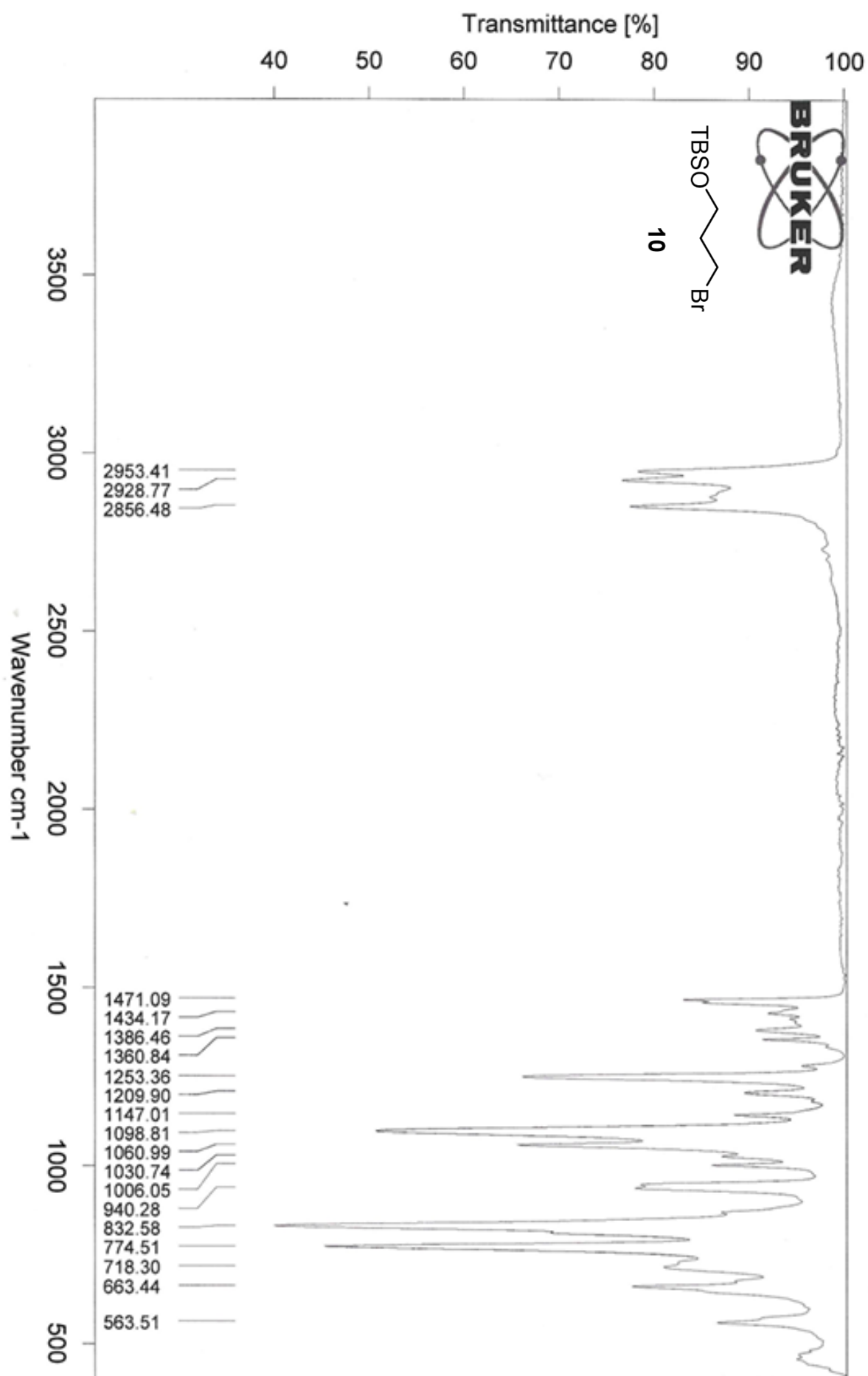
- APPENDIX 23:  $^{13}\text{C}$  NMR spectrum of aromatic ketone **38**
- APPENDIX 24: IR spectrum of aromatic ketone **38**
- APPENDIX 25:  $^1\text{H}$  NMR spectrum of isopropenyl ketone **18**
- APPENDIX 26:  $^{13}\text{C}$  NMR spectrum of isopropenyl ketone **18**
- APPENDIX 27: IR NMR spectrum of isopropenyl ketone **18**
- APPENDIX 28:  $^1\text{H}$  NMR spectrum of cyclopentenyl ketone **14**
- APPENDIX 29:  $^{13}\text{C}$  NMR spectrum of cyclopentenyl ketone **14**
- APPENDIX 30: IR spectrum of cyclopentenyl ketone **14**
- APPENDIX 31: HH COSY spectrum of cyclopentenyl ketone **14**
- APPENDIX 32: HSQC-edited spectrum of cyclopentenyl ketone **14**
- APPENDIX 33:  $^1\text{H}$  NMR spectrum of butyl ketone **45**
- APPENDIX 34: IR spectrum of butyl ketone **45**
- APPENDIX 35:  $^1\text{H}$  NMR spectrum of trisubstituted alkene **15**
- APPENDIX 36:  $^{13}\text{C}$  NMR spectrum of trisubstituted alkene **15**
- APPENDIX 37: IR NMR spectrum of trisubstituted alkene **15**
- APPENDIX 38: HH-COSY NMR spectrum of trisubstituted alkene **15**
- APPENDIX 39: 1D NOE spectrum of trisubstituted alkene **15**
- APPENDIX 40: HSQC-edited NMR spectrum of trisubstituted alkene **15**

## APPENDIX 1



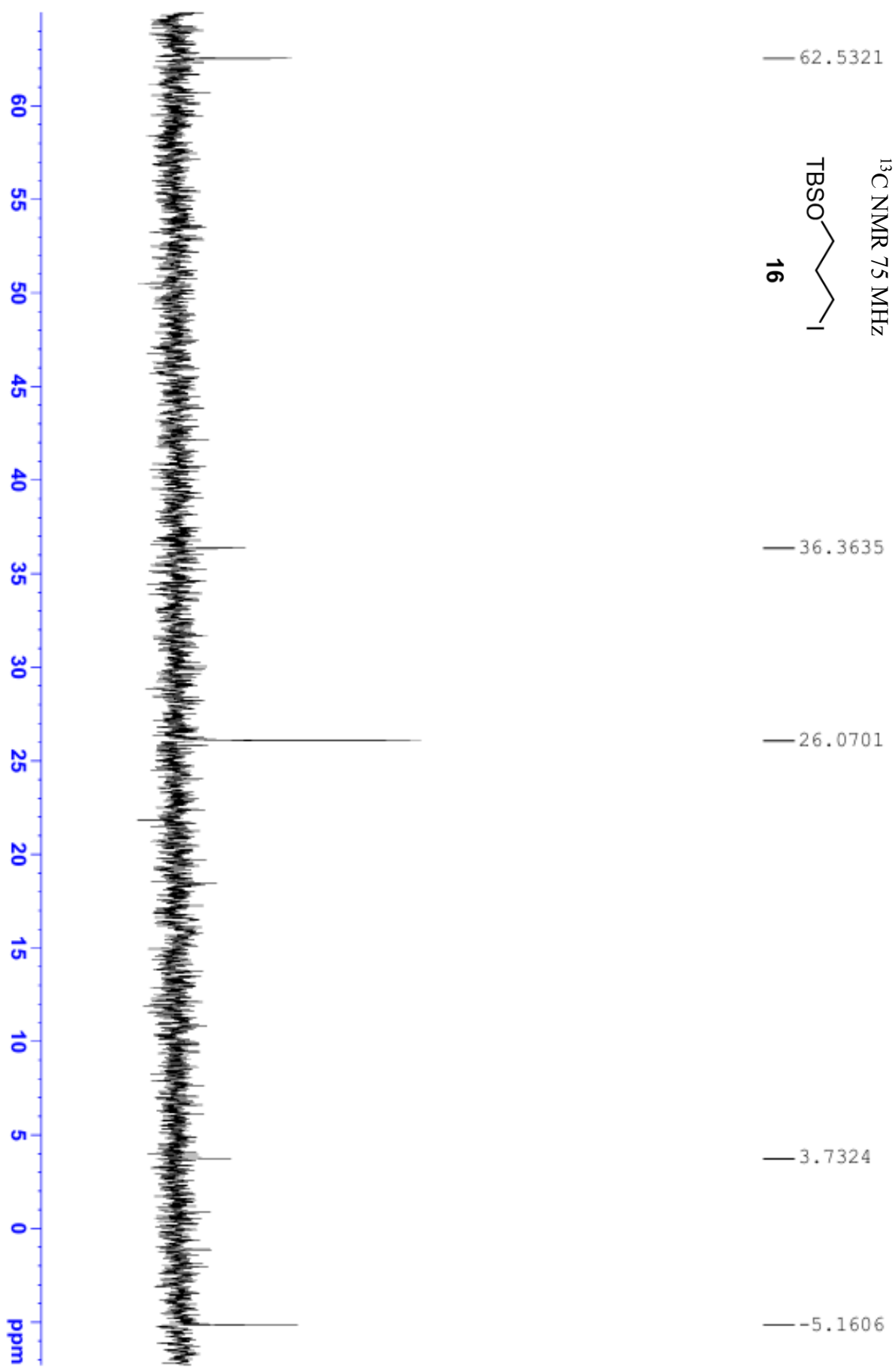
## APPENDIX 2

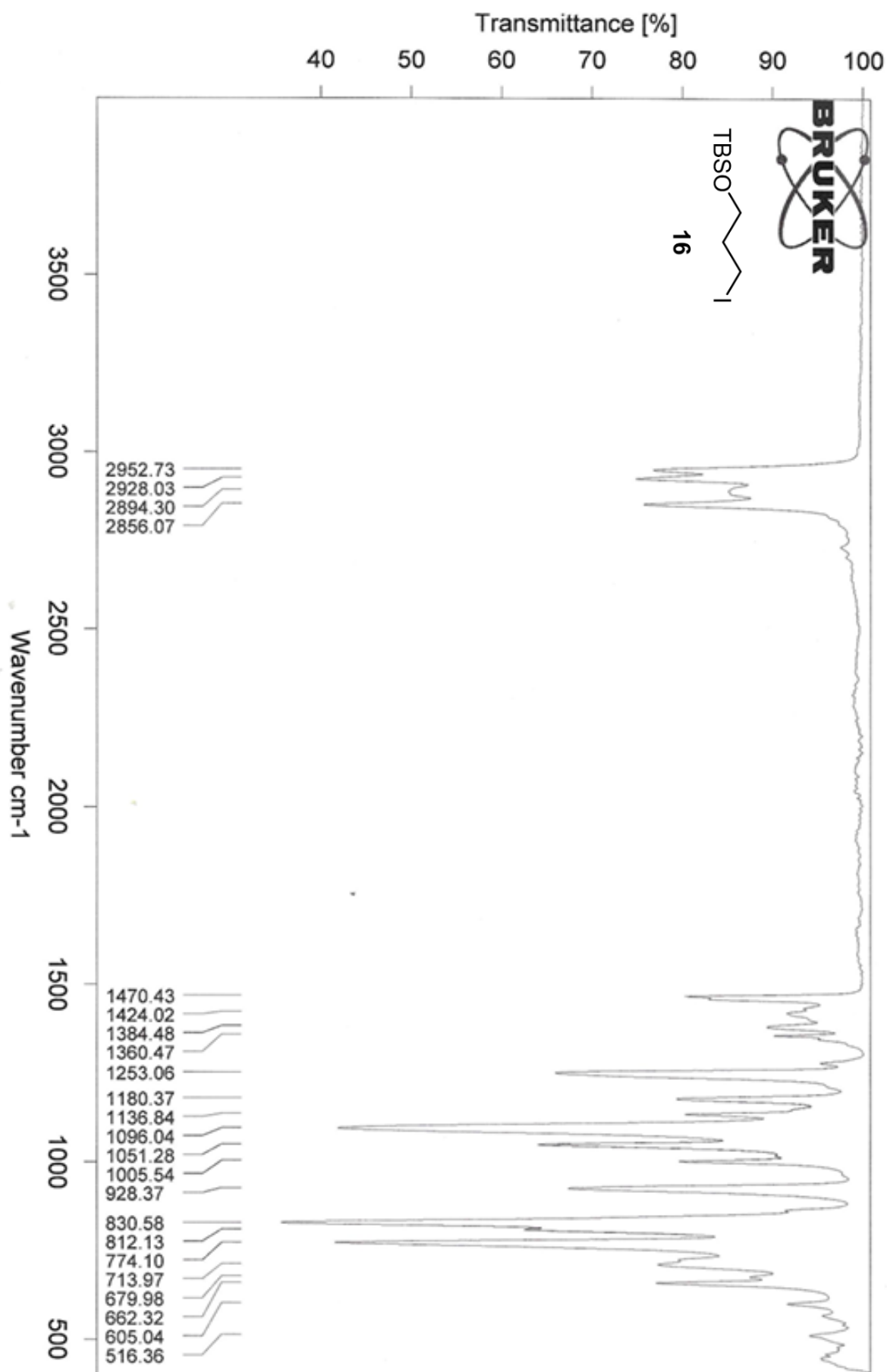






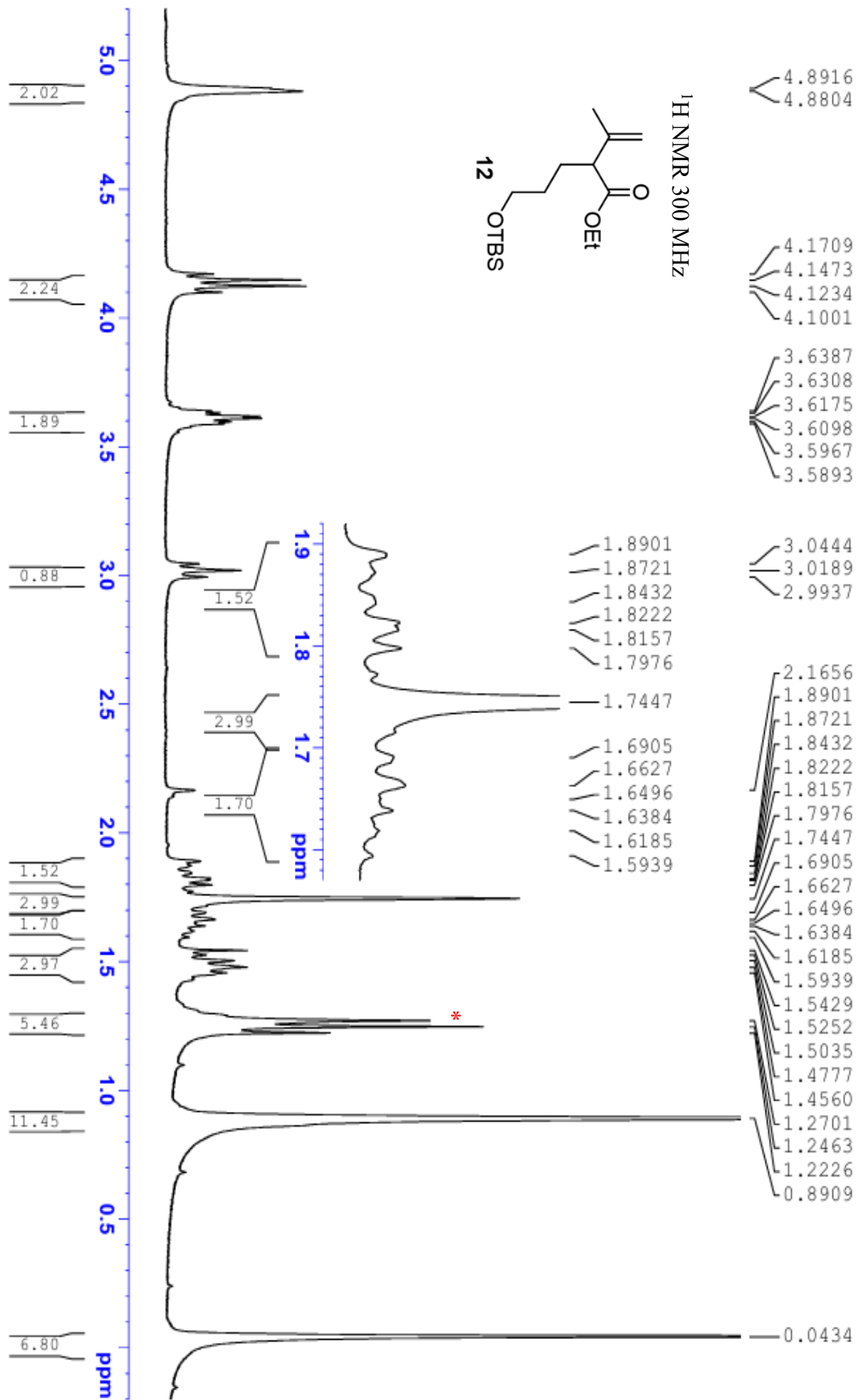
## APPENDIX 5



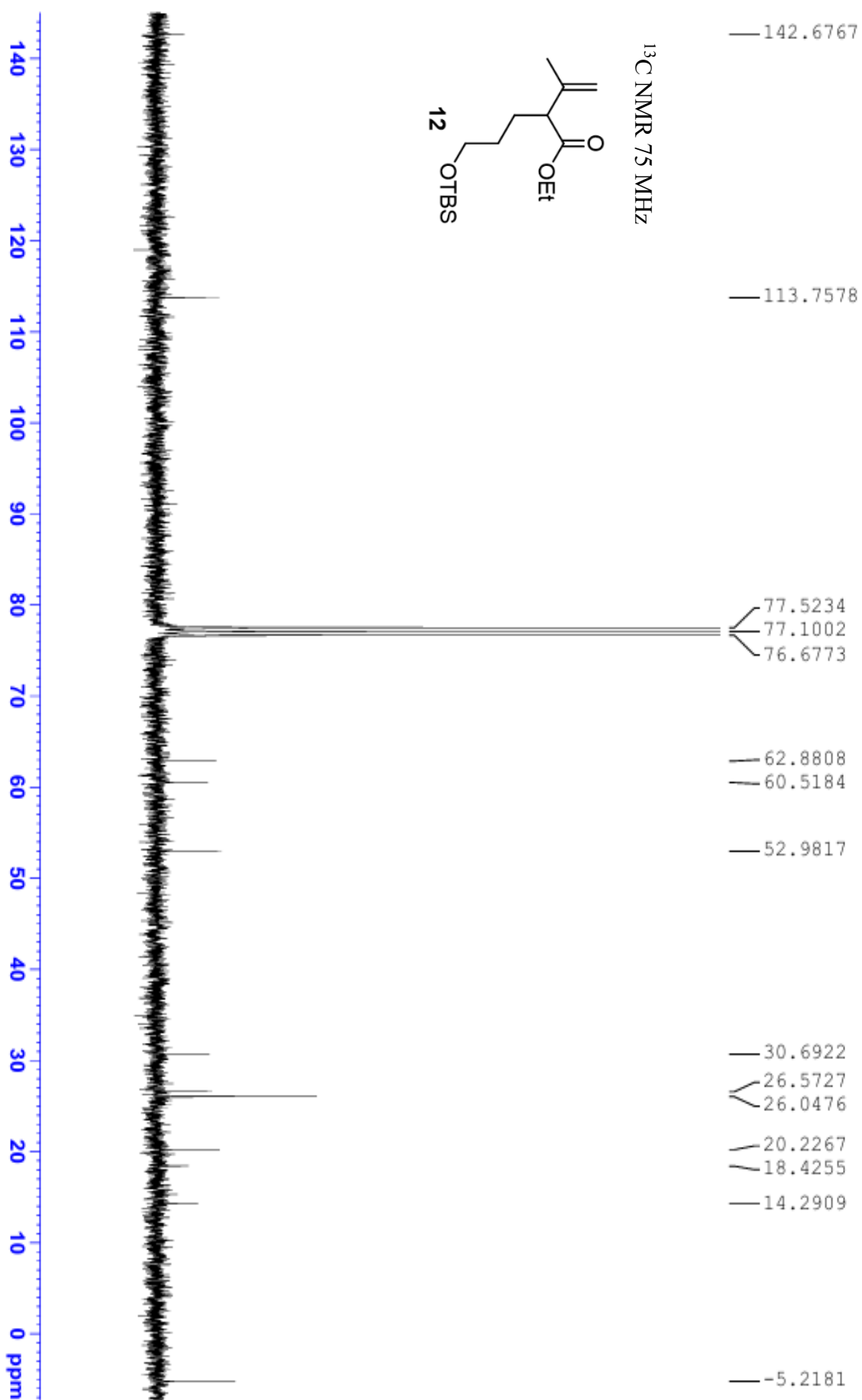


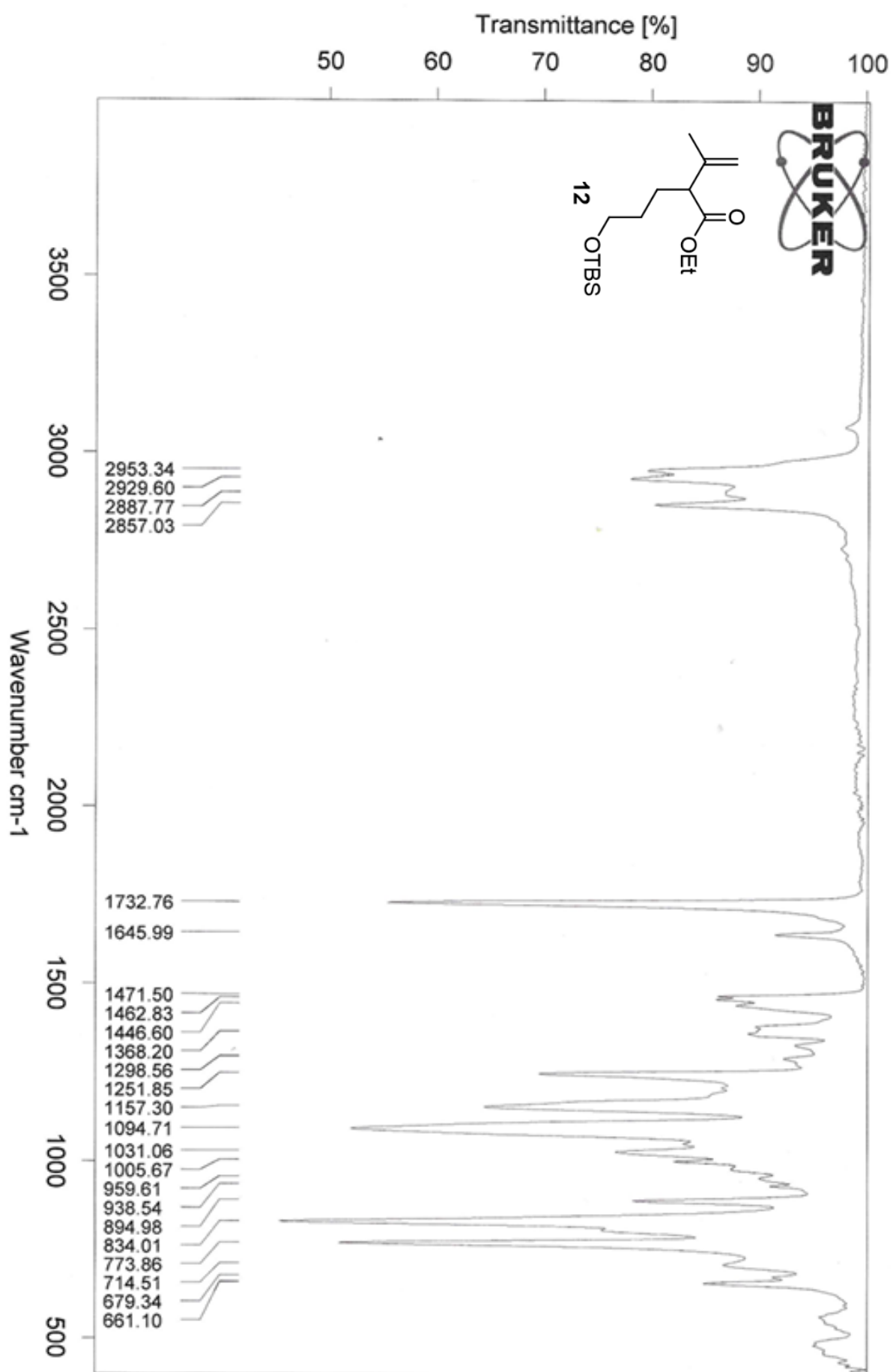


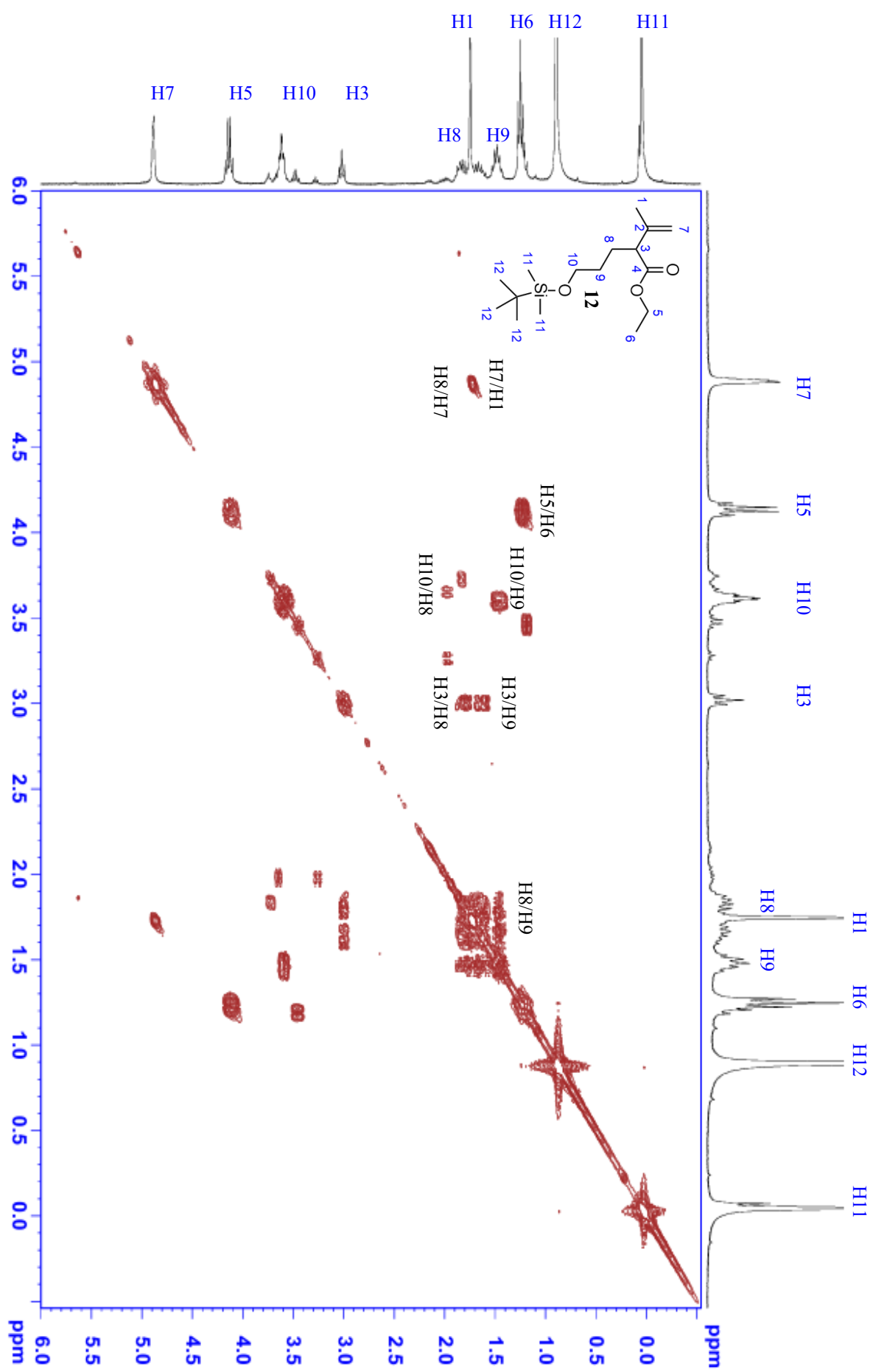
## APPENDIX 7

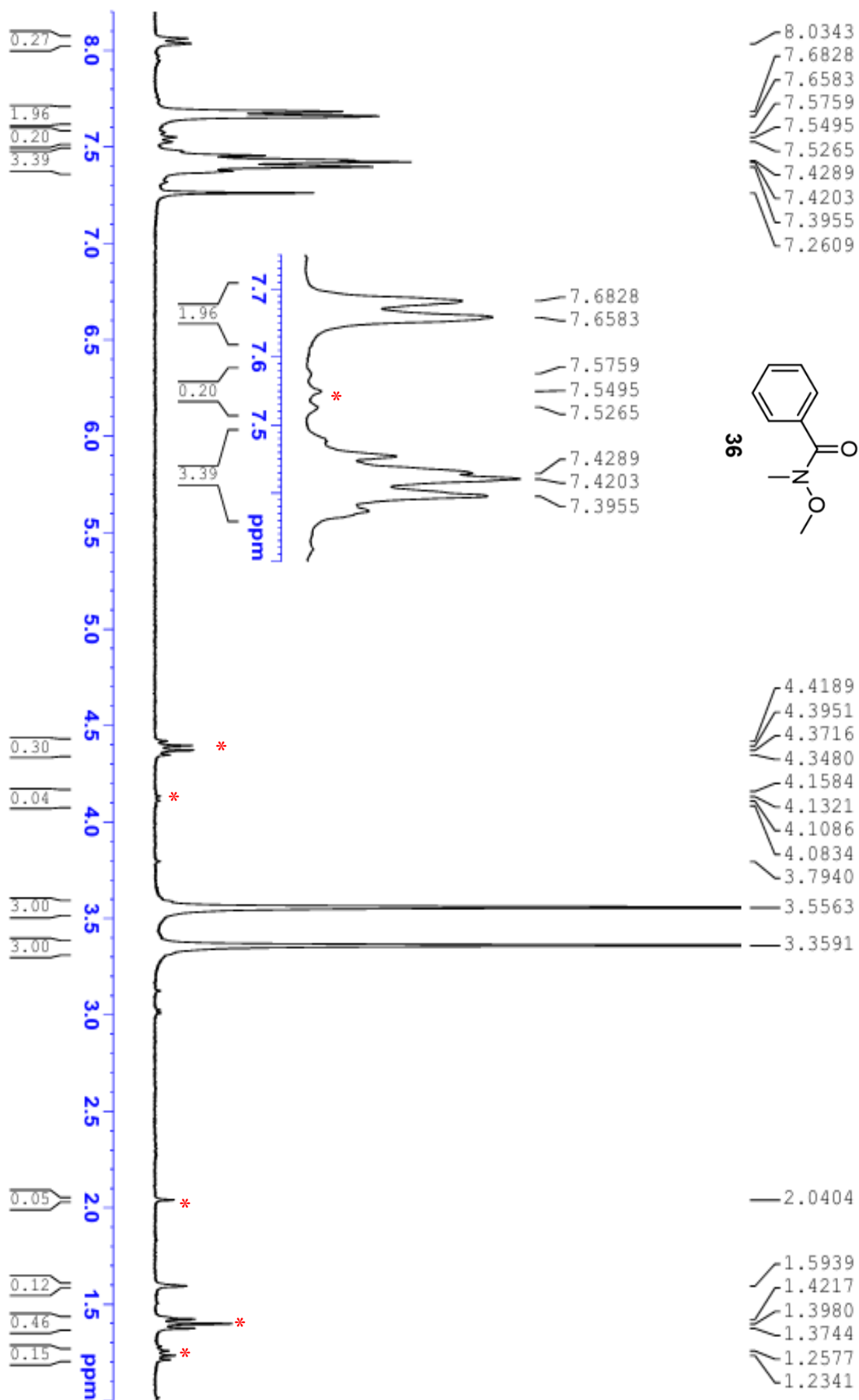


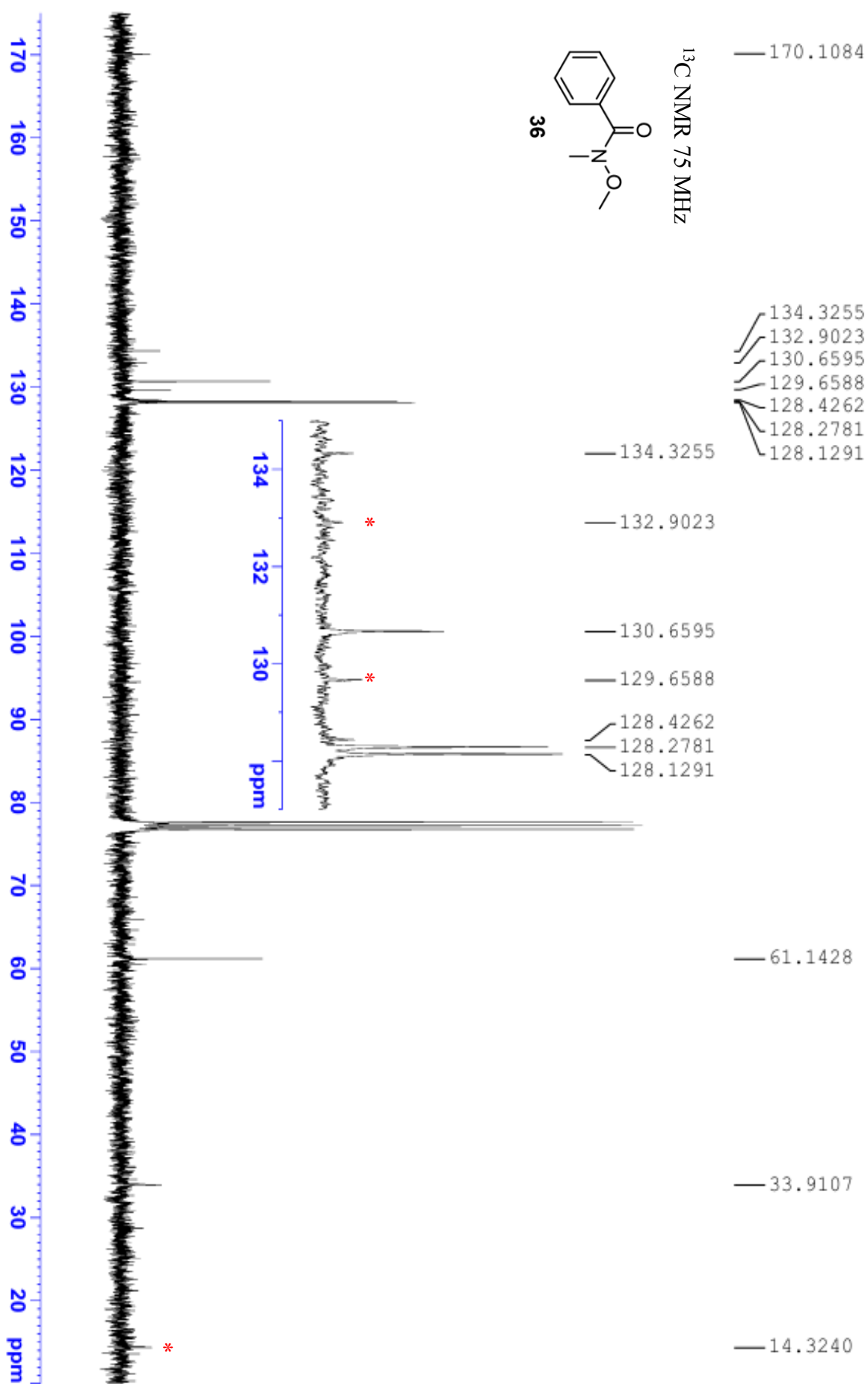
## APPENDIX 8

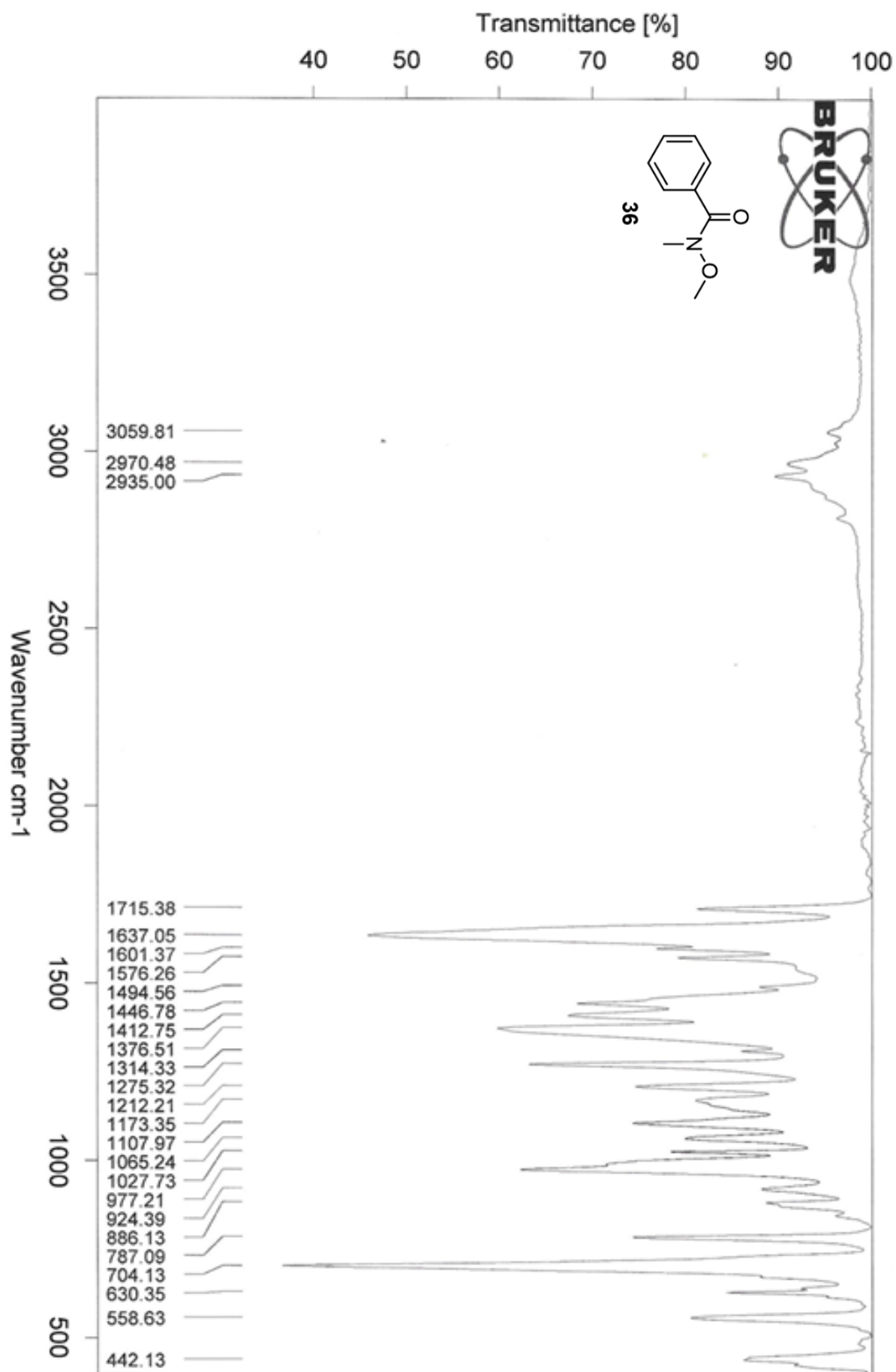


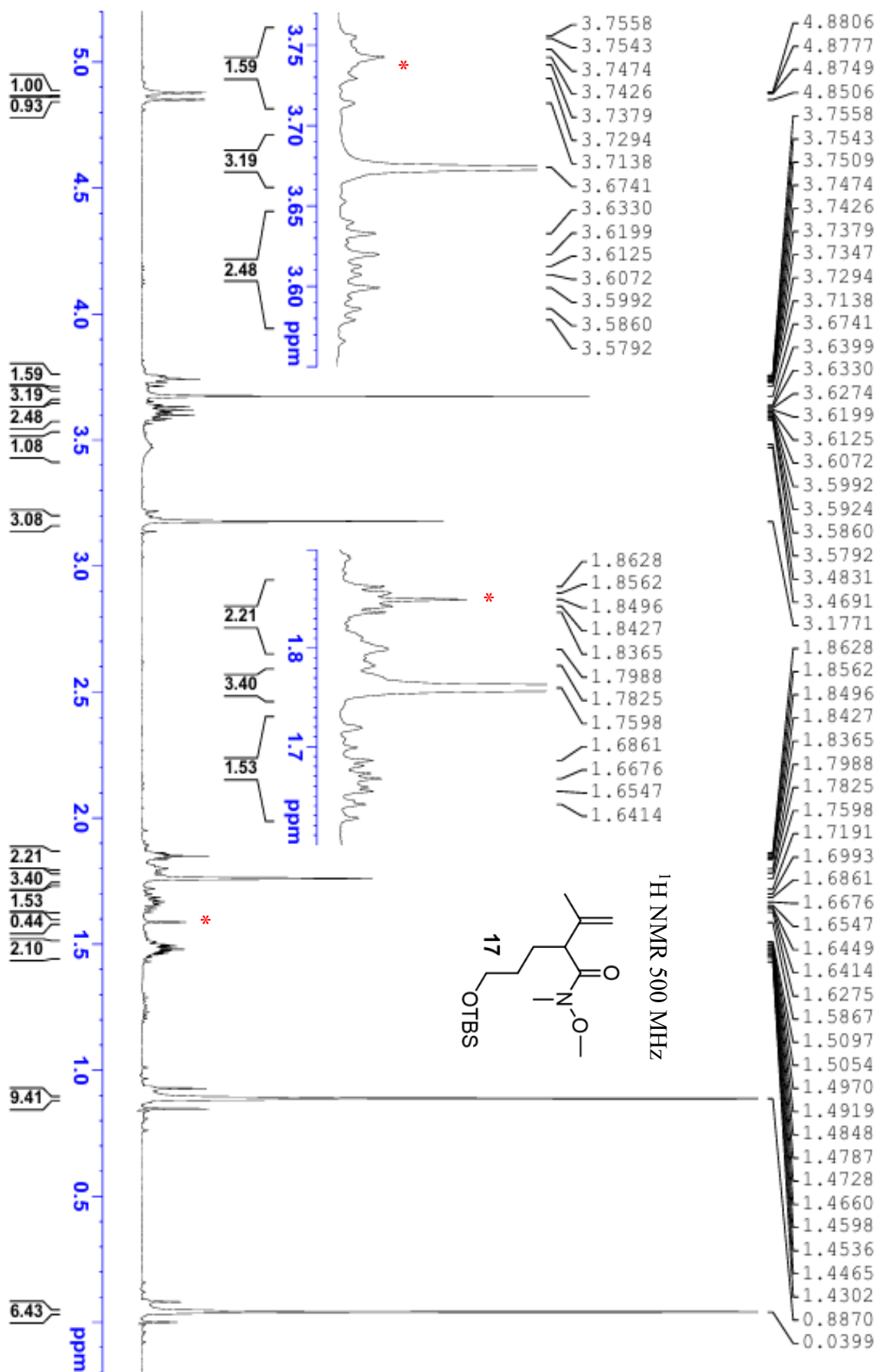






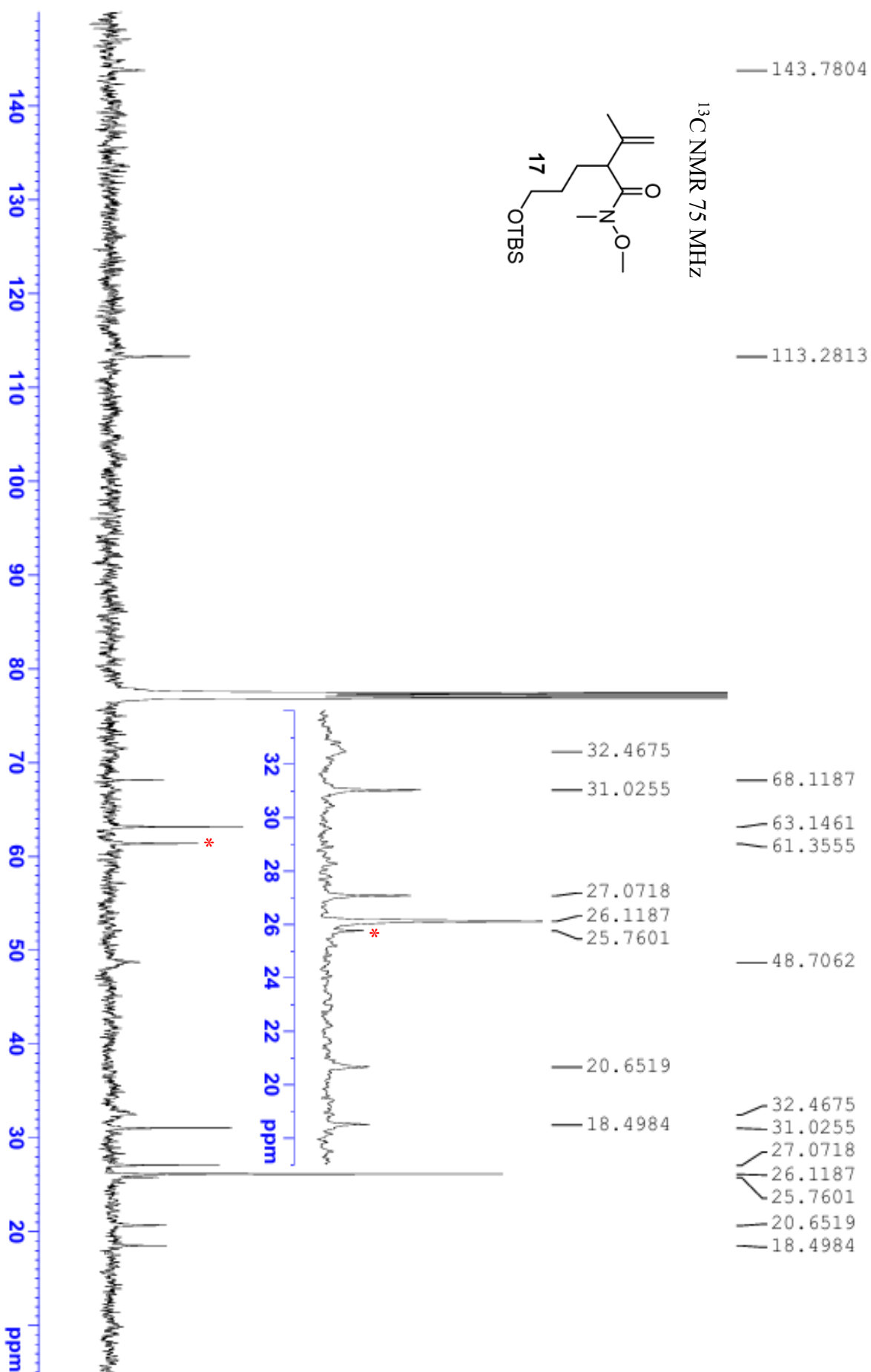


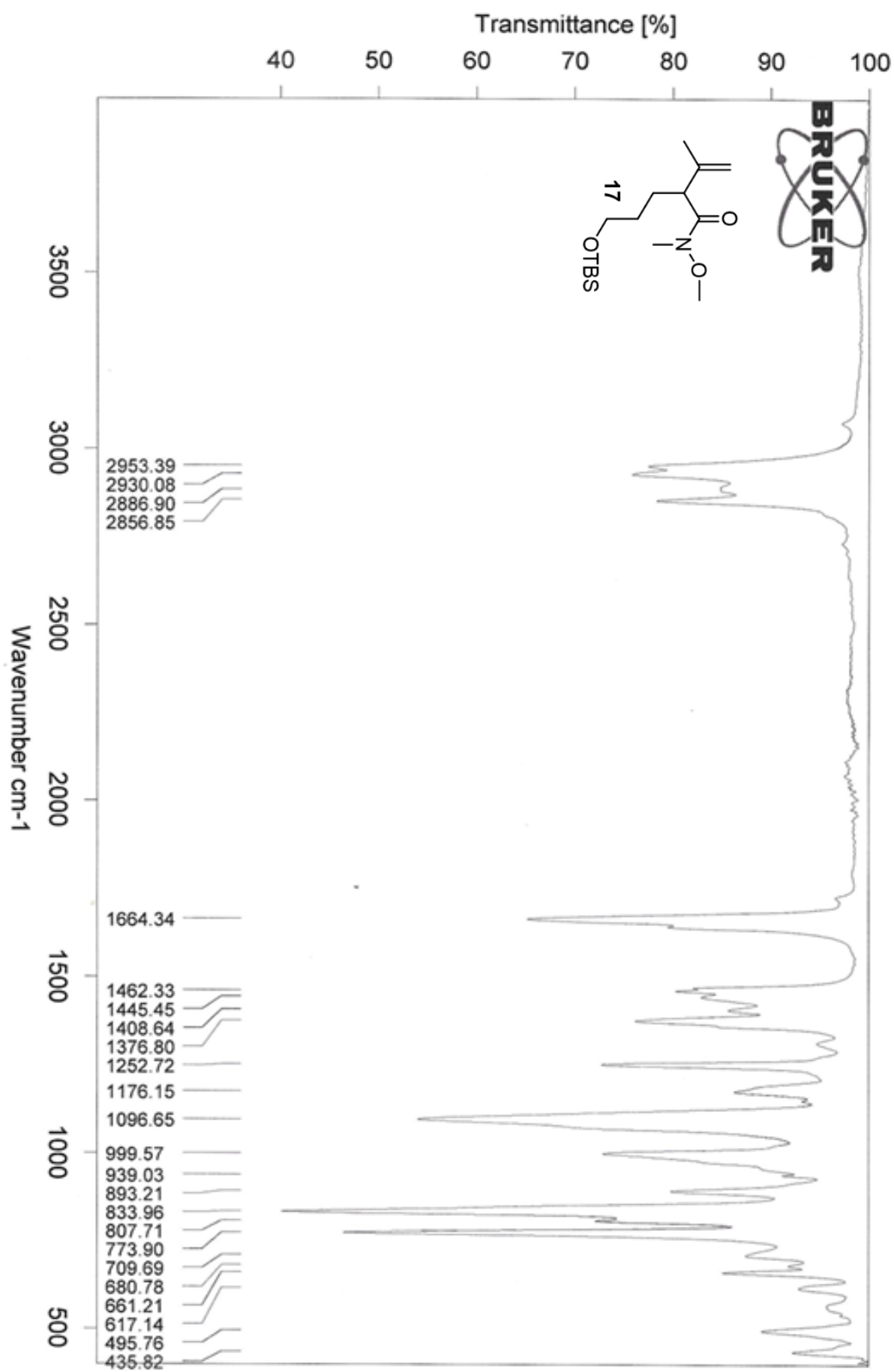


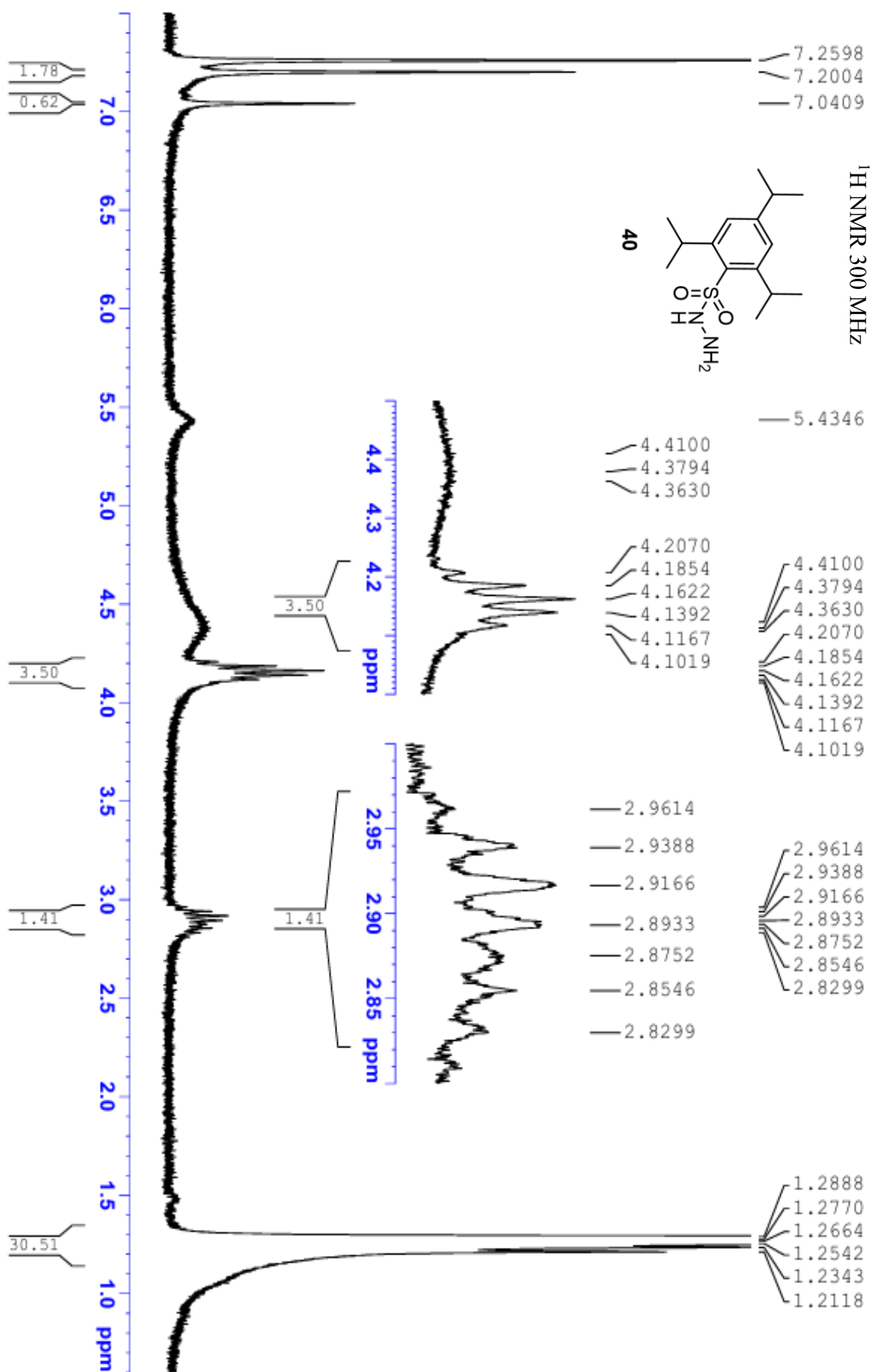


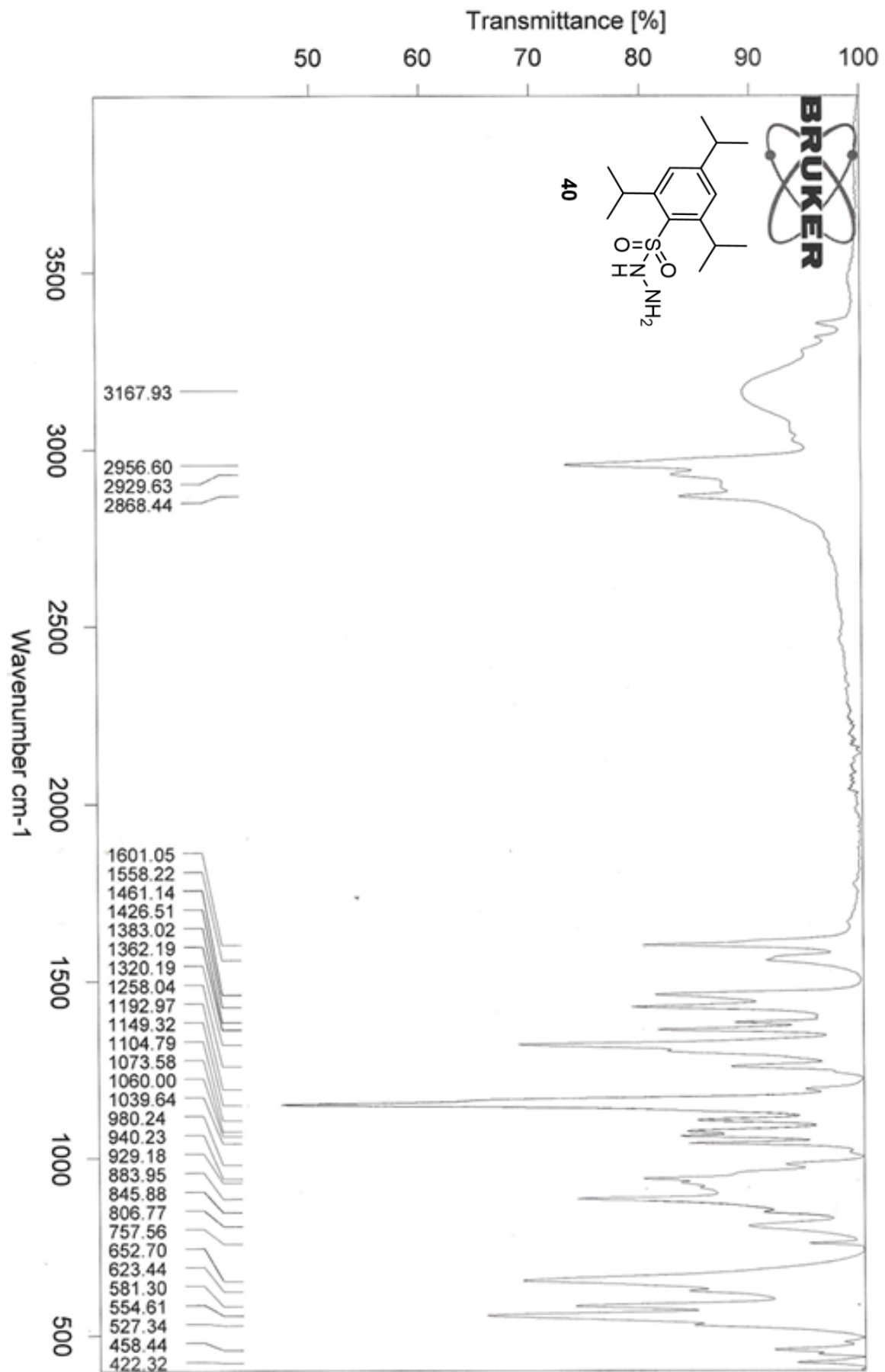


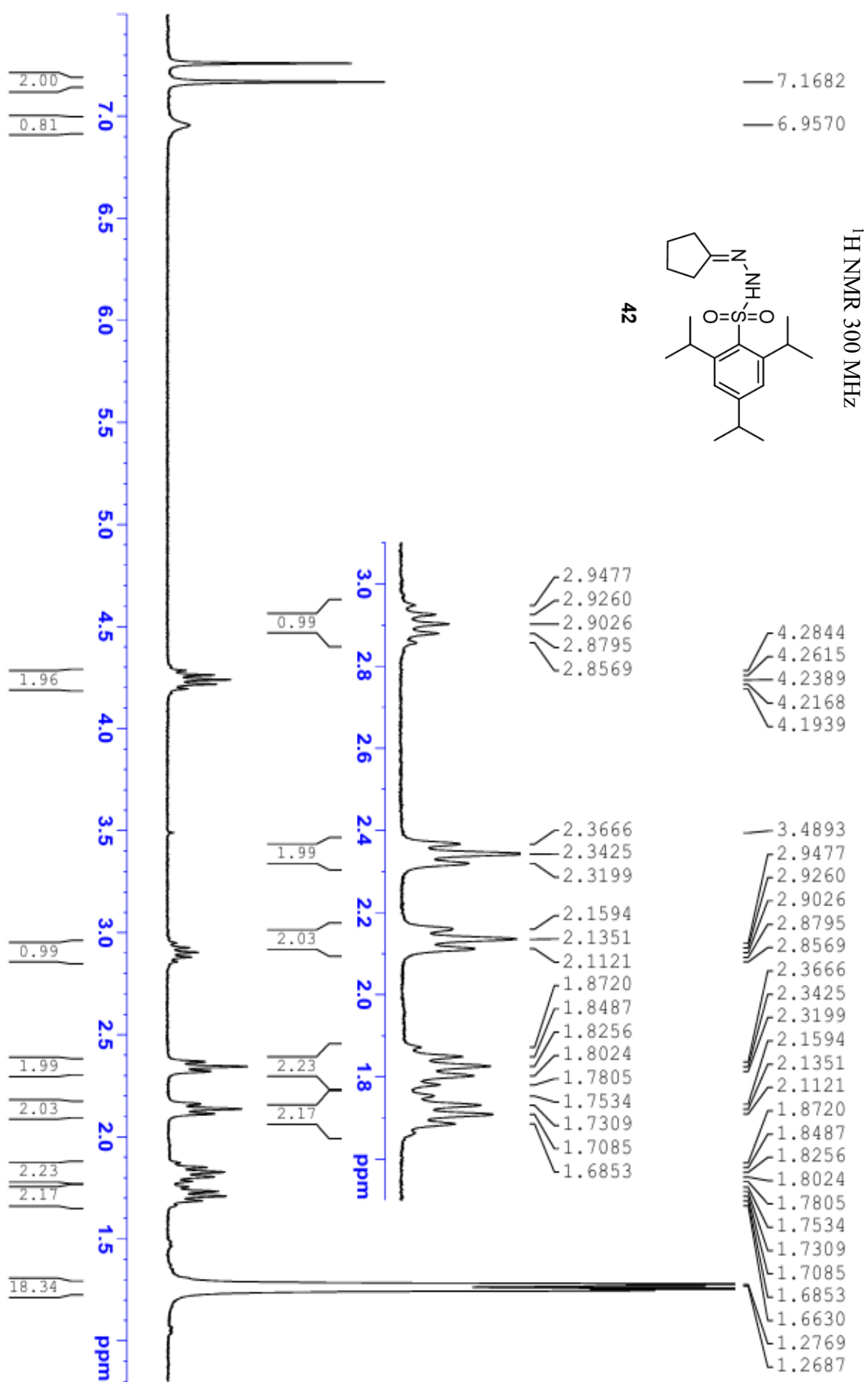
## APPENDIX 15

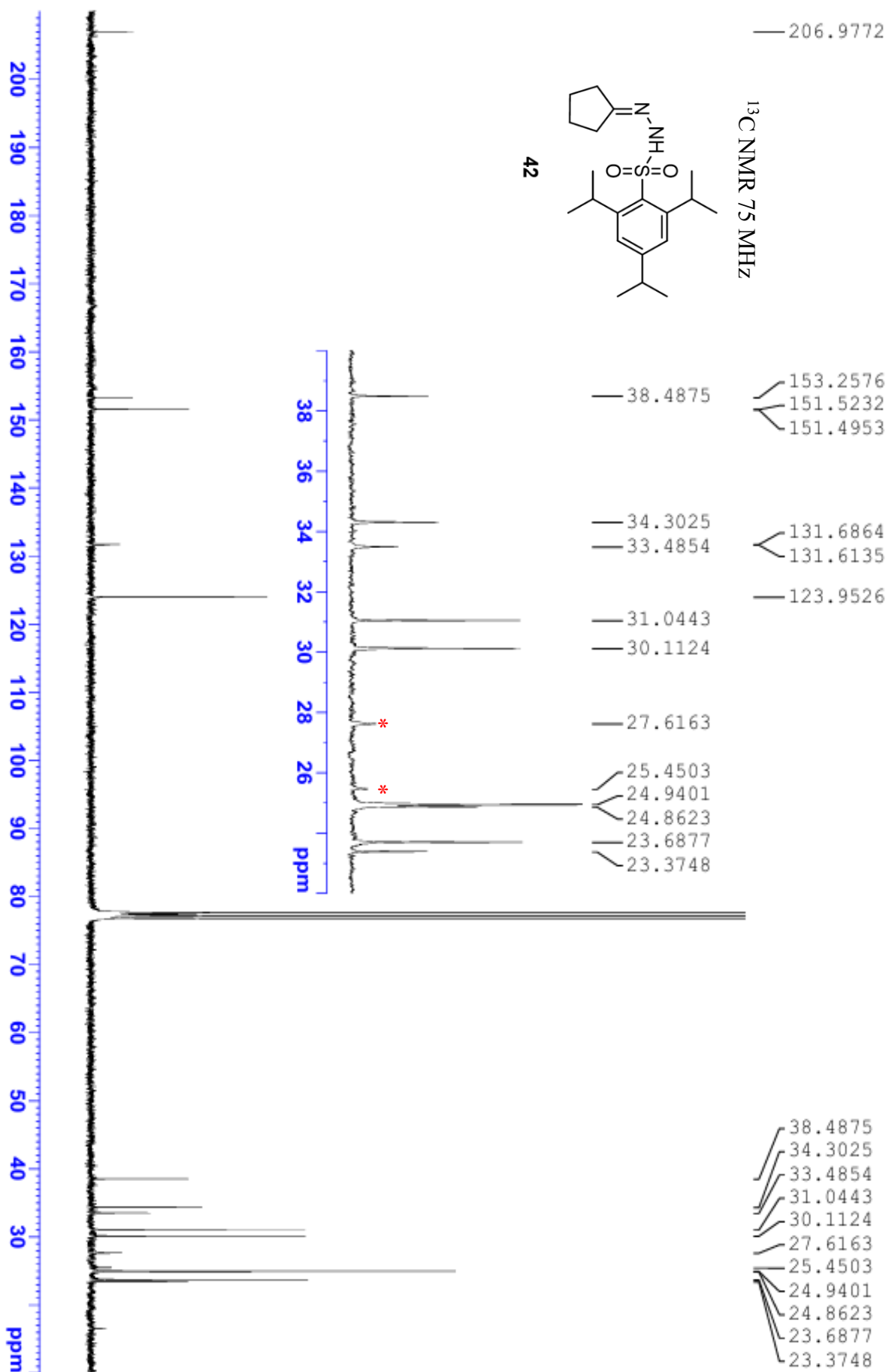


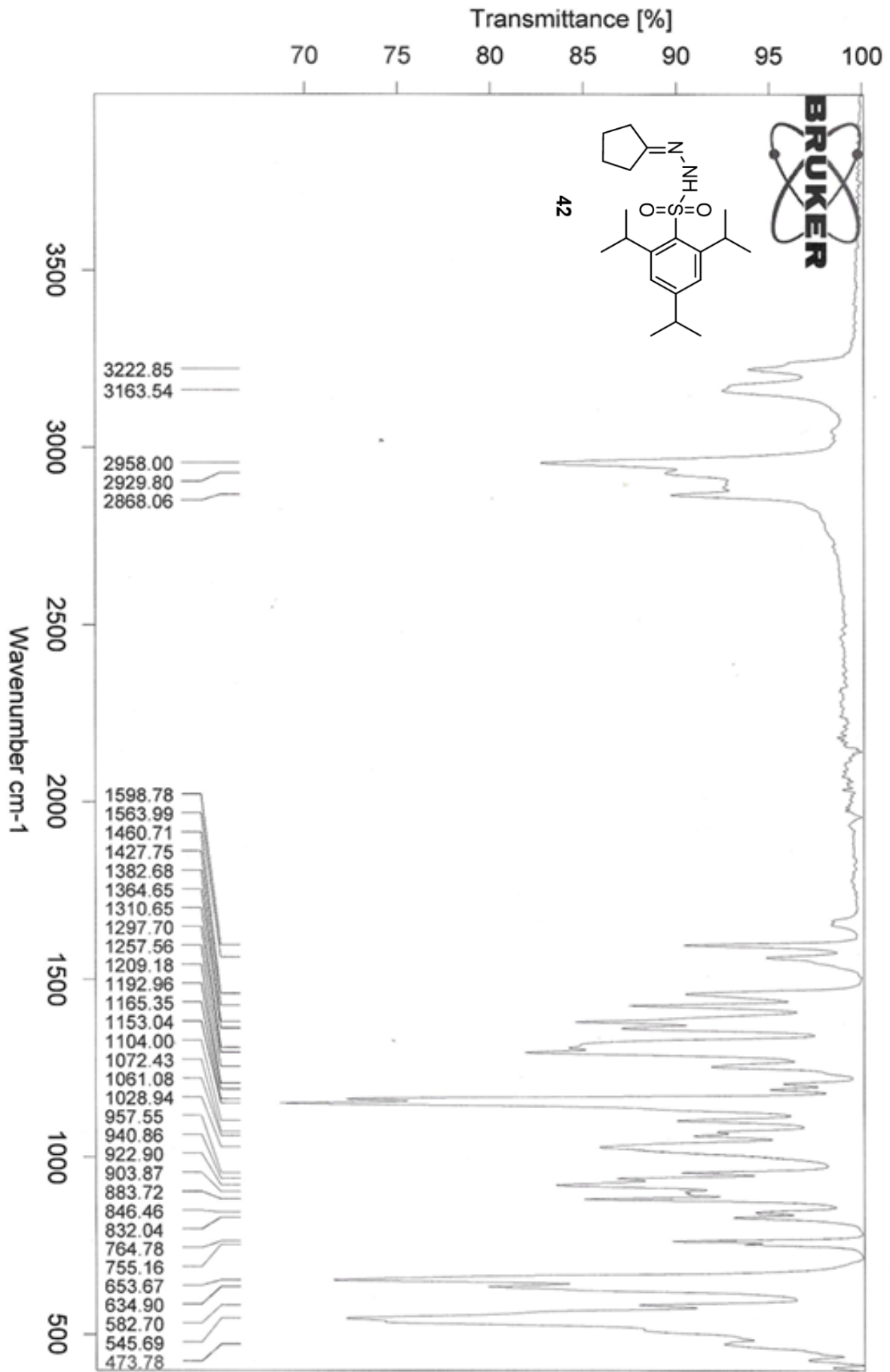


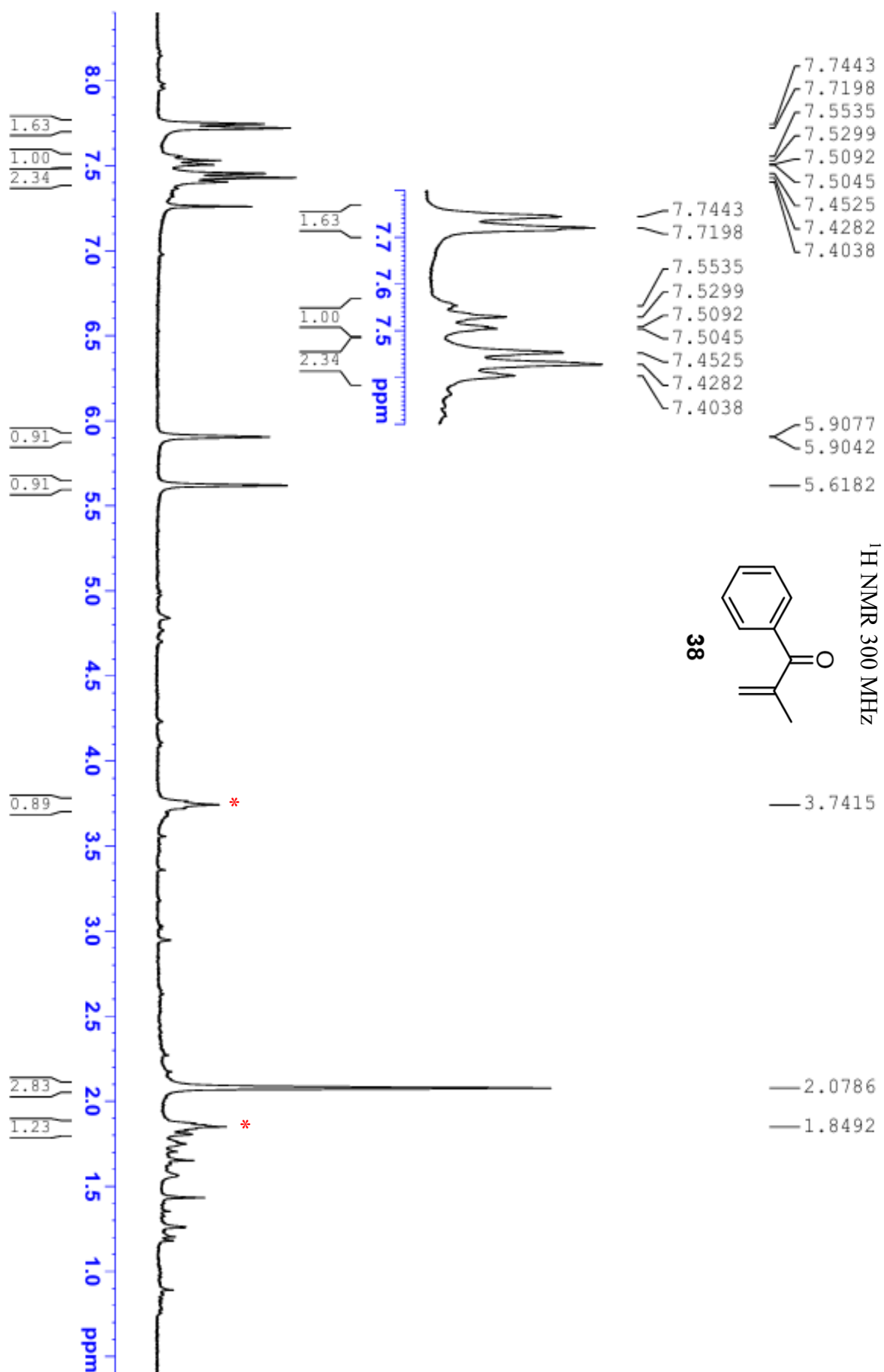






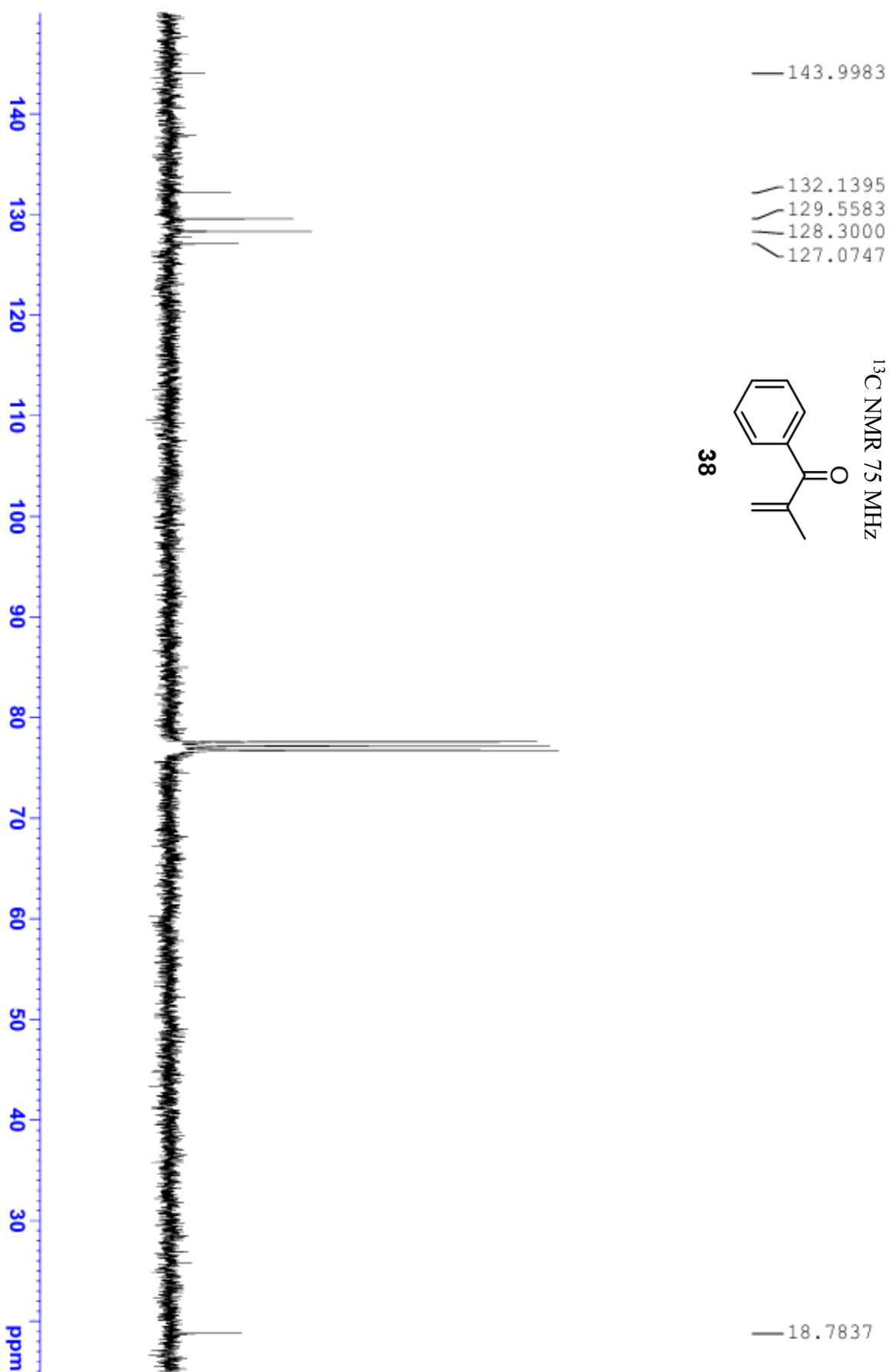


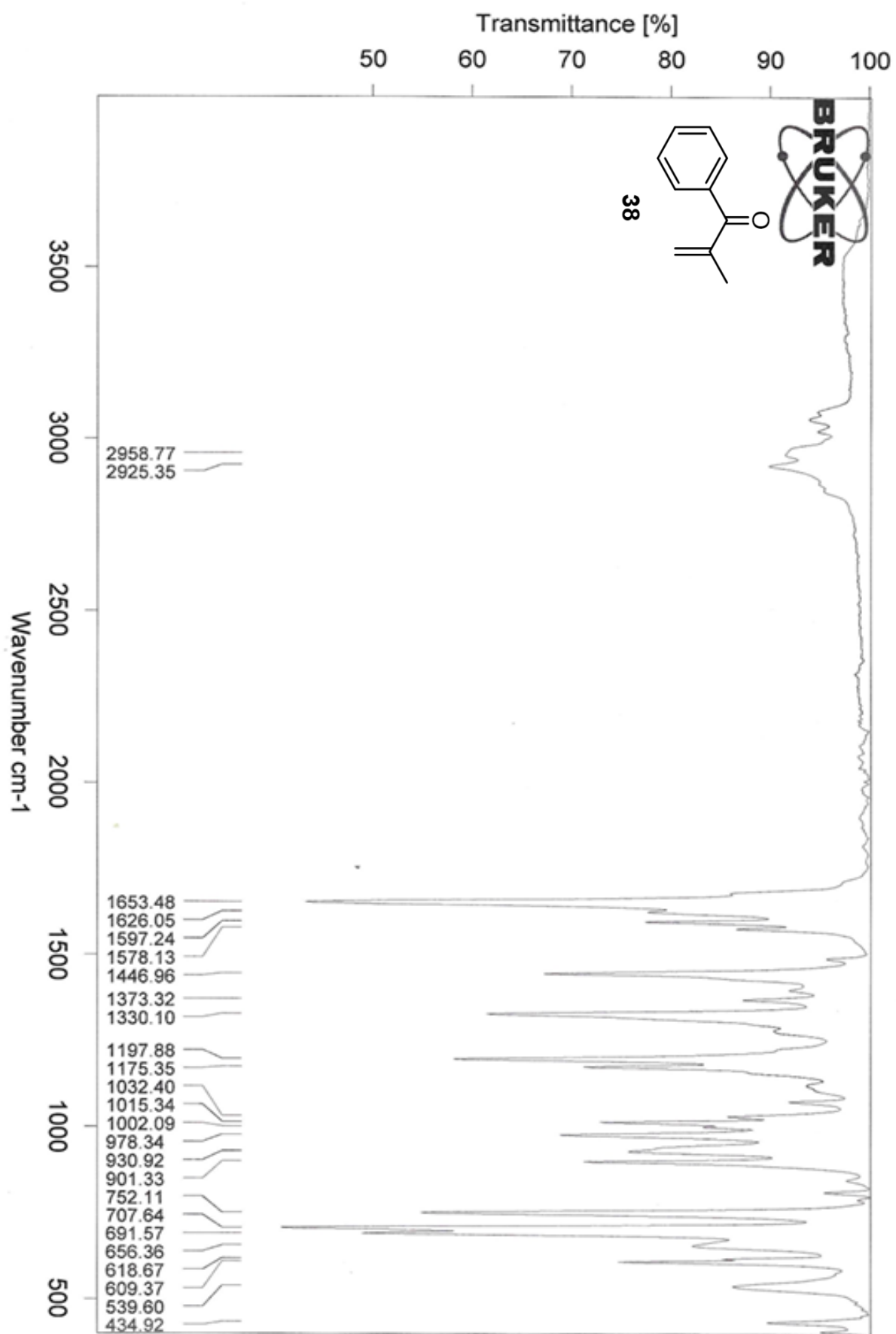






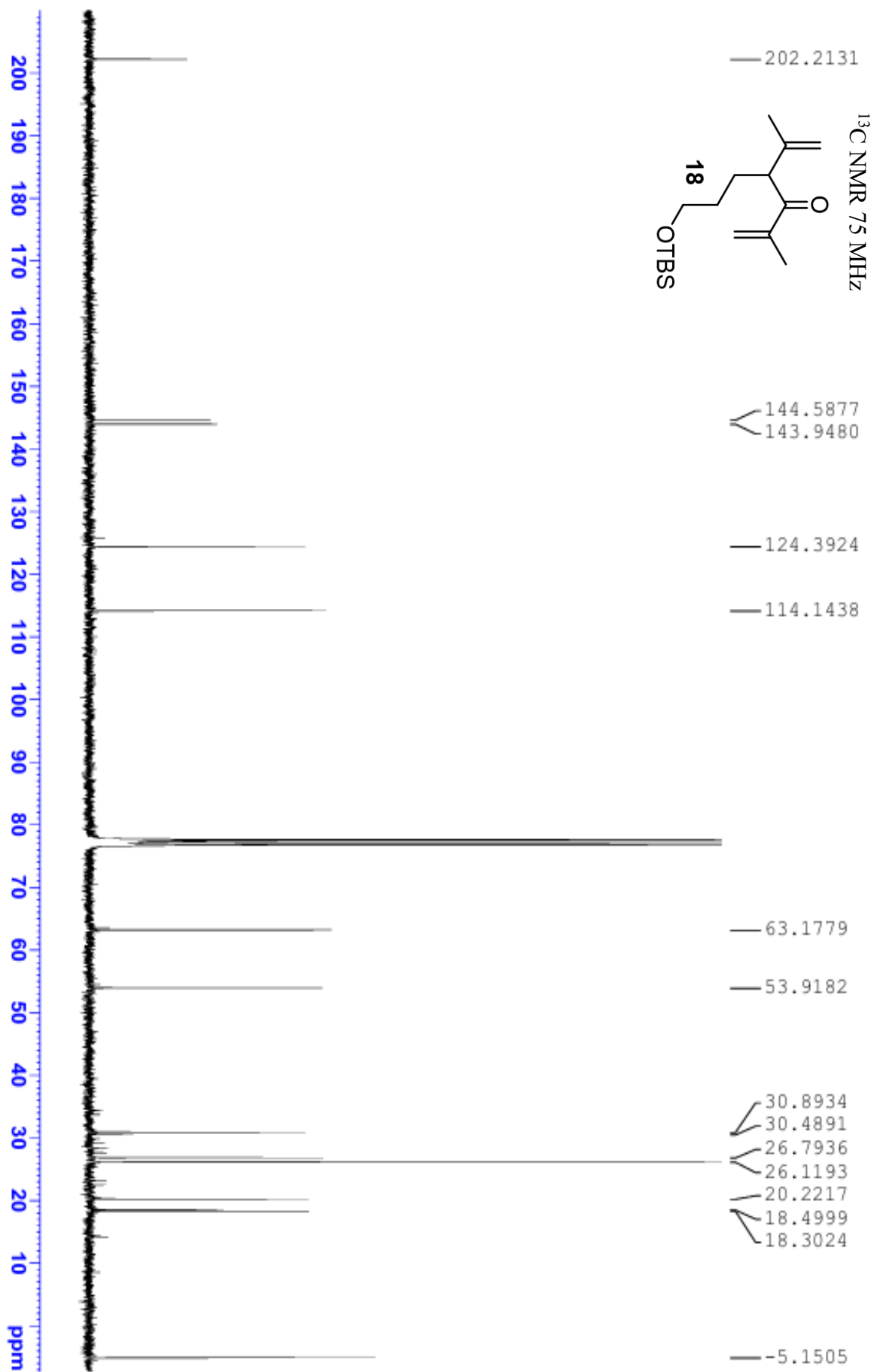
## APPENDIX 23

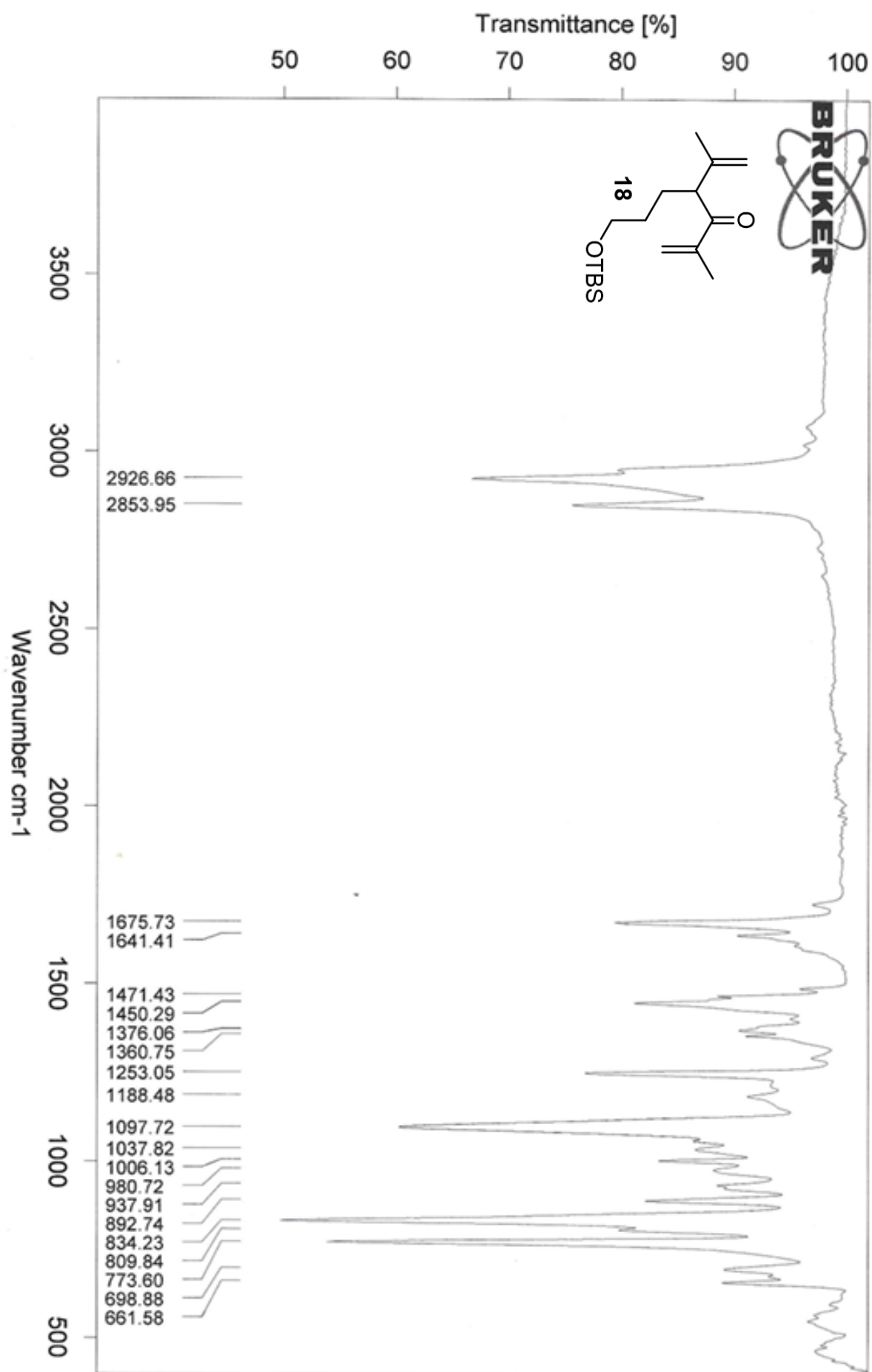






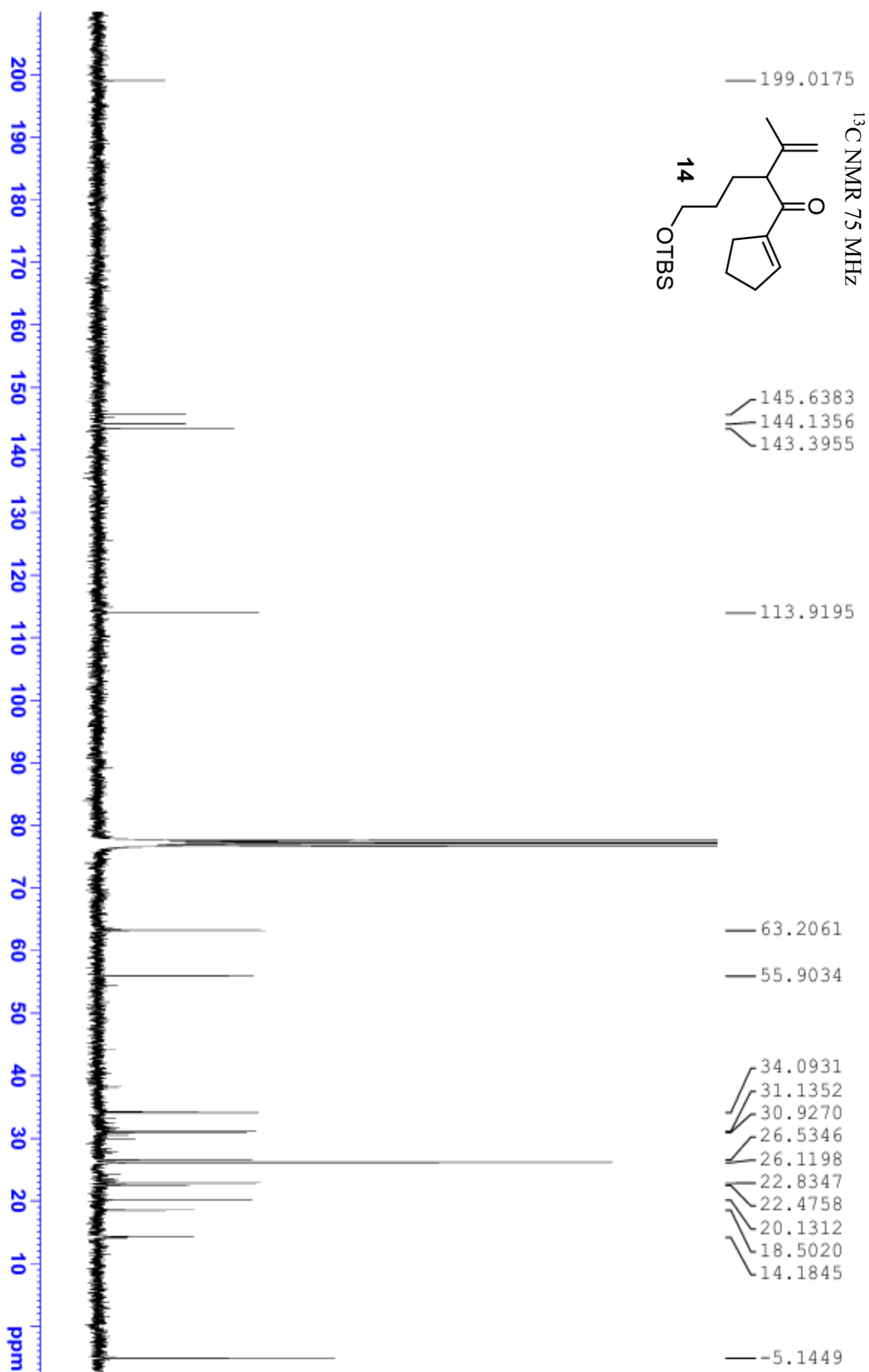
## APPENDIX 26

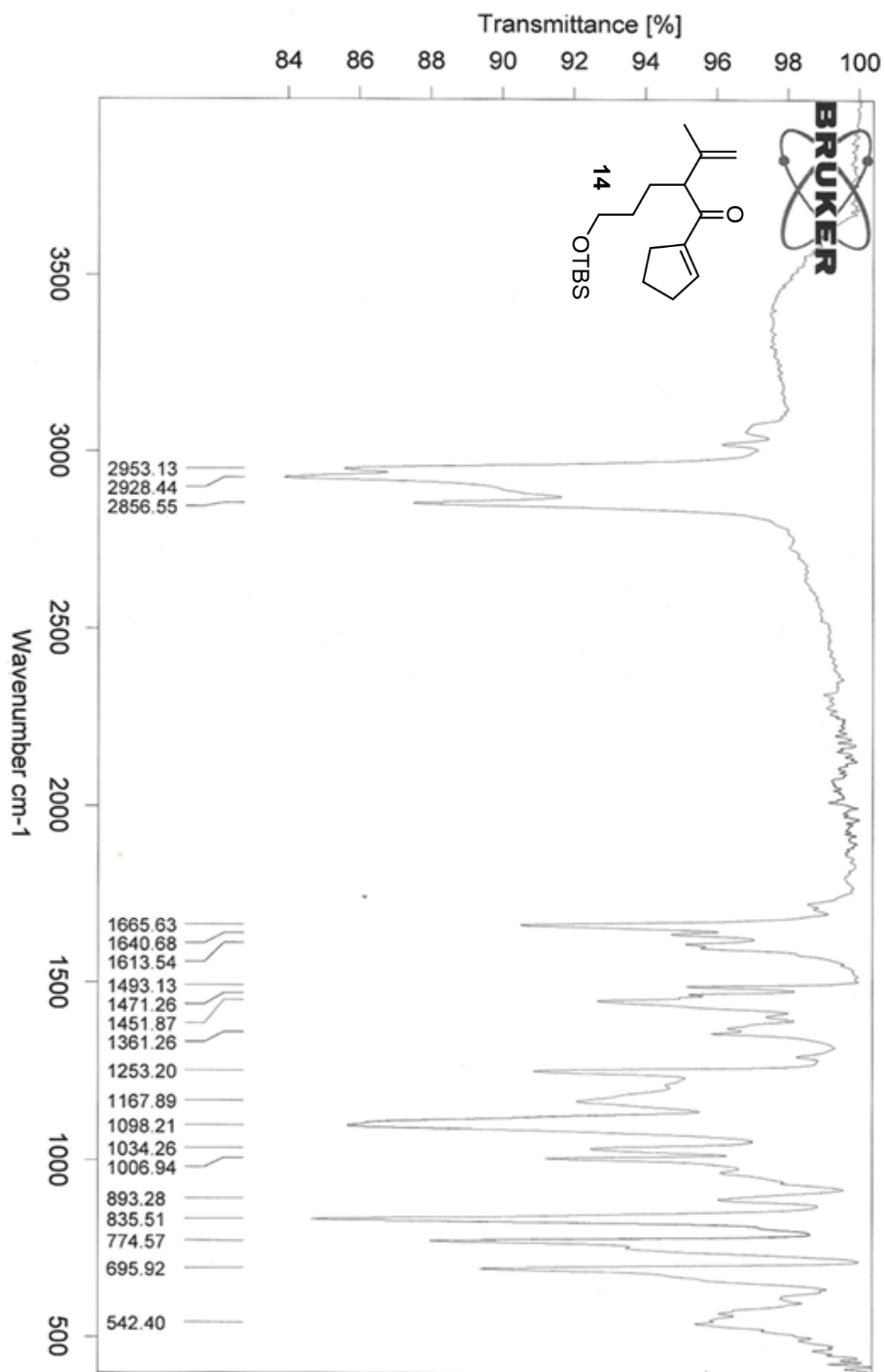




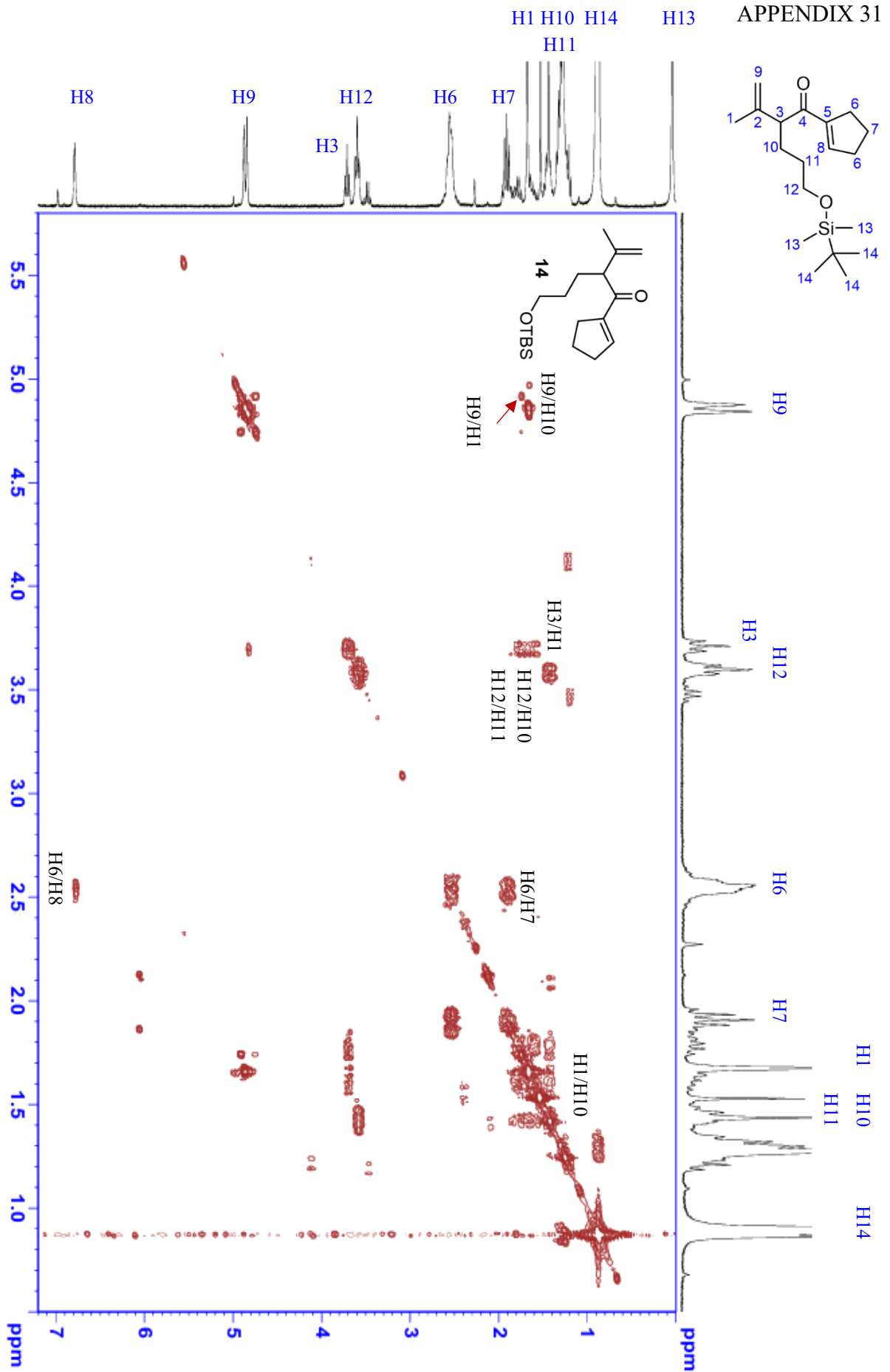


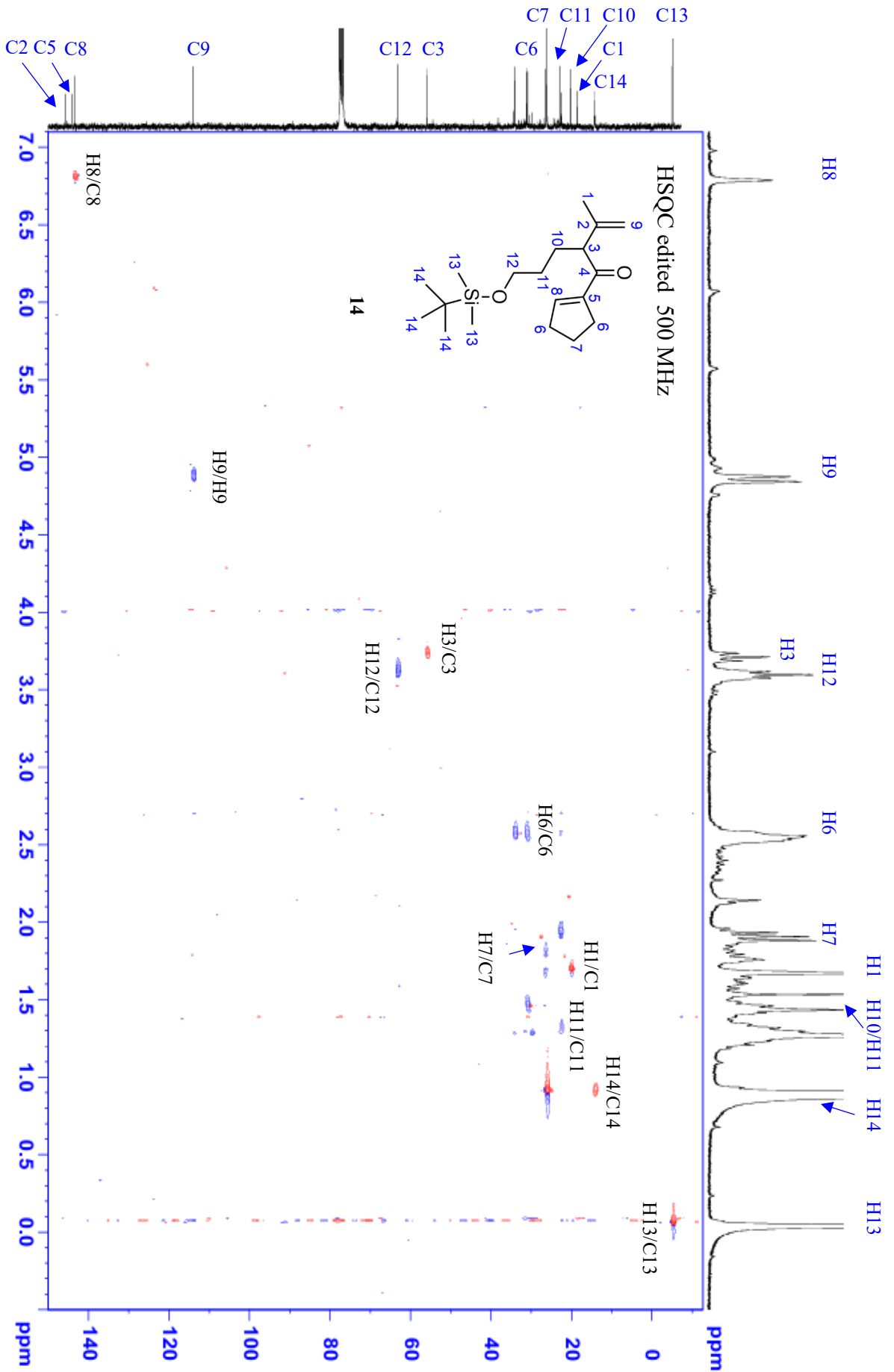
## APPENDIX 29

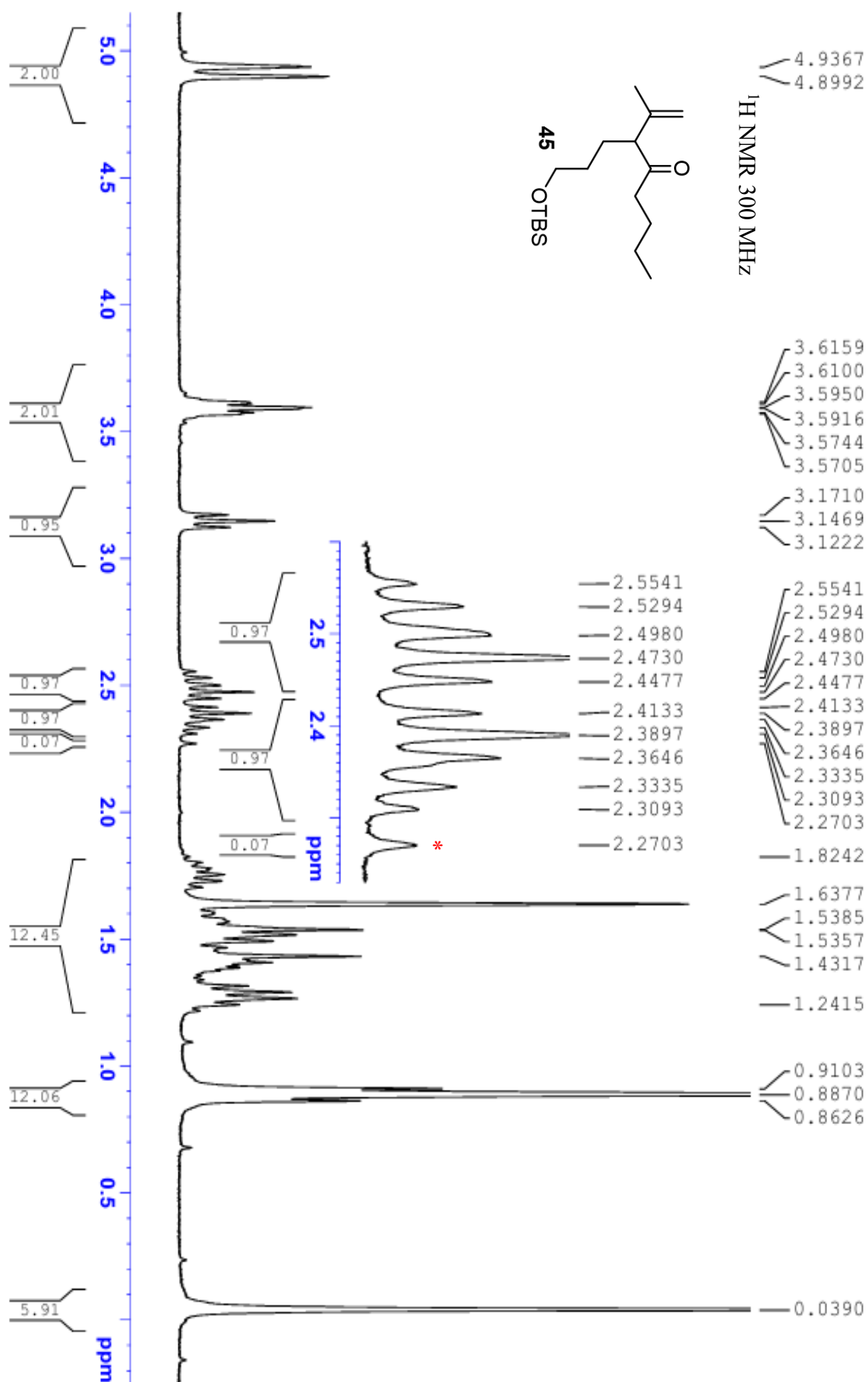


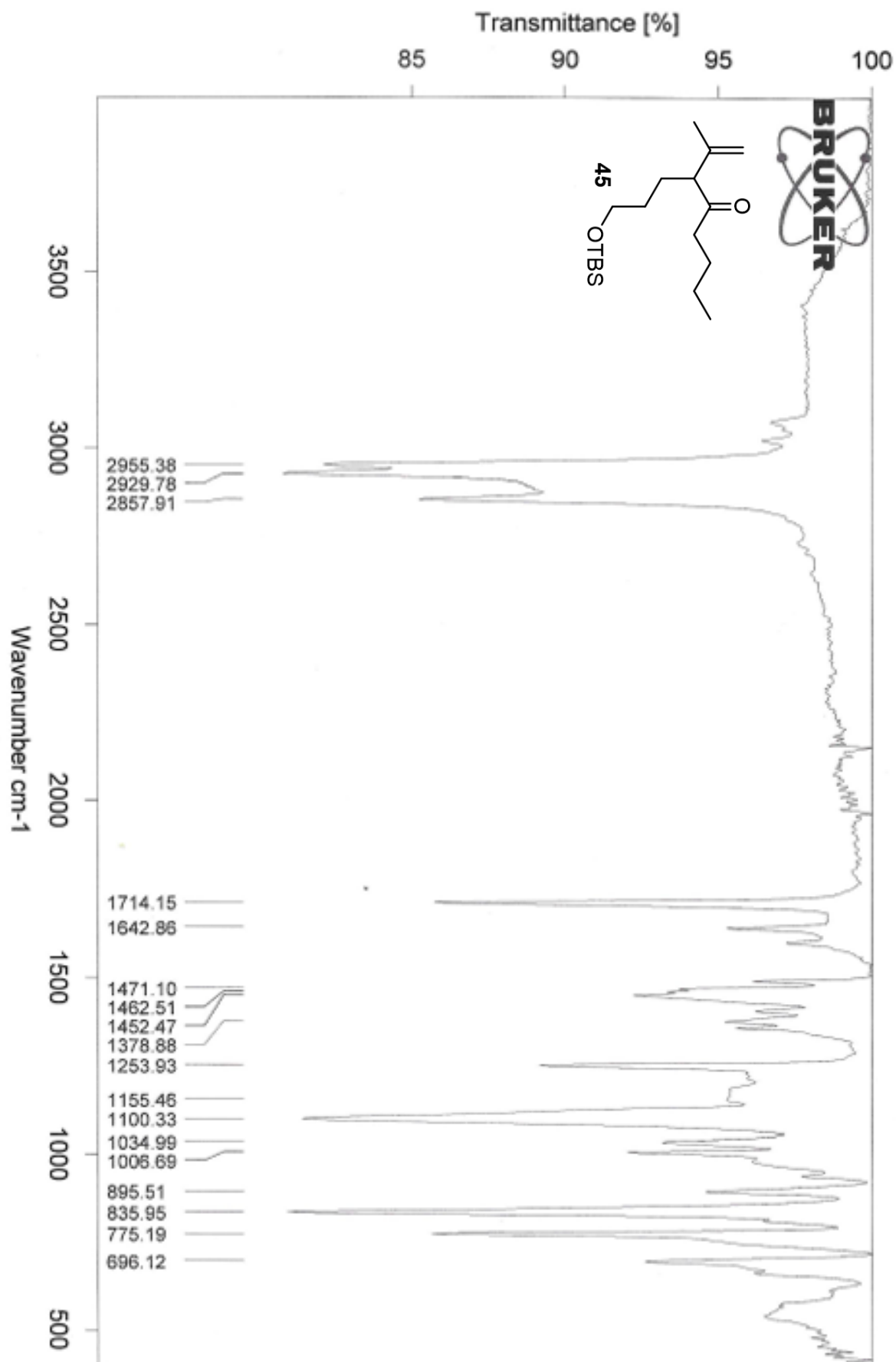






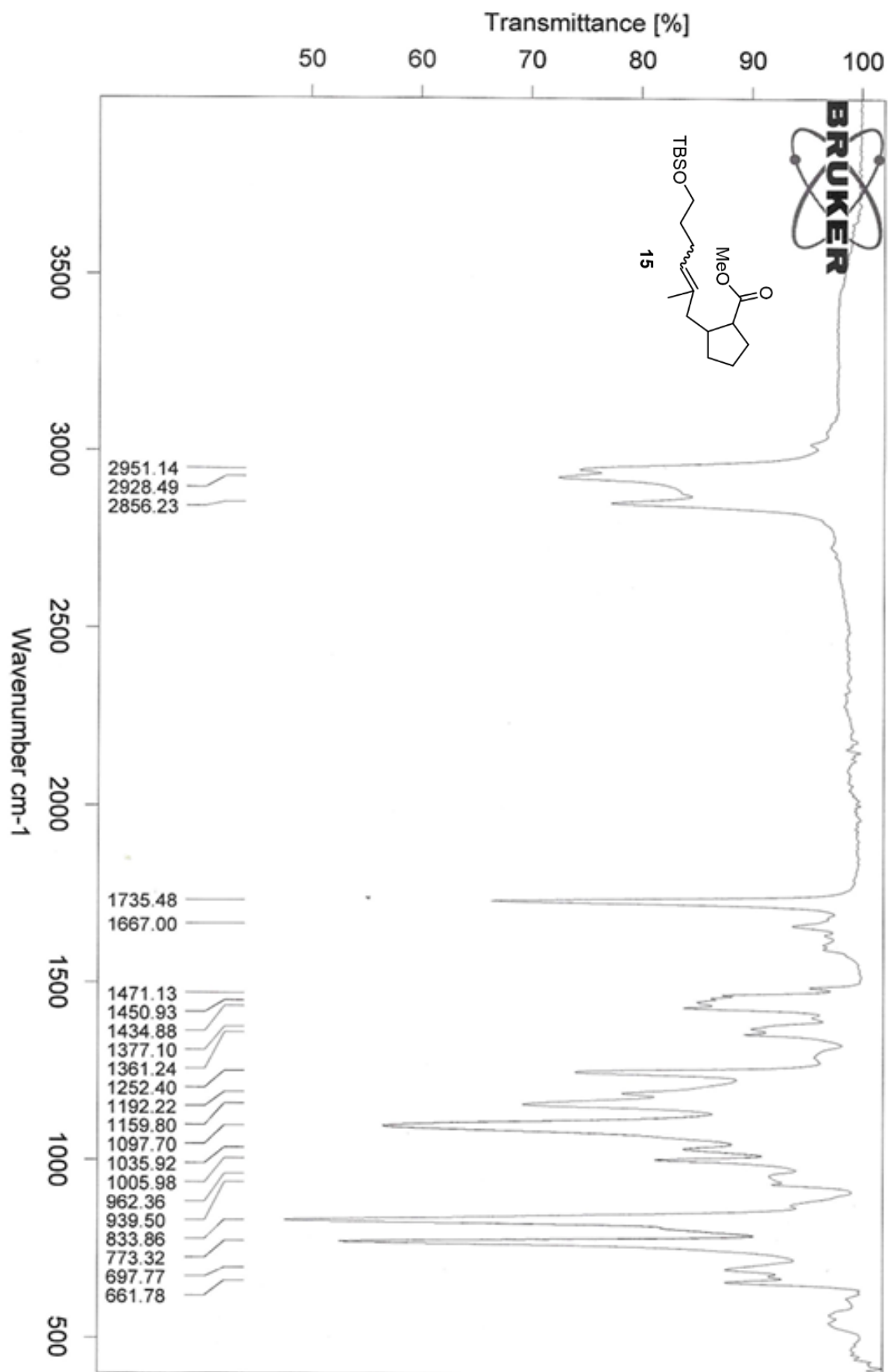


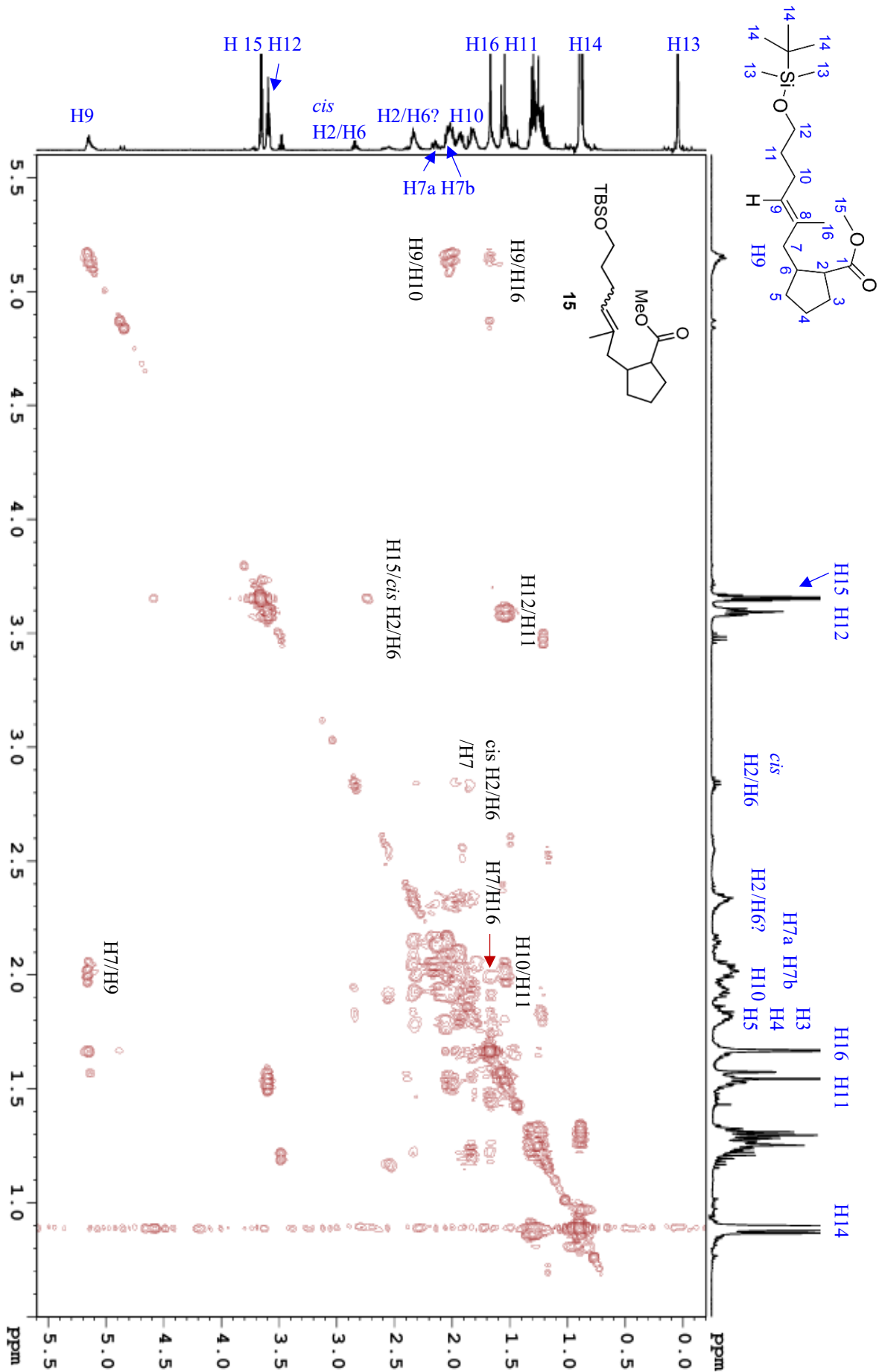






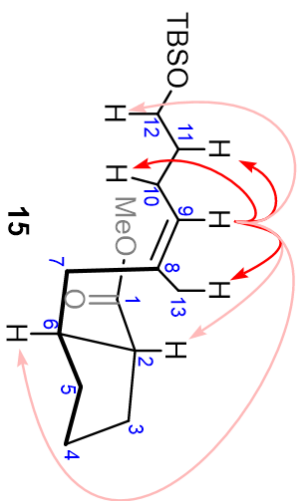








ID-NOE NMR 500 MHz  
irradiation 5.16 ppm



Red = 1H NMR  
Blue = 1D NOE

